LIGAND-BASED BIOSENSOR PLATFORMS FOR RAPID DETECTION OF BACTERIA AND CANCER

by

Hashem R. Ali Etayash

A thesis submitted in partial fulfillment of the requirements for the degree of

Doctor of Philosophy
in

Pharmaceutical Sciences

Faculty of Pharmacy and Pharmaceutical Sciences
University of Alberta

ABSTRACT

The availability of robust and handheld devices for detection is of growing importance in environmental safety, food analysis, and human diagnostic areas. The currently accessible approaches for detection of bacteria and/or diagnosing cancer, suffer from a number of constraints that hinder their wide-scale applications, such as stability, sensitivity, specificity and the time-independent functionality that is needed for real-time analysis. Identification of bacteria, for instance, has relied exclusively on specific microbiological culture media to grow, segregate and then enumerate only existing viable bacterial cells. This traditional method of detection is inconvenient, labor-intensive, time-consuming, and entails trained personnel in equipped laboratory settings. Likewise, examining cancer is mostly implemented through techniques like mammography, colonoscopy, echocardiogram, ultrasound exams, magnetic resonance imaging (MRI) and [18F] fluorodeoxyglucose positron emission tomography, which are typically followed by ex-vivo biopsies and further checkups. These methods are inconvenient, very expensive, and time-consuming, require skilled trainees and are occasionally not accurate in diagnosis; thus, they may lead to unnecessary treatment, false treatment or an actual disease go untreated.

In this dissertation, I present preliminary studies towards the development of highly reliable, cheap and noninvasive ligand-based platform technologies that can be used to detect bacteria and/or to identify breast cancer biomarkers. In chapter 1, a general introduction to the current diagnostic methods and the challenges they face are presented. Chapters 2 and 3 report novel biosensing approaches for detecting pathogenic foodborne *Listeria monocytogenes* (*L. monocytogenes*) using an antimicrobial peptide (AMP) from class IIa bacteriocins and monoclonal antibodies (mAbs) assimilated in an electrochemical impedance spectroscopy (ESI)

and microcantilever sensors (MCS). The results demonstrated a label-free detection of *L. monocytogenes* at very low concentrations (down to 1×10^3 CFU per mL) and also highlighted the feasibility of using short-ligand AMPs for selective detection of bacteria alternatively to mAbs as they are cheaper, hold better stability and easier to produce.

In chapters 4, 5 and 6, rapid and non-invasive tools for spotting breast cancer biomarkers, including circulating tumor cells (CTCs) and breast cancer cell-derived exosomes, are presented. The results showed the capability of peptide-based MCS to detect CTCs (represented by MCF7 spiked human blood samples) at a limit of 50 – 100 cells per mL with a capture yield of 80% from whole blood samples. Exosomes from breast cancer cell lines were also selectively identified by targeting over-expressed membrane-proteins CD24, CD63, EGFR, and GPC1, with an excellent selectivity was achieved when targeting the cell-surface proteoglycan, at extraordinary limits (~200 exosomes per mL, ~0.1 pg mL^{-1}).

The current research emphasizes the development of portable, non-invasive ligand-based nano and micro platform technologies for rapid detection of pathogenic foodborne bacteria and breast cancer biomarkers.

PREFACE

This thesis is an original work carried out by **Mr. Hashem R. Ali ETAYASH**. All experiments related to human blood samples were approved by the University of Alberta Health Sciences Policy and Committee.

- Chapter 2 of this thesis was published in **ACS Analytical Chemistry** journal. Arthurs in order, Etayash H, Jaing K, Thundat T, and Kaur K. I (Etayash H) had designed the research project, conducted experiments and analyzed data. Jaing K. had helped in in samples preparations and data analysis. Thundat, T. and Kaur, K. have supervised the project and contributed to the article composition and edition.
- Chapter 3 of the thesis was published in **Nature Communications** as Etayash H, Khan MF, Kaur K, and Thundat T. I (Etayash H) had designed the research project, conducted the experiments, and analyzed data. Khan M had designed and fabricated the microchannel cantilever and helped in data analysis. Thundat, T. and Kaur, K. have supervised the project and contributed to the manuscript composition. I was responsible for writing the manuscript. All authors have read and proof edited the manuscript.
- Chapter 4 was published in **NPG Scientific Reports** as Etayash H, Jaing K, Azmi S, Thundat T, and Kaur K. I (Etayash H) designed the research project, conducted the experiments, and analyzed data. Jiang K helped with SPR experiments and cantilever set up. Azmi S, helped in cells cultures and numerations. Thundat, T. and Kaur, K. supervised the project and contributed to the manuscript composition. I (primarily) and Kaur K (secondarily) were responsible for writing the manuscript. All authors have read and proof edited the manuscript.
- Chapter 5 was published in **RSC Nanoscale**. I (Etayash H) had designed the research project, conducted the experiments, and analyzed data. McGee R had helped in conducting the Scanning Electron Microscopy (SEM) experiments. Thundat, T. and Kaur, K. had supervised the project and contributed to the manuscript composition. I was responsible for writing the manuscript. All authors have read and proof edited the manuscript.
- Chapter 6. (**Unpublished**). I (Hashem Etayash) have designed the research project, experiments and run experiment and data analysis. Keren Jiang has helped in the impedance experiments and data analysis. Rania Soudy has helped in isolation and sample preparations.

Thomas Thundat and Kamaljit Kaur supervised the project and contributed to the manuscript composition. I was responsible for writing the current draft.

……
,,

DEDICATIONS

I would like to dedicate my thesis to my parents, My Dad and My Mom, whom I miss so much, AND to my lovely Wife and our cute little child☺ who is 10 months old. They were here for me side by side with their supports, encouragements and prayers. I also dedicate it to my brothers and sisters who have been here from far distance with their love, compassions and inspirations.

……
,,

ACKNOWLEDGMENT

I would like to acknowledge all the people, who have been here for me throughout my Ph.D. program, and who have helped me in many different ways to reach my goals.

- First, special acknowledgment and appreciation to my thesis supervisor Dr. Kamaljit Kaur. Thank you for the opportunity, for the fabulous support, help, guidance, and the affection which helped me being a very well-focused researcher.
- My gratitude and thanks to the Professor and Canada Excellence Research Chair, Thomas Thundat for his valuable supervision, supports, encouragement, and guidance.
- Many thanks to my lab members and collaborators Dr. Faheem Khan; Dr. Rania Soudy; Mr. Keren Jiang; Mrs. Parmiss Mojir Shaibani; Mr. Ryan McGee; Dr. Sharfuddin Azmi, and Dr. Ramana Azmi, for their help, support and assistance.
- I acknowledge my advisory committee members Dr. Arno Siraki and Dr. Carlos Velázquez for their guidance and treasured discussions throughout my studies.
- I would also like to thank CanBiocin Edmonton Inc. for providing me with the bacterial indicators to run the experiments.
- Last but not least, I would also like to express my gratitude and acknowledge all the funding agents for their support and trust. Special thanks to the Libyan Government and the Libyan-North American Scholarship Program, CBIE, for the financial support during my program. Special thanks to Alberta Innovates Future Technology for the financial support, for their magnificent coordination and assistance throughout my Ph.D. program. Thanks to NSERC, CHIR and CERC programs, and finally, special acknowledgments to the Faculty of Pharmacy and Pharmaceutical Sciences, University of Alberta, Edmonton, Canada.

TABLE OF CONTENTS

TABLE OF FIGURES

Chapter 1 . Introduction

1. Introduction

There is an immense global need of new tools for chemical and biological analysis that can provide a fast and accurate diagnosis for bacteria and/or cancer, allowing at the same time the functionality of in-situ real-time analysis[1, 2]. The necessity of rapid and sensitive sensing techniques for detection have become a critical need for alarming broad clinical problems that may include cancers[3], hepatitis[4], acquired immune deficiency disease (AIDS)[5]as well as foodborne and pathogenic superbugs outbreaks[6, 7].

1.1 DETECTION OF FOODBORNE PATHOGENS

Foodborne diseases are costly – yet preventable – and life-threatening problem for millions of people around the world. Although it is difficult to estimate the incidents of foodborne illnesses, the Centers for Disease Control and Prevention (CDC) estimates that each year thousands of people in the United States only, get sick, or die of foodborne illnesses. Almost fifty percent of the deaths result from consumption of food contaminated with pathogenic bacteria including *Salmonella, L. monocytogenes, E. coli* O157:H7 and others[8-10]. In this new era of shortages in the development of new antibiotics, new bacterial resistance mechanisms emerge and spread quickly, threatening our ability to treat common infectious diseases and booming up the mortality rates and disability of individuals[11-13]. As a consequence, the demand for real-time portable and biosensing devices is crucially required to detect contaminations and alarm infections before they happen. The survival rate from the invasion of harmful bacteria exclusively depends on accurate diagnosis of the bacteria and right-treatments, both of which are difficult to achieve when laboratory supports and antibiotics are limited due to superbugs' resistance. As of such consequences, it's very important to identify bacterial strains in contaminated food and/or clinical samples as soon and accurate as possible.

*L. monocyto*genes is one of the most deadly forms of foodborne pathogens if they infected neonates, pregnant women, immune deficient patients or people with other diseases like leukemia, Hodgkin's and diabetes mellitus[14]. The microorganism causes a disease known as Listeriosis, which occurs centrally (meningitis) or locally[14]. Although the Listeriosis is relatively

rare, it is often severe and the mortality rates can be up to fifty percent[14]. The estimated infective dose of *L. monocytogenes* is approximately 10 – 100 million CFU in healthy individuals, and about 0.1 – 10 million CFU in high-risk individuals[15]. The research in this dissertation focuses mainly on *L. monocytogenes* as a target bacteria but the application is not exclusively limited to *L. monocytogenes*.

Techniques for detection of food-borne pathogens

1.1.1 Conventional culture methods

The culture methods perhaps remain the standard microbiological test for bacteria detection and enumeration[16]. The basic principle is based on incubation of the contaminated samples in nutrient media with specific formulations that allow specific microorganisms to growth and replicate. The microorganisms can then be detected and enumerated after incubation for 24 – 72 hours depending on the type of strains[16]. The methods may include culturing the bacteria in agar plates, broth diluted in tubes, or in microwell plates. These conventional methods are very simple, adaptable, very practical and generally inexpensive. Nevertheless, they are inconvenient to some extent and require a minimum of 24 h to complete[16]. In addition, these laboratory culture techniques are unable to detect uncultured bacteria, which make approximately 99% of all bacterial species in the environments[17]. Accordingly, they might not be adequate for precise monitoring of the microbiological quality of food, water, and other pharmaceutical products[16].

1.1.2 Rapid methods of detection

The recent advancement in biotechnology has made the detection of bacteria much faster, more convenient and highly sensitive than the old traditional culture assays[18]. These new approaches are often referred to as “Rapid Methods” of bacterial detection. The techniques typically describe a vast array of tests that may include the miniaturized biochemical assay, the antibody, and nucleic acid based tests, and also the stat of the art biosensor platforms.

1.1.2.1 Miniaturized biochemical assay

It is a widely spreading method used to identify bacteria from food samples. Generally, the miniaturized biochemical kit consists of a deposable device contains 15 – 30 activated substrates full of media specifically formulated to identify specific bacterial groups. Usually, those miniaturized biochemical platforms are similar in format and show 99% accuracy in detection.

Despite that few assays may take a short period of time, the majority of the miniaturized biochemical tests require 18 – 24 hours to complete[19].

1.1.2.2 DNA-based hybridization methods

The nucleic acid-based techniques fundamentally rely on detecting specific DNA or RNA sequences in the genes of the targeted bacteria. This method is carried out by hybridization – an interaction of synthetic oligonucleotide sequences (probes) to their complementary sequences in the genes of the targeted cells[20, 21]. There are many foodborne pathogens that have been targeted using nucleic acid-based assays, which may include *Clostridium botulinum*[22], *Vibrio cholera*[23], *L. monocytogenes*[24], *Staphylococcus aureus*[25], and *Escherichia coli* O15:H7[26]. These microorganisms produce toxins that cause illnesses. Thus, the genes that produce these toxins can be targeted by nucleic acid probes. The recently described nucleic acid techniques for bacterial detection may include the polymerase chain reaction (PCR), real-time/quantitative polymerase chain reaction (qPCR), multiplex polymerase chain reaction (mPCR), nucleic acid sequence-based amplification (NASBA) and the DNA microarray technology.

- **Polymerase chain reaction (PCR):** PCR is one of the most effective techniques used in molecular biology. It is widely used in the detection of bacteria in food and other pharmaceutical products[27]. The approach has enabled the recognition of a single pathogen by targeting the complement DNA sequence of the targeted bacterium. PCR works by amplifying specific nucleotides in a repetitive cycle. At initial, the target double stranded DNA is denaturized into two basic strands by a specific enzyme and at high temperature, while two single stranded synthetic probes, known as primers, present in the solution. These primers, which are complementary to the two single stranded DNA, attach to their complement sequence and extend in the presence of deoxyribonucleotides and thermally stable polymerase enzymes[27]. The PCR amplification is usually visualized at the end using standard gel electrophoresis with a molecular stain[27]. A number of studies have reported PCR for detection of foodborne pathogens including the detection of *L. monocytogenes*[28], *Escherichia coli* O157:H7[29], *Staphylococcus aureus*[30], *Campylobacter jejuni*[31] and *Salmonella* spp[32].
- **Real-time or quantitative PCR (qPCR):** In principle, the qPCR is exactly the same as the simple PCR, except that it does not require gel electrophoresis after DNA hybridization for

product read-out[33]. Instead, the qPCR is able to monitor the PCR product consciously by measuring a fluorescence signal produced by specific dual-labeled probes or intercalating dyes incorporated directly into the external deoxyribonucleotides. The fluorescence intensity is directly proportional to the quantity of the PCR product; thus, it provides a real-time signal read-out[33]. The most common fluoresce probes used in qPCR may include SYBR green, TaqMan probes and molecular beacons. A number of reports have been presented using qPCR for detection of foodborne pathogens that may include the detection of *L. monocytogenes*[34], *Salmonella* spp[35], the detection of tdh-positive *Vibrio parahaemolyticus* in tropical shellfish[36] and also, the detection of *Staphylococcus aureus* strains[37].

- **Multiplexing PCR (mPCR):** The technique offers a faster screening tool than the conventional PCR as it uses multiple primers to amplify multiple gene targets. The design of multiple primers is very crucial for mPCR technology as they must have the same annealing temperature in order to produce successful multi-PCR assays[38]. In addition, the concentrations of the primers need to be carefully adjusted as it may originate doubled primers and test failure[38]. Recently, the technique has been used to detect foodborne strains simultaneously including the detection of *Salmonella typhi* [39], *Staphylococcus aureus*[40], *L. monocytogenes*[41] and *E. coli* O157:H7[42] using pairs of primers that target invasion proteins.
- **Nucleic acid sequence-based amplification (NASBA):** Unlike PCR, which requires thermocycling system, the NASBA technology operates by amplification of nucleic acids under isothermal condition. It also uses RNA instead of DNA[43]. Typically, a single-stranded RNA is converted into complementary DNA or cDNA, using a reverse transcriptase enzyme. The amplified product can be seen at the end of the experiment using gel electrophoresis as it's the case with standard PCR[43]. Nevertheless, a real-time NASBA also exists and uses florescence probes for quantitative real-time monitoring. The method has been used to detect a number of pathogenic strains including, *Salmonella enterica*[44], *Vibrio cholera*[45], *Staphylococcus aureus*[46], *Campylobacter jejuni*[47] and *L. monocytogenes*[48]. Other DNA-based methods such as the loop-mediated isothermal amplification (LAMP) and the DNA microarrays are also available in the field of DNA biotechnology for real-time detection[49], although their scaled application is narrowed to gene expression analysis studies. In overall, the DNA-based technology for detection has produced highly sensitive and specific approaches to detect pathogenic bacteria in food samples. They are very powerful,

quantitative and can reach significant levels of accuracy[18]. On the downside however, they are limited by the cost and the instability. PCRs and advanced PCRs require very well trained personnel's to handle the experiments and carry out their analysis. PCR materials including reagents, deoxyribonucleotides and DNA primers are very expensive for a general routine screening. They are time-consuming and require a preprocessing (sample enrichment before analysis). Due to the inability of these technologies to detect a small number of bacteria, they require an enrichment process before analysis[50, 51]. The enrichment process is applied to support growth of the targeted bacteria while inhibiting others; it leads to bacteria pre-concentration in the samples; i.e., it increases the number of bacteria to a detectable level[51]. The other downside of these technologies is the nucleic acids stability in food, which is very limited.[18, 51]. Therefore, the PCR and the current DNA-based detection may not be suited for nowadays bacterial general screening and day to day food and water analysis.

1.1.2.2 The immune assay-based technology

It is one of the most powerful approaches in diagnosis. The detection is simply based on antigen-antibody interactions, whereby, a specific antibody binds to a specific antigen expressed on the surface membrane of the target[52]. The strength of the binding determines the sensitivity and specificity of the detection. The immune assay may involve using polyclonal antibodies (pAbs) or monoclonal antibodies (mAbs)[53]. The pAbs is produced by more than one B cell and target multiple epitopes on one antigen on the surface of the cell. The mAbs; however, is generated by one cell and target one epitope in the antigen. Thus, the pAbs have higher affinity but lower specificity than the mAbs[53]. The Enzyme-linked immunosorbent assay (ELISA)[54] and the lateral flow immunoassay[55] are the most common approaches to the immune technology in the detection of foodborne bacteria.

ELISA is extensively used method for a variety of diagnostic applications including the detection of harmful bacteria in food and water samples. Perhaps the sandwich ELISA[56] is the main and the most effective form of ELISA assays. The method involves two antibodies; the first is attached to the surface of a microwell plate and the second is conjugated with a specific enzyme[56]. While the first captures the targeted bacteria antigen as the sample is loaded into the wells; the second antibody captures the first antibody-bound cells on the wells as it is introduced after washing the wells from the sample and the unbound cells[56]. The detection is achieved by

adding a colorless substrate, which converts to a colorful product by the antibody-conjugated enzyme (see **Figure 1.1** for further illustration of the basic principle of the sandwich ELISA assay).

A large number of studies have reported the detection of bacteria using ELISA which includes detection of *Salmonella*[57] using the commercially available ELISA kit, the detection of *Clostridium perfringens* α, β[58], and ε toxin, the detection of Staphylococcal enteroxins[59], *botulinum* toxins[60] and also the detection of *E. coli* enterotoxins[61] and others[62]. Recently, high-throughput and automated ELISA methods have made to the market and are available for detection of foodborne pathogens, (VIDAS (BioMerieux) and Assurance EIA (BioControl), for instance.

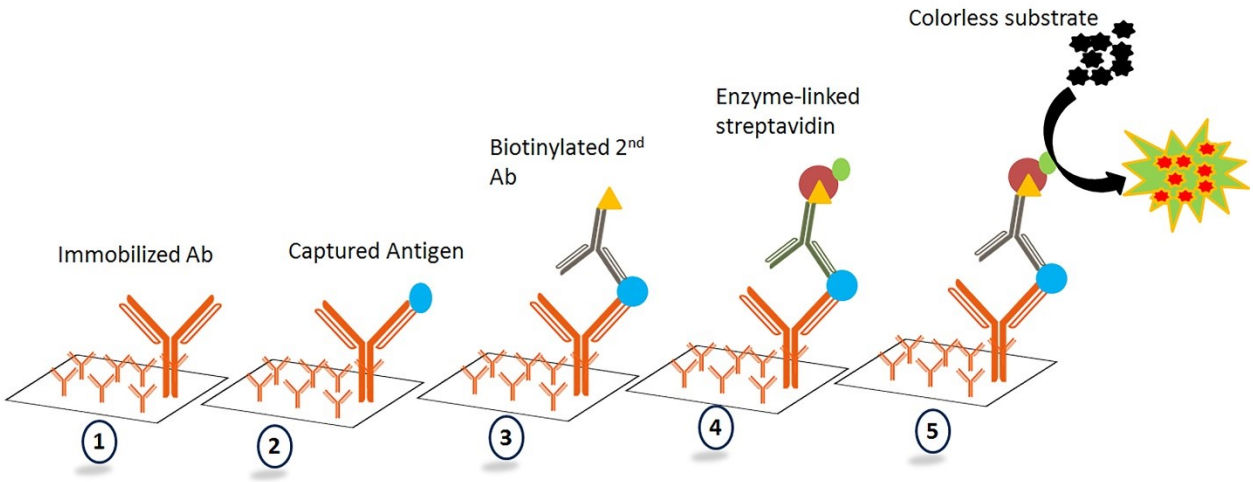

Figure 1-1| The basic principle of the sandwich ELISA assay in detection

Lateral Flow Immunoassay: Distinct from ELISA, this technique is designed to provide rapid and on-site detection. The lateral flow immunoassay may include the dipstick assay and the immune chromatography strips for rapid detection of antigens[55]. Typically in this approach, the sample "fluid" migrates along four sections arranged orderly in a plastic backing. It starts with a sample pad, followed by a conjugate pad, then a nitrocellulose pad and finally an absorbent pad. While the sample is migrating through, it will mix with the conjugate, which can be antibody or antigen coupled to colored particles. At the time the sample passes to the nitrocellulose line, which functionalized with a specific antibody of particular antigens, the colored particles bind to

the immobilized antibodies of the antigens and generate a colorful band that can be visualized[55]. A number of studies have explored the use of lateral flow immunoassay for detection of pathogens such as the detection of *L. monocytogenes*[63], *E. coli*[64] *and Salmonella*[65]; however, the achievable detection limit was always between 10^5 to 10^6 CFU per mL.

Despite the powerful fact of the ELISA and the other immunoassay in detection, they still have some limitations. The ELISA has low sensitivity in comparison to the PCR and advanced PCRs[18]. It may also produce false negative results due to the cross-reactivity with closely related antigens. To achieve higher level of sensitivity and specificity a pretreatment process (sample enrichment) is required for the samples before proceeding with the detection[18]. The experiments require very well trained personnel and very expensive due to the use of fluorescent labelling[18]. Consequently, the use of rapid detection methods such as label-free biosensor platforms could be a valid alternative to detect bacterial contamination.

1.2 DETECTION OF BREAST CANCER

Cancer is a group of diseases that involve abnormal or uncontrolled cell growth[66]. All types of cancer including lung, brain, liver, breast, pancreatic, colon and others share selected characteristic (hallmarks) features, common to generate malignant tumors[67]. Those hallmarks may include, uncontrolled cell proliferation due to abnormal signal transduction, loss of the apoptosis or programmed cell death, tissue invasion and metastasis permitting the spread of cancer and angiogenesis leading to the enhanced blood supply to the tumor[67].

Like most cancer diseases, breast cancer has a long period of growth prior to reaching a stage when the woman experiences symptoms or when the tumor is detected during examinations[66]. In other words, there is a long period, believed to be a “curable” period, prior to the tumor becoming symptomatic and detectable. As breast cancer is diverse (i.e., heterogeneous) disease, it may spread to other parts of the body before the tumor becomes large enough to be detected or yield symptoms. In fact, some types of breast cancer do not spread until the tumor becomes quite large[66]. Thus, there is no way to define with certainty if a patient has or will have a breast cancer, and if he or she does, how aggressive that breast cancer can be[66]. Consequently, there is an immense global need for new techniques that can detect breast cancer disease early before it

spreads and become aggressive or untreatable. If breast cancer is detected when it is very small and undeveloped, the majority of the patients can be cured of the disease[66].

Current Techniques used for breast cancer diagnosis

1.2.1 Medical History and Physical Exams

Patients will be checked by specialists about their medical history and whether they have a past link to breast cancer or not. Normally, doctors will ask about breast diseases, hormone replacement therapies, and any previous radiations to the chest or a family history of breast cancer. The physical exams will include examinations of the breast for any symptoms such as lumps, hardening or thickness in the breast, changes in tissue color in specific areas or suspicious feeling in the texture and size of the tissues and skin muscles surrounding the breast[68]. The doctor will also check the history of the patient for any other symptoms that may indicate cancer spreading such as enlargement of the lymph nodes under the armpit and above the collarbones. If results of the physical exams suggested that a breast cancer might be present, more investigations will take place such as x-ray imaging, testing samples of nipple discharges, carrying out biopsies of suspicious areas and others[68]. The physical symptoms of breast cancer are usually very accurate in diagnosis, but the main issue is that those physical symptoms appear at late stages of the disease and if the symptoms appeared then the chance of curing the disease is low[66].

1.2.2 Mammography

The diagnostic mammography is an x-ray image of the breast using a small dose of radiations[69]. It is used typically to look for any changes the patients' chest may have. Usually, the mammography is taken at two views, i.e., two x-ray images are taken from two different angles of each breast, and that is to get a closer look of any abnormal areas[69, 70].

The mammography is considered the best breast cancer screening tool so far. However, the screening still comes with its own limitations. Sometimes x-ray looks normal even though breast cancer exists, and this is what is known as false negative results. Or in contrary, the results look positive when no cancer exists, and this is known as false positive results. This can be a very serious issue as the patient may expose to unnecessary stress when she or/he has no cancer, or the patient is left without follow-ups when she or/he has the disease[70]. In addition, even though

the mammogram can show breast cancer that is too small to be felt, it's still unable to detect fast growing, aggressive metastatic cells[69, 70].

1.2.3 Breast Ultrasound

The Ultrasound scan, which is also known as Sonography, uses high-frequency sound waves to outline deep structures in the body[71]. The technique is very beneficial to look at some changes on the breast, but it is not as sensitive as the mammography. It may also be useful to examine small changes that can be felt but unseen by the mammogram and can be very helpful to determine whether the breast lump is filled with fluid or it is a solid or semisolid mass. In other words, the ultrasound is very suitable to distinguish between solid and fluid-filled cysts. While the technique is widely available and perhaps less expensive than the mammogram, it shares a number of drawbacks with the mammograms including false positive and false negative results[71].

1.2.4 Magnetic Resonance Imaging (MRI)

The MRI uses very powerful magnetic force and radio frequency waves instead of x-ray[72]. The produced energy from the frequency waves initially absorbed by the body organ or tissue and then released in a form of patterns (cross-sectional images) corresponding to that organ or the tissue structure[73]. A computer then translates the patterned images into very detailed three-dimensional pictures. Unlike the mammograms and the ultrasound, MRI is not routinely used for breast cancer screening; yet, it is applied in certain cases such as finding the primary tumor in breast cancer or finding affected axillary lymph nodes or whether the patient has a Paget disease of the nipple or not[73]. Furthermore, the technique is very useful when tested results from physical examination, mammography or ultrasound are not clear[72]. Despite its advantages as a powerful, highly sensitive and a noninvasive tool of detection, MRI suffers from few limitations as well, which can be pointed as following,

- The test can be very expensive ($1000 - $1500)
- Unable to find all breast cancers
- Cannot distinguish between malignant and benign tumors
- False positive results may occur
- Maybe problematic with implanted metals patients as they will be affected by the strong magnetic field of the MRI[73].

1.2.5 Ductogram (galactogram)

It is an x-ray technique that is mainly used in case of nipple discharges[74]. Typically, a small metal tube is placed in the opening of the nipple to outline the shape of the duct using the x-ray. The technique is very helpful to diagnose the intraductal papillomas, which is a common non-cancerous cause of nipple discharge[74].

1.2.6 Biopsy tests

The biopsy tests examine tissue samples taken from specific parts of the breast for cancer[75]. The test is usually done after mammography or ultrasound exams to confirm the presence of cancer. The tissue areas which look abnormal to the doctor known as lesions are generally prone to biopsy tests[75, 76]. There are particularly two kinds of biopsies and nearly all of them involve using a sharp tool to remove a small amount of tissue.

1.2.7 Blood chemical tests

The blood chemical tests are used to determine the presence of certain chemicals, hormones or cancer biomarkers that may reveal the presence of the disease. The tests can also suggest how well certain organs work and in what stage cancer might be[68].

Other tests such as the blood count, hormones receptor testing, HER2 (human epidermal growth factor receptor 2) testing, chest x-ray, and others may also be performed to confirm the diagnosis and plan for the treatment options[68].

1.2.8 Circulating Tumor Cells (CTCs) as a cancer biomarker

CTCs are cancer cells that shed from primary tumors and move into the peripheral blood circulation or the lymphatic system[77]. Hence, they constitute the seeds for the subsequent growth of other tumors in other parts of the body[78]. The size of CTCs can vary from 6 – 8 microns (small CTCs) to ~ 15 – 20 microns (large CTCs) and they can be found in very low numbers (approximately 1 – 100 cells per mL of whole blood)[78, 79]. This number is significantly low compared to millions of WBCs and billions of RBCs. Recently, molecular and clinical studies have revealed that CTCs may escape into the blood circulation at early stages of tumor development, putting an emphasis on the particular importance of sensitive and selective detection of CTCs in blood[79, 80]. Due to the presence of selective markers on CTCs that are not present in other blood cells, their detection can be achieved with high selectivity[80].

To date, a number of methods have been developed in order to isolate CTCs. However, the only FDA approved approach is the CellSearch system, which is based on labeled antibodies on detection[78]. Other techniques are also under developments. In those techniques, CTCs are usually captured first from the blood by using specific antibodies that can target specific tumor markers. Usually, anti-Epithelial cell adhesion molecule (anti-EpCAM) antibodies are used in this case[78]. Other labeled Abs are then applied to recognize CTCs from the hematopoietic cells. Despite the efficiency of the approach in certain cases, it is limited by the need of sufficient expression of EpCAM antigens on the tumor cell membrane[77], a necessary enrichment step. The issue is that EpCAM is not expressed in some CTCs and down regulated in others[77]. In addition, inabilities of the system to screen sufficient blood samples make it difficult to catch small numbers of CTCs[81, 82]. Therefore, further investigation and research to improve the detection are needed. Our aim in this research is to develop sensitive and accurate tools that can detect CTCs at low concentrations as we believe that CTCs detection can provide valuable information on cancer prognosis, diagnosis and monitoring of tumor sensitivity to anticancer therapy.

1.2.9 Exosomes as a cancer biomarker

Exosomes are small nanovesicles shed from various cells including tumor cells into the peripheral blood circulation[83]. Their size ranges from 40 nm to 120 nm depends on their source of origin[83, 84]. These vesicles have an aqueous, cargo covering core enclosed by a circular membrane bilayer. They carry various proteomic and genetic contents such as signaling proteins, receptors, nucleotides, and carbohydrates, which are identical to that present in their parental cells[85]. Cancer cells secrete significantly more exosomes than noncancerous cells and this has recently been proven with cell lines and in serums of cancer patients, where levels of the exosomes in serums of breast cancer patients was found significantly higher than in healthy donors[83]. In addition, cancer cell-derived exosomes were found to express different proteins or proteins in different expression levels than what is exist in normal cell-derived exosomes. These unique properties make them potential diagnostic markers for cancer detection[86].

Recently, exosomes have become a subject of interest for a wide-range of applications including their substantial use as biomarkers to recognize cancer early before it spreads[84]. Simple blood tests to detect those exosomes in biofluids of cancer patients would be a complement to other approaches to disease diagnosis and treatment monitoring. Unlike CTCs and other cancer

biomarkers, exosomes exist in high quantity in most biofluids of the body including; blood, urine, saliva, breast milk, and amniotic fluids[87, 88]. They are also present in much higher concentrations than CTCs. The quantity of CTCs in the circulation may reach 1 to 100 cells per mL, which is extremely low. On the other hand, a number of circulating exosomes in the plasma may reach 10^9 to 10^{11} vesicles per mL[88]. Not only as biomarkers, are exosomes also considered as interesting stable carriers of genetic materials and cytotoxic medications.

They are a portion of cancer process; they are involved in tumor angiogenesis, metastasis, cells talks, and reproduction[89]. Similar to CTCs, exosomes encompass various nucleic acids and proteins that can be used as targets for selective detection of cancer. Tumor cells were recently found to shed millions of exosomes daily into the blood circulation at earlier and late stages of cancer. These exosomes; thus, hold significant potential as biomarkers to identify cancer earlier and to further study cancer cell properties[89].

Unfortunately, the limitations of the currently available methods for isolating and detecting exosomes have hindered the clinical use of these nanovesicles as biomarkers in cancer to improve patient care[89]. In this thesis, we present the use of a microcantilever array sensor for detecting breast cancer cell exosomes at ultra-low concentrations. We compare the approach to currently available methods and we show a new form of a nanomechanical sandwich assay to achieve an extraordinary limit of detection.

1.3 BIOSENSORS

Biosensors have been in the developmental phases as alternative techniques for rapid detection for few decades and increasingly find applications in different fields including, chemical analysis, drug discovery, blood analysis, and glucose monitoring[90]. They are indeed making inroads into applications in different areas such as microbial detections[1, 91], food/water analysis[92, 93], and medical diagnosis[1]. In principle, biosensors are biochemical-engineered devices that sense specific analytes and measure the physicochemical and biological properties of the surrounding environments[90],[91].Typically they are derived from chemical, biological or biomimetic sensitive elements able to interact or recognize analytes under specific conditions. Since biosensor technology led to simultaneous sensing of chemical and biological entities in a single

experimental set, they have become essential tools in drug discovery, clinical detection, safety, and life science research[1, 90, 95].

A typical biosensor contains three major parts: a bio-recognition element, a transduction component and an output detector[90]. According to the transduction mechanisms, biosensors can be classified into optical, electrochemical, electromechanical sensors, and some others[96]. **Figure 1.2** shows a schematic representation of a number of new advanced biosensor techniques where the cataloging is based on their mode of transduction. Usually, the bio-recognition elements used in the biosensors are peptides, antibodies, proteins/enzymes, nucleotides, and other chemical recognition molecules[91]. Those recognition elements are attached physically or chemically into the interfaces of the sensor, and their interactions with the target-analytes lead to specific responses in the sensor that can be displayed in different user-friendly means. In this thesis we describe two advanced biosensors that have been recently applied to detect bacteria and cancer, namely the electrochemical impedance spectroscopy (electrochemical based sensor)[97, 98] and the microcantilever sensor (electromechanical based sensor)[99, 100].

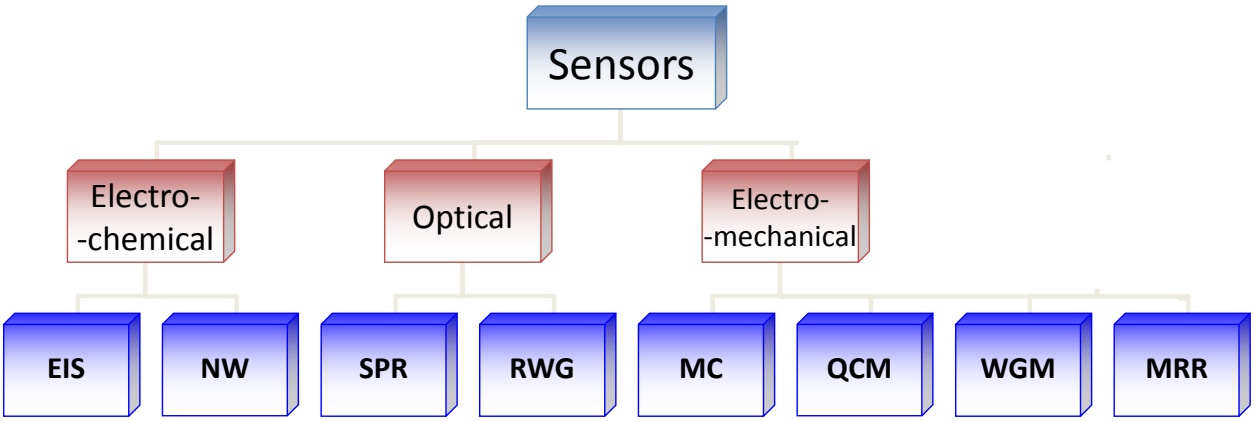

Figure 1-2| Bio and nanotechnology shows the present state-of-the-art biosensors. The classification based on the transduction mechanisms of the techniques; in each class we show examples of the most communal biosensors. EIS: electrochemical impedance spectroscopy; NW: Nanowire; SPR: surface-Plasmon resonance; RWG: resonant waveguide grating; MC: microcantilever; QCM: quartz crystal microbalance; WGM: whispering gallery mode; MRR: microring resonator.

1.3.1 Electrochemical impedance spectroscopy (EIS)

The electrochemical impedance spectroscopy is a relatively new and powerful technique that can characterize many of electrical properties of analytes and their interactions with electronically conducting electrodes[101]. The device can be very useful in different fields including diagnostic purposes by characterizing changes at the electrodes interface under specific system parameters. The technique measures the impedance of a system over a range of frequencies, and thus the frequency of the system, including the energy storage and dissipation properties, is revealed[101].

Principle of EIS:

The fundamental principle of EIS relies primarily on Ohms law, with the omission that impedance does not obey certain simplifying properties of the resistance[101]. Impedance measures the resistance and capacitance developed in solution through conductive or semiconductive electrodes and any deposition on these electrodes, or changes in the surroundings or damages of the electrodes would reflect on the impedance reading signals. Ohm's law defines the resistance in terms of the ratio between voltage €, and current (I) (Equation 1).

$$R = E/I \qquad (1)$$

The EIS is usually measured by applying an alternating current (AC) potential to an electrochemical cell and then measuring the current through the cell. Assume that we apply a sinusoidal potential excitation. The response to this potential is an AC current signal. This current signal can be analyzed as a sum of sinusoidal functions (a Fourier series)[101].

In our impedance spectroscopy system, integrated gold microelectrodes in an array format are functionalized with specific ligands (biorecognition molecules that may include antibodies or peptide targeting) that capture specific molecular analytes[97, 98] (**Figure 1.3**). Interaction of the immobilized ligands with their target analytes generates changes in the impedance reading signal. In other words, it changes the electrical double layer capacitance in the vicinity of the gold electrodes, and thus, changes in the impedance signal that is detected in real time. Binding of the analytes into the coated ligands produce impedance changes over substantial frequency ranges, which are regularly set in each experiment. Since the detection is performed while binding occurs, no molecular labeling is required. Although impedance has been well

established for decades, it is still primarily confined to laboratory research due to the lack of the solid integrated platform that can enable the development of commercial bio-affinity assay sensors for broad market use. Such platforms require multiple stage integration, including a microarray of transducers and supporting circuitry[102, 103]. Other limitations of the technology would be the nonspecific signal from the electrodes that could be easily read as specific interactions. Therefore, it's necessary to run parallel reference control experiments to eliminate any false-positive results[104].

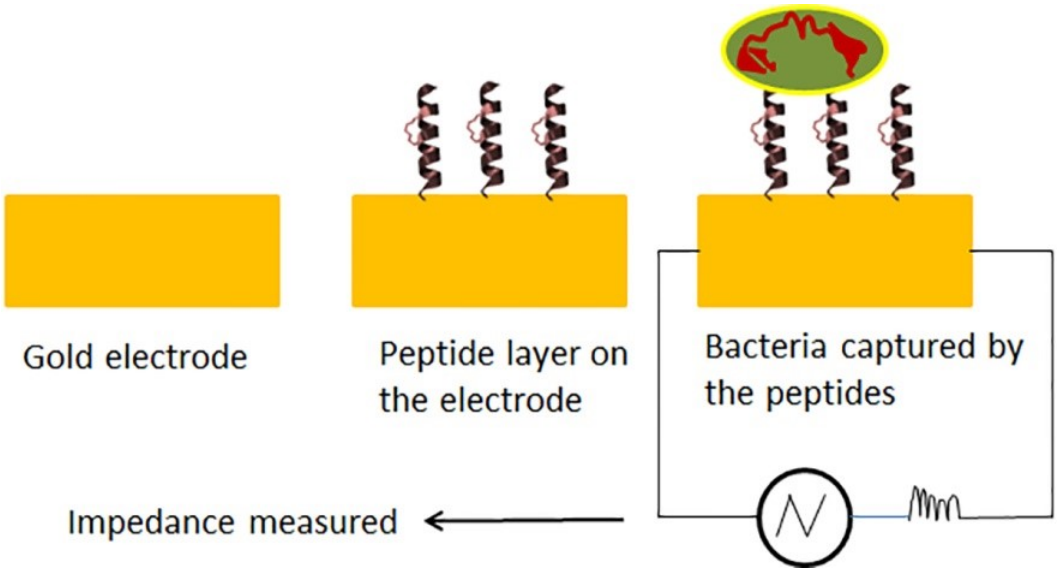

Figure 1-3| The basic principle of impedance detection in microelectrodes gold interface. On electrode interface, ligands such as bacteria targeting peptides can be immobilized prior to analysis. Insertion of the target analyte such as bacteria will lead to bacteria-peptide interaction of the electrode interface. Impedance can then read. Analyte-ligands interactions give a clear change in impedance that can be read instantaneously. At a given frequency, the interaction can be measured as a function of time.

The main advantages of using EIS biosensors is the platform flexibility, simplicity and the cost associated with it, which is very cheap and label-free in comparison to other biosensors[103, 105, 106]. In addition, the impedance offers a high performance, a new promising platform that will allow rapid access to a new biotech market, due to its high sensitivity, low-cost paradigm, miniature size, ease of assembly, and flexibility for multiplexed lab-on-a-chip device. Areas of a high

market potential of impedance may include research and development (R&D), food safety and water analysis, environmental monitoring, medical diagnostics, and drug development[106].

Impedance for detection of bacteria and cancer

Numerous studies on impedance spectroscopy have been reported for detection of foodborne pathogens and cancer biomarkers[98, 102, 103, 107-109]. A notable example would be the use of the antimicrobial peptide (megainin I) on microcapacitive electrode arrays for sensitive and selective detection of *E. coli*[110]. The study revealed a detection limit of approximately 1 bacterium per µL, which is a clinically useful detection range. The hybrid peptide microcapacitive device demonstrated also Gram-selective detection and interbacterial strain differentiation while maintaining recognition capabilities toward pathogenic strains of *E. coli* and *Salmonella*. In our study (presented in chapter 1)[97], we also demonstrate the selective and sensitive detection of *L. monocytogenes* using antimicrobial peptides from class IIa bacteriocins on impedance microelectrode arrays. These two studies on impedance and others have demonstrated the capability of the relatively simple impedance-based transduction architecture to directly detect bacteria, suggesting a promising alternative to traditional techniques of bacterial detection.

The impedance sensor has also been utilized for detection of cancer by direct quantification of CTCs in blood[107, 108]. The device offered a highly sensitive noninvasive approach of detection. It has been reported that cells size and properties can be characterized using impedance spectroscopy. As impedance devices consist of small microfluidic channels with microelectrodes in it from the bottom or the surrounding walls, they can measure the electrical properties of the inertial cells in suspension as they come in contact with the electrodes. *Nwankire* et al., proposed a microfluidic EIS device for automated quantification of ovarian cancer cells from whole blood samples[111]. In another study, *Kang* et Al., made an impedance based microfluidic sensor with interdigitated electrodes that cover the bottom of the microfluidic channels[112]. When cells pass through the fluidic channel it engages directly with the electrodes; thus, generate impedance signals. When the two studies were performed with normal human breast cells (MCF-10A) and human breast cancer cells (MCF-7), results showed a difference in the real part of the impedance and the phase response[112]. *Holmes* et al., had proven this concept and showed that lymphocytes, monocytes, and neutrophils can be identified and counted using this EIS approach[113]. A recent study by Arya *et al*., demonstrated the selective detection of breast cancer

cells using antibody-coated impedance spectroscopy[114]. In their study, an anti-EpCAM antibody was immobilized on the impedance microelectrodes and the capture of the cancer cells was monitored directly by the EIS sensor. An average modification of 2.2 10^7 Ω in the impedance value was noticed once the cell is trapped on the electrode surface. In this thesis, we do also report the use of impedance in the detection of breast cancer circulating exosomes using peptide targeting ligands instead of antibodies (chapter 6) and that is in order to enhance sensitivity, selectivity and generate a long stable cancer detection device. The study showed specific impedance signature towards cancer exosomes at low concentrations in human serum, and with a discrepancy between cancer and normal cell-derived exosomes.

The development of electrochemical impedance and the new microfabrication techniques would allow a single cell analysis on microfluidic devices, conferring new opportunities for cancer detection and cell-to microvesicles characterization[115].

One of the major challenges in impedance biosensor assay developments is associated with the selectivity and the non-specific response of the impedance. Nonspecific binding of the targets to the non-complementary ligands and the sensor surface is a problem in electrical sensors[116]. This technical problem is prominent for impedimetric detection in real-time as the assay workflow does not include washing steps. Therefore, both high and low-affinity complexes may remain on the transducer surface altering the impedance response, with subsequent interpretation as binding signals. In this thesis, one of our goals is to develop an impedance assay that can clearly distinguish between high-affinity specific binding and non-specific (or less specific binding) events and apply that to selectively detect bacteria and/or cancer.

1.3.2 Microcantilever biosensor

The current advances in micro and nanofabrication technologies allow a wide range of new technologies, including the development of mechanical devices with nano-sized touching portions. In the early 1980s, microcantilever was introduced as a probe in atomic force microscopy (AFM) for surface topography explorations and characterizations[117]. Shortly afterward it was recognized as a very sensitive tool for detection of temperature and humidity variations[118]. In the mid of 1990s, abilities of functionalized cantilevers with molecular probes in

showing selective responses to target biochemical compounds have opened a new field of biosensor technology based on electromechanical properties and surfaces structures[119]. Despite the reality of its relative new introduction, cantilever detection methodology has attracted significant attention as an approach to label-free sensing device in addition to its extreme sensitivity in diagnosis[99]. Recent studies sensing cantilevers to biomolecules in liquid at picogram to femtogram levels and sensitivities of nano to femtomolars[99]. It has been used for detection of numerous of chemical and biological entities including nucleotides[120, 122], proteins[123], microbes[124] and wide range of toxic chemicals and heavy metals[125]. The advantages of using ultra-small sizes of cantilevers allow the sensor to exhibit very fast responses to the evolving biological and chemical deviations on timescales of micro and milliseconds[126].

Cantilever Principle and Modes of Operation

Generally, cantilevers are micro to nano-sized beams produced from silicon materials, gold and sometimes certain polymer substances are also involved in the fabrications[127]. Typically in most biochemical analysis and diagnostics, cantilevers made from silicon and coated with a thin layer of bare gold (20 – 100 nm). The dimensions can vary from one design to another; however, the emblematic dimensions of microcantilever are nearly 50 μm (wide) and 350 μm (long) by 1 μm (thickness). The nanoscale cantilevers; on the other hand, are usually dimensioned with 600 – 950 nm (wide), 300 – 650 μm (long) and 50 – 100 nm (thickness). **Figure 1.4** illustrates the basic principle of cantilever sensor technique basing on beam deflection[128].

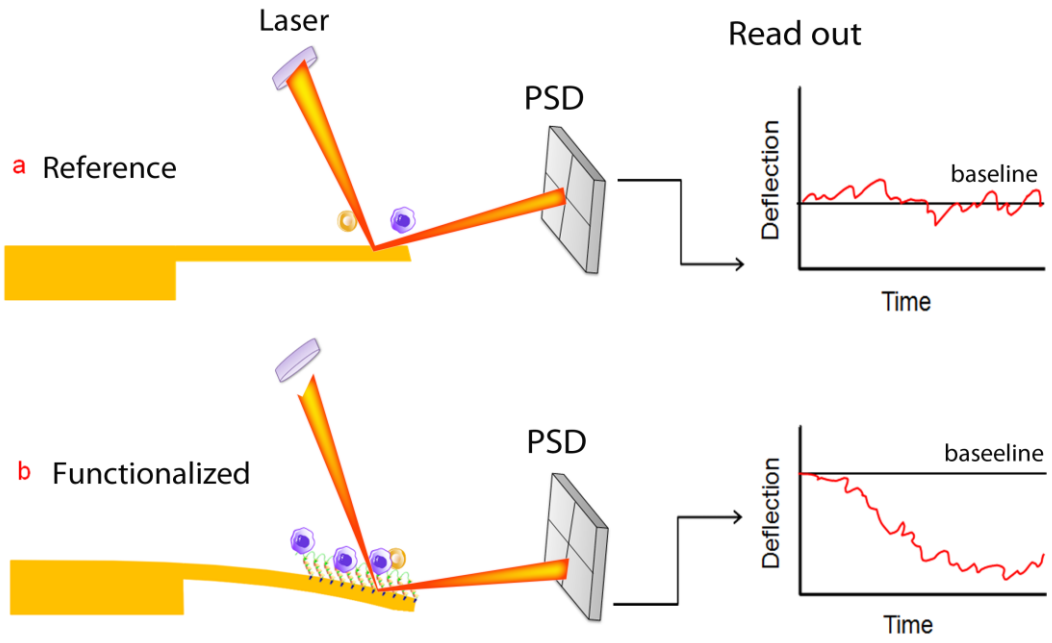

Figure 1-4| Basic principle of cantilever technique; when samples contain target analyte flow through the cantilevers, responses will be obtained based on interaction of the immobilized ligands on the cantilever with the introduced samples. Cantilever response is recorded in form of deflection by a position sensitive detector (PSD). a – no deflection from a reference cantilever (no binding to the target analyte); b – cantilever deflection as a result of the ligand-analyte interaction.

For most biochemical studies, cantilevers are functionalized with specific ligand molecules at which the target analytes are binding[3, 129-131]. During the detection the ligands are selectively capture the target molecules from the surrounding medium causing bending of the cantilevers, and/or resonance frequency changes depending on the mode of the cantilever's operation. In other words, the detection deeply relies on the bio-recognition between the predesigned detective agents (ligands) and the unknown sample molecules (targets).

Modes of Operation

Static mode of operation (surface stress mode): Micro and nano-cantilevers are applicable to operate by a static deformation mode, which means that cantilever beam bends as a result of increasing or decreasing of the surface stress generated by analyte-ligand interactions on the

surface of the sensor. While an increase in the surface stress (compressive stress) leads to downward bending of the cantilever, the decrease in the surface stress (tensile stress) leads to upward bending of the cantilever[127] **(Figure 1.5**.) As the cantilever remains immovable after attaining an equilibrium state, the operational mode is therefore, called the static deformation mode of operation. Basically, specific adsorption of the molecules into a one side of the cantilever results in a decrease in the surface free energy. From the change in the surface free energy of one surface and not the other as it's completely inert, different surface stress is generated between the two surfaces of the cantilever. The difference in surface stress between the functionalized surface and the passive (non-functionalized surface) leads to cantilever deflection (bending) and the value of this bending can be estimated according to Stoney's formula[128]. [2]

- $\Delta\sigma = \left[\frac{E\Delta h}{4(1-\nu)}\right] \times \left(\frac{t}{L}\right) 2$ [2]

Where Δσ is the change in surface stress (or surface-energy) due to the molecular adsorption, E is the elastic modules of the cantilever; *v* is the poisson ratio while L and t are the length and thickness of the cantilever, respectively. The Young's modulus is an indicator of the elasticity of the material and a lower value of the Young modulus brings about a higher sensitivity.

Dynamic Mode of operation (resonance mode): The basic principle of the dynamic mode of operation is mostly relies on cantilever's vibration at a resonance frequency. **Figure 1.6**; shows adsorption induced cantilever vibration with at a specific resonance frequency; i.e. the resonance frequency changes by analyte adsorption to the surface of the cantilever[127, 128]. The fundamental resonance frequency f_0 of a single harmonic oscillating cantilever is expressed as [3]:

- $f_0 = \frac{1}{2\pi}\sqrt{\frac{k}{nm}}$ [3]

where k is the spring constant of the lever, *n* is a geometrical parameter for the fundamental vibration of the cantilever beam and m is the effect of mass of the cantilever.

- **Quality factor (Q):** the Q factor can be useful in determining the reliability and accuracy of

the resonance frequency measurements as it determines the slope of the amplitude and phase curves near the resonance[127]. The Q factor is defined by equation [4].

- $Q = \frac{2\pi Ws}{Wd}$ [4]

where is Ws is the stored vibrational energy and Wd is the lost of energy per vibrational cycle. The Q factor therefore, can be expressed in a form:

- $Q = \sqrt{3\,\frac{f_0}{\Delta f}}$ [5]

Where the Δf is the resonant peak frequency full-width at half maximum.

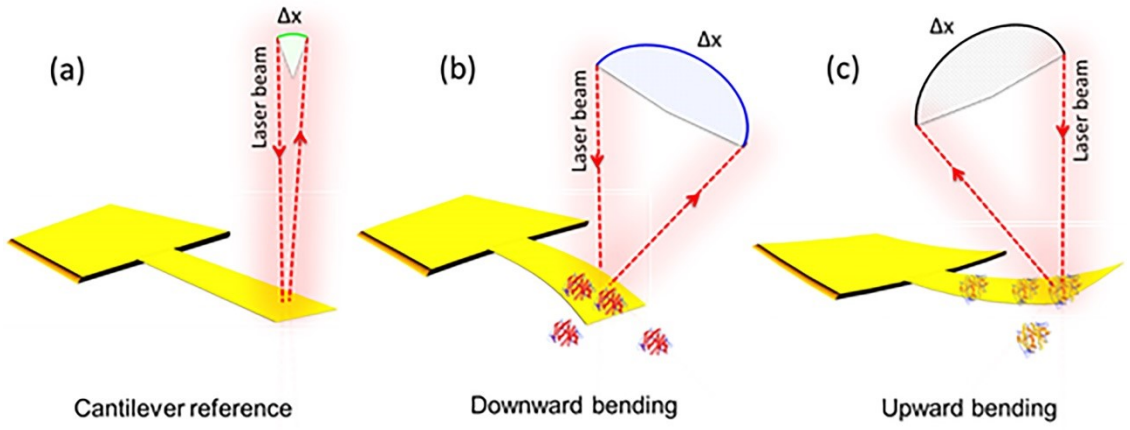

Figure 1-5| Cantilever transduction principle, the static deformation mode of operation. (a) Cantilever reference where is no clear shift on the cantilever beam (no bending); the asymmetric molecular binding to the cantilever surfaces could lead to increase the surface stress, compressive stress (b) downward bending, or decrease on the surface stress, tensile stress (c) upward bending.

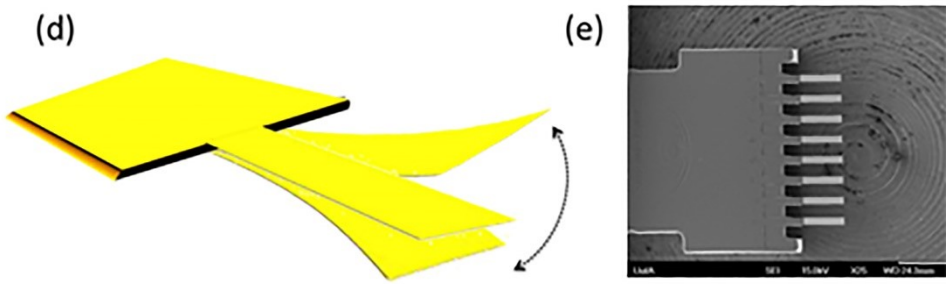

Figure 1-6| (d) A cartoon shows cantilever dynamic mode of operation, where vibration cause oscillation, the resonance mode. The dynamic mode detecting mass changes by measuring the resonance frequency changes (e) a graphic scanning of eight cantilevers array.

Bimetallic mode of operation (Thermal mode): In the bimetallic mode of operation, the cantilevers undergo a static deflection in response to heat changes because of different coefficients of thermal expansion between the metallic thin film and the underlying coating layer[128, 132]. This mode of operation is also referred to as a heat mode of operation because it causes cantilever bending as a result of differing thermal expansion coefficients of the sensor substrate and cantilever materials. The mode is widely used for temperature related applications such as thermal actuators[133]. The heat changes on the surface of the cantilever can be driven by external influences such as changing temperature due to catalytic and reactions of analyte-receptor and/or other chemicals. Materials attachment to the apex of the cantilever could also cause heat changing and cantilever bending. The sensitivity of the cantilever heating mode is orders of magnitude higher than that of the conventional calorimetric methods.

Cantilever Surface Functionalization

Attachment of chemical or/ biological detectives such as proteins, DNA, cells, and other semiselective biochemical elements have drastically enhanced the strength of several biosensors including cantilevers in recognition applications[128, 133]. The stimulating advantages of surface functionalization are the ability to detect specific targets in an unknown mixture as well as addressing different particles using multiplexed array at the same time. It is a fact that the cantilever itself does not have the specific adherence to specific molecules; in other words, it does not have any inherited chemical /or biological selectivity. However, coating the cantilever

surface with specific ligands (recognition agents) – molecules that have specific and strong interactions to particular biomolecules – leads to specific responses from the cantilever that convey the specificity of the interactions. Thus, the vital part of the specific sensing is attaching biochemical detective elements to the surface of the cantilever prior any applications.

There are many approaches that can be used to functionalize the cantilever with specific recognition molecules based on the final applications of the sensor. On silicon cantilevers, for instance, the functionalization can be performed by so-called a silicon-chemistry, using polylysine, aminosilane, epoxysilane or nitrocellulose in case of the silicon chips/silica glass etc.[129, 134]. On the gold-coated cantilevers, the functionalization can be implemented easily using thiol-chemistry, by taking advantages of the strong covalent interaction between the Au and the thiol group of the ligand molecules[135]. The challenging in these approaches is adopting a healthy reaction chemistry that can assure a well-mannered condition that maintains the required chemical selectivity, stability and complete bioactivity of the attached molecules. The immobilization mechanism is always determined by both the chemical nature of the molecular probes and its reactive functional groups. In the case of operating the cantilever sensor on a surface stress mode, which requires binding of the target analyte to only one side of the cantilevers in order to produce a stress and consistence cantilever deflection, the functionalization must be done only on one surface of the cantilever, not both. Failure to do so, a stress from the opposite surface will cancel the first and cantilever will fail to bend. To avoid that issue from occurrence, the inactive surface of the cantilever should be passivated by coating it with a material that does not interact with the analyte or other solution components. Typically in cantilevers, one surface is passivated by salinization or grafting with inert polymer substances such as polyethylene glycol[128].

Functionalizing one separate cantilever has not been that thought provoking, as it is the case with the cantilever array. The process is simply performed by dipping the tip of the cantilever in the solution of the functionalized molecule. Although the procedure is simple and easy, it is not applicable to individually functionalize a cantilever array (8 cantilevers in an array, for example, **Figure 1.6b-e**). The cantilever array could have four to eight cantilevers in the same track and it has been a very useful strategy for competitive studies by making one or two of the cantilevers as internal nonspecific references[128]. The challenge in here is how to functionalize such an array

individually without affecting each other's. Few methods have been used such as evaporating the Au selectively and using the spray-coating or pipetted droplets of a polymer solution to cantilevers[136]. These methods, however, turned to be inconvenient, lack the reliability and difficult to produce. Lately, other techniques were proposed to locally functionalize microscale cantilevers such as arrays of dimensional matched separate micro capillaries[137] and ink-jet printing[138]. These approaches are very effect but suffer from challenges in controlling evaporation and drying of the samples[137]. Furthermore, these methodologies are neither likely to produce submicron patterns, nor to be scaled up to create large and multiplexed arrays. In addition to those techniques, there are other approaches that have been used recently such as the photolithographic approach[139], liquid drop dispensing tools[140] and the micro contact printing[141].

Microcantilever in bacteria and cancer detection

Micro and nano-cantilever biosensors are extremely vital and swiftly progressing in fields of chemistry and biomedical sciences. In the recent years, cantilever biosensors have broadened their applications to include every sense of detection and diagnostics.

As biological sensing devices, microcantilever applications have included studying antigen-antibody interactions[142], DNA hybridizations[143], detection of superbugs such as pathogenic bacteria[144], fungus and viruses[145], and most recently, in the monitoring and detection of cancer biomarkers and gene transmutations[120, 146]. Observations that multiple DNA hybridizations and antigen–antibody interactions can collectively produce a nanomechanical motion in a cantilever make the platform suitable for developing sensors based on DNA. Several studies have shown the applicability of using cantilever sensors to detect DNA hybridizations and mismatching. The detection is simply based on the interaction of immobilized DNA-probes (oligonucleotides) with complementary DNA-strands in solutions. The process also requires reference cantilevers functionalized with negative oligonucleotides that do not match the target DNA-strands. It has been demonstrated that the cantilever biosensors offer interesting possibilities for label-free detection of biomolecules such as proteins and enzymes and carbohydrates based on nanomechanical motion[125]. Recent advances in cantilever technology developments have shown the ability of microcantilevers to detect a number of pathogenic microorganisms and cancer biomarkers. A large number of published works show the capability of cantilever technologies to detect bacterial cells at very low concentrations in different samples[98, 132, 147-149]. For example, a

report by *Mutharasan* et al., showed the capability of a piezoelectrically excited millimeter cantilever (PEMC) functionalized with a virulent gene stx2 to detect *E. coli* O157:H7 (EC) in both buffer and proteinous sample at very low concentrations (~700 cell per mL) and without any sample pre-treatment steps[148]. Recently *Huber F* et al., showed a gold standard assay for detecting the BRAF gene mutation using an array of microcantilever sensors[150]. The BRAF gene mutation is a characteristic indication of malignant melanoma, the deadliest form of skin cancer. This study indicated the applicability of cantilevers assays to distinguish between mutated-cell lines and wild-type cell lines and gives hope for the system to be used for real-time cancer detection.

In this thesis, I applied the microcantilever array sensor in combination with AMPs and antibodies to detect *L. monocytogenes* and identify bacterial resistance (chapter 3). We also utilized the sensor to detect circulating tumor cells and breast cancer cell-derived exosomes (chapter 4 and 5).

1.4 BIORECOGNITION MOLECULES IN BIOSENSORS

Molecular biorecognition is an essential part in biosensor design. The biosensor can be defined as seen in **Figure 1.7**, as an analytical device incorporating a biological sensitive receptor with a physiochemical transducer[96]. The biorecognition molecules in biosensors can be available naturally from biological bodies such as enzymes and antibodies or it can be made synthetically in laboratories. The currently used biorecognition elements in biosensors include enzymes, antibodies, nucleic acids, aptamers, peptides and other synthetic chemicals[91, 128].

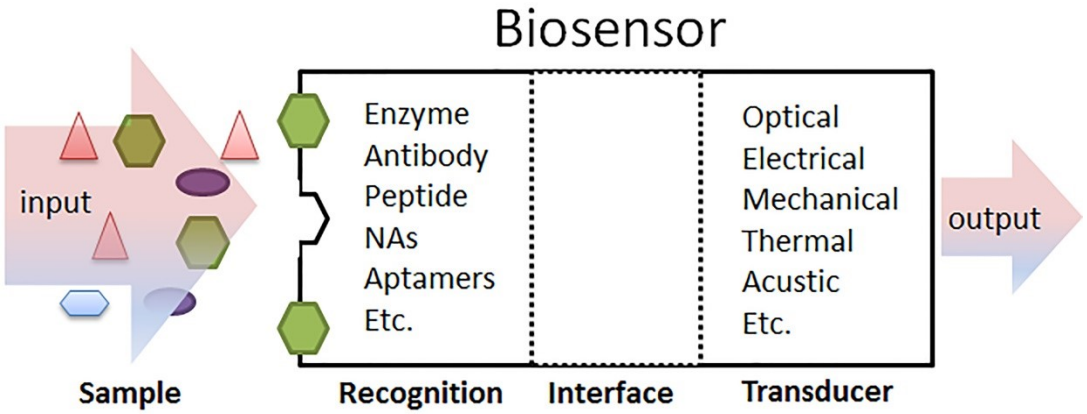

Figure 1-7| Basic biosensor components may include, input, a recognition element, a transducer, and an output reader**.**

1.4.1 Enzyme-based biorecognition

The use of enzymes in biosensors was the basis of biosensors[151]. Enzymes are very attractive molecules as biorecognition elements in biosensor applications due to the variety of reaction products arising from the catalytic route of enzymes, which include protons, electrons, light, and heat[151]. Today, perhaps the most spread biosensor in the world is the glucose sensor, which is based on enzyme biorecognition[152]. The sensor is used to measure the concentration of the glucose in the blood especially for routine screening in diabetic patients. There are few enzymes which are used in glucose detectors, many of which require cofactors. The most stable enzyme; however, is the glucose oxidase, which also does not require cofactors. The enzyme was used to develop first biosensors in 1962 by *Clark* and *Lyo*n[152].

In microbial detection, the most common technique, based on enzyme recognition, used in bacterial detection is bioluminescence[153]. This method takes the advantage of the ability of certain enzymes to emit photons as a byproduct of their reactions, a phenomenon known as bioluminescence. The system has been used to detect a wide range of microorganisms and foodborne pathogens such as *L. monocytogenes*, *Salmonella* spp. and others. Despite the strength of the enzyme based systems, generally, the affinity-based sensors are preferred over enzymatic biosensors for detection of bacteria, due to their enhanced selectivity and specificity and lack of extra reagents required. In addition, some drawbacks of the current enzyme-based biosensors

such as poor stability, critical operational conditions, pH variations and temperature fluctuations limit their broader utility for real-time applications[153].

1.4.2 Antibody-based biorecognition

The majority of the currently available rapid detection methods use antibodies (mAbs or pAbs) for recognition, identification, and quantitation of the target analytes[154]. The antibodies are exclusively used for detection purposes and their popularity has significantly enhanced since the discovery of mAbs in 1999[155]. The principle is based on the biomolecular interaction of the sensor interface (antigen-antibody interactions), which then detected and transformed into a digital signal interpreted by a computer aided readout. The strength of the signal usually depends on the affinity of the antibody to the target antigens[154].

The antibody-based sensors have been extensively used in the detection of pathogenic bacteria. They have been employed to detect a wide variety of bacterial strains, including *Listeria, Salmonella, E. coli* and many others[156, 157]. The main advantage of antibody-based sensor biorecognition is that the immunogen or the targeted antigens does not need to be purified prior to detection. A variety of signal transduction methods has also been utilized including, optical, electrochemical, mechanical and others. The most useful signal generation was based on enzyme fluorescence with a catalytic turnover resulting in amplification of the output signals, thus increasing the sensitivity of the assays[157].

Despite the fact that antibodies are the most successful binders, they still exhibit limitations associated to their biophysical properties such as poor solubility, low thermal stability, and the cross-linkage that may cause false positive or false negative results. The other issue which is associated with antibodies in biosensors is that due to their length it can be very hard to immobilize them on the sensor substrates. Their immobilization may cause aggregation and retention in their binding affinities to the target antigens[158].

1.4.3 Aptamers-based biorecognition

Nucleic acids are very small molecules, well known to carry and pass genetic information and possess remarkable structural and functional characteristics[159]. Recently, nucleic acids (DNA and RNA) have emerged as very powerful and versatile biomolecular recognition elements in biosensors. They have found a key role in the biological detection and analytical monitoring.

Nucleic acid aptamers are nucleic acid species that are engineered through repeated cycle of in vitro selection procedure identified as SELEX (systematic evolution of ligands by exponential enrichment) in order to bind specifically to various molecular targets[159]. Aptamers can be designed against various targets such as small molecules, proteins, nucleic acids, and even cells, tissues and organisms.

A variety of aptamers based biosensors has been designed and reported for detection of a large number of biomolecules including cancer and pathogenic bacteria. The main advantages of using aptamers in biosensors are that they can provide strong binding selectivity to low molecular weight substrates or to relatively big macromolecules. The binding affinity of aptamers towards their targets is very strong and the binding constant can reach picomolar ranges compared to what is seen with antibodies[159]. The high specificity of base pairing properties of nucleic acid enables for selective replication and transcription processes in the biosensor. Therefore, aptamers based biorecognition represent a novelty in analytical biosensors and there are great expectations for their promising performance as an alternative to conventional analytical tools. The main disadvantages of using aptamers in biosensor are the cost, instability at harsh environmental conditions and also the need for professional trainees to handle the preparation and sample preprocessing[159].

1.4.4 Peptide-based biorecognition

Peptides are the building unit of the proteins; they consist of a few number of amino acids (between 2 – 50 residues) linked together through peptide bonds. Several recent studies have explored the application of short ligand peptides in biosensors for detection of various biomolecules including bacteria and cancer[131, 160-162]. The principle idea is based on the ability of the peptide to bind selectivity to specific targets on the biosensor substrate. Typically, the biorecognition molecules (peptides) are immobilized on a solid substrate in such a way that a specific signal is generated from the sensor when the peptide selectively interact, or bind to the targeted antigens (i.e., the detection relies on the bio-recognition between the predesigned peptide and the unknown target on the sample[110, 163].

There are a number of bio-detection approaches based on peptides as these biorecognition elements have been successfully used for detection of bacteria and/or cancer. A number of analytical techniques have also utilized peptides in detection including fluorescent techniques,

surface-enhanced Raman spectroscopy, microcantilever[164], surface plasmon resonance, quartz crystal microbalance[165] (QCM), impedance spectroscopy[166] and others[167].

In contrast to other biorecognition molecules, peptide ligands may hold a number of advantages as delineated below:

- Peptides have remarkable ability to form various folding and tertiary structures that make them valuable molecules to interact with numerous receptors. They may share this characteristic feature with antibodies as well[168].
- They hold unique selective binding properties such as that existent in the antimicrobial peptides (AMPs)[168] and cancer targeting peptides.
- Peptides can be produced naturally from various sources including bacteria, plants, insects and even human and animals. They can also be synthesized in small laboratories using various techniques such as the solid phase peptide synthesis (SPPS) or the liquid phase peptide synthesis[169].
- Peptides are inexpensive to produce and can be produced quickly in high quantities
- Perhaps the main advantage of peptides as biorecognition elements in biosensors is their stability at various experimental conditions. Conformationally constrained peptides such as cyclic peptides or lasso peptides can be designed thermally stable at harsh chemical conditions[169].

In this dissertation, I do highlight the prospect of using peptides as biorecognition molecules in biosensors. I also discuss their advantages, disadvantages and provide experimental evidence of various peptide probes as biorecognition elements for cancer and bacteria detection.

1.4.5 Other biorecognition elements

There are more biorecognition elements used in biosensors for varieties of other diagnostic applications and those may include, carbohydrates[170], lecitin[171], the molecular imprint based recognition[172] and others. We limit our discussion in this dissertation to the aforementioned biorecognition elements in biosensors due to the complexity of the field and due to the existence of extensive reviews on biosensor recognition elements.

1.5 THESIS PROPOSAL

1.5.1 Rational and Hypothesis

In this thesis, we emphasize on the development of rapid detection tools for detection of bacteria and/or cancer; therefore, we have divided the dissertation into two parts. The first part focuses on the detection of pathogenic foodborne bacteria and the second section centers on the early detection of breast cancer using noninvasive biosensors.

The rapid and early detection of bacteria play vital role when it comes to food safety, drinking water, combating infectious diseases and preventing bioterrorism. Today, there is an essential need for the development of quick and easy approaches to detect pathogenic bacteria in food, water, and other pharmaceutical ingredients. In addition, tools that can detect bacterial resistance in the first place would be crucially important to prevent the spreading of resistant bacterial strains and enhance the development of new antibiotics. As effective testing tools in diagnostic analysis require obeying certain criteria and rules, the sensitivity, selectivity and the time functionality required for real-time analysis remain the main limitations of the current detection approaches. Henceforth, inexpensive sensors for the rapid detection of bacteria and the determination of their susceptibility to antibiotics are urgently needed in order to combat the emergence of drug-resistant bacterial strains.

In cancer research, the detection of breast cancer at early stages has and continues to be a hassle and technically challenging task due to the nature of the disease. In the early-stages of breast cancer, CTCs and cancer-derived exosomes are present in the bloodstream at low concentrations. Their existences carry such valuable information about primary tumors and serve as potential biomarkers for disease diagnosis and progression. It is now evident that early detection of CTCs or cancer cell-derived exosomes would be a promising new pinpointing field for identifying the disease, estimating the metastatic regressions and monitoring risk of progressions in patients with cancer. The currently available methods for detecting CTCs or cancer exosomes require improvement as the majority of those techniques lack the sensitivity, specificity and the time-functionality needed for rapid analysis.

The availability of robust and portable biosensing devices to detect CTCs or cancer-derived exosomes would be of a great importance. Biosensors with a multiplexing detection system such as that exist in impedance spectroscopy or the microcantilever array sensors will offer great advantages over other techniques and will overcome some limitations of the currently available diagnostic methods. Therefore, **we hypothesize** in this dissertation that, integration of biosensor technologies such as microcantilever array sensors and electrochemical impedance spectroscopy with biomaterial recognition elements such as antibodies or targeting peptides could offer excellent diagnostic tools for real-time detection of bacteria, CTCs and circulating cancer cell-derived exosomes.

We also emphasize on the feasibility of using small peptide molecules as biorecognition elements in biosensor platforms. Their distinguishing properties as antimicrobials and cancer targeting could make them particularly interesting candidates as biomolecular recognitions for the detection of bacteria and cancer, respectively. Here, we validate the hypothesis of using peptides in biosensing platforms for specific detection of *L. monocytogenes* (Chapter 2 and 3) and also in detection of breast circulating tumor cells (Chapter 4) or exosomes (Chapter 6).

1.5.2 Objectives

The main aim of this research is to address preliminary studies towards developing real-time, sensitive, and reliable biosensors for detection of bacteria or cancer using ligands-based biosensor platforms such as the impedance spectroscopy and/or microcantilever array sensors.

1.5.2 Specific objectives

- **Chapter 2.** Explores the possibility of using antimicrobial peptides from class IIa bacteriocins as targeting ligands or bio-detection molecules in impedance spectroscopy for detection of foodborne *L. monocytogenes*. The ultimate goal was to establish a peptide-based electrochemical impedance sensor for real-time detection of foodborne bacteria in food, water, and other pharmaceutical products.
- **Chapter 3.** I aimed to overcome some limitations of conventional cantilever sensors and enhance the detection sensitivity that could not be reached by impedance technology and other electrochemical sensors. We targeted *L. monocytogenes* as a foodborne pathogen in

order to establish a highly sensitive platform for detecting *Listeria* in water and food samples. Our major goal was to achieve a single cell detection limit in small confined volume. In this chapter, we also intended to explore the feasibility of using the designed bimaterial microfluidic cantilever (BMC) for real-time sensing of multidrug resistant bacteria and measure bacterial response to antibiotics through monitoring their metabolic cycle.

- The objective of **Chapter 4** was to develop a peptide-based microcantilever array sensor for the detection of CTCs in a buffer and human blood samples as a target for early diagnosis of breast cancer. Short ligands cancer targeting peptides were employed to develop a cost-effective peptide-based biosensing approach for sensitive and selective detection of CTCs.
- The goal of **Chapter 5** was to explore the possibility of using breast cancer cell-derived exosomes as a new biomarker for early detection of breast cancer. We aimed to develop a rapid method to separate and differentiate cancer exosomes from noncancerous exosomes using a microcantilever array sensor. We also aimed to the discover the expression affinity of some membrane-bound receptors including CD24, CD63, EGFR and Glypican 1 on the surface of breast cancer exosomes via the nanomechanical signal of the microcantilever sensor.
- **Chapter 6** aimed to compare the electrochemical impedance spectroscopy in detecting cancer exosomes with the above-indicated study of the microcantilever array in detecting breast cancer cell-derived exosomes. The detection of cancer exosomes using small peptide molecules as exosomal-targeting ligands instead of antibodies will be explored. The ultimate goal was to design and develop a biosensor device to isolate and selectively detect cancer exosomes in human serum and thereby identifying breast cancer at early stages.
- Finally**, Chapter 7** concluding remarks and general discussion of the outcomes from the work is presented along with few future directions.

Chapter 2 . Impedimetric Detection of Pathogenic Gram-Positive Bacteria Using an Antimicrobial Peptide from Class IIa Bacteriocins

Etayash H, Jiang K, Thundat T, Kaur K. Impedemetric detection of pathogenic gram-positive bacteria using an antimicrobial peptide from class IIa bacteriocins. ***Anal Chem***., 1693-700 (2014)

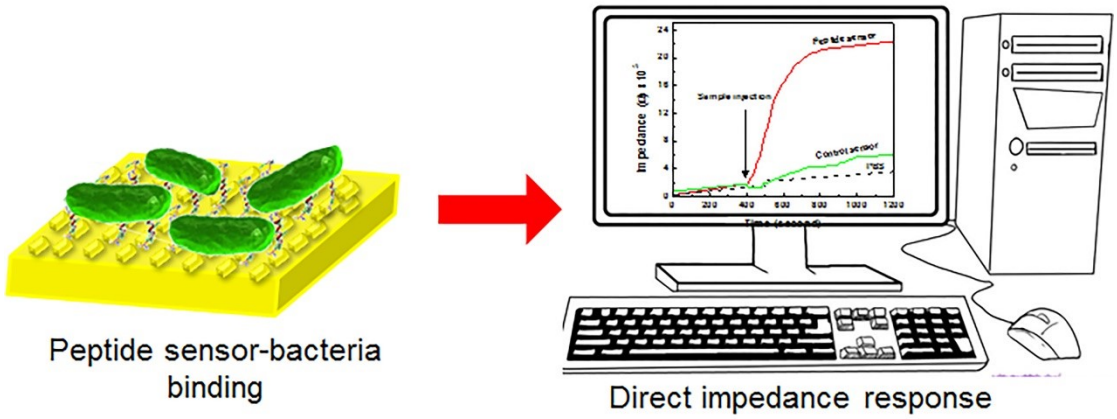

2.1 Introduction

Food contaminations and resistance of bacterial infections remains as one of the critical concerns in developed and developing nations due to the lack of handheld or portable devices for fast detection with high sensitivity and selectivity.[173, 174] For nearly a century, the conventional approaches for bacterial testing have relied and "continue to rely" almost exclusively on specific microbiologic media to segregate and enumerate the existing viable bacterial cells.[175] The steps involved in these detection techniques are labor intensive, time-consuming and require trained personnel in a laboratory setting. Therefore, conventional methods are inadequate for making timely assessments on microbiological safety of food and pharmaceutical products. Over the years many biological procedures have been simplified and faster methods for detection with significantly reduced assay time and enhanced sensitivity have been developed.[93] Most importantly, these advanced biotechnological assays, which referred to as "rapid detection techniques" have spawned a new generation of analytical methods that no longer relied exclusively on agar media.[27, 176] These techniques encompass a large and diverse group of systems and devices including miniaturized biochemical assays,[175] physicochemical tests based on bacterial metabolites, antibody-antigen interactions,[29, 177] DNA and enzyme based tools,[176, 178-180] and even fully automated diagnostic systems. The majority of these advanced detection approaches rely on antibody and nucleic acid probes for recognition, identification, and quantification of the target bacterial cells. These techniques include polymerase chain reaction (PCR) [27] and immunoassays,[29] as well as biosensor-based platforms with immobilized receptors.[1, 181, 182]

Despite the fact that these methods are very powerful and versatile tools for detecting, monitoring, and clinical diagnosis of pathogen infections with specificity and sensitivity, they still suffer from a number of constraints that limit their widespread applications. Antibody-based platforms, for instance, lack ample stability at harsh environmental conditions, the high cost of monoclonal antibody developments, and the need for a well-trained microbiologist to perform the tests.[183] Similarly nucleic acid probes based techniques are very costly, labor intensive, and require pretreatments to extract the DNA.[180] In contrast to antibody and DNA–probes, AMPs are intrinsically more stable in harsh environments, easier to synthesize, and exhibit broadband of activities and affinities against a wide range of Gram-positive and Gram-negative strains of bacteria[184]. Indeed, several recent studies have explored the viability of using the AMPs as

molecular recognition elements in biosensor platforms and have demonstrated the ability of naturally occurring AMPs to serve as robust bio-recognition probes in electronic biosensors.[110, 160, 167, 168, 185] For example, Mannoor *et al* reported self-assembling of antimicrobial peptide onto a wireless graphene nanosensor and showed bio-selective detection of bacteria at single-cell levels.[186] We recently showed that surface anchored peptide segment of class IIa bacteriocin is able to bind selectively without exhibiting biological activity only to Gram-positive bacteria.[187]

Here we report on utilizing the antimicrobial peptides as selective probes for label-free, real-time detection of foodborne pathogens using a new generation of impedance array analyzer that works at very low frequencies. We have functionalized the arrays with antilisterial, antimicrobial peptide, of class IIa bacteriocin for selectivity.[188] The impedance spectroscopy is a promising sensor platform due to its simplicity, high sensitivity, miniature size, ease of assembling and flexibility for multiplexed lab-on-a-chip applications.[103, 185] It has lately been proven to be a very effectual tool for studies including detection of DNA hybridization,[103] antigen-antibody interactions and most recently in the detection of cancer biomarkers.[108, 189] Leucocin A (LeuA) is a well-known, naturally occurring AMP of class IIa bacteriocins.[190, 191] It consists of 37 amino acid residues (**Figure 2.1b**) and similar to other class IIa bacteriocins, it is characterized by a conserved disulfide bond and a YGNGV sequence near the N-terminus and a C-terminal domain with an amphiphilic α-helix ending with a hairpin-like structure at the C-terminal tail.[191] Distinguishing from other antimicrobial peptides, class IIa bacteriocins exhibit high potency against particular species of *L. monocytogenes*, which therefore known as antilisterial antimicrobial peptides.[187, 188] In addition to that, LeuA exhibits very potent activity against *L. monocytogenes* in a nanomolar range [minimum inhibitory concentration (MIC) of 0.1 nM].[192] Although the exact mechanism of specificity of class IIa bacteriocins remains a matter of controversy, there is a consensus that they exert their antimicrobial specificity and activity by binding to invariant components of microbial surfaces through specific membrane-located proteins of the mannose phosphotransferase system (man-PTS).[193-195] Different expression levels of this mannose receptor on surface of the bacterial cells from one to another lead to various sensitivities and activities of bacteriocins.[195]

The antimicrobial peptide of class IIa bacteriocins, when immobilized on electrode arrays for impedance spectroscopy, offers an ideal sensor platform for real-time detection of *Listeria*

monocytogenes in solutions. We used the multiplexing capabilities of our custom designed antimicrobial peptide impedance microelectrodes for demonstrating the detection of different types of foodborne pathogens in contaminated samples.

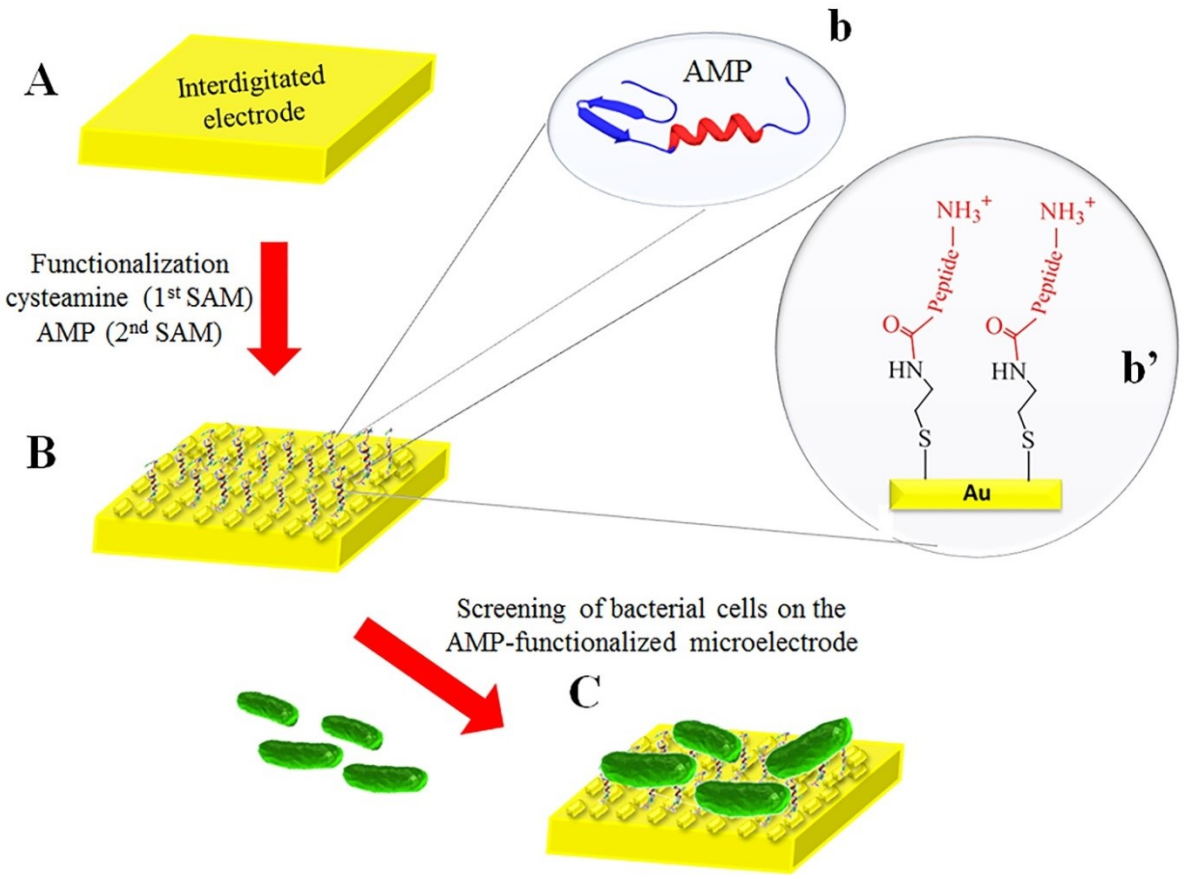

Figure 2-1| Graphic depiction of AMP-based biosensor (A) simulated cartoon denotes the interdigitated microelectrode. (B) AMP immobilized on the microelectrode array. (C) Bacterial detection is achieved via binding of the target cells to the immobilized AMP. The (b) shows NMR solution structure of the AMP (Leucocin A), while (b') displays chemistry of the surface functionalization.

2.2 Materials and methods

2.2.1 Antimicrobial peptide and cell culture

Antimicrobial peptide of class IIa bacteriocin (Leucocin A), having a sequence of 37AA (KYYGNGVHCTKSGCSVNWGEAFSAGVHRLANGGNGFW) was chemically synthesized

using solid phase peptide synthesis as descried previously.[196] Stocks of pathogenic bacterial cells (*L. monocytogenes* ATCC 43256, *Enterococcus faecalis* ATTC 19433, and *Staphylococcus aureus* ATCC 13565) and non-pathogenic (*Listeria innocua* ATCC 33090) were obtained from CanBiocin Edmonton Inc. and were grown overnight in an APT medium at room temperature. All the experiments regarding the pathogenic bacterial subculture, maintenance, and treatments were carried out in a level II biosafety cabinet.

2.2.2 Impedance Analyzer (IA-2)

Impedance Spectroscopic Analyzer (SHARP IA-2) developed by the Sharp Laboratory of America was used in this study. The instrument is capable of measuring up to 15 channels simultaneously at a fixed frequency in the range of 10 - 1000Hz and a stimulation voltage of 10 - 212mV. The sensor array consists of 15 interdigitated gold electrodes enclosed in three separate reaction chambers. The individual impedimetric sensor electrode had a typical dimension of 3350 μm×100 μm×150 nm, and the spacing between the sensor electrode and the common electrode is 40 μm. The size of each die of fabricated impedimetric microarray was 20 mm×18.5 mm. The impedance analyzer is also equipped with a sensor for temperature control which is adjusted at 25 °C.

2.2.3 Impedance array functionalization

Surface functionalization with antimicrobial peptide was based on covalent interaction between the accessible carboxylic group of the peptide and a free amine group of a thiol linker pre-attached onto the electrodes surface. **Figure 2.2.1** is a schematic outline of the sensing platform revealing the immobilization approach. First, the gold interdigitated electrodes were functionalized with a cysteamine ($SHCH_2CH_2NH_2$) by treating them with 0.01M of cysteamine hydrochloride in concentrated (8 x PBS, pH 8.1) buffer solution for 6 h.[197] The electrodes were then rinsed with 1 x PBS, pH 7.4, to remove any unbound thiol linkers. Stock solution of AMP (800 μg mL^{-1}) in 1 x PBS, pH 7.4, containing an activating agent, 0.2 M EDC, was injected into the sensing chambers and incubated overnight at room temperature. The functionalized electrodes were then rigorously washed with 1 x PBS to remove any unbound AMP, rinsed with deionized water and dried in liquid nitrogen.

2.2.4 Impedance set up and measurements

The IA-2 analyzer operation is based on electrochemical impedance spectroscopy.[198] When the AMP captures its specific target bio-molecules from the surrounding medium, the molecular interactions lead to changes in the sensor's impedance that are correlated to the type and amount of the bound analytes. The changes thereby, are detected, measured and analyzed by monitoring impedimetric parameters. The experiments presented in this study were performed at 10-100 Hz and 100 mV stimulation signal for bacterial detection in both PBS and milk samples. Initially, to optimizing an adequate frequency for the detection, bacterial cells at 10^3 cfu mL^{-1} were exclusively incubated with the peptide sensor arrays and the impedance reading were taken at different frequencies ranging from 10 to 100 Hz. In each study, prior measurements of the peptide-bacteria interactions, the sensor array fluidic chamber were filled with target-free sample (No bacteria) and subjected to impedance reading for 400 seconds to establish the base line. Target contains sample was then incubated in the sensor chamber and subjected to another impedance reading for ~ 800 seconds.

For sensitivity measurements, *L. monocytogenes* at serial concentrations of (10^2, 10^3, 10^4, 10^5, 10^6 cfu mL^{-1}) were individually injected into the sensor array fluidic chambers, incubated with the immobilized peptide, and subjected to impedance reading for ~ 800 seconds at 100 Hz. The detection selectivity experiments were performed with various bacterial strains (10^3 cfu mL^{-1} each) at a 100 Hz and 25 °C. For the real-time measurements, the impedance vs. time data were recorded while buffered dilutions of bacterial solutions incubated in the microfluidic channels. All experiments were repeated at least three times. For real-time bacterial detection in milk samples, fixed concentration of *L. monocytogenes*, 10^3 cfu mL^{-1} was mixed with PBS samples having different milk densities. The samples were then independently incubated in the microfluidic chambers and impedance reading was recorded at 100 Hz at 25 °C. Finally, the sensor device was regenerated via cleaning the microfluidic chambers (removing all adhered bacterial cells) with a 70% ethanol followed by rinsing with DI water and drying under nitrogen.

2.2.5 Data analysis:

Data analysis software is based on a previously described algorithm,[103, 105] which incorporated into the IA-2 instrument user interface. The interaction chemistry suggests that the immobilized antimicrobial peptide captures the target bio-molecules (bacteria) at a rate that follows an

exponential function. This rate changes with time after introduction of the target molecules into the fluidic chamber. Therefore, the binding curve at a fixed frequency is analyzed as an exponentially varying impedance signal Z over time t according to Eq. (1): [105]

$$|Z(t)| = B + A[1 - \exp(-st)] \quad \textbf{(1)}$$

Where, s, A, and B are independent constants. B is the offset at which the exponential begins, and denotes the array impedance baseline of the target-free buffer solution. Both s and A hold important biochemical parameters. The first is the amplitude of the impedance signal response, and the latter is correlated to the rate of exponential time constant associated with target binding. The algorithm automatically extracts the kinetic parameters from the Eq. (1) and computes the amplitude of impedance response corresponding to the peptide bacteria interactions. The curve was analyzed as an exponentially varying impedance signal and the parameters calculations reflect the target concentration, sensor surface coverage and target binding kinetics. The analysis window was set manually onto 1 min after sample injection in order to prevent the mechanical disturbance caused by emptying and refilling the microfluidic chambers from affecting the calculations. The integrated impedance signal response (integrated area) was calculated as the area under the binding curve starting at the point of sample injection and ending at 1200 second.

2.3 Results and Discussion

The objective of our investigation was to explore the feasibility of employing antimicrobial peptides of class IIa bacteriocins in an impedance analyzer for selective and sensitive detection of harmful microorganisms and in particular, *L. monocytogenes*. Optimum impedance frequency range for the detection was determined by exposing the peptide sensor to various samples with and without target cells at different frequencies (10, 25, 50 75, and 100 Hz). **Figure 2.2A** illustrates the optimum frequency for using the AMP designed sensor in detecting spoilage bacterial species. Although all the investigated frequencies exhibited clear impedimetric responses to bacterial cells, 100 Hz appeared to be the optimum frequency within the constraints of our experimental setup. This comes in agreement with previous reports that show a 100 Hz is an optimum frequency in impedance for detection of bacteria[199-202].

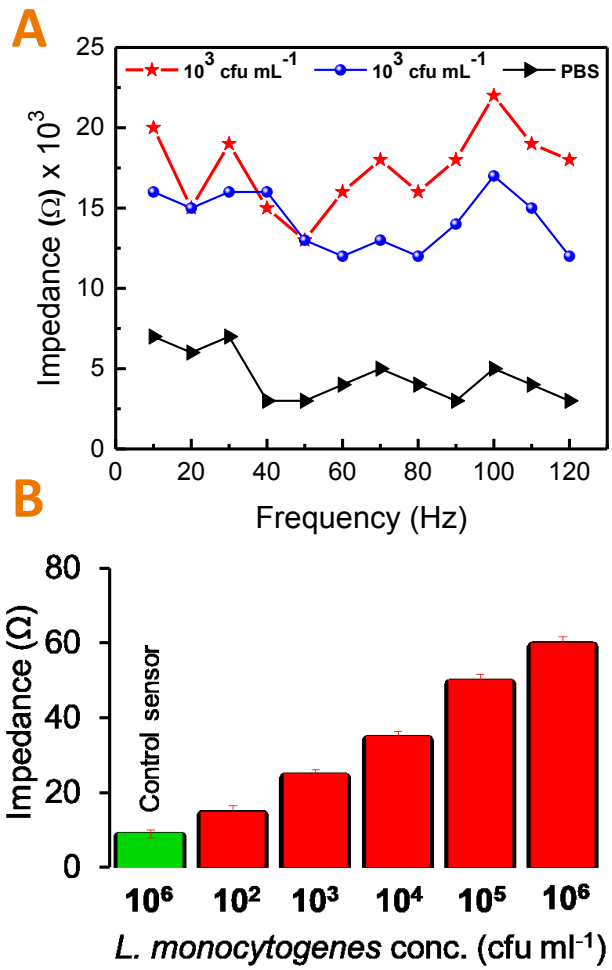

Figure 2-2| (A) Impedance spectra of the peptide sensor response to *L. monocytogenes* (red) and E. faecalis (blue) at concentrations of 10^3 cfu mL^{-1} as well as its response to a PBS solution (purple) at multiple frequencies. (B) Impedance spectra of various concentrations of *L monocytogenes* at fixed frequency (100 Hz). A control sensor (cysteamine-functionalized sensor) was used for a comparison purpose. Error bars show the standard deviation.

2.3.1 Sensitivity: The sensitivity of microbial detection is a very critical parameter in determining the practical applicability of the functionalized sensor.[1, 203] To this end, the sensitivity of the LeuA functionalized sensor (peptide sensor) in detecting microbial cells was probed by exposing the sensor to various concentrations of bacteria. Figure 2B shows the results of measurements performed after incubation of the peptide sensor with pathogenic *L. monocytogenes* in concentrations ranging from 10^2 – 10^6 cfu mL^{-1}. A "Control Sensor" with cysteamine-functionalized microelectrode array treated with the same concentrations of bacteria, and a "blank", peptide sensor treated with target-free samples were also subjected to impedance readings for comparisons. The results revealed that variation in the impedance signal response is directly proportional to the number of bacterial cells bound to the peptide sensor (LeuA-immobilized array) and that variation is expressed in a logarithmic increase with respect to serially diluted bacterial cells. The lowest limit of detection of this peptide microelectrode device

to *Listeria monocytogenes* was found to be 10^3 cfu mL^{-1}, i.e., one bacterium per microliter, which is significantly a clinically relevant edge,[204] and indeed it compares well with other detection assays such as antibody-based impedance and AMP-based fluorescence tests.[168, 205]

In order to simulate the applicability of this peptide sensor in everyday applications and in on-site detection, the detection was performed in a real-time, without any extrinsic labels. The dynamic parameters of the peptide bacteria interactions were further estimated accordingly. As shown in **Figure 2.3**, impedance microelectrodes (**Figure 2.3A**) were firstly functionalized with LeuA as described in the experimental section. A microfluidic chamber having three separate cells was then attached to the functionalized microelectrodes, where each cell is hosting 5 microelectrodes (**Figure 2.3B**). The fluidic chambers were initially filled with buffer solution (target-free sample, without bacteria) and subjected to impedance reading for 400 second to determine the baseline. Subsequently, 20 μL of *L. monocytogenes* solution (10^3 cfu mL^{-1}) was incubated with the functionalized microelectrodes and the impedance was measured for 800 seconds. The impedance response was continuously monitored before and after injection of the bacterial samples. As it is seen in **Figure 2.3C**, the peptide sensor produces a measurable response to bacterial sample relative to the blank and the control sensors. A clear signal and strong response begins immediately after sample injection, indicating adhesion of the bacterial cells to the immobilized peptide on the sensor surface. The impedance shows large changes that are clearly attributed to the binding of the immobilized AMP to the target bacterial cells. The results are in an agreement with a similar study done by Mannoor *et al*. 2010, where they revealed that peptide micro-capacitive hybrid impedance was able to demonstrate both Gram-selective detection and interbacterial strain differentiation, while maintaining recognition capabilities toward pathogenic strains of *E. coli* and *Salmonella*.[110] The same study was also able to reveal a detection limit of approximately 1 bacterium per μL.[110]

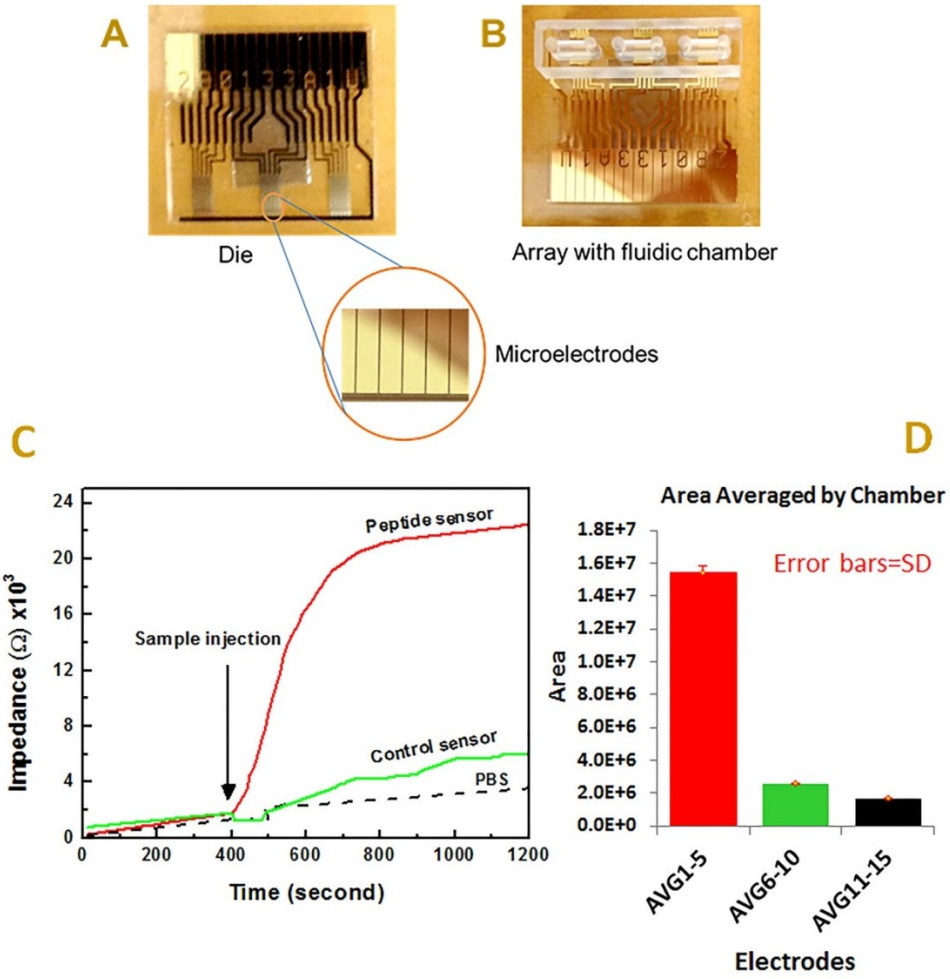

Figure 2-3| Real time measurements of binding of bacteria to the peptide sensor (A) Die or impedimetric sensor microarray showing the interdigitated gold microelectrodes (B) Photograph of the impedance array attached to a microfluidic chamber. (C) Binding curves for the normalized impedance signals from specific binding of *L. monocytogenes* (10^3 cfu mL^{-1}) to a peptide sensor (red-line), and a control sensor (green-line). A peptide sensor response to a phosphate buffered saline (PBS) was used also as a blank (black dashed-line). Each impedance response is an average calculation of 5 replicates. (D) The binding curve parameter (integrated area under the curve) for the peptide sensor response to *L. monocytogenes* (red), the control sensor (green), and PBS response (black). Each calculated area is an average calculation of 5 responses.

Further insight on the selectivity of the immobilized AMP towards *L. monocytogenes* was achieved by analyzing the kinetic parameters of the peptide-bacteria interactions. The integrated area under the binding curve was algorithmically calculated for each sensor and a representative

graph was plotted in **Figure 2.3D.** Clearly, the integrated areas show a strong correlation between specific binding of the peptide sensor to *L. monocytogenes* and the physical adsorption to the controls sensors.

2.3.2 Selectivity: We investigated the selectivity in binding of the AMP functionalized sensor towards various bacterial species and determined the binding kinetics of each strain. In particular, binding affinity of the peptide sensor was explored against *L. monocytogenes*, *Listeria innocua*, *Enterococcus faecalis*, and *Staphylococcus aureus*. In a previous study, we have shown the capability of surface immobilized with a short segment of class IIa bacteriocin (LeuA) to bind selectively to Gram-positive strains at high concentrations using fluorescence microscopy methods.[187] The method however, did not demonstrate high sensitivity, nor did it show capability for label-free multiplexed detection of different strains on a real-time.[187] This study on the other hand demonstrates that combining the antimicrobial peptide with the impedance spectroscopy allows discrimination between various bacterial species at a concentration of 10^3 cfu mL^{-1}. **Figure 2.4A** reveals a real-time impedimetric response of the peptide sensor to various bacterial species at 100 Hz. The red signal corresponds to peptide sensor responses to *Listeria monocytogenes*; while the blue, green, and orange represent the peptide sensor interactions for *Enterococcus faecalis, Listeria innocua* and *Staphylococcus aureus*, respectively. The peptide sensor clearly displays the highest impedimetric signal response against *L. monocytogenes*, where the amplitude is increased from 500 Ohms (Ω) at the baseline to reach ~ 2.4×10^3 Ω. The next uppermost impedance signal was observed against *Enterococcus faecalis*, where impedance shifted to nearly 1.8×10^3 Ω from its starting point after the sample injection. Finally, impedance reached 1.35×10^3 and 1.43×10^3 Ω due to peptide sensor responses to both *Listeria innocua* and *Staphylococcus aureus*, respectively. The variation in the impedimetric responses between bacterial strains is attributed to a number of potential factors; for instance, differential expression level of the man-PTS receptors on the surface of the target cells from one strain to another would give rise to different binding sensitivity of the immobilized AMP to bacterial strains, which thereby, lead to distinctive impedance sensor responses. Indeed, few studies have recently shown that number of the molecular receptors at the cellular membrane of the bacterial cells play very crucial role in peptide-bacteria interactions, and that biological activity of the AMP depends on the level of the expressed receptors at the bacterial cell membrane.[194, 195, 206] Likewise, Kjos *et al*. showed that the level of bacteriocin susceptibility of the bacterial cell was predominantly

dictated by differences in expression of man-PTS proteins and that bacteriocin sensitivity can vary within the same species, due to differential expression levels of the same man-PTS receptor.[194]

The algorithm [105] we used allowed obtaining further insight of the peptide bacteria interactions by extracting the kinetic parameters of the peptide sensor responses to bacterial species. The integrated areas under the binding curve of each strain that interacts with the immobilized AMP were calculated and graphically plotted in **Figure 2.4B.** In agreement with the real-time measurements, the integrated areas showed that the highest area accounted for peptide sensor responses to binding of *L. monocytogenes* to the immobilized AMP.

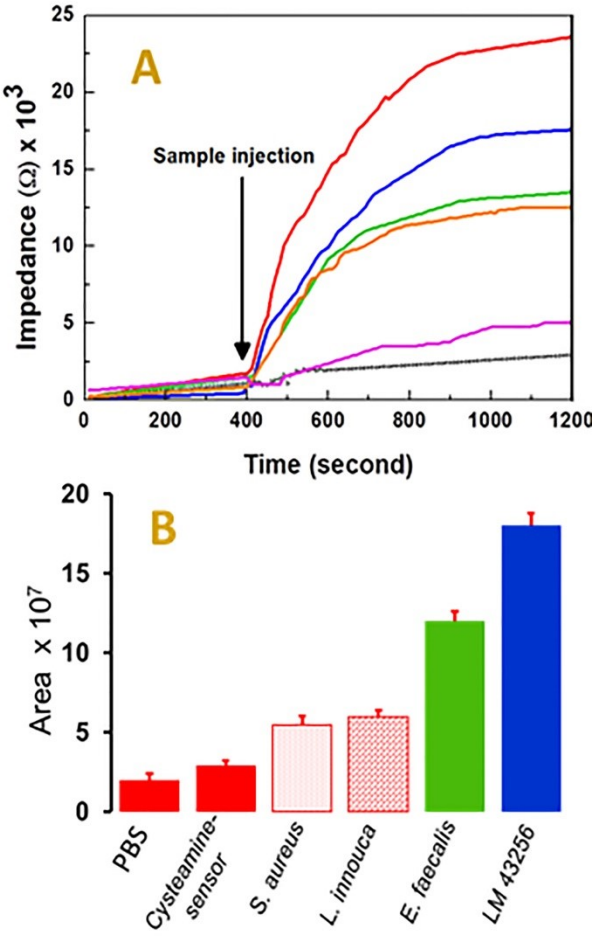

Figure 2-4| (A) Real-time impedimetric response to various bacterial species (10^3 cfu mL^{-1}) at 100 Hz. The red signal corresponds to the peptide sensor response to *L. monocytogenes* (*LM* 43256); while the blue, green, and orange show the peptide sensor response to *Enterococcus faecalis* (*E. faecalis*), *Listeria innocua* (*L. innocua*) and *Staphylococcus aureus* (*S. aureus*), respectively. The pink colored signal is the control sensor response to *L. monocytogenes* and the dashed black-line is the peptide sensor signal against the PBS solution. (B) The binding curve parameter (integrated area under the curve) for impedance sensor responses to the corresponding strains. Note that each impedance response is an average calculation of 5 replicates and error bars indicate corresponding standard deviations.

For a comparative quantification of binding of the different species to the peptide sensor, the parameters A, s and A × s were algorithmlly calculated for the different bacterial species (**Appendix Figure 1**). The intended parameters revealed the target concentration, sensor surface

coverage as well as the binding kinetics. While the amplitude A is proportional with the sensor surface converge of the target cells and indicative to the affinity of the analytes-receptor interactions, the time constant (s value) is relative to the binding rate constant, which is in fact independent of the Amplitude A. The A × s value represents the initial rate of binding. We can infer that a combination of both parameters A and s provided a signature of the binding event and allowed one to obtain further comprehensive characteristic of peptide-target binding behavior.

2.3.3 Real-time detection in milk samples: In order to investigate the applicability of the present AMP-based sensor array in real-life applications, we have used it for detection of bacteria in artificially contaminated milk. First, we optimized the milk concentration for the impedimetric detection. Unlike the PBS, the milk has a very high molecular density due to its components from fats, sugars, enzymes and proteins. Those components unfortunately, could cross-react and interfere with the target bio-molecules in the detection and lead to false positive or negative results.[207] For these reasons, a concentration of 10^3 cfu mL^{-1} of *Listeria monocytogenes* was incubated with a number of serially diluted milk samples ranging from 10% − 100% in PBS solution. A 20 μL from each sample was incubated with the AMP fabricated microelectrodes in the impedance microfluidic chamber and the impedance measurements were carried out for 800 seconds at 100 Hz. The optimization of the assay was performed through the analysis of the amplitude of specific binding versus non-specific (controls) signals (**Figure 2.5A**). The calculated ratio of specific and non-specific signal amplitude A shows a sharp optimum at 10% concentration of milk in PBS (1:9). In contrast, plain milk with 100% concentration shows very different pattern and depraved signal response indicating interference. Milk proteins and fats beside other components seem to interact non-specifically with the peptide sensor and lead to strong impedance changes. In fact, it has been previously shown that milk components non-specifically interact with the impedance response of the interdigitated electrodes giving rise to an increase in the resistance.[207-209] Furthermore, high density of fats and proteins could raise the possibility of peptide-protein and/or peptide-lipid interactions that could lead to false positive results. [210, 211]

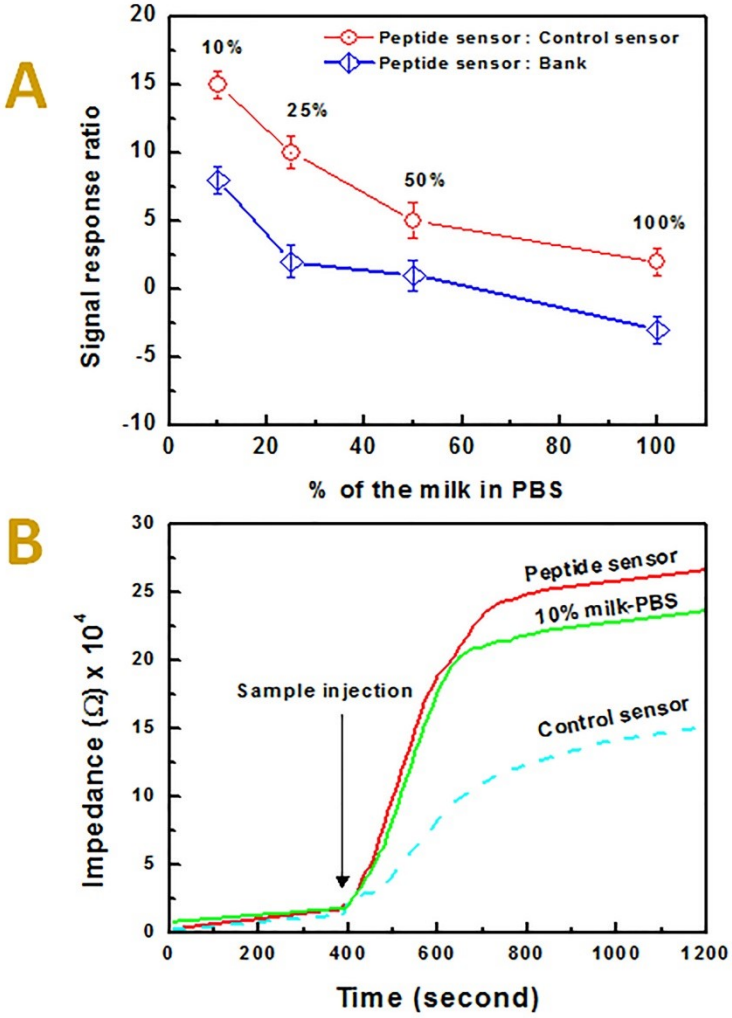

Figure 2-5| Signal response ratios of specific targets versus negative controls; while the red signal corresponds to Amplitude of peptide sensor response: Amplitude of the control sensor response to *L. monocytogenes* at 10^3 cfu mL^{-1}, the blue signal correlates to amplitude of peptide sensor response to *L. monocytogenes* at 10^3 cfu/mL: Amplitude of the peptide sensor response to the same sample with no bacteria. Ratios were calculated at different concentrations of the milk in PBS solution. Each parameter value is an average estimated from measurements of 5 different microelectrodes within the same reaction chamber; error bars indicate corresponding standard deviations. (b) Real-time label-free detection of *L. monocytogenes* in milk sample (10^3 cfu mL^{-1}) in 10% milk at 100 Hz. The red-line corresponds to the peptide sensor response to *L. monocytogenes* while the green-line is the response for the blank (10% milk-PBS with no bacteria). The dashed cyan-line is the control sensor response to *L. monocytogenes* in 10% milk. Each impedance response is an average calculation of 5 replicates and error bars indicate corresponding standard deviations.

Figure 2.5B, depicts a Real-time label-free detection of *L. monocytogenes* (10^3 cfu mL^{-1}) in 10% milk at 100 Hz. The curves showed sufficient resolution on impedance responses between peptide sensor response to *L. monocytogenes* and the negative controls. Analyzing the binding curve parameters such as integrated area (**Appendix Figure 2-A**), amplitude A (**Appendix Figure 2-B**), time constant s (**Appendix Figure 2-C**) as well as the initial rate of binding A × s (**Appendix Figure 2-D**), revealed further substantial resolutions with approximately 3-4 fold difference between the peptide senor responses to bacterial samples and the negative controls.

The experiment establishes that the sensor responses show significant non-specific adsorption of the fats, proteins and carbohydrates present in the milk with no clear detection of bacteria at high density of the milk. On the other hand, at a concentration of 10% milk/PBS, the peptide sensor was able to provide excellent specific: non-specific resolution and detect *L.* monocytogenes at very low level of concentration.

2.3.4 Sensor array regeneration: The microelectrode array was regenerated through vigorously washing the microfluidic chamber with 70 % ethanol in order to completely remove all adhered bacterial cells and making the functionalized array accessible for the next detection process. The array performance after regeneration was evaluated against *L. monocytogenes* at a concentration of 10^3 cfu mL^{-1} in 1X PBS solution at a fixed frequency. **Appendix Figure 3** shows the dependence of assay parameters A, s, and A × s on the number of array re-uses. The amplitude A declined rapidly after the third re-use to approximately 50% of the initial value. The time constant and the initial binding have also changed erratically from the first time use. In agreement with previous studies[198], the results could be due to partial detaching of the peptide from the surface of the sensor array during treatments. A reduction in the peptide graft density would lead to decay in the binding capacity of the sensor array and reduced signals. Furthermore, the excessive use of the ethanol for washing the cells from the sensor surface could damage the sensor array electrical properties and lead to improper integration of the results. Owing to the semiselective nature of the interaction of AMPs with pathogenic bacteria, specifically *L. monocytogenes,*[188, 212] the discrimination of multiple species of pathogenic bacteria has been achieved in buffer solutions. However, it has been very challenging to detect bacteria in pure milk samples. Future work will focus on obtaining a well-defined discrimination pattern between bacterial species in milk samples and other food products. The approach will involve exploring different strategies to improve sensitivity and selectivity via employing alternative techniques for covalent and non-covalent functionalization of the AMPs, investigate multi-ligands and using other sensor platforms in parallel to achieve better detection limit with relevant selectivity using multi-modal approach.

2.4 Conclusion

An impedimetric biosensor platform for bio-affinity assay was developed based on a real-time, label free detection using antimicrobial peptide of class IIa bacteriocins. The biosensor was

capable of distinguishing between closely related bacterial strains and was able to detect very low concentration of *L. monocytogenes* with limits of detection as low as 10^3 cfu mL^{-1}, or one bacterium μL^{-1} - a clinically relevant limit. The data analysis algorithm extracted multiple parameters of binding curve kinetics, all of which were essential for analysis of target–peptide interactions in a real-time. This fully integrated AMP-based sensor array can be potentially used for detection of a wide range of analytes of practical significance, and has the prospective of use as a robust, portable biosensor device to efficiently detect pathogenic strains in food samples.

Chapter 3 . Microfluidic Cantilever Detects Bacteria and Measures their Susceptibility to Antibiotics in Small Confined Volumes

Etayash H, MD Khan, Kaur K, and Thundat T**. "**Microfluidic cantilever detects bacteria and measures their susceptibility to antibiotics in small confined volumes". ***Nature communications*** 7, 12947 (2016)

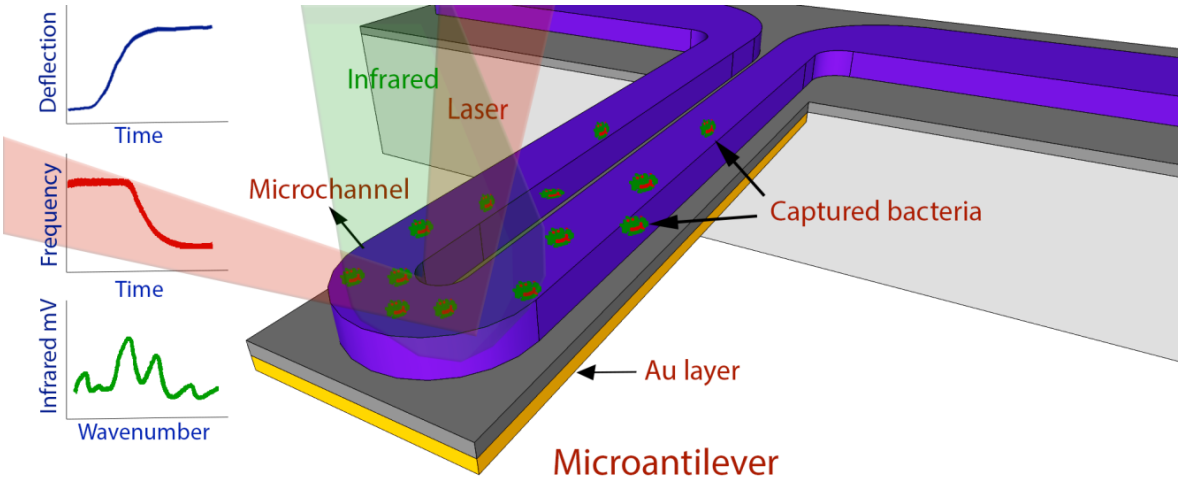

3.1 Introduction

Current methods for detecting bacteria and measuring their response to antibiotics lack sensitivity, selectivity, stability, and the ability for real-time analysis[173]. Laboratory-based detection methods, such as agar plates and broth dilutions assays, are inconvenient and require a minimum of 24 hours to complete, depending on the bacterial species[213]. Rapid detection techniques, such as antibody-antigen assays (e.g., ELISA)[214], resazurin-reduction assays[215] (for bacterial resistance), the mycobacterial growth indicator[216] and/or polymerase chain reaction-based methodologies[217], are very sensitive and powerful detection tools. However, they are expensive and they are unable to distinguish between living and dead species. In addition, high sensitivity and selectivity in real-time measurements in the stated techniques are still challenging[173]. Hence, inexpensive sensors for the rapid detection of bacteria and the determination of their susceptibility to antibiotics are urgently needed in order to combat the emergence of drug-resistant bacterial strains.

Recent developments in micro and nanofabrication allow the integration of multiple signal generation techniques into a single device to obtain orthogonal signals, which enhances the detection sensitivity and selectivity[218]. A number of versatile, highly sensitive sensors, based on microcantilevers for microbial detection, have been developed[128, 144, 219]. These sensing concepts rely on immobilizing specific receptors on the cantilever surface for selectively capturing the target bacteria and translating the binding into mechanical signals, as either cantilever deflection (static mode) or a shift in resonance frequency (dynamic mode)[128]. Despite the many advances in these conventional modes of cantilever operation, a number of constraints still exist that limit their widespread application. First, sensitive measurement of the resonance frequency shift in a liquid environment has been limited by the low-quality factor (Q-factor) of the cantilever, due to liquid damping[128]. Second, the response of the cantilever is often affected by liquid flow, which increases the signal-to-noise ratio. Laminar flow around the cantilever creates a potential barrier for the efficient capture of targets from the flowing solutions[220]. In addition, the small dimensions of the sensor decrease the capture cross-section, resulting in the reduced adsorption of target molecules. Therefore, the mode and volume associated with fluid delivery play a crucial role in the capture rate of the target molecules[220].

A suspended microchannel resonator, where a microfluidic channel is embedded inside a microcantilever, overcomes the limitations of liquid damping and achieves unprecedented mass resolution[221]. Since the liquid is inside the cantilever, the cantilever can be excited into resonance in a vacuum for increased mass resolution and higher reproducibility[222, 223]. Despite its extraordinarily high mass sensitivity, this resonator still lacks selectivity in detection. Incorporating multi-modal detection, by which multiple orthogonal signals can be monitored simultaneously, is a way to achieve the desired selectivity. Pre-concentrating analytes also increases the selectivity and sensitivity of detection. We have fabricated a microfluidic channel on a bimaterial cantilever (BMC) so as to obtain three orthogonal signals - adsorbed mass, adsorption stress, and mid-infrared spectroscopy of the adsorbates, as shown in **Figure 3.1**. Functionalizing the interior surfaces of the BMC with specific receptors allows the target bacteria to be selectively trapped inside the channel in a 50-picoliter volume. Adsorption of the bacteria causes changes in the cantilever resonance frequency, resulting from changes in the inertial mass of the liquid-filled cantilever. In addition, adsorption of bacteria also results in the cantilever bending, due to adsorption-induced surface stress which results from the microfluidic channel being fabricated on top of the cantilever with cross-sectional asymmetry. Adsorption-induced stress originates from changes in free energy (free energy per unit area is surface stress) due to adsorption. A third orthogonal signal can be obtained by illuminating the cantilever with IR radiation. Absorption of specific IR wavelengths by the adsorbed bacteria causes additional cantilever deflection due to non-radiative decay. The nanomechanical bending of the cantilever, as a function of illuminating wavelength, resembles the IR absorption spectrum of the bacteria. Since IR absorption spectroscopy is an established technique, incorporating this into the BMC system enables selective identification of bacterial strains and accurate discrimination between injured cells and intact cells. In this article, we applied the BMC sensor to enrich and detect *L. monocytogenes* in picoliter sample volumes with high sensitivity and selectivity using three orthogonal signals. In addition, the metabolic activity of the adsorbed bacteria resulted in nanometer scale fluctuations that are larger than the Brownian motion of the cantilever. Sensitive monitoring of this fluctuation allows the sensor to discriminate between intact and dead *E.coli*, as well as characterize the metabolic response of *E. coli* to antibiotics.

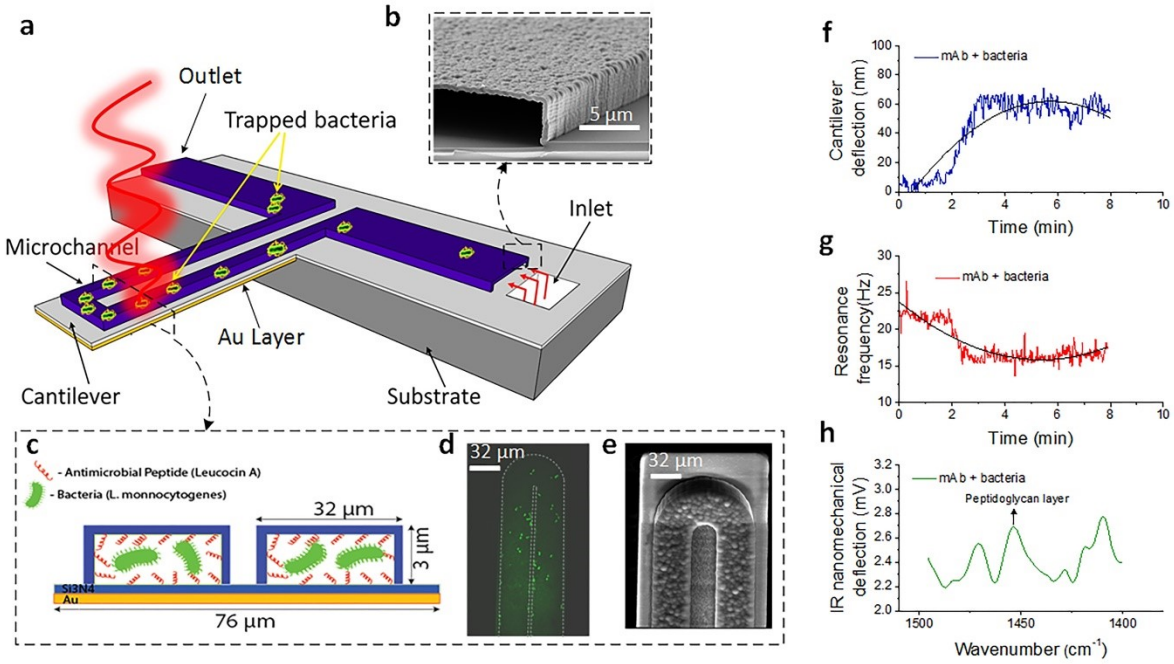

Figure 3-1| The schematic representation of the BMC and its multi-mode of operation. (a) BMC filled with bacteria supported on a silicon substrate. At the bottom, the BMC is coated with a 300 nm-thick layer of gold, which serves as a second element (mismatched expansion coefficients between the silicon nitride and gold layer facilitate the cantilever deflection as a localized heat is produced). The BMC was coated with a bacteria-targeted receptor and irradiated with a specific wavelength of tunable infrared light. (b) Scanning electron microscopy (SEM) image of the cross-section of an inlet, located on bottom side of the chip. An aqueous solution of bacteria is loaded from the inlet. (c) Cross-section of the 32 mm wide microchannel of the cantilever. The inner surface of the cantilever's microchannel was functionalized either with a mAb or an AMP (Leucocin A) from class IIa bacteriocins, which acted specifically against L. monocytogenes. (d) Fluorescent image from the top side of the BMC, filled with bacteria. (e) SEM image of the tip of the BMC. The round microchannel helps to ensure clog-free flow. (f) When the bacteria inside the BMC absorb infrared light, local heat is generated that results in the nanomechanical deflection of the BMC. (g) The resonance frequency is sensitive to the increased mass caused by the adsorption of bacteria inside the BMC. (h) When the BMC is illuminated with a certain range of infrared light, a plot of the nanomechanical deflection of the BMC shows the wavelength where the bacteria absorb infrared light. This can provide excellent selectivity in a complex mixture.

3.2 Methods

A bi-material microcantilever (32 μm wide, 600 μm long) with a microfluidic channel (cross section 32 μm x 3μm) embedded on it was used in this study (**Figure. 3.1a**). The cantilevers were mircofabricated using silicon nitride and a thin layer of gold (300 nm) was deposited on one side to make them bi-material. When the bacteria inside the BMC absorb a specific wavelength of IR, they produce localized heat, which is then transferred to the gold layer beneath the silicon nitride. Due to a mismatch in the thermal expansion coefficients of silicon nitride and gold, the BMC deflects upwards. Changes in BMC deflection (ΔA) are measured by reflecting a laser off of the cantilever to a position sensitive diode detector. In the detection experiments, the microfluidic channel of the cantilever was functionalized using bacteria-targeting molecules to capture the analytes and enhance the detection sensitivity and selectivity. Two targeting molecules of *L. monocytogenes* were employed [anti-*L. monocytogenes* monoclonal antibody (mAb) and *Listeria*-selective antimicrobial peptide (AMP) from class IIa bacteriocins]. A peptide with non-specific binding to *Listeria* was used as a negative control (**see Appendix for further details**).

In the experiment, 100 μl water samples, free from bacteria or artificially contaminated with bacteria at various concentrations ($10^2 – 10^5$ cfu ml^{-1}), were injected into the sensor and subjected to nanomechanical monitoring while the BMC filled with liquid. Measurements of the cantilever deflection, nanomechanical IR spectra and mass adsorption (measured as resonance frequency shifts) were taken simultaneously. As targeted bacteria pass through the narrow microfluidic channel embedded on the cantilever, they are trapped by the immobilized ligands. The bacteria absorb IR photons at certain wavelengths and release heat to the background, through the non-radiative decay process of vibrational energy relaxation. This results in a small change in the temperature of the bimetallic cantilever, causing it to bend in proportion to the quantity of the released energy. While the IR-induced nanomechanical spectra represent the molecular signature of the bacteria inside the microchannel, the resonance frequency shifts provide real-time measurements of the specific mass of the captured bacteria. The bacteria-adsorption induced cantilever bending was monitored at IR wavelengths where bacteria did not absorb the IR. Note: The interference due to IR radiation-induced bending of the empty cantilever is eliminated by taking the differential deflection of the cantilever, which will then represent the specific binding signals of bacteria binding to the immobilized receptors. The differential deflection is obtained

by subtracting the deflection of the cantilever filled with sample (bacteria) from the deflection of an empty cantilever exposed to the same IR radiation.

For the bacterial drug-resistance experiments, the sensor was chemically treated using a linker molecule (APTES), which provided a loose attachment of the bacteria to the surface, holding the cells in place without affecting their metabolic activity. After the treatment, the BMC was introduced into the sensor chamber to complete the analysis. Calibration of the cantilever was performed at this point by injecting a bacteria-free PBS solution and monitoring the IR-induced nanomechanical bending, cantilevers deflection, fluctuations, as well as frequency shifts associated with the loaded materials. The measurements were used as a baseline in the analysis of subsequent experiments. The nanoscale dynamic deflection, cantilever motion, IR absorption and the resonance frequency shifts were collected after each step. A solution containing a small aliquot of living bacteria (~10^5 cfu ml^{-1}) was introduced into the BMC and left to incubate for 10 minutes at ambient temperature. The BMC chamber was then rinsed with PBS to ensure removal of any floating cells that might impact the results. Afterward, a standard bacteria growth LB media was introduced onto the sensor in order to promote metabolic activities and data was subsequently collected. The growth media was then exchanged with LB media containing antibiotics; either ampicillin or kanamycin at a concentration of 10 μg ml^{-1} and the data of resonance frequency, IR absorption, fluctuation and cantilever nanomechanical deflections were collected twice at ~5 min and ~30 min of exposure. The antibiotics were then removed and the LB medium was re-introduced prior to collecting data. To enhance the metabolism of the bacteria, we also introduced a 5% glucose solution to the bacteria after their exposure to the antibiotics. Each experiment was repeated at least five times to verify the consistency of the results and statistical difference analysis was performed using either the unpaired t-test or the one-way ANOVA test, as specified. The multivariate statistical analysis technique of principal component analysis (PCA) was used for analyzing the IR data of the bacteria, to differentiate injured *E. coli* from intact *E. coli*. In all statistical analysis, the significance level (P value) was set as 0.05.

3.3 Results

The BMC is fabricated using silicon nitride with a 300 nm thick layer of gold on one side for enhanced thermal sensitivity (bi-material effect). Changes in the BMC deflection amplitude (ΔA)

are measured using an optical-beam-deflection method, which enables recording of the resonance frequency and deflection of the cantilever simultaneously. In addition, sequential exposure to IR radiation excites the bacteria inside the cantilever, producing heat which deflects the cantilever further. Monitoring the deflections as a function of illuminating wavelengths shows the IR spectra of the targeted bacteria. Since the IR spectroscopy is chemically specific, non-selective absorption can be used for trapping the bacteria. Details of the experimental set-up, bacterial subculture and preparations, receptor immobilization, characterization and surface density studies are described in the **Appendix section**.

3.3.1 Bacterial detection: To demonstrate bacterial detection, we used *L. monocytogenes*, a serious food-borne pathogen which has a mortality rate that exceeds 20%[224]. Prior to bacterial injection into the sensor (10^2 cells in 100 μl), the inner surface of the chip was functionalized with either the anti- *L. monocytogenes* monoclonal antibody (mAb-coated BMC) or the *L. monocytogenes* targeted antimicrobial peptide (AMP-coated BMC). In addition to its binding selectivity, the immobilized receptors on the inner BMC interface served as a pre-concentrator, increasing the number of bacteria in the channel. The detailed chemistry of surface functionalization is shown in the **Appendix Figure 4**.

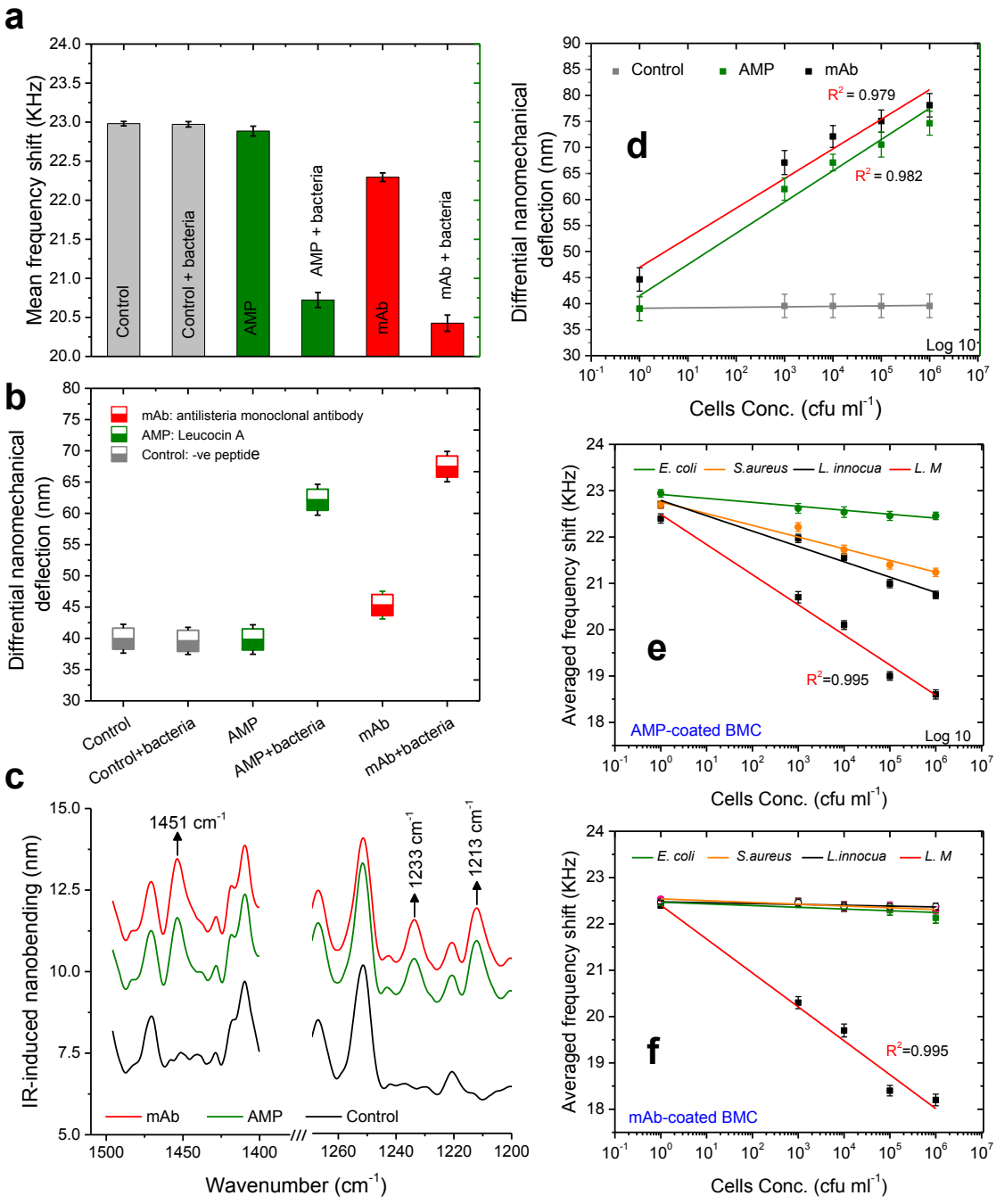

Figure 3-2| BMC multi-mode signal readout as a function of bacterial adsorption. (a) The mean descent in the resonance frequency shifts as a result of captured *L. monocytogenes* by either AMP or mAb-coated BMC; frequency drops as higher-density bacteria attach to the inner surface of the cantilever. In comparison with a control BMC (coated with a negative peptide), the AMP- and mAb-coated BMCs show significant responses to *L. monocytogenes* (P¼0.032). (b) Nanomechanical bending of the cantilever as a result of bacteria adsorption-induced surface stress. Statistically significant deflection is observed for both AMP- and mAb-coated BMCs in

comparison with the control (P>05; n=5). Differential deflection represents the specific binding event of the immobilized receptor to the bacteria, derived by subtracting the infrared-induced deflection. (c) Typical segments of BMC infrared nanomechanical spectra show the distinctive infrared absorption bands of bacteria (1,451, 1,233 and 1,213 cm^{-1}). The spectra were subtracted from the background signal and smoothed 45% to decrease the noise. (d) Nanomechanical deflection of a BMC after exposure to serial concentrations of L. monocytogenes demonstrates the sensitivity of the BMC. The corresponding fit is a linear function and error bars show the corresponding s.d.'s (n=5). (e,f) The selectivity of the BMC towards *L. monocytogenes*; the resonance frequency of the BMC changes with the type of bacteria species tested. It shows selectivity (higher affinity to *L. monocytogenes*) with an AMP coated BMC and specificity (capturing only *L. monocytogenes*) with a mAb-coated BMC. The data represent an average of five replicates and error bars correspond to s.d.'s.

Figure 3.2 shows cantilever deflection and resonance frequency shift as a function of bacterial adsorption. Resonance frequency changes result from changes in the inertial mass caused by the immobilized receptors capturing bacteria (**Figure 3.2a**). The mass of bacteria captured in the channel can be measured from the resonance frequency shift as 24.5 ng and 24. 9 ng in both AMP and mAb-coated BMC, respectively. In addition to the frequency shift, the cantilever deflection changes simultaneously as a result of the bacteria adsorption-induced surface stress, with an average differential deflection of 62±4 nm and 68 ±5 nm in both the AMP and mAb-coated BMCs (**Figure 3.2b**). Figure 2c shows differential cantilever deflection as a function of illuminating wavelength due to IR absorption by the bacteria trapped in the channel. The differential deflection is obtained by subtracting the IR-heating induced deflection of an empty cantilever from that obtained with bacterial sample loaded in the BMC. This mechanical IR absorption of the bacteria displays a typical spectrum with a distinct absorption peak at 1451 cm^{-1}, suggesting a peptidoglycan layer of the bacterial cell wall (**Figure 3.2c**). Absorption bands observed at 1233 cm^{-1} and 1213 cm^{-1} (**Figure 3.2c**) are due to the C-O-C ester and P=O vibrations of the bacteria phosphate diester groups, respectively. Two other vibrational bands also appear during irradiation of the sensor with higher wavelengths, indicating a P-OH (1100 cm^{-1}) and polysaccharide group (1023 cm^{-1}) in the bacterial cell wall (**Appendix Figure 6**). As reported previously, these observed IR absorption bands are a characteristic fingerprint of the bacteria[225-228].

3.3.2 Sensitivity: Since sensitivity is a key determinant to the applicability of using the sensor in real applications, we conducted experiments where different concentrations of bacteria, ranging from 10^3 – 10^6 cfu mL^{-1}, were injected into the BMC. We measured the nanomechanical deflection and plotted the responses against bacteria concentrations in the samples (**Figure 3.2d**). While the deflection signals of the control device (peptide-coated BMC) showed negligible response upon exposure to various concentrations of bacteria, the AMP and mAb coated BMCs showed increased bending with increased concentrations of bacteria. As the concentration of bacteria increases, so does deflection, which suggests a direct relationship to the number of bacteria bound to the functionalized surface. The results show the lowest detection limit of 100 cells per 100 μL (a single cell μL^{-1}), for a signal-to-noise ratio of 3. This detection limit is clinically relevant and compares well with other reported techniques.[97, 110, 229, 230] The advantages of the BMC sensor include its ability for multi-modal detection with very small volumes and its enhanced sensitivity and selectivity. Other label-free devices, such as the surface plasmon resonance (SPR) or quartz crystal microbalance (QCM), can only provide a single signal and are only suited for applications involving low molecular weight (LMW) analytes[165, 231]. Unlike conventional cantilevers and/or AFM cantilevers, the BMC offers multi-modal detection of liquid phase analytes with higher selectivity, sensitivity, and increased reliability.

3.3.3 Selectivity: The selectivity study intended to explain the selectivity matrix as it depends on gram-positive vs. gram-negative and the different strains of gram-positive bacteria, via elucidating the selectivity rejoinder of *L. monocytogenes* in contrast to other gram-positive strains. **Figures 3.2e-f** show the selective detection of *L. monocytogenes*. Cantilever deflection and resonance frequency shifts for different strains in serial concentrations (**Figures. 3.2 e-f**) revealed substantial discernment patterns and selective responses to *L. monocytogenes*. The differential nanomechanical cantilever deflections for different strains were clearly discernable for targeted strains (**Appendix Figure 8**). Control experiments carried out using fluorescence microscopy verified these results (**Appendix Figure 8**). In addition, the nanomechanical IR spectrum shows differences among bacterial species (**Appendix Figure 9**). These variations can be attributed to the asymmetric stretching of P=O in the phosphodiester backbone of nucleic acids (at ~12123 cm^{-1}), the asymmetry of the peptidoglycan layer of the bacterial cell wall (at 1451 cm^{-1}) and the lipid groups (between 1000 - 1023 cm^{-1}) in the bacterial cell wall. Specificity

in the IR spectra also comes from lack of interference as the flow through approach selectively captures the targeted strains, while still allowing the untargeted strains to pass through the channel. It is clear from these results that the AMP-coated BMC exhibited preferential binding towards *L. monocytogenes* relative to other strains by approximately 2 -3 orders of magnitude, while the mAb-coated BMC showed absolute specific response to *L. monocytogenes*, in comparison to other tested strains. We explain this differentiality towards *L. monocytogenes* by a mechanism-related behavior of the immobilized ligands[191, 193]. In an AMP-coated BMC, Leucocin A is a very distinctive AMP, which targets a specific membrane-bound receptor on the surface of the bacteria[232, 233]. This receptor is more prevalent in *L. monocytogenes* than in other species. As a result, Leucocin A has a higher affinity to *L. monocytogenes* than other strains. The mAb-coated BMC targets a specific antigen on the surface of *L. monocytogenes* which is not present in other strains. The AMP-coated BMC offers a broad spectrum diagnostic tool by allowing the detection of pathogenic bacteria. The sensor is sufficiently stable and reusable (**Appendix Figure 10**) and provides a cost-effective alternative to currently available techniques. On the downside, it is not specific for *L. monocytogenes*, as it can capture other strains with lower affinities. This can be tackled by differentiating the measured responses with respect to their strengths and flaws. In contrast, the mAb-coated BMC proposes a specific detection methodology to *L. monocytogenes*, at a higher affinity rate. Although the sensor is very specific and sensitive, it cannot be used to detect multiple strains simultaneously (**Appendix Figure 10**).

3.3.4 Antimicrobial resistance

In order to demonstrate the feasibility of using a BMC sensor to detect bacterial response to antibiotics, a small aliquot of living *E. coli* (~10^5 cfu ml^{-1}) was inserted into a BMC chip. Prior to insertion of the sample, the internal walls of the BMC were coated with a thin film of bacteria-adhesion molecules (APTES), which allowed the loose attachment of bacteria without affecting their metabolism[234]. In the first set of these experiments, the response of *E. coli* DH5α to ampicillin and kanamycin were monitored. We measured the deflection and resonance frequency shifts before and after the attachment of *E. coli*, after injecting LB (liquid broth) media, and LB-containing 10 μg ml^{-1} either, ampicillin or kanamycin (**see methods in the appendix**).

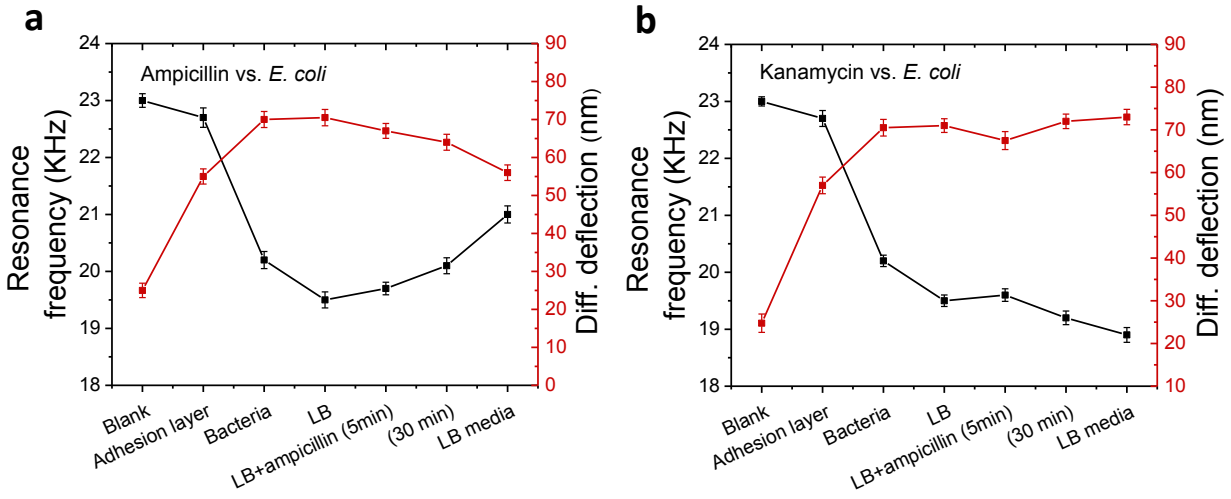

Figure 3-3| The BMC sensor displays the response of *E. coli* DH5a to antibiotics (ampicillin and kanamycin) at 0.1 mg ml^{-1}. (a,b) The resonance frequency shifts and the nanomechanical deflections as a result of serial steps starting from a blank cantilever to removal of the drug and re-introduction of the LB media. A decrease in the frequency is observed with the introduction of both bacteria and LB media (a,b). Introducing ampicillin (a) led to an increase in the resonance frequency and a decrease in the nanomechanical deflection. Injection of kanamycin, however (b), led to a decrease in the resonance frequency and an increase in the nanomechanical bending. Removing antibiotics and adding LB media further confirmed that bacteria have been killed by ampicillin (no dormancy), but not by kanamycin (b). An average of five replicates is presented with error bars, indicating s.d.'s.

Figure 3.3 shows cantilever deflection and resonance frequency, as a result of *E. coli* exposure to antibiotics (ampicillin and kanamycin). The introduction of *E. coli* causes the cantilever to deflect (~70 ±4.1 nm) as well as resonance frequency to shift (~ – 2.6 KHz from the background). An injecting aliquot of LB media led to a slight increase in the cantilever's deflection and a decrease in the resonance frequency (+71±3 nm and –0.7 KHz). Five minutes after the injection of LB-containing ampicillin, the resonance frequency showed an increase of ~ 0.2 KHz, while the deflection dropped by ~ 4 – 5 nm. After 30 minutes of exposure, the resonance frequency showed a larger shift (~ +0.4 KHz –**Figure 3.3a**), while the deflection further decreased by ~ 7 – 9 nm (**Figure 3.3a)**. Similar to the ampicillin response, injecting kanamycin showed an increase in the resonance frequency (~ +0.1 KHz – **Figure 3.3b**) and a drop in the deflection (~ 4 – 6 nm) after 5 min of exposure **(Figure 3.3b**). However, unlike ampicillin 30 minutes after exposure, the resonance frequency dropped and the deflection

increased compared to what was observed prior to the injection of kanamycin (~ +6 nm – **Figure 3.3b**). The measured noises in the *E. coli*-immobilized BMC cantilever deflections before and after the injection of antibiotics show significant variation between ampicillin and kanamycin (**Figure 3.4**). It has been reported previously that changes in bacterial metabolic activity change the different stresses on the cantilever.[234] Thus we assume that this effect may due to metabolism-induced stress and may indicate bacterial resistance to the drugs. As can be seen in **Figure 3.4 upper panel**, the fluctuation decreased dramatically (variance 0.65 ±0.053 nm^2) compared to that observed before the ampicillin injection (variance 6.16 ±0.26 nm^2). However, after the kanamycin was injected (**Figure 3.4 lower panel**), the fluctuation was consistently higher and compared well with the observation before kanamycin injection (variance 5.61 ±0.046 nm^2). In both cases, the bacterial cells seem to deactivate their metabolic processes initially after exposure to the antibiotics (short dormancy state), and then either die or recover with the addition of nutrients. Drug-induced bacteria death (ampicillin) resulted in changes in frequency, surface stress, and decreased cantilever bending and fluctuation. In contrast, the bacteria exposed to kanamycin appear to have full metabolic recovery, resulting in a decrease in frequency, increase in cantilever's deflection and nanomechanical noise. Our results are in agreement with previous reports of nanomechanical noise associated with the viability of bacteria and metabolic activity[234].

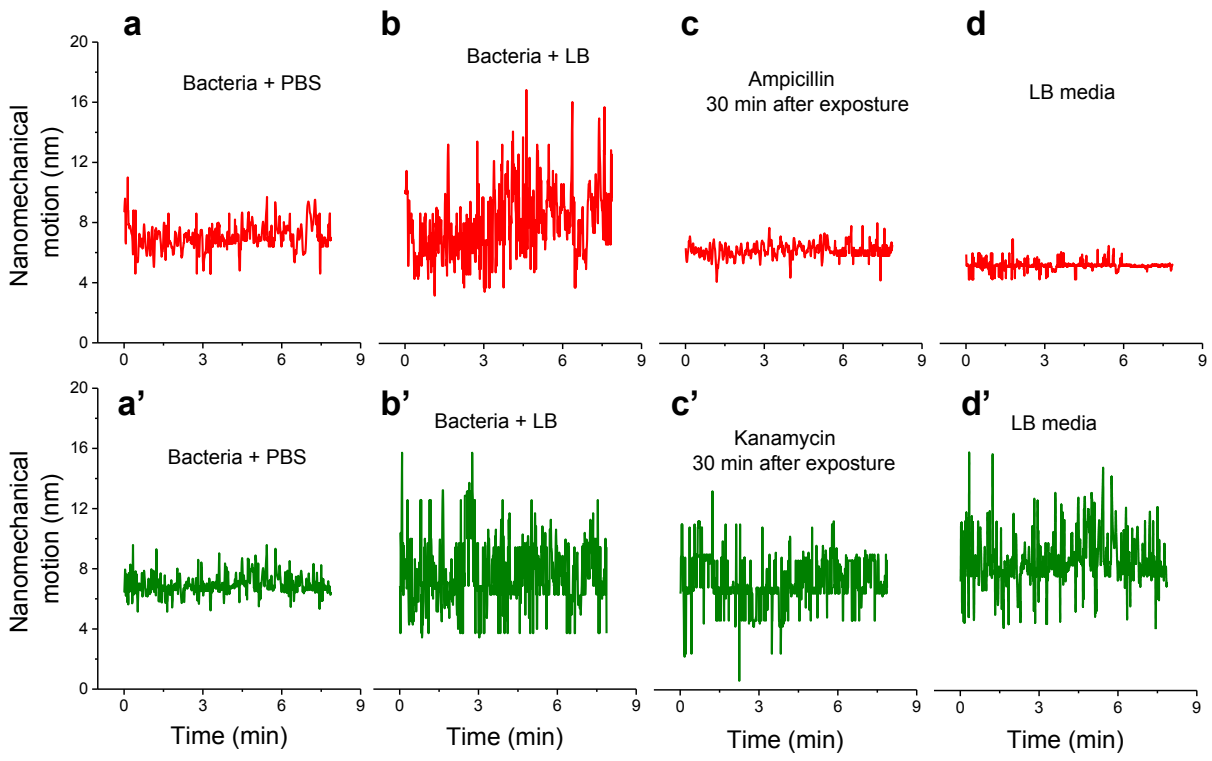

Figure 3-4| Nanomechanical fluctuation shows bacterial susceptibility to ampicillin (upper panel) and kanamycin (lower panel). (a, a') The results of bacteria in PBS; b,b' show the enhanced fluctuation due to the insertion of LB media into the bacteria. (c,c') The fluctuation after exposure to antibiotics, ampicillin and kanamycin, respectively (measurement was performed 30 min after the exposure). This suggests that the *E. coli* have been killed by ampicillin but that they resist the antibacterial effect of kanamycin. Removal of the antibiotic and re-introduction of LB media to the bacteria confirmed that bacteria exposed to ampicillin have been killed (d), while the *E. coli* exposed to kanamycin are alive (d')

To support this hypothesis and to investigate whether bacteria have been killed or placed in a dormancy state (a period in the bacteria life cycle when physical activities are temporarily stopped in order to survive unforeseen circumstances), we removed the drugs and re-introduced LB broth media (**Figure 3. 3 and Figure 3. 4**). As expected, the bacteria exposed to ampicillin were killed, showing a further decrease in cantilever deflection (**Figure 3. 3a**), an increase in the resonance frequency (**Figure 3.3a**) and a decrease in the vibrational noise (**Figure 3.4d**), compared to the bacteria exposed to kanamycin, which showed increase in deflection (**Figure 3.3b**), decrease in resonance frequency (**Figure 3.3b**) and an enhanced cantilever fluctuation

(**Figure 3.4d'**). A multivariate analysis of the nanomechanical IR spectra was carried out to determine the difference between intact and injured bacteria. **Figure 3.5** shows the second derivative transformation analysis of the nanomechanical IR spectra of *E. coli* placed in LB, exposed to ampicillin (**Figure 3.5a**) or kanamycin (**Figure 3.5b**), then further incubated with LB after removal of the drugs. The spectra (**Figure 3.5a and b**) showed unique IR absorption features for the bacteria exposed to ampicillin and kanamycin. As shown in **Figure 3.5**, the spectral data were processed by separating overlapping absorption bands and by removing baseline shifts, to show the difference between intact and injured bacteria. Also, analyzing the data using the principle component analysis (PCA) showed distinct clusters, corresponding to intact and injured bacteria (**Figure 3.5c**). These results show that bacteria exposed to ampicillin have been lysed (killed) while bacteria exposed to kanamycin are alive. The distinct differences in IR-nanomechanical spectra are arising primarily from the vibration of the molecular moieties on the bacterial cell wall (bands at 1451 cm^{-1}). Changes in the IR spectra of bacteria during exposure to ampicillin may originate from denaturation and/or redistribution of the cell contents. It is clear that exposure to drugs such as ampicillin (which causes rupture of the cell walls or cell membranes of the bacteria) and protein re-distribution may also result in unique spectral features. These results were further confirmed by confocal microscopy imaging (**Figure 3.5d**), which shows both live and dead bacteria (after exposure to ampicillin or kanamycin). In this experiment, the viability of the attached bacteria to the internal surface of the cantilever was evaluated by incubating the bacteria with life/dead stain for 10 min at 37 ºC. The live/dead stain contained two different fluorescent dyes, which stains live cells green while staining the dead cells red because the red pigment can only adhere onto damaged cell membranes. As indicated from **Figure 3.5d** and from bacteria counting analysis, most of the *E. coli* exposed to ampicillin were killed (red stained) while 75% of the *E. coli* exposed to kanamycin were alive (green stained). The results support the conclusion that BMC readout signals, including cantilever deflection, resonance frequency shift, nano-fluctuation, and the mechanical IR-bending, are associated with the viability and metabolism of the bacteria.

To verify the connection between the nanomechanical fluctuations of the BMC and bacterial metabolism, we introduced a media that supports bacterial metabolism, consisting of 5% glucose, and collected the BMC data (**Appendix Figure 11 and 12).** The drastic increase in the

nanomechanical fluctuations of the cantilever clearly supports the hypothesis of increased fluctuation with an active metabolic process of the bacteria. Responses of *L. monocytogenes* and *E. coli* DH5α, confined in the BMC to Leucocin A (a ribosomally synthesized AMP of class IIa bacteriocins), were comparable to those obtained with ampicillin. These results show that a BMC can be an ideal sensor platform for testing bacterial responses to a variety of drugs (**Supplementary Fig. 13**).

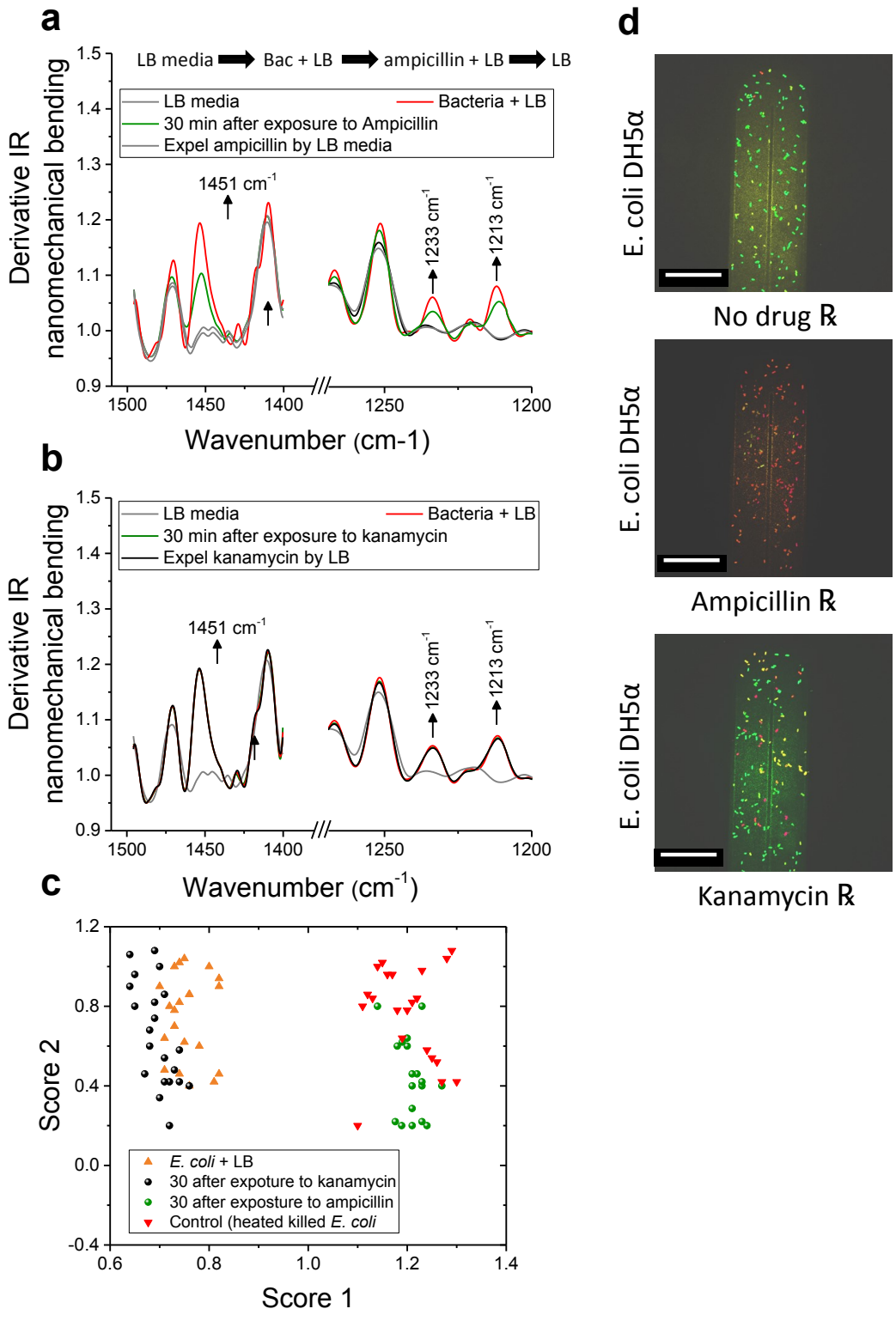

Figure 3-5| Nanomechanical infrared spectra of E. coli. Representative infrared second deviation analysis in the mid-infrared region for bacteria exposed to ampicillin (a) and kanamycin (b). The measurements were performed as indicated on top of the spectra, first LB media alone, followed

by LB bacteria, and the later addition of an antibiotic in LBþbacteria, and finally, exchanging the antibiotics with LB media. The infrared spectra were algorithmically preprocessed (binning, smoothing and second deviation transformation) to reduce the number of data points so as to eliminate noise. (c) Representation of the multivariate statistical analysis technique of principal component analysis (PCA), which selectively differentiates dead from intact bacteria after exposure to ampicillin or kanamycin, respectively. (d) Confocal microscopy images of the antibiotic–bacteria interaction inside the BMC were obtained (B30 min after exposure to drugs); a live/dead viability kit was used to stain living cells green and dead cells red. Images were taken using confocal microscopy (scale bar, 22 mm).

3.3.5 Discussion

The integration of photothermal infrared spectroscopy with a bimaterial microchannel cantilever – with its internal surface functionalized with receptors – overcomes the sensitivity and selectivity challenges presented by the real-time detection of bacteria and their interactions with antibiotics. By exploiting the semi-selective nature of the AMP from class IIa bacteriocins and the specific properties of mAbs, we were able to capture *L. monocytogenes* and detect it at very low concentrations, down to a single cell per μL. The BMC platform has also enabled us to monitor bacterial response to antimicrobials more closely when compared to existing approaches. The detection of resistant bacteria using the nanoscale motions of living bacteria exposed to ampicillin, kanamycin, and AMP are also demonstrated. In contrast to other bacterial monitoring tools, the BMC combines the selectivity of IR spectroscopy with the thermal sensitivity of the bimaterial cantilever to obtain the IR spectra of analytes in picoliters of samples. This nanomechanical IR spectroscopy, based on calorimetry, is complementary to that of the conventional IR spectra, which uses the Beer-Lambert law of counting photons for signal generation. However, heat-based nanomechanical spectroscopy is a direct technique for measuring IR absorption by a sample and since the mid-IR is free from overtones, this wavelength range is ideal for molecular recognition. In addition, the BMC is capable of measuring the mass density of analytes with high resolution and detects analytes, including bacteria, as they pass through the cantilever's microchannel. These BMC cantilevers can be mass-produced for low cost using conventional microfabrication techniques. Capturing the target analytes inside the channel by surface immobilization enhances sensitivity as well as selectivity. Since a BMC can support multiple orthogonal signal generation concepts, the technique is highly

versatile and has achieved better sensitivity, selectivity, and faster responses, when compared to other approaches such as the optoplasmonic nanosensor[218]. We anticipate that these IR integrated BMC sensors will be useful for a wide variety of applications, ranging from food and water analysis to drug discovery and testing pharmaceutical ingredients. In the near future, it will be possible to integrate sample separation techniques with BMC platforms to achieve the full potential of the lab-on-a-chip concept.

Chapter 4 . Real-time Detection of Breast Cancer Cells Using Peptide-functionalized Microcantilever Arrays

Etayash H, Jiang K, Sarfuddin A, Thundat T, Kaur K. Real-time Detection of Breast Cancer Cells Using Peptide-functionalized Microcantilever Arrays. ***Scientific Report***s, 5:13967 (2015)

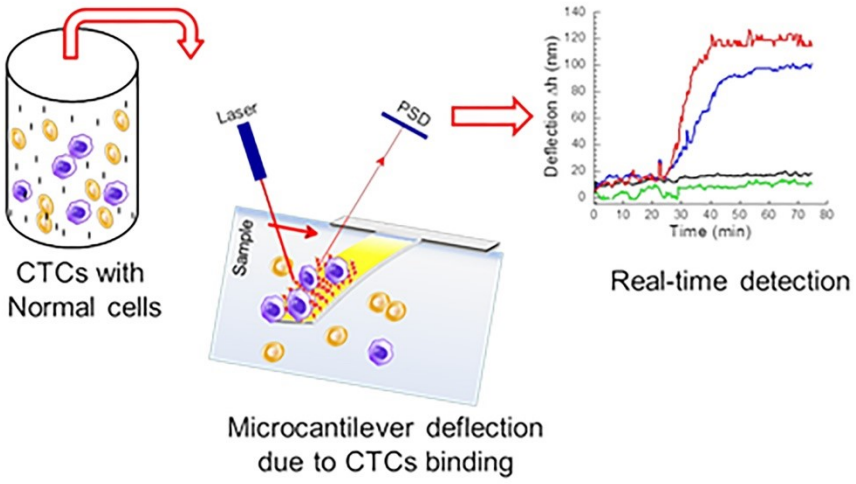

4.1 Introduction

In-vivo examinations of breast cancer is mainly implemented through techniques like mammography (an x-ray of the breast), ultrasound exams, magnetic resonance imaging (MRI) and/or [18F]fluorodeoxyglucose positron emission tomography, which are typically followed by ex vivo biopsy and further checkups.[235] A simple blood test to detect circulating tumor cells (CTCs) that flow in the bloodstream of cancer patients due to cell shedding from primary tumors could complement other detection methods for disease diagnosis. In recent years, molecular and clinical findings have revealed that cancer cells may invade into the blood circulation at early stages of tumor developments, putting an emphasis on the particular importance of sensitive and specific detection of CTCs in the blood.[78] Developing a sensitive and accurate tool for detection of CTCs would provide valuable information on cancer prognosis, diagnosis, monitoring of tumor sensitivity to anticancer drugs as well as in personalization of anticancer therapy. [78, 236]

Numerous approaches have been developed for reliably identifying and quantifying CTCs in blood samples.[237-242] The presence of CTCs or cancer cells in blood (~ hundreds per mL) is masked by normal blood cells that appear at a billion times higher concentration, making their detection challenging. The classical methods for isolation and enumeration of CTCs are time consuming and cannot be used for easy, routine screening to determine disease recurrence and response to treatments. Evolving technologies in the past few years have allowed identification and quantification of CTCs with applicable specificity and sensitivity. Methods such as the immunohistochemistry (IHC) [243], flow cytometry (FC)[244] and the polymerase chain reactions (PCR) [245] are very sensitive and compliant approaches for detections. However, with respect to their applicable use, they continue to suffer from numerous constrains such as the need for the trained cytologist to handle the sample assessments, time-consumption associated with the handling and pre-treatment procedures, as well as the cross-reactivity of the antibodies and nucleotides used during the detections.[77, 240] Other alternative label-free biosensing technologies to the classical approaches of CTCs detection are under developments, such as nanowire sensor[246], the graphene oxide nano-sheets [247], the electro-impedance cytometry [107] and microcantilevers. [150, 248-250] One platform based on the immunomagnetic beads conjugated with an antibody to EpCAM (CellSearch®, Veridex™, Warren, PA), is now clinically used for enumeration of CTCs from human blood samples.[19] Majority of these advanced detection

platforms rely on antibody and/or oligonucleotide probes for recognition, identification, and quantification of the target cells.

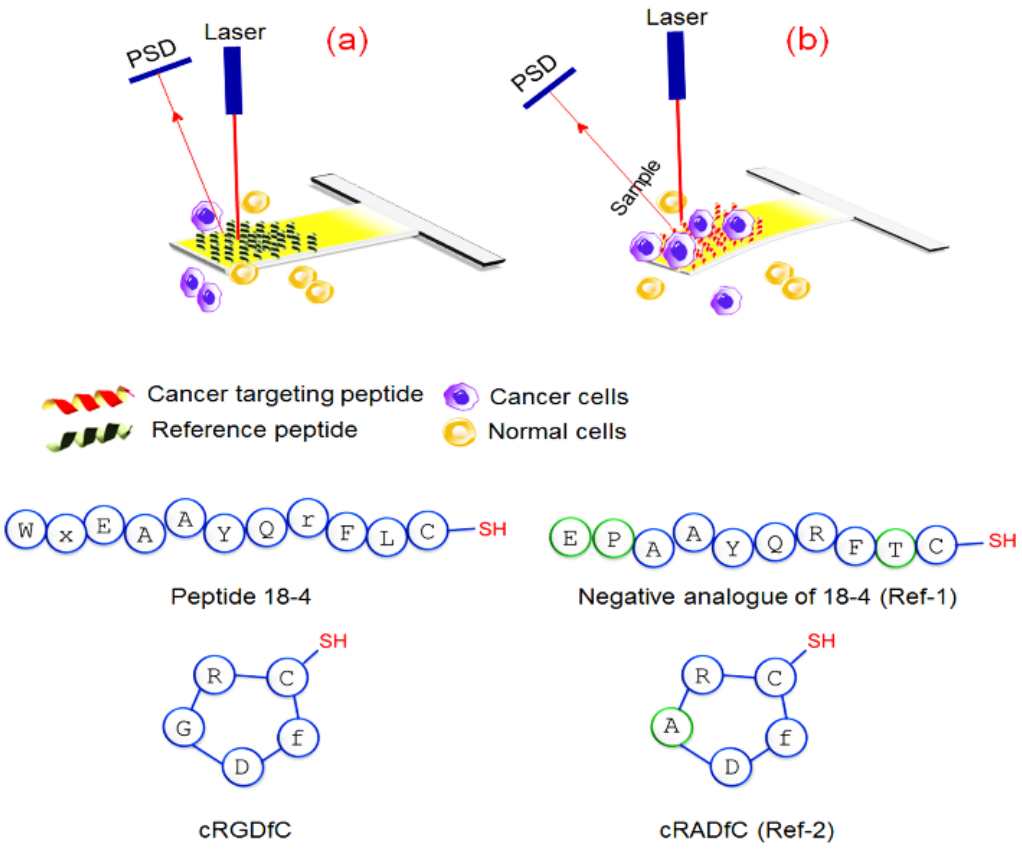

Figure 4-1| Schematic showing principle of microcantilever sensor operation. (a) Microcantilever coated with non-specific reference peptide (Ref-1 or Ref-2) shows no response to the presence of normal or cancer cells (no deflection). (b) Microcantilever functionalized with cancer targeting peptide (18-4 or cRGDfC) demonstrates a strong response (deflection) to cancerous cells due to peptide-cancer cell interactions. PSD, Position Sensitive Detector

In this study, we report the development of a peptide-based microcantilever array sensor for efficient capture of intact representative cancer cells at low concentrations without pre-requisite labeling or sample processing (**Figure 4.1**). The microcantilever array was functionalized separately with two cancer targeting peptides, namely, a decapeptide **18-4** (WxEAAYQrFL) with an additional C-terminal cysteine or a cyclic RGD peptide (cRGDfC) [135] using the thiol group of cysteine residue. Peptide **18-4** is a proteolytically stable engineered breast cancer targeting

peptide derived from a 12-mer peptide p160 that was identified using in vivo phage display for cancer targeting. [251, 252, 23] Peptide **18-4** exhibits high affinity for breast cancer cell lines (MCF7, MDA-MB-231, and MDA-MB-435), most likely through a receptor-mediated mechanism, with almost no binding to the noncancerous cells (MCF10A and HUVECs). RGD is a well-studied tumor homing peptide that interacts with specific integrin receptors (αvβ3) overexpressed on several tumor epithelial cells.[253-255] However RGD also targets non-tumorigenic tissues as it is recognized by several integrins (8 out of 24 heterodimers) and is therefore deemed less specific. To explore whether cancer cells can be selectively captured with these peptides, breast cancer cells (MCF7 or MDA-MB-231) alone or in combination with non-cancerous MCF10A (derived from the same breast tissue as MCF7) were spiked into a buffer or blood solution to obtain mimics of CTCs in human blood. The cancer cells were detected by recording the nanomechanical bending of the cantilevers in real-time based on the surface stress induced by adhesion of the cancer cells to the immobilized peptides.

4.2 Methods

4.2.1 Peptide Design and Synthesis. Two cancer-targeting peptides, peptide **18-4** (WxEAAYQrFLC) and cRGD (cyclicRGDfC) and the corresponding negative control peptides, Ref-1 (XEPAYQRFTC) and Ref-2 (cyclicRADfC) were used in this study. In each peptide an additional cysteine residue has been added at the terminus in order to enable adequate anchoring to the cantilever gold interfaces and the SPR gold chips through the well-known gold-thiol chemistry immobilization method[135, 187] Peptides were synthesized chemically using standard N-Fmoc solid phase peptide synthesis as described previously[21]. Briefly, the first amino acid was coupled into a 2-chlorotrityl resin (NovaBiochem, San Diego, CA) at 5-fold excess using the N,N diisopropyl ethylamine (DIPEA) at room temperature. Further amino acids were added automatically using an automated peptide synthesizer (Tribute, Protein Technology, Inc., USA). The completed peptide was ultimately released from the resin with a mixture of 90% trifluoroacetic acid (TFA), 9% dichloromethane (DCM), and 1% triisopropylsilane (~10 mL) for 90 min at room temperature. The cleaved peptide combined with TFA was then concentrated, washed with diethyl either, dissolved in water and purified using reversed-phase HPLC (**Appendix Table 1**).

4.2.2 Microcantilever Sensor Preparation. Microcantilever arrays (Concentris GmbH – Switzerland) of eight gold-coated cantilevers (500 μm long, 100 μm wide and 1 μm thick) were used in the experiments. The apex – top gold surfaces of the cantilevers (20 nm gold thickness) were functionalized with our designed thiolated peptides following the procedure described for gold-thiol chemistry immobilization[135, 187]. Briefly, cantilevers were cleaned with Piranha solution (30% H_2O_2:96% H_2SO_4, vol/vol) for 15 minutes, rinsed three times with MilliQ-water (18 MW) followed by ethanol, and dried in air. The arrays were incubated in 2-[methoxy(polyethyleneoxy)propyl]trimethoxysilane (10 mM, Gelest Inc. Frankfurt, Germany) for 20 minutes, rinsed with ethanol and dried in air in order to make the backside of the levers inert and reduce nonspecific binding to the silicon side. Subsequently the microcantilevers were coated with the peptides of interest. In order to make sure that only cantilevers tips were functionalized with the peptide, only the tips were dipped-in the peptide solution (1 mg/mL) and kept for 6 h; the process was also repeated once to ensure an adequate peptide coupling to the cantilever surface. Prior to use, the arrays were rinsed with 70% ethanol and copious amount of PBS solution to remove any physically adsorbed materials.

4.2.3 **Cantilever Setup and Deflection Detection.** All cantilever experiments were carried out using an in-house built microcantilever array sensor **(Appendix Figure 14)**. Briefly, the cantilever setup consists of a fluidic cell within which the functionalized cantilever array was mounted. The cell is attached to an inlet port connected to a syringe pump for introduction of the sample and an outlet port which is attached to a fluid reservoir. To detect cantilever deflections, a low-power (~1 mW) laser beam was reflected off the free-end of the cantilever and was focused onto a position sensitive detector (PSD Thorlabs. Inc. New Jersey, USA). Data from nano-mechanical cantilever deflections were recorded in real-time using a multifunctional data-acquisition board driven by LabView-based software. The functionalized cantilever array was initially placed in the fluidic cell and equilibrated in running phosphate buffered saline (PBS) at a constant flow rate of 5 mL h^{-1} until a stable baseline was achieved. It was then exposed to running PBS solution for approximately 50 scans followed by flow of sample solutions containing cancer cells. An optimum flow rate for detection was determined by exposing the peptide **18-4**-functionalized cantilever to a solution of cancer cells at various flow velocities. The results led us to select a flow rate of 1-2 mL h^{-1} for all our subsequent experiments. The

experiments were performed for four different peptides as indicated in the text and four different cell lines including the non-cancerous control cells.

4.2.4 Cell Culture. The human breast cancer cell lines MCF7 and MDA-MB-231 (American Type Culture Collection, Manassas, VA) were cultured in DMEM medium containing 10% fetal bovine serum (FBS), 100 IU mL^{-1} penicillin, and 100 IU mL^{-1} streptomycin. The human mammary epithelial cell line MCF-10A was cultured in minimal essential growth medium (MEGM, Lonza, Cedarlane) supplemented with the same additives as mentioned before. Human umbilical vein endothelial cells (HUVEC), kind gift from the laboratory of Sandra Davidge, University of Alberta, were cultivated using endothelial cell growth medium (EGM, Lonza, Cedarlane) containing 20% FBS, 2 mM L^{-1} glutamine, 100 IU mL^{-1} penicillin, 100 IU mL^{-1} streptomycin, and 2 ng/mL basic fibroblast growth factor (Roche Diagnostics, Mannheim, Germany). All cell lines were cultivated at 37 °C in a 5% CO_2 – 95% O_2 incubator, and growth media were replaced every 48 h.

4.2.5 Cantilever and Cell Capture Assay. For running the cantilever assay and performing the capture efficiency experiments, cells were diluted in serum-free medium, starting at an initial concentration of 10^3 mL^{-1} determined by a hemocytometer. Subsequently the cells were centrifuged at 500 rpm, and re-suspended in phosphate buffered saline (PBS, 1 mL). Cells were aliquoted into a low-attachment 96-well plate to obtain a serial dilution of cells ranging from 100 - 5 cells mL^{-1} in each well (optical microscopy was used for cell counting). Mixed cells samples were obtained by following the same protocol, where aliquots of MCF7 and MCF10A were mixed to give final ratios of 25:75, 50:50, and 75:25 for MCF7:MCF10A with 100 cells mL^{-1} in each well. Before the cell capture assay, MCF7 cells were stained with fluorescent dye (CyQUANT, green – Life Technologies Inc., Burlington, ON, Canada) following the manufacture's protocol, washed with PBS, centrifuged and re-suspended at 100 cells/mL in PBS solution. The sample with seeded cells was then introduced into the cantilever sensor after calibrating the baseline with PBS solution for ~ 20 min. After taking the deflection reading the cantilevers were scanned by a fluorescence microscope (Olympus America, Melville, NY, USA) and sets of images corresponding to the captured cells were taken at different positions. The images were imported and cell numbers were computed using ImageJ software package. The

capture efficiency was defined as the ratio of the number of target cells captured to the number of target cells initially seeded.

Human blood samples were collected from healthy donors with informed consent and in accordance with the approved guidelines by the University of Alberta. All experiments were performed following protocols as approved by the ethics committee. All samples were collected in EDTA tubes and were processed within 3 h. Blood without plasma sample was prepared by spinning a tube of a fresh blood containing anticoagulant in a centrifuge at 2000 rpm for 10 min until the blood cells fall to the bottom of the tube.[54] The blood plasma as a supernatant was drawn from the tube and the remaining sediment was suspended in PBS. Before each injection into the cantilever system, the samples (whole blood or the blood without plasma) were diluted to 10% concentration in 1x PBS solution, spiked with various concentrations of MCF7 cells (25, 50, and 100 cell mL-1) and subjected to nanomechanical reading. The capture yield was determined as discussed above.

The MCF7 and centrifuged white blood cells (from 1 mL blood) were stained green and red, respectively, suspended in PBS solution (1 mL) and injected to the cantilever device. Note that in order to get the red probe (propidium iodide) inside the WBCs, the hematological cells were incubated with the stain for ~ 1 h at room temperature. Captured cells were then examined using fluorescence microscopy at 20x magnification and excitation wavelength of 488 nm (CyQUANT) and 543 nm (propidium iodide). The emitted fluorescence was detected through spectral detection channels between 500−530 nm and 555−655 nm for green and red fluorescence, respectively. Capture efficiency was defined as mentioned above.

4.2.6 SPR Measurements. Surface Plasmon Resonance (SPR) measurements were carried out using a SRP Navi 200 instrument (BioNavis Ltd., Tampere, Finland) that uses the Kretscheman prism configuration having a goniometer with dual flow channels and cohesive peristaltic pump with 100 μL sampler loops. Briefly, the experiments were performed in angular scan mode in order to determine the SPR angular position changes in a real-time. The critical angle of total internal reflection was measured as the reflection index changes due to the surface absorption on the chip. A flow rate of 10 μL min^{-1} was used throughout the experiments with a sensor temperature fixed at 25 ºC. A laser with a wavelength of 670 nm was used as a light source to excite the surface plasmon at the dielectric gold interface. A freshly cleaned gold-coated SPR

chip (50 nm gold, 5 nm Titanium adhesion layer) was functionalized with peptide **18-4** by immersing in peptide/PBS solution (1 mg mL^{-1}) for 12 h at room temperature. The measurements started by introducing the peptide chip into the sample holder and running 1x PBS solution at a 7.4 pH to stabilize a baseline. Two Samples of PBS (1x) solution, containing cancer cell line MCF-7 (100 cell mL^{-1}) or the corresponding normal cell line MCF-10A were injected separately through the flow cell. A continuous scan was performed on a liquid range of 50-77º and the recorded data were processed using the BioNavis software package.

4.2.7 Statistical Analysis. For all the experiments, signals of identically functionalized cantilevers were averaged and each experiment was performed at least three times. All data are presented as mean ± SD of the calculations throughout the manuscript. The statistical difference was tested either using the unpaired t-test or the one way ANOVA test as specified.[55] In all statistical analysis the significance level (*P* value) was set at 0.05.

4.3 Results and Discussion

4.3.1 Functionalization of Microcantilevers. Microcantilevers in an array were functionalized with self-assembled monolayers (SAMs) of cancer cell binding peptides, which can act as specific ligands for cancer cells. As illustrated in **Figure 4.1**, the detection principle is based on static mode of cantilever operation, which means that cantilever beam bends as a result of changes in the surface stress generated by analyte-ligand interactions.[127] Specifically in this study, selective adsorption of the cancer cells to the immobilized peptide on the surface of the cantilevers results in a decrease in the surface free energy which in turn leads to generate a differential surface stress between the functionalized and non-functionalized sides of the lever. This differential surface stress causes cantilever to deflect or bend by a certain extent that can be expressed according to Stoney's formula[27]. An in-house built microcantilever array sensor was used for the cantilever experiments **(Appendix Figure 14)**.

One of the essential parameters that determine the efficiency of the cell capture on the microcantilever system is the flow velocity of the sample throughout the system.[256] Therefore, in order to optimize the flow rate, a number of experiments were conducted to determine the sensor capture efficiency at different flow velocities. We spiked cancer cell lines (MCF7) into

phosphate buffered saline (PBS) at ~100 cells mL^{-1} and dispensed on a peptide (**18-4**) coated microcantilever array as a function of flow rates ranging from 1 to 5 mL h^{-1}. The capture yield was calculated for each flow rate and results were charted as shown in **Appendix Figure 15**. We found that the estimated capture efficiency increased by decreasing the flow velocity of the samples, indicating an inverse proportion of the capture yield to the sample flow velocity. The capture yield was significantly enhanced at 1 mL h^{-1} flow rate (81%) compared to that at faster flow rate of 5 mL h^{-1} (54%). Based on these results that suggest enhanced binding of the cancer cells to the immobilized peptide with increased incubation time, the subsequent studies were performed using a flow rate of 1-2 mL h^{-1}.

4.3.2 Cancer Cell Binding to the Peptide-functionalized Microcantilevers. First, we aimed to assess and compare the binding efficiency of the designed peptide-based microcantilever sensor (peptide **18-4** sensor) to other peptide-sensors including cRGDfC sensor against the human adenocarcinoma breast cell line MCF7, which is a good mimic for circulating breast tumor cells in human blood. The thiolated peptides **(Appendix Table 1)** were chemically synthesized and independently immobilized on cantilever beams in arrays using the tip-dipping method as described in the material and methods section. Cancer cells were spiked into PBS (25 cells mL^{-1}, pH ~7.4) and were allowed to flow through the microcantilever array. Reference cantilevers functionalized with control peptides were treated with the same concentration of cancer cells and subjected to nanomechanical readings for comparisons. Results of the analysis revealed significant beam deflection for peptide **18-4** functionalized sensor with approximate deflection of 120 ± 7 nm achieved after sample introduction (**Figure 4.2a**). The deflection, however, showed to be slightly less in case of cRGDfC functionalized array with a deflection distance of 102 ± 3 nm. Compared to the peptide **18-4** and RGD sensors, the reference cantilevers (Ref-1 and Ref-2) exhibited insignificant bending when subjected to the cancer cells, indicating weak binding properties of the control peptides.

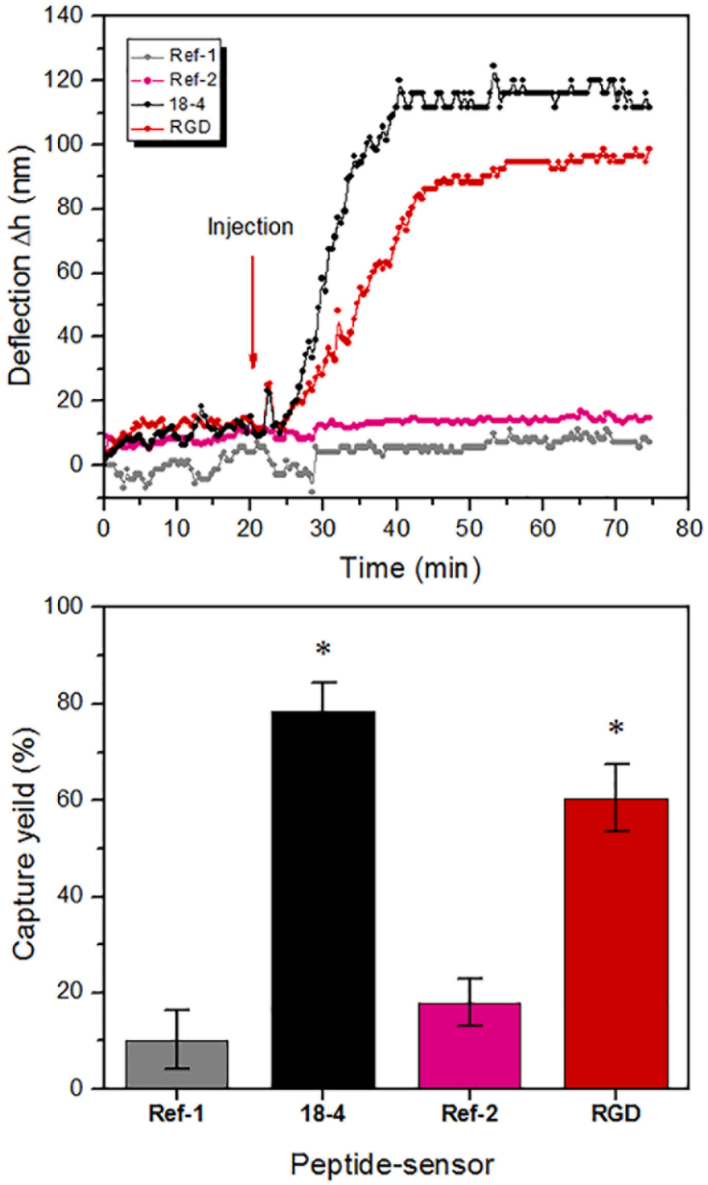

Figure 4-2| Label-free real time detection of cancer cells using peptide-functionalized cantilever array. (a) Real time detection of MCF7 human breast cancer cells mimicking the circulating tumor cells at 25 ± 5 cells mL^{-1} using peptide-functionalized cantilever array. Cantilevers were functionalized with four different peptides, two cancer-targeting peptides (18-4 and RGD) and two non-specific reference peptides (Ref-1 and Ref-2). (b) Capture yield of cancer cells corresponding to each peptide sensor. Each cantilever differential deflection represents an average calculation of eight replicates and error bars indicate standard deviations, *P < 0.05

.

Further insight on the peptide binding efficiency to cancer cells was gained by estimating the capture yield of cancer cells of each peptide sensor. **Figure 4.2b** displays the capture yield (%) of the peptide cantilever sensors in contrast to the reference cantilevers. The calculated capture efficiency was found to be around 80 ± 4 % in the case of peptide **18-4** sensor and almost 60 ± 6 % for cRGDfC sensor. In contrast to the sensing peptides, the reference cantilevers showed only 14–19 % for both Ref-1 and Ref-2. The cantilever results demonstrated that peptide 18-4 sensor has better binding affinity to cancer cell lines than the cRGDfC sensor. These results match well

with the previous studies of peptide array whole cell binding assay for screening of cancer targeting peptides using fluorescence microscopy. [251, 252]

4.3.3 Specificity of Peptide-functionalized Microcantilevers. In order to determine the specificity of the designed sensor, we applied the peptide **18-4** functionalized cantilever array to distinguish between cancerous and non-cancerous cell lines in real-time **(Figure 4.3)**. Here the binding affinity of the peptide sensor was explored against two types of breast cancer cell lines, namely, MCF7 and MDA-MB-231 and two non-cancerous cell lines, MCF10A and HUVEC. MCF10A are non-cancerous cells derived from the same human mammary tissue as MCF7, whereas HUVEC endothelial cells are isolated from normal human umbilical vein. When cells were injected at a concentration of 100 ± 10 cells mL^{-1} separately to each peptide cantilever, the cantilever showed significant deflection for cancerous cell binding (280 ± 25 nm) compared to non-cancerous cell binding (90 ± 15 nm, **Figure 4.3a**). The variation in cantilever deflection upon binding cancerous or noncancerous cells is most likely due to the differential expression levels of specific peptide-binding receptors present in cancerous and noncancerous cells. We and others have shown that peptide **18-4** and the original lead peptide p160 enter cells by a receptor-mediated endocytosis.[21,23] The receptor is not known yet, however, it is clear that the receptor is overexpressed in breast cancer cells compared to normal cells. The results confirm our conjecture that peptide **18-4** binds breast cancer cells with high specificity. Previously we showed that a similar peptide, peptide **18** (WXEAAYQRFL), binds MDA- MB-435 breast cancer cells with an apparent K_d of 41.9 μM. [252]

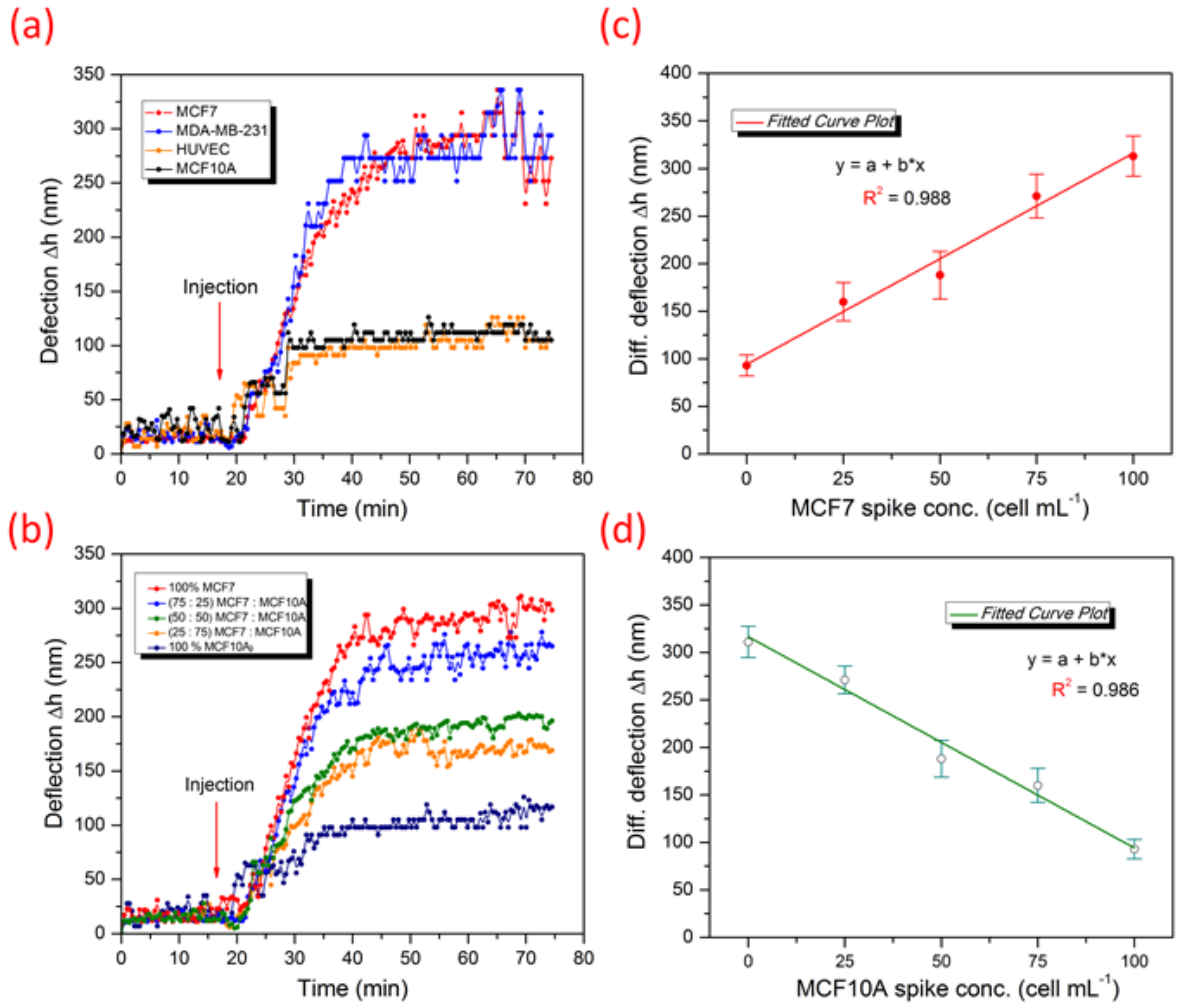

Figure 4-3| Specific binding of peptide-cantilevers to breast cancer cells. (a) Label-free real time recognition of cancer cell lines (MCF7 or MDA-MB-231, 100 ± 10 cells mL^{-1}) from non-cancerous cell lines (MCF10A or HUVEC, 100 ± 10 cells mL^{-1}) with microcantilever array functionalized with **18-4** cancer targeting peptide. (b) Cantilever deflection in response to a function of different concentration ratios of cancerous to non-cancerous cells (MCF7 to MCF10A) in PBS solution as indicated. (c) and (d) demonstrate the concentration dependence of cantilever response to the number of cancerous or non-cancerous cells, respectively, present in the co-culture sample (100 cells mL^{-1}). The representative graphs show an increase in cantilever deflection with an increase in the number of MCF7 cells (c), and a decrease in cantilever deflection with an increase in the number of MCF10A (d) in the media. Each cantilever differential deflection represents an average calculation of eight replicates and error bars indicate standard deviations.

Thi

s finding highlights that such tumor binding peptides are not only useful for tumor imaging or targeted drug delivery, but can also be useful as recognition elements to develop peptide-based biosensor platforms for cancer cell detection in real-time. In recent years, several studies have explored the feasibility of using short-ligand peptides as molecular recognition elements in biosensing techniques and have validated the ability of natural and synthetic peptides to serve as robust biorecognition probes in biosensors.[110, 164, 257, 258] We have recently shown that an antimicrobial peptide from class IIa bacteriocins can be used for the detection of Gram-positive *L. monocytogenes* at 1 bacterium μL^{-1} using impedance spectroscopy [259]. Furthermore, Mannoor *et al*. showed bio selective recognition of pathogenic bacteria at a single-cell level using peptide assembled onto a wireless graphene nanosensor[186]. Here we have employed a cancer-targeting peptide, engineered from a phage display library and synthetic peptide array library for breast cancer cell binding, as a sensing molecule to detect cancer cells in a cantilever array for the first time.

The differential deflection of the peptide microcantilever sensor to cancer cells was also explored by injecting samples with different ratios of cancer cells (MCF7) to noncancerous (MCF10A) cells. **Figure 4.3b** demonstrates cantilevers deflection after injection of cancer cells only (100 cell mL^{-1}) as well as after dilution with MCF10A (MCF7:MCF10A; 1:0, 3:1, 2:2, 1:3, 0:1). The cantilevers selectively responded to MCF7 cells and showed amplitude of deflection proportionally scaled with concentration of the MCF7 cells in the sample (**Figure 4.3c**). In a co-culture of cancerous and noncancerous cells, the cantilever was able to detect cancer cells in the presence of ~ 75% normal cells (MCF10A). Similarly, as the concentration of normal cells was increased, the deflection signal decreased (**Figure 4.3d**) indicating the ability of peptide probes to discriminate between cell types. The results suggest that the presence of normal cells (MCF10A used here) does not prevent cancer cells from binding to the immobilized probes; it might however, impede their transportation to the sensor probes at lower concentrations dropping the limit of detection. Non-specific binding, sample delivery and improper cell dispersion (mixing) may also contribute to reduced capture sensitivity. [260]

Peptide **18-4** binds to breast cancer cells most likely via a receptor-mediated mechanism.[252] We attribute the variation in cantilever responses between cancerous and non-cancerous cells to the presence of different receptors or different expression levels of a specific receptor on surface of

cancer cells. It is well known that certain receptors or/markers are over expressed on cancer cells and deficient in the normal ones [261, 262], and such receptors are being targeted for diagnosis and drug delivery using different types of ligands such as antibodies, aptamers, affibodies and peptides.

The sensitivity of detection is one of the key features for practical application of the sensor in medical and biological applications. To this end, the sensitivity of the peptide based cantilever array was determined by exposing the sensor to various concentrations of cancer cells (MCF7) spiked in PBS ($5\pm3 - 10^3 \pm 10$ cell mL^{-1}) (**Appendix Figure 16**). The results showed the ability of sensor to detect as low as 25 ± 5 MCF7 cells per mL in pure buffer solution from the background deflection (baseline). The signal, however, was not distinguishable from the background at lower concentration, suggesting a minimum detection limit of 25 cells per mL. Several studies have shown that biosensor performances are often affected by the analyte transport in the vicinity of the sensing area[256, 263] as well as dispensing of the cells in the microfluidic system.[260, 263] Therefore in flow through systems like microcantilevers, it is possible to achieve a low detection limit by controlling the fluid delivery with a proper mixing regime. In addition, cantilever with a continuous fluidic flow allows analysis of relatively large sample volumes with few CTCs, thereby improving the detection limit, as opposed to other detection methods with fixed sample volumes.

4.3.4 Cancer Cell Binding using Surface Plasmon Resonance. In order to validate microcantilever results, surface plasmon resonance (SPR) was utilized to study the specific recognition of cancer cells by surface immobilized cancer targeting peptides. SPR is routinely used as a standard characterization tool for bimolecular interactions and serves as a complementary transduction method to the piezoresistive microcantilever system.[40] SPR is a highly sensitive method, however, piezoresistivity, the change in electrical resistivity under stress or deflection is a simple method that eliminates the complexity inherent to optical instruments such as SPR without the loss of sensitivity. The ligand peptide **18-4** was covalently immobilized on SPR gold slide using the thiol chemistry as described above. The peptide functionalized slide was inserted into the instrument and PBS solution was allowed to flow at a constant flow rate of 10 μL min^{-1}. SPR slide functionalized with a reference peptide (Ref-1) was used at the same time on another SPR channel for comparison. The sensor selectivity to the

target cells was measured by SPR reading after injecting samples of cancerous (MCF7) and noncancerous cells (MCF10A) simultaneously at a concentration of 100 cells mL^{-1}. **Figure 4.4a** displays a typical SPR spectrum illustrating responses of the SPR sensor functionalized with peptide **18-4** or Ref-1 to MCF7 or MCF10A cells. A sharp SPR signal was generated for specific interaction between the peptide **18-4** sensor and MCF7 cancer cells compared to the other signals. A low response was observed for peptide **18-4** binding to MCF10A cells followed by similar response signals by the reference sensor to both MCF7 and MCF10A cells. The responses, however, are likely related to non-specific interactions with the sensor surface since no clear differentiation exists between the two cell lines. In agreement with the cantilever results, peptide **18-4** SPR sensor exhibited highest signal to MCF7 cells indicating a specific interaction to the corresponding cells and confirming the applicability of the assay to distinguish between cancerous and noncancerous cells in real-time.

The sensitivity of the peptide functionalized SPR sensor was evaluated by injecting serial concentrations of MCF7 cancer cells (5±3 to 100±10 cell mL^{-1}) to the peptide **18-4** sensor at a fixed flow rate of 10 μL min^{-1}. **Figure 4.4b** shows a representative SPR spectrum where an increase in SPR intensity was observed with an increase in concentration of the injected MCF7 cells. Similar to the microcantilever studies (**Appendix Figure 16**), the number of cells bound to the immobilized ligand is directly proportional to the number of cancer cells in the sample, up to a maximum of ~500 cell mL^{-1}, where the saturation takes place.

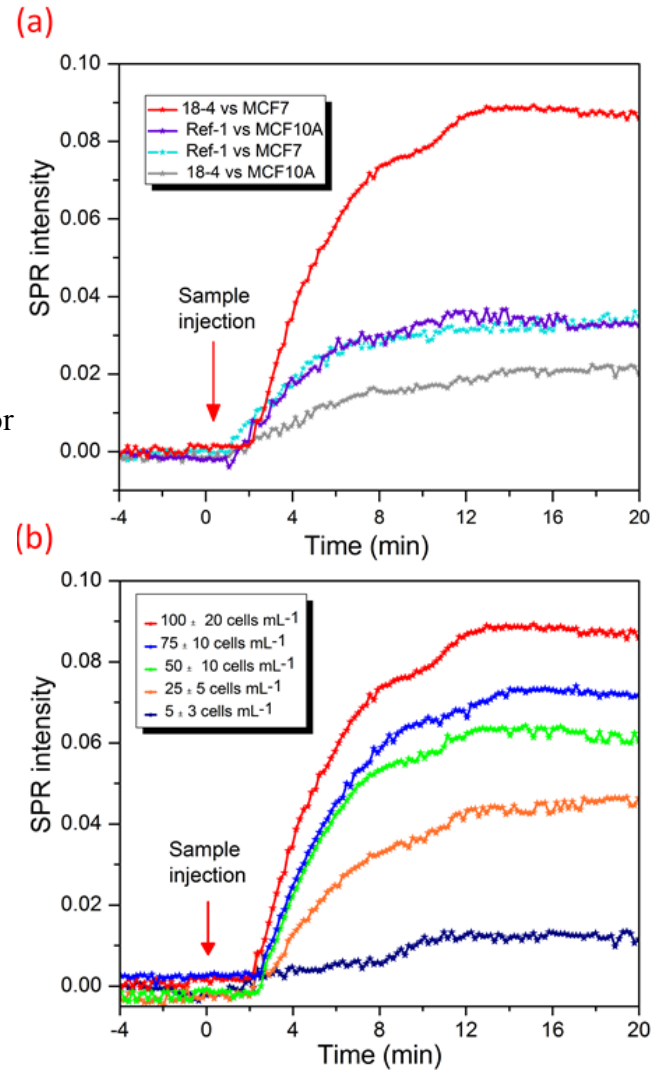

Figure 4-4| Direct discernment of cancer cells from non-cancerous cells by a peptide-based SPR sensor. (a) SPR intensity signal resulting from interaction of 18-4 functionalized SPR chip (or functionalized with reference peptide) with MCF7 or MCF10A cells. (b) SPR sensitivity spectra for peptide 18-4 against various concentrations of cancer cells (MCF7) at a constant flow rate of 10 μL min^{-1}.

4.3.5 Cancer Cell Detection in Whole blood Samples. To mimic the detection of CTCs from patient blood samples, the designed peptide-based microcantilever were exposed to MCF7 cells spiked in human blood samples. First, the blood was made less viscous by diluting it with buffer solution (90%) in order to facilitate the injection and diminish the viscosity effects. In addition, to enhance the sensitivity, the plasma was removed from the blood by centrifugation. Plasma is routinely removed from the blood for CTC enrichment from whole blood.[41,42] Subsequently, blood or blood without plasma spiked with different concentrations of MCF7 cells (25, 50 or 100 cells/mL) was allowed to flow over the peptide **18-4**-cantilever. The cantilever system was initially equilibrated by injecting the blood sample (with or without plasma), followed by injection of MCF7 spiked blood. This was done to clearly observe the deflection after introduction of the spiked blood. Instead when the system was equilibrated by injecting PBS,

followed by blood and then spiked blood, the deflection due to spiked blood was less apparent (Figure S4). We envisage the patient samples can be run in the clinics by equilibrating the system with normal human blood followed by injection of the patient blood in the cantilever flow through system to obtain a clear read out. **Figure 4.5** shows the differential deflections of microcantilever arrays after injecting the blood (**Figure a-b**) or blood without plasma (**Figure c-d**). An increase in cantilever deflection was observed with an increase in number of MCF7 cells in the sample. Both the MCF7 spiked blood samples, whole blood or blood without plasma, showed a substantial deflection compared to the MCF7 free specimens at a concentration of 100 ±10 cancer cells/mL. Blood without plasma showed higher response (87±10 nm) compared to whole blood sample (62±10 nm). In addition, for the blood without plasma specimen (**Figure 4.5d**) the nanomechanical bending was significant (40 ±10 nm) even at 50 ±10 cancer cells/mL, suggesting interference from plasma components such as proteins and other interfering biomolecules.

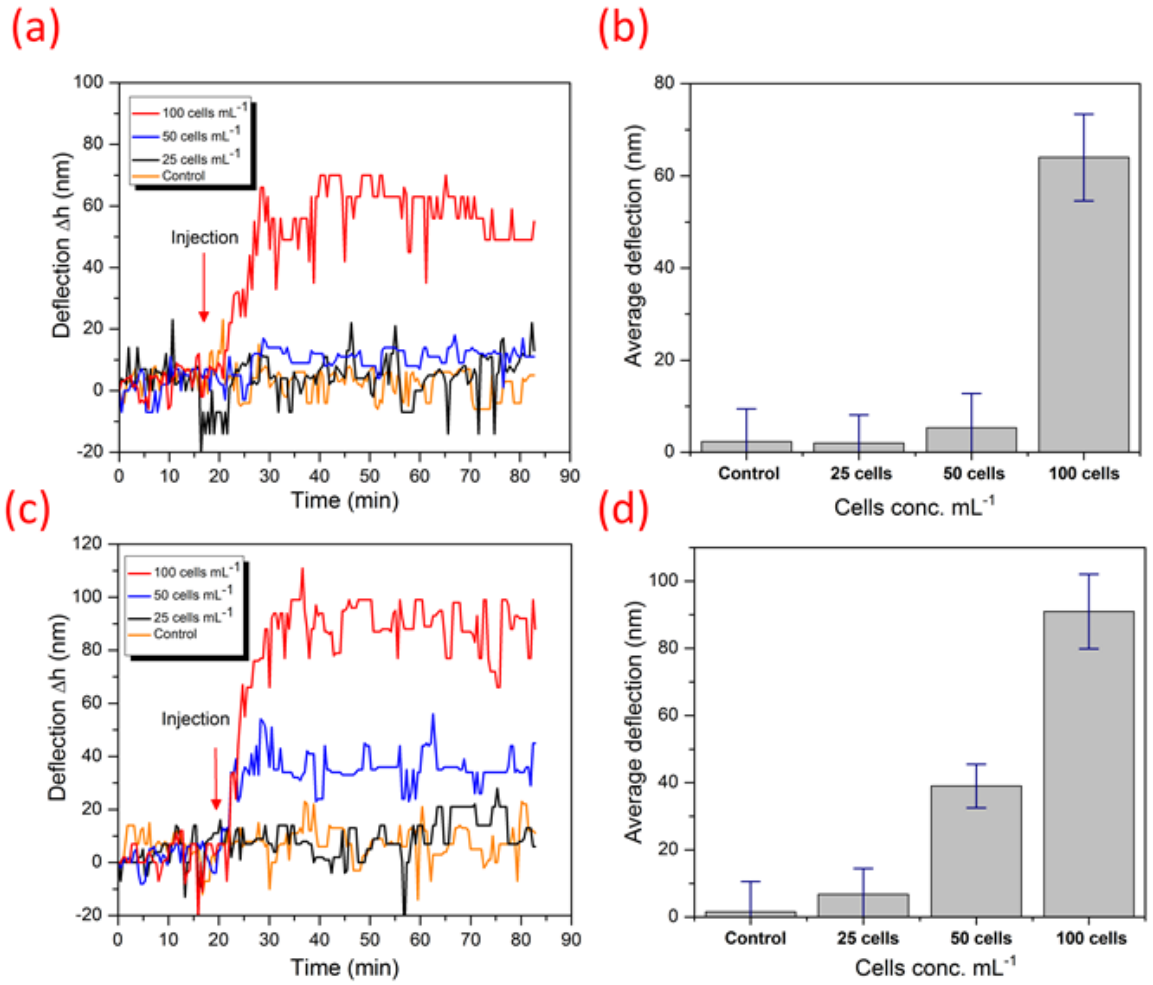

Figure 4-5| Differential deflection of microcantilever arrays with MCF7 spiked into human blood samples. (a) Top figure shows results from injection of whole blood, whereas (c) lower figure shows data from injection of blood without plasma, both spiked with MCF7 cells. The system was first equilibrated by injection of blood samples, free from MCF7, followed by injection of MCF7 containing 25, 50 or 100 cancer cells/mL. The control represents the response of a negative analogue of peptide 18-4 to ~100 cells mL-1 spiked samples. Figures (b) and (d) show the average deflection of peptide 18-4 coated cantilevers in both, whole blood and blood without plasma, respectively, based on three individual studies performed under the same conditions. The error bars indicate corresponding standard deviations.

Further, we examined the cancer cell capture from whole blood samples using fluorescence microscopy with comprehensive image analysis. MCF7 and white blood cells (WBCs) in blood samples were fluorescently labeled green and red, respectively, followed by injection into the cantilever. The eight microcantilevers were exposed to two spike cell concentrations, 50 or 25 cells/mL of blood at 2 mL/hour (**Figure 4.6a**). The captured cells were imaged using fluorescence microscopy. **Figure 4.6b** shows images of two of the eight cantilevers with captured MCF7 and hematological cells (WBCs). While the control peptide cantilevers captured almost no cancer cells, the peptide 18-4 cantilevers captured 5 ± 2 MCF cells/cantilever. Overall, the average number of captured MCF7 cells per 8 cantilevers, when seeded at a concentration of ~50 cell/mL, was found to be 40 ± 5 cell/mL for the peptide **18-4** coated sensor which is significantly higher than the control sensor (5 ±2 cell/mL). These results are statistically significant as specified using the unpaired student t-test (P=0.008). In contrast, at seeded concentration of 25 cancer cells/mL, poor significant difference was observed for the peptide **18-4** sensor compared to the control sensor (P=0.056; *n*=5). From the optical images of single cells (MCF7) bound to microcantilevers, we can clearly see the results correlate reasonably well with the cantilever deflection measurements (**Figure 4.2b**). An increase in bound cancer cells was observed with an increase in its seeded concentration. At 50 cells/mL, high capture efficiency (80 ± 5%) was achieved using peptide 18-4 functionalized microcantilevers. It is interesting to note that a similar capture yield (80%) was obtained for MCF7 cells present in PBS (Figure 2b) or whole blood samples (Figure 6c), whereas the cantilever deflection was decreased when MCF7 cells were present in whole blood (Figure 5a) compared to when present in PBS (Figure 2a). This is likely due to the higher baseline deflection for the spiked whole blood sample, where other biomolecules from the blood bind to the peptide cantilever before cancer cell binding.

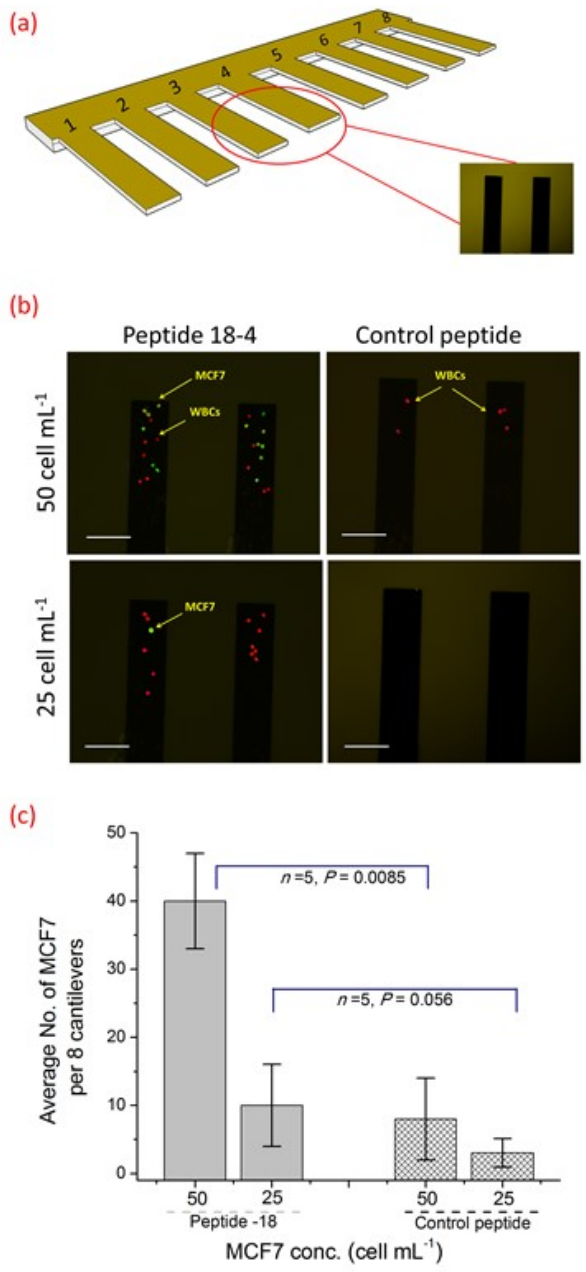

Figure 4-6| Cancer cell capture on the peptide coated microcantilevers (eight) using fluorescence microscopy. (a) Schematic of 8 cantilevers used to capture cancer cells when exposed to 50 or 25 cells/mL sample. (b) Fluorescence microscope images of the captured MCF-7 cells on the peptide-coated (18-4 or control) microcantilevers (two of the eight cantilevers are shown here). The eight cantilevers were exposed to MCF7 spiked whole blood samples (50 or 25 cells/mL). Cancer cells (MCF7) and the white blood cells (WBCs) were stained separately, green and red, respectively, before mixing. Scale bar is 100 μm. (c) The average number of captured MCF7 cells per microcantilever as computed from the set of fluorescence microscopy images. Assay

was repeated five times, and mean ± SD is presented. The P values were computed using the unpaired *t*-test to signify the statistical difference between the comparable groups.

Owing to the high specificity of peptide **18-4** to breast cancer cells, detection of cancer cells was achieved in buffer and blood samples at reasonable concentration levels. Although it has been very challenging to detect cancer cells in pure blood samples, we achieved the detection limit of approximately 50 cell mL^{-1}, which compares well with other reported data.[13] Typically, antibodies or nucleotides are used as molecular recognition elements in cancer detection[79, 264]. The only test that has been approved by the US Food and Drug Administration to measure CTCs in patients is the CellSearch® system (Veridex™, Warren, PA). This system is based on epithelial cell adhesion molecule (EpCAM) recognition by anti-EpCAM antibody[265]. The system is very sensitive, achieves robust capture efficiency, and is used for clinical prediction of CTCs with enumeration count of 5 or more cancer cells per 7.5 mL human blood. It is reported, however, that even with CellSearch a number of cancer cells escape from the detection due to the lack of the EpCAM molecule or due to the multiple steps that are required for the enrichment process[77]. There are several other platforms that use EpCAM antibody and are under development, such as nanowire based platform and platinum microelelctrodes coupled with electrochemical impedance[44,45]. Lee and co-workers reported an integrated nanowire based platform where the EpCAM antibody immobilized in the quartz nanowire arrays captures CTCs from blood samples and laser scanning cytometry is used to enumerate the CTCs[44]. Similarly, in another study EpCAM antibody is used to capture cancer cells and the binding event is monitored using highly sensitive electrochemical impedance sensor[45]. In this case, however, the detection sensitivity is dependent on the ionic strength of the sample and the frequency at which the electrical impedance is measured.

More recently, a genetic-based approach is reported where nanoconstructs called "NanoFlares" are used to detect live circulating tumor cells from blood.[46] NanoFlares consist of gold nanoparticles functionalized with single-stranded DNA (antisense recognition motif) that binds to short DNA complement containing a fluorescent reporter, whose fluorescence is quenched when it is present near the gold particle. In the presence of cancer cells the NanoFlares bind to target mRNA, and the fluorescent reporter is away from the gold nanoparticles displaying

enhanced fluorescence which is quantified using flow cytometry. Other methods for CTC detection include capturing CTC based on the cell size difference.[47,48] CTCs are typically larger than peripheral blood cells and different filtration approaches are being developed to isolate and detect CTCs[47].

Our study explores an alternative selective biomolecule (peptide) to detect cancer cells in combination with highly sensitive microcantilevers. The technique not only detects cancer cells by peptide capture, it also sorts cells in a single step. Unlike other techniques, peptide-based cantilever arrays are very simple to prepare, can be readily fabricated on silicon wafers and/or other materials using conventional microfabrication techniques, are inexpensive and can be used in an array format to detect simultaneously several cancer phenotypes. The ultra-small size of cantilevers, which resembles a miniature diving panel, allows the sensor to exhibit quick responses to the biological and chemical deviations for real-time, in-situ monitoring[49]. Peptide functionalized cantilever arrays can be developed to capture multiple receptors expressed on cancer cells increasing sensor sensitivity. Our future work will focus on obtaining a well-defined peptide array with different binding affinities for cancer cells in blood samples and the normal haematological cells. The approach will encompass exploring strategies such as employing different techniques for peptide immobilization, investigating multi-ligands for targeting and using other sensor platforms in parallel to achieve better detection limits with high selectivity. Peptide **18-4** works well to capture the immortalized cells spiked into human blood. Future work warrants the evaluation of peptide **18-4** binding to patient derived CTCs to validate the peptide-based microcantilever approach. Currently peptides are being used clinically to detect cancer.[50-52] For instance, RGD that binds αvβ3 integrins on cancer cell surface is used in cancer patients as a radiotracer to detect breast cancer lesions by positron emission tomography (PET).[50]

4.3.6 Conclusion

Functionalization of microcantilevers with breast cancer-targeting peptide **18-4** has enabled label-free sensing platform for real-time detection of cancer cells in human blood samples. The peptide **18-4** functionalized cantilever sensor can detect cancer cells in whole blood which contains significantly large number of hematological cells. The achieved detection limits with the cantilever sensor are 25, 50, and 100 cancer cells/mL in buffer, blood without plasma and blood, respectively. The higher sensitivity toward the blood without plasma sample suggests that

the microcantilever sensing can be further improved by removing the non-cellular components from the blood. Further a capture yield of 80% from spiked whole blood samples was achieved with the peptide **18-4** functionalized cantilevers, which is comparable to the antibodies based systems.[14] These results suggest that the peptide-based microcantilever sensor can be developed into a diagnostic platform for detection of circulating tumor cells as well as to monitor the therapeutic outcomes in cancer patients.

Chapter 5 . Nanomechanical Sandwich Assay for Multiple Cancer Biomarkers in Breast Cancer Cell-derived Exosomes

Etayash H, McGee R, Kaur K, Thundat T. Nanomechanical Sandwich Assay for Multiple Cancer Biomarkers in Breast Cancer Cell-derived Exosomes. ***Nanoscale***, , 15137- 41 (2016)

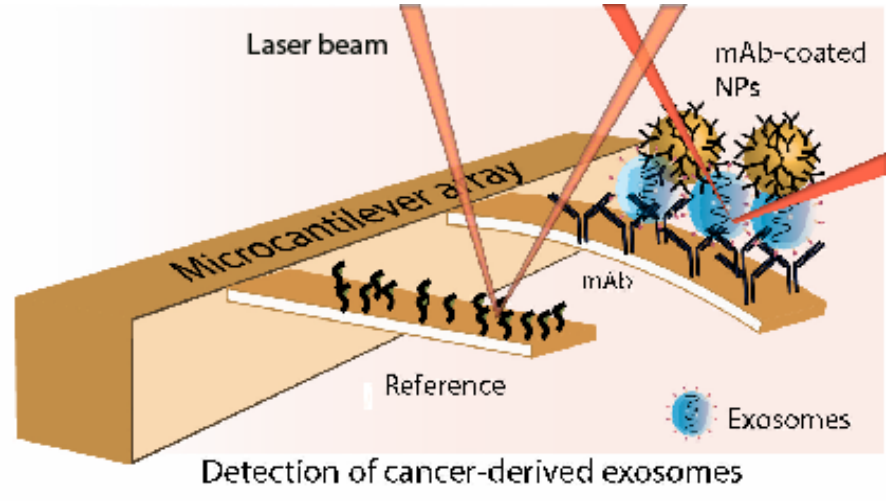

5.1 Introduction

Exosomes are nanoscale vesicles with sizes in the range of 30 nm – 100 nm shed by many cell types into the bloodstream[266]. As they harbor numerous bioactive receptors, nucleic acids, and signaling proteins for cell-to-cell communication, they have become increasingly attractive as diagnostic and therapeutic targets[84, 267]. Recent studies have shown the potential use of circulating exosomes as biomarkers for predicting and monitoring a number of complex diseases, including cancer[268]. It has been reported that circulating exosomes may carry valuable information about their parental tumors[84], which make them ideal biomarkers for early detection of cancer. Selective detection of cancer specific exosomes; however, is currently limited by their size, their identical composition to exosomes from non-tumorigenic cells and most importantly, their lack of specific markers that can discriminate them from other extracellular vesicles. Therefore, developing a technique for selective isolation and characterization of cancer exosomes are very important to overcome the challenges towards their use as biomarkers for detecting cancer. The current available approaches for detecting tumour-derived exosomes are either inept or impractical. Ultracentrifugation for instance, is time consuming and lacks the ability to differentiate between tumorigenic and non-tumorigenic exosomes[269, 270]. ELISA and western blot analysis require large amounts of samples and extensive labelling; thus, they are impractical for routine screening with high throughput[270]. The commercially available nanoparticle tracking analysis (NTA) is an ideal tool to sort nanoparticles in the size range of 10 nm – 2 μm. However, the system can only detect high concentrations of nanoparticles (10^6 to 10^9 particles mL^{-1}). Other novel approaches such as nano-plasmonic sensors[271], Raman scattering[272], miniature magnetic resonance[273] and others[274], are presently under development.

Here, we report the use of a sandwich technique of multiplexed cantilever array sensor for real-time, high-throughput screening of cancer cell-derived exosomes. We use the cantilever to discriminate between tumorigenic and non-tumorigenic exosomes and to detect ultra-low concentrations of breast cancer exosomes spiked in human serum. The technique has the potential to circumvent the limitations of other analytical methods in detecting low-abundant tumorigenic exosomes secreted into the blood stream by tumours at the initial stages of their development.

5.2 Methods:

5.2.1 Probes for Targeting Exosomes. The following monoclonal antibodies were used without any further modification; antiCD24 (Abcam, clone eBioSN3), antiCA63 (Abcam, clone SPM110), antiGPC1 antibody (EMD Millipore, clone 4D1) and antiEGFR antibody (Abcam, clone EGFR.1).

5.2.2 Microcantilever Arrays Preparation. Microcantilever arrays with eight gold-coated microcantilevers (Concentris GmbH – Switzerland), 1000 μm long, 100 μm wide and 1 μm thick, were used in the experiments. The top surfaces of the cantilevers (20 nm gold thickness) were functionalized individually with the above designated monoclonal antibodies, following a previously described protocol[97]. Initially, the arrays were cleaned with Piranha solution (3:1 by volume 96%H2SO4:30%H2O2) for 15 minutes, rinsed with MilliQ-water (18 MW), ethanol and dried in air. The arrays were then incubated in 2[methoxy (polyethyleneoxy) propyl] trimethoxysilane (10 mM, Gelest Inc. Frankfurt, Germany) for 20 minutes in order to render the backside of the levers inert to interactions. The cantilevers were then rinsed again with ethanol and dried in air. In order to immobilize the antibodies, the arrays were first coated with a thiolated linker ($HSCH_2CH_2NH_2$) by treating the surface with a cysteamine hydrochloride (0.01 M) in a concentrated buffer solution (8× PBS, pH 8.1) for 6 h. The arrays were then rinsed with 1× PBS (pH 7.4) to remove any unbound cysteamine. The accessible carboxylic terminal of monoclonal antibodies (at a concentration of 50 μL mL^{-1}) was activated by NHS/DCE (solution of 0.10 M NHS and 0.4 M EDC in deionized water) for 10 min and allowed to interact with the free amine groups of the pre-attached cysteamine linker. *Note*: functionalization of the two self-assembled monolayers (cysteamine and the mAbs) was performed using the capillary coating apparatus (Concentris – Switzerland) in order to differentially functionalize each cantilever in the array with different antibodies. Prior to use the array was rinsed with 70% ethanol and copious amounts of PBS solution to remove any physically adsorbed materials.

5.2.3 Cell Lines. Human breast cancer cell lines (MDA-MB-231, MCF7) and human mammary epithelial cell line MCF-10A (American Type Culture Collection, Manassas, VA) were used in the experiments. The first two were cultured in a DMEM medium containing 10% exosomes-depleted fetal bovine serum (FBS), 100 IU mL^{-1} penicillin, and 100 IU mL^{-1} streptomycin. MCF10A however, was cultured in minimal essential growth medium (MEGM, Lonza,

Cedarlane) supplemented with the same additives as mentioned above. All cell lines were incubated at 37 °C in a 5% CO_2–95% O_2 incubator and the growth media were replaced every 48 h.

5.2.4 Exosomes Isolation from Cell Lines. When cells reached confluence, the media was collected and centrifuged at 800g for 5 min, followed by a centrifugation step of 2,000g for 10 min to discard dead cells and cellular debris. The supernatant was filtered through a 0.2 μm pore syringe filter (ROSE Scientific Ltd, CA). The collected media was then ultra-centrifuged at 100,000g for 2 h at 4 ºC and exosomes pellet was subjected to a PBS washing steps followed by another ultra-centrifugation at 100,000g for 2 h at 4 ºC. While the supernatant was discarded, the exosomes pellet was suspended in 500 μl of sterile PBS. Frothy microliters of these exosomes were used for DLS analysis after dilution in PBS for independent measurement of exosomes concentrations.

5.2.5 Concentration of Exosomes Proteins. The proteins concentration (surface proteins) of the exosomes was determined using Bradford Protein Assay (Bio-Rad, Hercules, CA) with bovine serum albumin (BSA) as a standard. Procedures were carried out according to the manufacturer's instructions.

5.2.6 Dynamic Light Scattering (DLS). Exosomes size distribution and concentrations determined via DLS was carried out using a Zetasizer nanoseries instrument (Malvern Nano-Zetasizer, 633 nm He- Ne laser (4 mW)), operating at a 173° angle. Samples (~ 0.5 mg ml^{-1} total protein concentration as measured by Bradford assay) were placed in solvent-resistant micro cuvettes at 40 μL and measured for light scattering at a fixed position with an automatic attenuator. The temperature was controlled at 25C°. The presented data is an average of five replicates. The extracellular vesicles (exosomes) intensity distributions P1(r) are presented in **appendix Figure 17**. According to previous studies,[18] when the area of P1(r) is aligned to the Rayleigh Ratio R(q), the integral of the number-weighted radius distribution PN(r), represents the number of exosomes per mL (**see appendix Figure 17e**). The refractive index of exosomes is currently unknown; therefore, it's imported from another reference[275] as 1.46. The size distribution of the purified exosomes, determined by DLS, was found between 86 nm to 112 nm (**appendix Figure 17a, b, c, d**), which is in a good agreement with data, published elsewhere[87, 268]. Moreover, three different concentrations of exosomes were perceived, 6.13×10^{12}, $5.1 \times$

10^{12}, and 4.3×10^{12} exosomes mL^{-1}, for MDA-MB231, MCF7 and MCF10A, respectively. Next, we adjusted the sample concentration by comparing the data from DLS to the Bradford protein concentration assay (**appendix Figure 18b**) and performed serial dilutions afterward, for the cantilever experiments.

5.2.7 Scanning electron microscopy (SEM). All samples were fixed with 3.7% glutaraldehyde (Sigma–Aldrich) in phosphate buffered saline for 10 min, washed twice with PBS and dehydrated with ethanol. The samples were then left to dry at room temperature for several hours on a silicon substrate and then analyzed by scanning electron microscopy with a 5keV accelerating voltage (Sigma FE-SEM, Carl Zeiss) after gold sputtering. **Appendix Figure 18a** shows selected SEM images of exosomes from the three different cell lines; MDA-MB231, MCF7 and MCF10A.

5.2.8 Microcantilever Measurements and Data Analysis. The cantilever experiments were carried out using a home-made microcantilever setup was previously described[100]. Prior to running the exosomes, the functionalized microcantilever array placed in the fluidic cell was equilibrated by running a solution of phosphate buffered saline (PBS): human serum solution (1:1 vol/vol) at a constant flow rate of 1 mL h^{-1} until a stable baseline was achieved (serum was diluted in PBS and filtered through a 0.2 μm pore-filter prior the use). The microcantilever array was then exposed to a running PBS/serum solution for approximately 50 scans followed by flow of a solution containing cancer cell exosomes. The experiments were performed for three different isolated exosomes (from MDA-MB231, MCF7 and MCF10A) and several different concentrations as indicated in the text (from 10^{-6} g mL^{-1} to 10^{-15} g mL^{-1}). After exosome injection, the microcantilever array was washed with PBS for 10 minutes at the same flow rate. For running the microcantilever assay and performing the capture efficiency experiments, mixed concentrations of exosomes from cancer cell line (MDA-MB231) and non-cancerous cells (MCF10A) were prepared with up to 20-fold excess of MCF10A-derived exosomes (**Appendix Figure 19**). The final concentration was fixed at 1 μg mL^{-1}. Samples were then injected individually into the cantilever sensor and the data was recorded in real-time. Data from nanomechanical cantilever deflections was recorded in real-time using a multifunctional data-acquisition board driven by LabVIEW-based software.

5.2.9 Antibody Conjugation to Gold Nanoparticles. Spherical gold nanoparticles (diameter = 100 nm) were purchased from Nanopartz^{TM}. The mAb-coated Au nanoparticles (NPs) were prepared according to the previously described immobilization technique. Briefly, 100 µL of 1 mg mL^{-1} Au NPs in PBS were mixed with 100 µL of 1 mg mL^{-1} cysteamine hydrochloride in PBS (8× PBS, pH 8.1) and incubated for 6 h at room temperature. 500 µL of 1% poly (ethylene glycol) (MW 20 000; Sigma) was then added to the mixture to prevent aggregation and the solution was centrifuged at 6000 rpm for 30 min. The supernatant was removed and the pellet (cysteamine-coated gold NPs) was redispersed in a 100 µL PBS solution (pH 7.4). 50 µL of antiGPC1 mAb was added to 450 µL PBS, containing 100 µL of carboxylic group activating agent (solution of 0.10 M NHS and 0.4M EDC in deionized water, prepared separately, then added to the mAb solution). The mAb solution was left for 10 min for activation before incubation with cysteamine-coated NPs for 12 h at room temperature. As previously proven[97], the accessible carboxylic terminal of mAb will be activated to interact with the free amine groups of the pre-attached cysteamine linker. The solutions were completed to 1 mL with PBS, 500 µL 1% poly (ethylene glycol) was again added to prevent aggregation and centrifuged at 6000 rpm for 30 min. The supernatant was removed and the pellet (antiGPC1-coated gold NPs) was redispersed in a 1 mL PBS solution (pH 7.4) and stored at 4^{0}C until its use.

5.2.10 Exosomes Detection in a Nanomechanical Sandwich Assay. The microcantilever array functionalized with antiGPC1 mAb was first equilibrated by flowing a solution of phosphate buffered saline (PBS): human serum solution (1:1 vol/vol) at a constant flow rate of 1 mL h^{-1} until a stable baseline was generated (note that the serum was diluted in PBS and filtered through a 0.2 µm pore filter prior its use). Following this, the cantilever array was subjected to 1 mL PBS/serum solution containing exosomes derived from cancer cell MDA-MB231 or normal cells MCF10A, at concentrations ranging from 10^{-9} g mL^{-1} to 10^{-15} g mL^{-1} (**See appendix Figure 20**). To amplify the cantilevers signal, a 2×10^{-12} g mL^{-1} solution of antiGPC1-coated nanoparticles (~ 500 NPs) was injected into the system and allowed to incubate for 1 hour before an ultimate wash with PBS solution. Note: the concentration of the antiGPC1-coated NPs was adjusted after several optimization experiments (**Appendix Figure 21**). Different concentrations of antiGPC1-coated NPs (10^{-6} to 10^{-12} g mL^{-1}) were introduced into the sensor following the injection of fixed concentration of exosomes (10^{-13} g mL^{-1}, ~ 200 exosomes mL^{-1}). From the results it can be seen that the noise from the NPs is a minimum at 2×10^{-12} g mL^{-1}, which correspondingly represents

the lowest noise ratio. The result is illustrated in the **appendix Figure 21**with averaged values of three replicates. A similar experiment was performed with control cantilevers, as indicated, for comparison. Data from nanomechanical cantilever deflections were recorded in real-time using a multifunctional data-acquisition board driven by LabVIEW-based software. Each experiment was repeated three times and the averaged values, mean ± s.d., were presented.

5.1.11 Statistical analysis. The statistical analyses were carried out using either, the unpaired student's t-test or the one-way ANOVA as specified elsewhere. All experiments were performed as a minimum of three independent repeats and the signals of identically functionalized cantilevers were averaged. P-values of less than 0.05 were considered statistically significant. Data is presented as mean ± s.d. throughout the manuscript.

5.3 Results:

The first set of experiments was designed to assess the specificity of detecting exosomes in human serum spiked with breast cancer-derived exosomes using cantilever arrays. We targeted a number of biological markers including, CD24, CD63, EGFR and Glypican-1 (GPC1), that are believed to be over-expressed on surface-membrane of exosomes originated from cancer cells. Monoclonal antibodies (mAbs) were used as probes to target those membrane-associated proteins. Therefore, the antibodies were chemically immobilized onto the cantilever surface using a multiplexed capillary tube technique (See Methods).

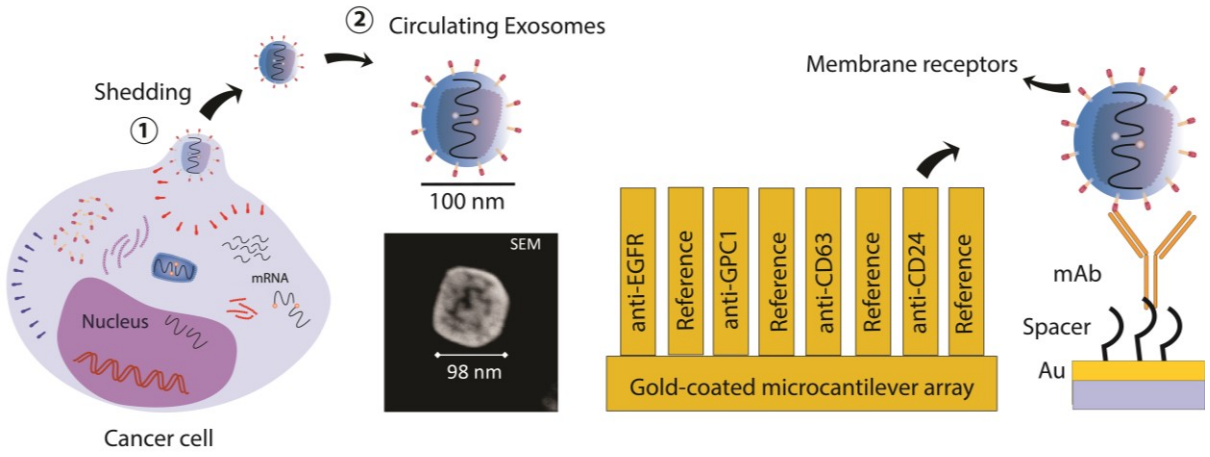

Figure 5-1| Tumor cells secrete exosomes through blending of the cell membrane to induce circulating extracellular vesicles in various biofluids with nanoscale sizes. These circulating nanovesicles carry arrays of biological markers including proteins, lipids and nucleotides, identical to that existing in their parental cells. High magnification scanning electron microscopy shows a single exosome from cancer cell lines (MDA-MB231) having a diameter of ~98 nm with no further characteristic details. The cantilevers in the array were either functionalized with exosome-targeting probes (monoclonal antibodies) as indicated, or with a reference control for differential detection of signal. The right-end diagram shows chemistry of surface coating, where a thiolated spacer was placed between the antibody and the Au-cantilever interface in order to enable the immobilization and reduce steric hindrance.

Exosomes derived from breast tumor cell lines (MCF7 and MDA-MB231) or non-tumorigenic cell lines (MCF10A), were isolated by multiple steps of ultracentrifugation and characterized by Dynamic Light Scattering (DLS) and Scanning Electron Microscopy (SEM) (supplementary). DLS and SEM results showed comparable extracellular vesicles with an average size of ~102 ±8 and ~89 ±5 nm diameter, respectively (**appendix Figure 17 and 18**). The isolated exosomes were suspended in 1 ml sterile-buffer/human serum samples (1:1 v/v) and introduced to the cantilever array functionalized as shown in Fig 1. Different cantilever bending signals were observed after injecting the exosomes (**Figure 5.2a, b, c)** with bending amplitudes scaled according to the targeted antigens. Differential deflection of the mAbs functionalized cantilevers displayed selective response to cancer cell-derived exosomes (**Figure 5.2a, and b**) when compared to that of non-tumorigenic exosomes (**Figure 5.2c**). The highest affinity (highest deflection) was observed when targeting the EGFR receptor (**Figure 5.2a, and b**); however, the lowest selectivity was observed when targeting the same receptor (c). Interestingly, the best

selectivity was achieved when detecting the cell-surface GPC1, as very low response to non-tumorigenic exosomes was observed (**Figure 5.2a, b and c**). In addition, by targeting GPC1, the tumorigenic exosomes could still be detected in the presence of a 20-fold excess of non-tumorigenic exosomes (**appendix Figure 19**), reaching a detection limit of 10^{-9} g mL^{-1}. When we compared the relative expression of the above-mentioned antigens on the tested exosomes from cancerous and non-cancerous cells (**Figure 5.2d**), the protein profiles showed significant discrepancy in their distribution with the best differential discrepant level with GPC1 ($P = 0.00158$), demonstrating its minute expression on non-tumorigenic exosomes. This compares very well with earlier evidence of proteins expression of breast cancer exosomes. The CD63, CD24 and EGFR are established exosomal markers and their expression is relatively higher in tumors exosomes than the levels on noncancerous-derived exosomes[274]. Recently, immunoblotting and FACS analysis have also identified GPC1 protein in much higher abundance in exosomes from breast cancer cells than in exosomes from noncancerous cells[268]. In addition, the relative concentration of GPC1 was found significantly higher in the sera of cancer patients compared to healthy donors[268]. Our nanomechanical results provide further support of elevated level of GPC1 on exosomes from breast cancer cells and raise the prospect use of this exosomal biomarker to identify breast cancer at its early stages of development.

To further understand response of the microcantilever to exosomes antigens, we carried out extra control experiments where GPC1-coated cantilevers were exposed to two samples; the first contained the exosomal bound antigen (GPC1) and the second one free of antigens. As in the previous experiments, following equilibration of the cantilever system with 1 ml of sterile-buffer/human serum sample of 1:1 v/v, the samples with or without the antigen was introduced into the sensor system and the response was monitored for 60 min. Results showed a substantial nanomechanical deflection (~104)

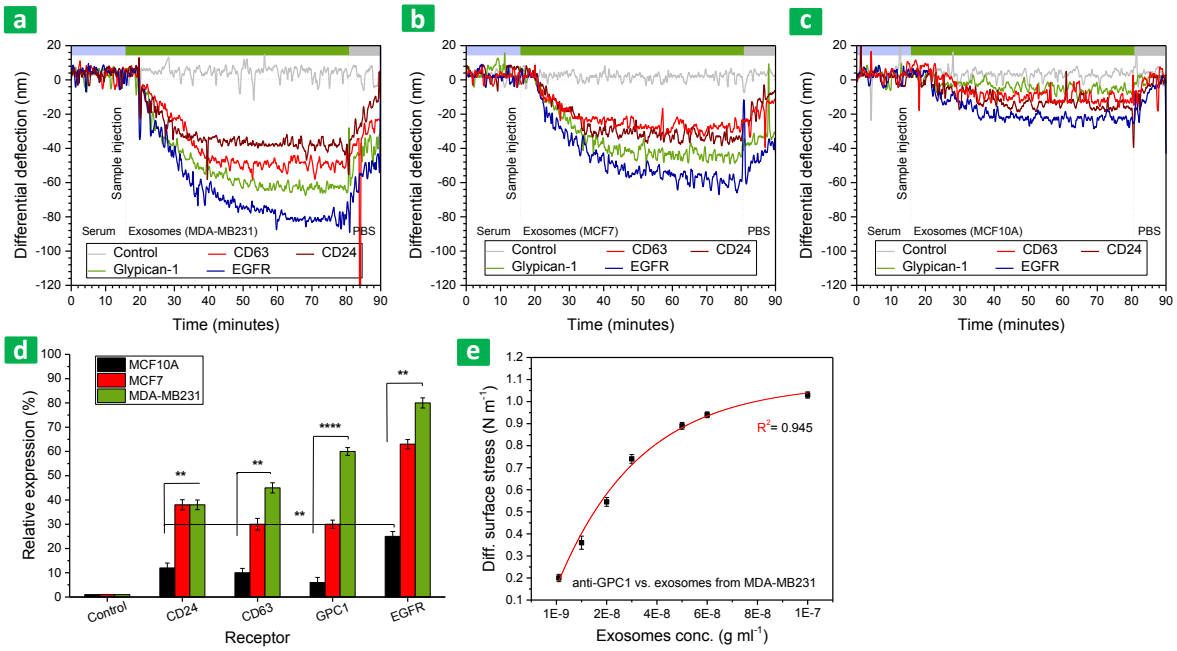

Figure 5-2| Real-time nanomechanical detection of exosomes with microcantilever arrays. Differential nanomechanical deflection (nm) is shown in response to exosomes derived from cancerous cells MDA-MB231 (a), cancerous cells MCF7 (b) or to exosomes from non-tumor cells MCF10A (c). The nanoscale deflection was measured in presence of 1 µg ml-1 exosomes in a solution of PBS/ human serum (1:1) using a 1000 µm-long and 1 µm-thick gold-coated silicon nitride cantilevers. (d) Surface stress measurement of the exosomes membrane-associated proteins with relative expression (%) in the tested cell lines, as indicated. Values represent mean ± s.d., n= 3 biological replicates. (e) Langmuir isotherm fit equilibrated according to surface stress values extracted from sensitivity experiments (supplementary). R2 = 0.94, indicating a consistent fit with the data. An average calculation of three replicates is presented with error bars indicate s.d.± 8 nm) when the samples were spiked with GPC1 antigen. The cantilever, did not exhibit any deflection when exposed to antigen's free samples (supplementary Fig 4). These results provide further support to our previous results and clarify further the behavior of the cantilever towards exosomal surface antigens.

Kinetics of real-time analysis showed exosomes quantification and protein profiling based on the cantilever's surface stress. The calculated dG value from GPC1 interaction to the cantilever (grafted with mAb) was found to be 197.9 kJ mol^{-1} calculated from a Langmuir isotherm fit (**Figure 5.2e**). The observed binding constant was ~0.1 nM, which is slightly lower than that of individual antigen-antibody binding ~3 nM[276]. The observed steady binding may be due to the presence of multiple binding sites per exosome. Likewise, the calculated dG values of other ligands showed 231.8 kJ mol-1, 139.6 kJ mol^{-1} and 121.8 kJ mol-1 for EGFR, CD24 and CD63

receptors, respectively, suggesting decent agreements with results previously reported for antigen-antibody experiments[271].

Next, to enhance the sensitivity and to detect ultra-low concentrations of exosomes based on GPC1 expression level, we used a sandwich cantilever assay, where a solution contains detective antibody (antiGPC1) grafted on 100 nm gold-nanoparticles was further introduced into the cantilever. The exosomes were captured first by the antiGPC1 mAb immobilized on the cantilever's surface, then further exposure to antiGPC1-tethered on the nanoparticles resulted in binding of the nanoparticles into the free region of the captured exosomes (**Figure 5.3a**), amplifying the nanomechanical cantilever's deflection (the sandwich assay is detailed in the online methods). Figure 5.3 illustrates the nanomechanical response of the cantilever to very low concentrations of exosomes (10-13 – 10-12 g mL-1). As presented in **Figure 5.3b**, adsorption of mAb-coated nanoparticles gives rise to an increase in the nanomechanical deflection, enhancing the mass limit of detection to 10-13 g mL-1 or/ 0.1 pg mL-1. The nanomechanical bending (nm) is scaled proportionally with the exosomes concentration in the samples at fixed level of antiGPC1 NPs (**appendix Figure 20**).

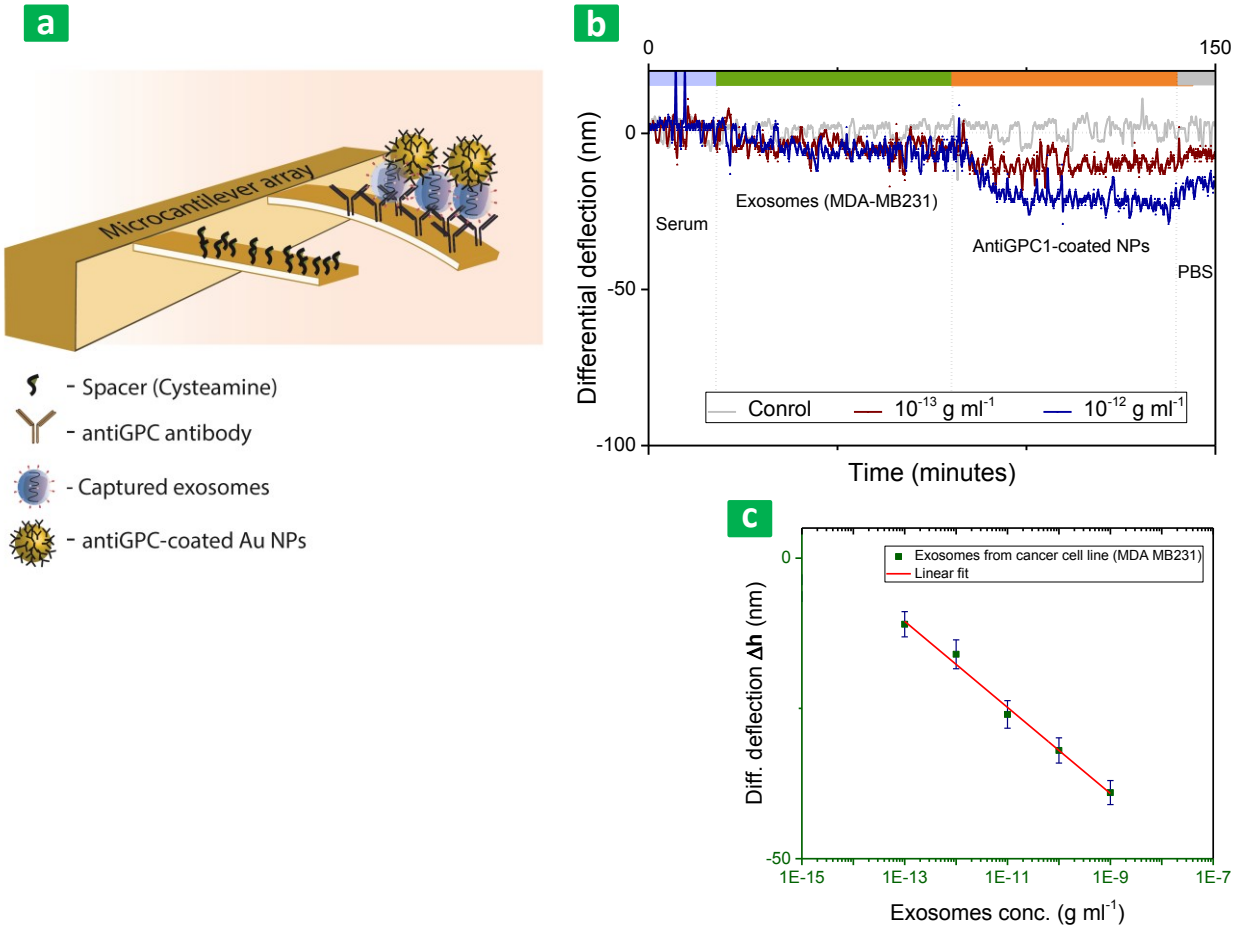

Figure 5-3| Sandwich assay for the cantilever and the effect on the nanomechanical deflection. (a) Schematic of the effect of the nanoparticle mass loading on the nanomechanical deflection of the cantilever. (b) Enhanced signals of the cantilever's nanomechanical deflections due to insertion of the mAb-coated nanoparticles (NPs). In the blue and wine signals, the cantilevers and NPs are bio-functionalized with antiGPC1 mAb. The sensitivity of the cantilevers before NPs binding (~10-9 g mL-1) was increased by the sandwich assay to ~10-13 g mL-1 (~2 × 102 exosomes mL-1), which is higher than the clinically relevant limit. The control signal (grey) is cysteamine-coated cantilevers subjected to exosomes solution (at 10-12) followed by anti-GPC1 coated NP at 2 × 10-12 g mL-1. (c) Resulting downshift of the nanomechanical bending is proportional to the concentration of the exosomes in the solution. An average calculation of three replicates is presented with error bars show s.d

From the geometrical limit, the estimated number of nanoparticles on the surface is ~500 NPs and the bending response due to mass loading can be estimated as 10^{-7} nm. This comes in agreement with the experimental data that shows an estimate number of NPs on the surface to

~400 (**appendix Figure 21**). According to the results, the observed bending enhancement is most probably due to additional surface stress caused by NPs binding to more than one exosomes. The amount of observed stress is around 0.1mN/m2. This limit is superior to the previously reported values due to the utilization of the functionalized NPs for mass enhancement[274]. Compared to the existing detection methods[274], the observed sensitivity is 103 times higher than that observed for western blot and 102 times higher than the ELISA. Unlike the state-of-the art microscopies[277] and fluorescence based flow cytometry[278], the cantilever approach is label-free, adequate for routine clinical screenings and supports the detection of smaller size of extracellular vesicles (≥100 nm). The ultra-small size of the cantilever, which resembles a miniature diving board, allows the sensor to respond quicker to the biological and chemical binding in real-time and in-situ. The cantilever can also be assembled into a microfluidic device with an embedded microchannel for single particle detection[221, 222]. We anticipate these findings to provide a significant positive impact on the use of exosomeic sensors to detect cancer early and monitor its prognosis. Yet, a number of key studies are remained to be undertaken including a comprehensive stoichiometric investigation of binding between mAbs and their targeted exosomal antigens and the detection of cancer exosomes in complex biological fluids such as blood, urine, saliva, etc. obtained from cancer patients.

5.2 Conclusions. We have presented a simple and multiplexed approach that uses alternative biomarkers for highly sensitive and selective detection of breast cancer cell-derived exosomes. The approach detects exosomes at ultra-low concentrations, compares the expression level of exosomal-surface antigens, and discriminates in real-time tumorigenic from non-tumorigenic exosomes. The technique is simple, inexpensive and able to sort exosomes in short time. Unlike other methods, the sensor can be used in an array format to capture multiple exosomal markers simultaneously increasing the sensitivity and selectivity of the detection. This finding offers opportunities for the development of exosome isolation technique for future diagnosis of breast cancer and monitoring in real-time its progression.

Chapter 6 . Impedimetric Detection of Breast Cancer Cell-derived Exosomes Using Cancer Targeting Peptides

6.1 Introduction:

Exosomes are membrane-enclosed extracellular vesicles with sizes ranging between 30 – 150 nm. They are shed from a large number of cells and circulate mostly in blood and other biological fluids including, saliva, lymph, ascites, amniotic, cerebrospinal fluids, and others[84]. As exosomes harbor a number of bioactive molecules such as membrane-associated enzymes, anchored proteins, membrane receptors, nucleotides such as DNA and microRNAs and other signaling proteins, they have become an attractive target as diagnostic biomarkers for prediction, diagnosis, and monitoring regression and progression of various diseases including cancer [83, 84].

Recently, a number of studies, including ours, have reported the possible use of exosomes as specific markers for predicting cancer early and monitor its progress. Nevertheless, identification and recognition of cancer cell-derived exosomes are still challenging and technically limited by a few factors including, exosomes' small size, heterogeneity and the complex procedure of isolation. The existing methods for detecting tumorigenic exosomes from blood are either impractical, expensive or lack the ability to differentiate tumorigenic from non-tumorigenic exosomes[274]. Only few techniques are under development[271, 272, 278-280].

In this study, we present a fully integrated peptide-based impedance array sensor for label-free detection of breast cancer cell-derived exosomes in an effort to contribute to the current evolution of exosomes detection. The technique offers a very simple, sensitive, and costly effective approach for high-throughput screening of breast cancer. We use peptide integrated platform in order to discriminate between tumorigenic and non-tumorigenic exosomes and to identify low concentrations of cancer-cell derived exosomes spiked in human serum.

6.2 Experimental Section

6.2.1 Peptide Probes for Targeting Exosomes:

Cancer targeting peptides P18-4 and RGD4C were synthesized in the laboratory using solid phase peptide synthesis (SPPS) as previously described[233, 281]. A control sensor with only cysteamine attached to the sensor was used for comparison purposes.

6.2.2 Impedance Analyzer IA-2:

An electrochemical impedance spectroscopic analyzer IA-2 (Sharp Laboratory of America) was utilized in this study[102, 282]. The sensor consists of an array having a 15 interdigitated gold-coated microelectrodes enclosed in three separate cells or chambers (5 electrodes per cell). Each electrode has a typical diameter of 3350 μm × 100 μm × 150 nm, holding up to 20 μL volume of liquid. The spacing between the electrodes is approximately 40 μm and the size of each die of the fabricated microarray is around 20 mm × 18.5 mm. The sensor is capable of measuring up to 15 channels simultaneously at a fixed frequency in the range of 10 − 1000 Hz and a stimulation voltage of 10 − 212 mV. The analyzer is also equipped with a temperature control sensor, which was set at 30 °C in this experiment.

6.2.3 Peptide Immobilization on Impedance Chip:

Impedance surface functionalization with cancer targeting peptides was based on a covalent interaction between the carboxylic groups of the peptide and a free amine group of a thiolated linker pre-anchored to the interdigitated gold electrodes. Briefly, a cysteamine linker (HSCH2CH2NH2) was immobilized first on the electrode interfaces via a simple thiol chemistry interaction[97]. Cysteamine hydrochloride (0.01 M) dissolved in concentrated buffer (8× PBS, pH 8.1) was incubated on the gold electrodes for 6h at room temperature. The electrodes were then washed with 1× PBS buffer (pH 7.4) to remove any unbound cysteamine molecules. We repeated this process twice to ensure sufficient coupling of the cysteamine onto the gold electrodes. Peptide solution at 1 mg per mL was activated by NHS/EDC (solution of 0.10 M NHS and 0.4 M EDC in deionized water) for 10 min and then allowed to interact with the free amine groups of the pre-attached cysteamine linker on the gold electrodes. The reaction was kept 12h and the chip was washed afterward with 1× PBS to remove any unbound peptides, rinsed with a copious amount of deionized water and dried in air. Prior to use, the array was rinsed with copious amounts of PBS solution to remove any physically adsorbed materials.

6.2.4 Cell Culture:

Human breast cancer cell lines MDA-MB-231 and human mammary epithelial cell line MCF-10A (American Type Culture Collection, Manassas, VA) were used in the experiments. The first was subcultured in a DMEM medium having 10% exosomes-depleted fetal bovine serum (FBS), 100 IU mL^{-1} penicillin, and 100 IU mL^{-1} streptomycin. The second (MCF10A) however, was cultured in minimal essential growth medium (MEGM, Lonza, Cedarlane) supplemented with the same supplements as indicated above, free from exosomes. Both cell lines as recommended were incubated at 37 °C in a 5% CO_2 – 95% O_2 incubator and the growth media were replaced every 48 h for refreshment.

6.2.5 Isolation of Exosomes from Cell Lines:

Circulating exosomes extraction from the culture media was performed as previously described in Chapter 6[279]. We repeated the procedure few times to get enough quantity of exosomes and we suspend the pellet (exosomes) in a 500 μL volume of 1× PBS buffer for concentration and independent measurements.

6.2.7 Concentration of Exosomes Proteins:

Determination of proteins concentration (surface proteins) of the exosomes was carried out using Bradford Protein Assay (Bio-Rad, Hercules, CA) with bovine serum albumin (BSA) as a standard. Procedures were performed according to the manufacturer's protocol.

6.2.8 Dynamic Light Scattering (DLS) and Scanning Electron Microscopy (SEM):

Dynamic Light Scattering (DLS) was used to determine the size distribution and concentration of the cell culture derived exosomes. The detailed procedure was described previously in our earlier study[279]. The presented data is an average of 3 replicate studies. Same as previously, SEM was carried out to determine shape and size of the collected exosomes. Fixed on silicon substrates the exosomes were analyzed using a 5keV accelerating voltage (Sigma FE-SEM, Carl Zeiss) after gold sputtering.

6.2.9 Impedance Measurements and Analysis:

The impedance analyzer IA-2 works by the electrochemical impedance spectroscopy principle, which relies primarily on Ohms law. When the immobilized peptides capture the target exosomes, the impedance reading signal changes based on type, strength, and magnitude of the interaction. This generated signal reflects the type and amount of the receptor-bound exosomes. The cancer exosomes thereby can be detected, measured and analyzed by monitoring the impedimetric parameters of the electrochemical spectroscopy[97, 282].

All impedimetric measurements were carried out at 10 Hz with 100 mV stimulation signal. Initially, we optimized the applied frequency for adequate impedance signals by exposing the sensor to cancer exosomes ($1\mu g\ mL^{-1}$) and recorded the impedance signal at various frequencies (10 – 100 Hz). Experimentally, the sensor array fluidic chamber was filled with 20 μL solution of (buffered saline (PBS): human serum solution (1:1 vol/vol)) having exosomes from the breast cancer cell line MDA-MB231 at $1\mu g\ mL^{-1}$. As sensor temperature was fixed at 30 °C and the stimulation voltage at 100 mV, the impedance amplitude was recorded at a various frequency range (10 – 100 Hz). Note that, prior to running the exosomes experiments, the functionalized impedance was equilibrated first by incubating a solution of phosphate buffered saline (PBS): human serum solution (1:1 vol/vol) in the sensor chambers and recording the impedance as a baseline signal (serum was diluted in PBS and filtered through a 0.22 μm pore filter prior the use). In each experiment, the solution free from exosomes was subjected to impedance reading for 400 s, before exosomes containing samples were exchanged and subject to another impedimetric reading for 800 s. As impedance holds an array with different cells (chambers), the measurements of impedance versus time data were performed simultaneously in real-time.

For the sensitivity measurements, samples having exosomes at serial dilutions (from 10^{-6} g mL^{-1} to 10^{-12} g mL^{-1}) were injected into the sensor coated with peptides and subjected to impedance reading. Note that a control sensor (coated with cysteamine) was always used side by side with the cancer targeting peptides to compare results. All data was analyzed using IA-2 impedance analyzer software based on an algorithm integrated directly into the IA-2 user interface[103, 282]. As the interaction between the immobilized peptides and their target analytes (exosomes) follows an exponential function, the interaction rate changes with time. This binding curve at fixed frequency follows the following formula:

$$|Z(t)| = B + A[1 - \exp(-st)]$$

Where Z is the exponentially varying impedance, time t, and s, A, and B are independent constants. While B is the offset at which the exponential starts and represents the impedance baseline of the samples free of exosomes, the parameters s and A hold important physiochemical properties of the analyte-receptor interactions. s is exponential time constant associated with exosomes binding and represents the binding rate constant. A is the amplitude of impedance signal and is relatively proportional to the sensor surface coverage of the targets. The extracted A×s value represents the initial binding rate. We can deduce that the combined parameters can provide a further knowledge of the binding event between the receptor and the targeted exosomes and allow obtaining a further comprehensive characteristic of peptide-exosomes binding behavior. The algorithm automatically extracts the kinetic parameters from the equation 1 and computes the amplitude of impedance relative to the interaction between the peptide and the exosomes. The analysis window was manually set to 1 minute after introducing the sample and that is in order to prevent any calculation error that may result from emptying and refilling the impedance fluidic cells. The integrated impedance signal response (integrated area under the curve) was also algorithmically calculated as the area under the binding curve[103, 282].

6.3 Results and Discussion

We aimed in this study to target breast cancer cell-derived exosomes in serum samples using cancer homing peptides on impedance spectroscopy. The goal is to develop a simple, sensitive, non-invasive and costly effective approach to capture selectively breast cancer exosomes. In the first set of the experiments, we intended to optimize the frequency of the sensor by conducting experiments using same concentration of exosomes (1 μg mL^{-1} based on protein concentration) and record the impedimetric signals at different frequencies (10 Hz – 120 Hz). According to our experimental setup, instrument and designed protocol, an optimum frequency for the detection was determined to be 100 Hz, which is the best frequency that gives highest impedimetric amplitude as exosomes interact with the immobilized peptide (**Figure 6.1**). Note that, exosomes isolation, quantity, and size distribution determinations were reported previously in the earlier chapter[261].

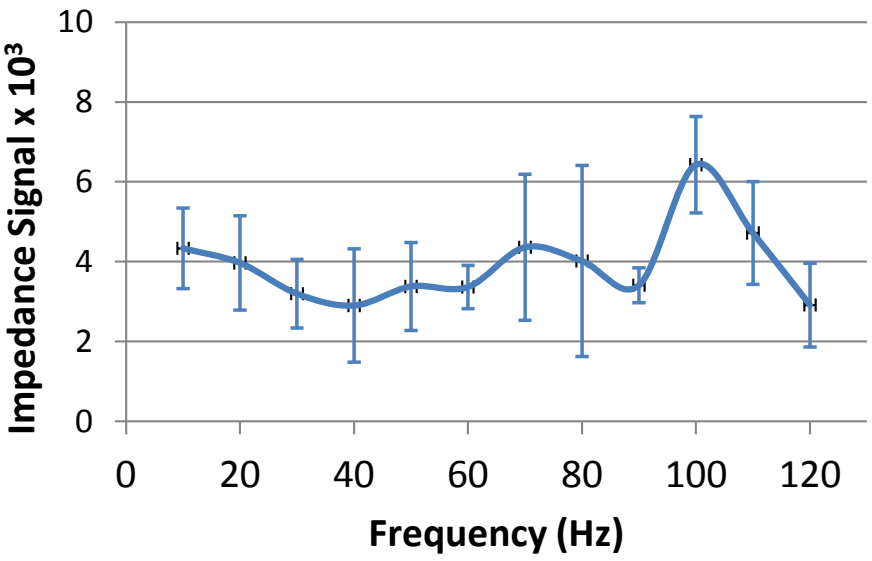

Figure 6-1| Impedance signal optimization for the best reading frequency (Hz). The test was performed with RGD4C against MDA-MB231 cell-derived exosomes at 1μg mL^{-1}.

Next, we tested the binding affinity of two different peptides namely, P18-4 and RGD4C against the breast cancer exosomes on the impedance platform. The two peptides were immobilized on two different impedance chips as described in materials and methods. The isolated exosomes from breast tumour cell lines (MDA-MB231) and non-cancerous cell lines (MCF10A), each separately, were added into 1 ml sterile-buffer/human serum samples (1: 1 v/v), introduced into the peptides functionalized chips (20 μL at 1 μg mL^{-1}) and subjected to impedance reading. We also probed the selectivity in the binding of the peptide-coated sensors to exosomes from cancerous cells and determined the binding kinetics of each tested peptide. **Figure 6.2** shows the selective impedimetric response of the peptide-sensors towards breast cancer exosomes with binding preferentiality of the RGD4C peptide to cancer exosomes. In particular, the RGD4C peptide showed higher impedance signal when exposed to cancer exosomes compared to what was seen by the P18-4 or the control sensor. Impedimetric responses of ~6.1 × 10^3 Ω, ~5.9 × 10^3 Ω were observed with RGD4C- and P-18-4 -coated sensors, respectively, in comparison to only ~0.3 × 10^3 Ω for the control sensor (cysteamine-coated sensor) when exposed to cancer cell-derived exosomes (**Figure 6.2a**). The results suggested that RGD4C peptide-sensor has slightly better affinity to breast cancer exosomes compared to P18-4. The results suggested also the

expression of RGD4C and P18-4 binding receptors on surface of cancer exosomes and that expression of these receptors might be higher than its level in normal cell-derived exosomes.

Further insight on the sensor's selectivity to breast cancer exosomes was attained by examining the kinetic parameters of peptide-exosomes interactions (area, s, A and A × s). Firstly, the calculated area under the binding curve (area) clearly showed the strong discrepancy between specific binding of the peptide-sensors to cancer exosomes and the physical adsorption to non-tumorigenic exosomes (**Figure 6.2b)**. In agreement with the real-time data of impedance measurements, the integrated areas under the binding curve reveal that the highest area accounts for RGD4C peptide sensor when it was exposed to cancer exosomes compared to what is seen with P18-4 and the control. This suggests the expression of the peptides bound receptors on the surface of breast cancer exosomes. Integrin αvβ3 is very well known to be over-expressed on the surface membrane of breast cancer cells, especially the circulated ones[254, 255]. However, further studies are needed to confirm its expression on breast cancer cell-derived exosomes. Other integrin's though, such as the integrin's α6β, α6β1 and αvβ5 are reported on exosomes from lung and liver cancer[283]. They also found to be associated with lung and liver metastasis[283]. We anticipate that this integrin subtype may also associate with breast cancer exosomes.

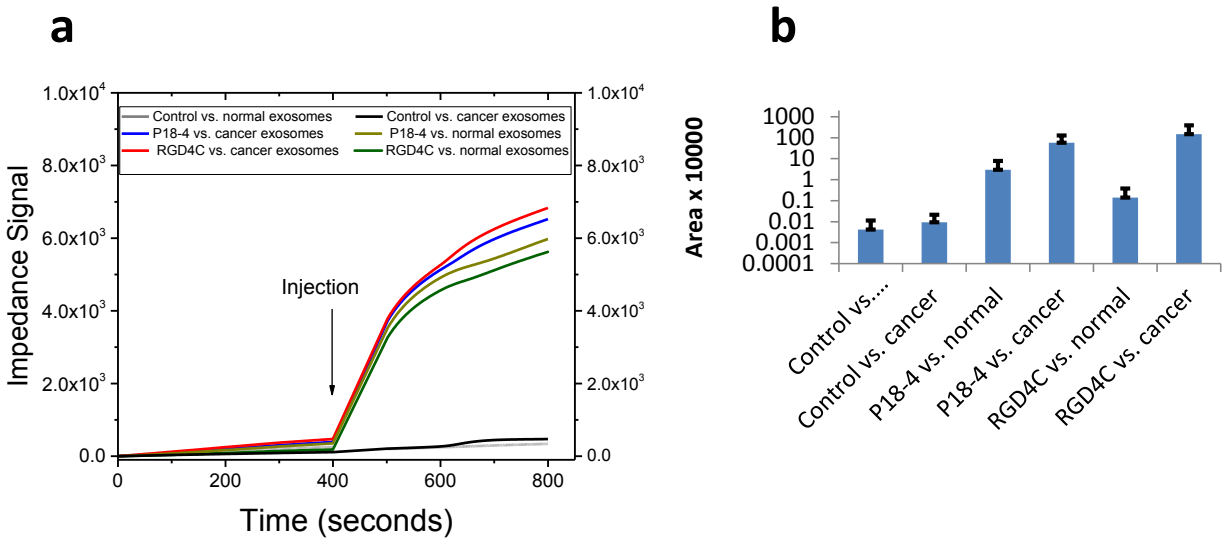

Figure 6-2| Real time detection of breast cancer cell-derived exosomes using peptide based impedance spectroscopy. Spectrum (a) shows real time impedance response to breast cancer exosomes as they interact to different peptides on the impedance chips. Chart (b) shows the integrated area under the binding curve of the impedance sensors functionalized with (RGD4C

and P18-4) against exosomes from normal and cancer cells lines. Cysteamine functionalized impedance chip was used as a reference control. Error bars represent standard deviation, a one way ANOVA shows $P < 0.05$ for the area under the binding curve.

The impedimetric parameters A, s and A × s were also algorithmically calculated using impedance to disclose useful quantitative binding parameters of the dissimilar peptide-sensors towards cancerous and non-cancerous exosomes (**Figure 6.3**). The intended parameter A, which is the impedance amplitude, is proportional to the sensor surface converge of the exosomes and indicates the affinity of the peptide-exosomes binding interaction as shown in **Figure 6-3a.** The s value or the time constant (**Figure 6-3b**) represents the binding rate constant, which is independent of the amplitude A. lastly, the A × s value (**Figure 6-3c**), which shows the initial binding rate. Those algorithmic parameters confirm with comprehensive details the selective capture events of cancer exosomes by the immobilized peptides. Thus provide a further signature of the peptide-exosomes interactions.

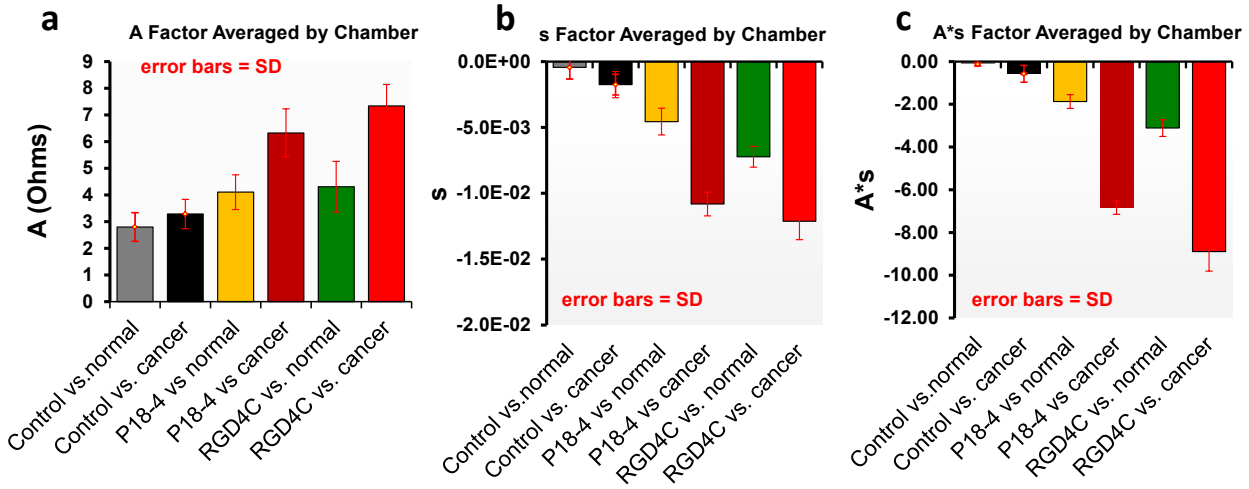

Figure 6-3| Binding kinetic parameters of the normalized impedance signal (A, s and A*s) of the peptide sensors interactions to cancer and normal cell-derived exosomes. a (amplitude), b (binding rate constant) and c is (initial binding rate). SD, standard deviation.

To identify the sensitivity of the sensor (RGD4C-coated impedance), we exposed the sensor to various quantities of exosomes according to protein concentration (10^{-6} g mL^{-1} to 10^{-12} g mL^{-1})

and measured the impedance reading versus time. The results, as presented in **Figure 6.4**, show variation in the amplitude of impedance signal with respect to the number of the exosomes in the sample. The response was scaled equivalently with number of exosomes in the samples. The lowest viable detection was found to be 10^5 exosomes per mL^{-1}, which is a bit higher than what we reported previously with the microcantilever array in exosomes detection[279], which was approximately 2×10^2 exosomes per mL. The sensitivity; however, still compares reasonably well to other methods reported for exosomes detection such as the plasmonic[271] and the surface plasmon resonance[284].

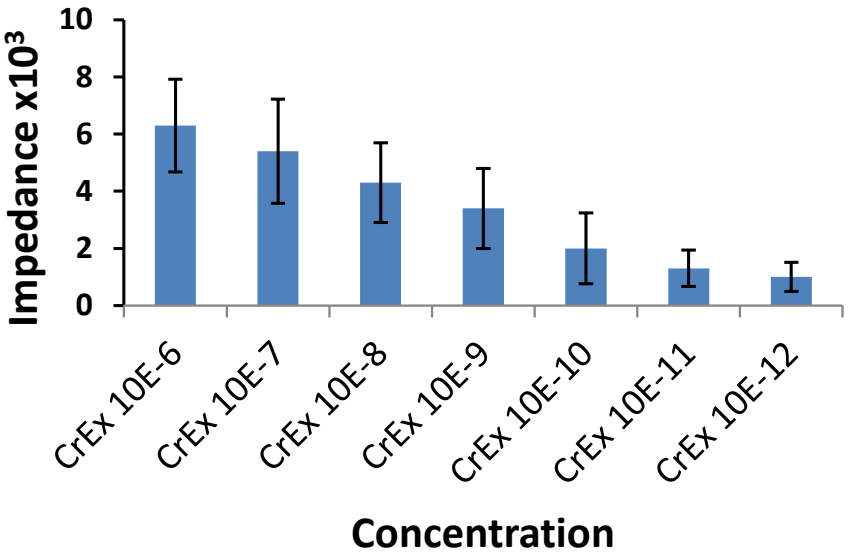

Figure 6-4| Concentration dependence, the resulting impedance signal of the peptide-exosomes interaction (RGD4C vs exosomes from MDA-MB231), is proportional to the concentration of the exosomes in the injected solution. An average calculation of two replicates is presented with error bars show s.d. CrEx (circulating exosomes.

6.4 Conclusion

We present in this study, the detection of breast cancer cell-derived exosomes using peptides with electrochemical impedance spectroscopy. Peptide molecules immobilized on impedance microelectrode chips allowed for a selective capture of cancer exosomes. Best selectivity

achieved by the RDG4C peptide, which showed better impedimetric affinity to breast cancer cell-derived exosomes than its counterpart peptides with a detection limit of ~10^5 exosomes per mL. The study has also suggested that the expression of the membrane bound receptor (integrin αvβ3) on the surface of breast cancer exosomes, highlighting its potential as exosomes biomarker. This implemented peptide-based impedance offers a high performance, a new promising platform that will allow rapid access to a new biotech market, due to its high sensitivity, low-cost paradigm, miniature size, ease of assembly, and flexibility for multiplexed lab-on-a-chip devices.

Chapter 7 . Conclusion and Future Direction

7.1 Conclusion

In this thesis, the development of reliable, sensitive and costly effective devices to detect foodborne pathogens and/or to identify breast cancer from in vitro spiked samples are presented.

Foodborne diseases are a significant problem that threatens human health and safety. It costs the economy billions of dollars[285, 286]. The current ways of detecting bacterial contamination are inconvenient, insufficient, and lack the time functionality needed for real-time analysis[173]. Accordingly, there is an immense global need for rapid, sensitive and highly specific techniques for bacterial detection that can fight infections worldwide and ensure the basic requirement of a safe supply of foods for human consumption.

In chapters 2 and 3, we aimed to emphasize on the development of novel biosensors based on surface immobilization of AMPs and/or mAbs for the detection of pathogenic foodborne *L. monocytogenes*. In chapter 2, an AMP from class IIa bacteriocins, namely, Leucocin A, assimilated on an electrochemical impedance spectroscopy (ESI) was used to selectively detect *L. monocytogenes*[97]. The result demonstrated the ability of the designed device to detect as low as 10^3 CFU mL^{-1}. The device; however, could not reach lower range than this and was not able to detect bacteria selectively in milk at lower concentrations. We then tried to use a new real-time sensing device known as a microfluidic cantilever in order to improve the limit of detection and develop robust, highly stable sensitive biosensor. We also incorporated the use of anti-*Listeria* mAbs in addition to the AMP Leucocin A to test multi-ligands for sensitive detection. As presented in chapter 3, the study showed extraordinary detection limit that reaches a single cell in small confined volume ~ 0.01μL. It also showed the ability of the designed multimodal cantilever sensor to differentiate between life and dead strains of bacteria and detect real-time bacterial response to antibiotics[132].

Yet further studies are needed to addressed the capability of the sensor to detect bacteria in samples from meat and milk products without any interference, the studies conducted here have concluded that ligand-based biosensors with impedance spectroscopy and microcantilever sensors are able to detect pathogenic bacteria at low concentrations in buffer samples. The

devices are highly selective, cost-effective and reliable in a real-time readout. Furthermore, both studies highlighted the feasibility of using short ligand AMPs for selective detection of *L. monocytogenes* and that those stable, inexpensive molecules can be used alternatively to mAbs and other ligands as they are less expensive and easier to produce. The use of hollow channel microcantilever has also allowed the detection of bacterial drug resistance and monitoring bacterial response to antibiotics in very short period of time. The finding suggested the ability of the microchannel cantilever to detect bacteria metabolism as it reacts to the injected antibiotics. It showed a clear metabolic recovery of *E. coli* after 30 minutes from exposure to kanamycin, while the case was different when exposed to ampicillin. This suggested resistance of *E. coli* to kanamycin and a positive response to ampicillin. Identifying bacterial metabolic response to antibiotics in such a short time will allow us to save many precious hours in clinical sample analysis and will prevent from prescribing unnecessary medications.

In the last three chapters, we intended to use the same transduction approaches (impedance spectroscopy and microcantilever) with different ligands to develop non-invasive and easy to use assays to identify breast cancer by targeting breast CTCs[100] and/or breast cancer-derived exosomes[279]. We thus hypothesize the development of quick approaches for spotting breast cancer at early stages. We target CTCs and circulating breast tumor-derived exosomes, as biomarkers of breast cancer growth. The results of the studies showed the capability of a peptide-based microcantilever sensor to efficiently detect cancer cells (MCF7 spiked human blood samples) at a limit of 50 – 100 cells per mL with a capture yield of 80% from whole blood samples. The study however, could not reach better sensitivity than 50 cells per mL which exceeds the clinically relevant limit of detection. The presence of CTCs in extremely low numbers makes it hard to achieve the clinical limit of detection. We thus explored the idea of detecting breast cancer cell-derived exosomes as prospective biomarkers for breast cancer and others. Exosomes from breast cancer cell lines were isolated using ultracentrifugation. Then they were exposed to a cantilever array coated with antibodies. We were able to selectively identify targeted over-expressed membrane-proteins CD24, CD63, and EGFR and GPC1 in breast cancer exosomes. An excellent affinity was achieved when targeting the cell-surface proteoglycan, GPC1, at detection limits of ~200 exosomes per mL, approximately 0.1 pg mL^{-1}.

In chapter 6 we investigated the detection of breast cancer-derived exosomes using peptide array in an impedance spectroscopy. The detection was achieved using cancer homing peptides including the P18-4, and the RDG4C. The findings showed bit better selectivity when using RGD4C over P18-4 peptide. The selectivity was not significant in the real time spectra compared to samples from normal cell lines. However, analysis of the binding parameters, (A, S, and A×S), showed a significant response of the peptides (P18-4 and RGD4C) to cancer exosomes. The study showed a sensitivity of ~10^5 exosomes per mL and suggested an embedding of the membrane-bound protein (integrin's) on the surface of breast cancer exosomes. Despite the fact that further studies are required to validate these findings, we propose that such peptides could have very potential use as exosomes detection agents.

The current dissertation emphasizes the development of portable, non-invasive ligand-based nano and micro biosensing platforms for rapid detection of harmful bacteria and breast cancer at early stages. It also, explores the viability of utilizing short ligand peptides, instead of antibodies, as less expensive, more stable and highly sensitive biorecognition molecules in biosensors for real-time detection of bacteria and/or cancer.

7.2 Future Plan

The future plan will focus on two areas. First, the positive results were obtained from the detection of bacteria and measuring its response to medications using the bimaterial microfluidic cantilever stimulate us to further examine the use of multiple strains with multiple targets as well as multiple strains with multiple antibiotics. I also intend to apply different AMPs and different mAbs in the system to examine the selectivity towards other strains of bacteria. for the sensor can also be improved to be more robust, stable, and sensitive with excellent reproducibility. The way of how samples are introduced can be improved to make the sensor easily handled by non-professional personals. The photothermal deflection can also be improved by checking with different bimaterials and different layer thickness.

- First, designing highly selective AMPs and/or mAbs will make sure that we are targeting the right bacteria and will eliminate any false results that may occur from receptor cross-talks with other similar strains. The AMP we used from class IIa bacteriocins is highly potent, easy to produce, and has an excellent stability. However, the nature of the semiselective properties of the peptide can be an issue when targeting closely related strains. We could

modify the peptide to achieve higher selectivity or we could use it in an array with other controls to eradicate any negative outcomes.

- The use of different chemical immobilization strategies may also have a potential effect on the sensor sensitivity. We would try to find better chemistry for APMs and mAbs immobilizations that would offer cost-effective and highly reproducible assembling.
- The cantilever can also be functionalized in a way that allows only the tip of the hollow channel to be activated with the active ligands (AMPs or mAbs). This will enable the sensor to detect a single cell level as no cell adhesion will happen in the hollow channel entrance. At present, It would be hard to achieve a single level of detection since the cantilever's entry has the same material as the cantilever tip. Photochemistry can be applied in this case to achieve this goal and activate the tip of the cantilever only. Thus, enabling much better sensitivity of the device and overcome the limitations of bacteria sticking.
- Finally, we will apply real samples and validate the techniques with the gold standards

Further studies towards detection of bacteria in food, water, drinks and other samples are under the plan. The study encourages also the in vivo experiments and clinical studies to examine the ability of the sensor detect bacteria from human samples, including blood, serum, urine, saliva and others.

With respect to the application in measuring bacterial response to antibiotics, we are further expanding the research to include a large number of bacteria and antibiotics. Designing a small scaled prototype of the device then would take place, which will require further optimizations and testing. The ideal device would have the ability to sense bacterial response to drugs in very short time and with high degree of accuracy.

The second area that needs further exploration is the ability to use cancer cell-derived exosomes as a biomarker to detect cancer early. To this end, our results showed the ability of the cantilever array to detect multiple markers of cancer exosomes on the same set. The multiple targeting (dual targeting) of cancer exosomes will display increased detection selectivity and perhaps specificity. In exosomes, the bioactive molecules packed on them make them unique nanovesicles that could serve as biomarkers. Those packed materials carry the same properties as exosomes origin cells and can be easily transferred into recipient cells, enabling them to change their biological properties[83]. Through this way tumor cells are believed to continuously modify

their surrounding environment and distant target cells favoring cancer metastasis[88]. Our plan is to further investigate the surface coating and targeting ligands specificity. Here are a number of future plans:

- As the study has conducted in nanoscale, it would be important to investigate the expression level of the targeted receptors. This can be obtained by conducting western blotting analysis, and ELISA.
- Isolation of exosomes needs to be improved by using different methods or combining methods with the current ultracentrifugation technique. Study the effect of other exosomes isolation methods on the results obtained by the cantilever is required. This investigation may lead to better results and enhance the system sensitivity and selectivity.
- The current isolation also consumes lots of samples and cell culture, an alternative perhaps can save samples and time. The ultracentrifugation may also not work with clinical samples; thus, an alternative is necessary.
- The detection of cancer exosomes in vivo can be totally different from what are seen in vitro samples. Therefore, an essential study would be exploring the ability of the sensor to detect cancer exosomes in vivo, either from animal models or samples from cancer patients.

Another avenue that can be further explored is the use of cancer homing peptides as exosomes targeting agents. The plan is to design exosomes specific peptides using peptide screening libraries or the phage display method in order to reveal peptides with strong affinities to exosomes. Peptides are unique in their properties as they are less expensive and hold much higher stability than antibodies, especially in biosensing platforms.

The utilization of nanoscale vesicles in cancer diagnosis is a quite new field. Thus, many challenges to overcome in exosomes diagnostics especially in vivo remained[274, 279]. Isolation of exosomes with high purity is one of the biggest problems and creating an efficient, stable and clinically feasible extraction method is quite challenging. In addition, the existence of potential biomarkers in cancer exosomes still requires large multicenter validations and the correlation between these exosomes markers and clinical practice requires deeper and more rigorous studies. The knowledge of the basic properties of exosomes is also insufficient ranging from the factors affecting exosome synthesis, release or secretion and transfer to storage conditions of exosomes all still require investigations as they are crucial to the accuracy of exosome diagnosis.

Bibliography

1. Arora, P., Sindhu, A., Dilbaghi, N. & Chaudhury, A. Biosensors as innovative tools for the detection of food borne pathogens. *Biosens Bioelectron* **28**, 1-12 (2011).
2. Rios, A.C. et al. Alternatives to overcoming bacterial resistances: State-of-the-art. *Microbiological Research* **191**, 51-80 (2016).
3. Joo, J., Kwon, D., Yim, C. & Jeon, S. Highly sensitive diagnostic assay for the detection of protein biomarkers using microresonators and multifunctional nanoparticles. *ACS Nano* **6**, 4375-4381 (2012).
4. Uliana, C.V., Riccardi, C.S. & Yamanaka, H. Diagnostic tests for hepatitis C: Recent trends in electrochemical immunosensor and genosensor analysis. *World Journal of Gastroenterology : WJG* **20**, 15476-15491 (2014).
5. Justino, C.I., Rocha-Santos, T.A. & Duarte, A.C. Review of analytical figures of merit of sensors and biosensors in clinical applications. *TrAC Trends in Analytical Chemistry* **29**, 1172-1183 (2010).
6. Kou, S., Cheng, D., Sun, F. & Hsing, I.M. Microfluidics and microbial engineering. *Lab on a Chip* **16**, 432-446 (2016).
7. Bell, R.L. et al. Recent and emerging innovations in *Salmonella* detection: a food and environmental perspective. *Microbial Biotechnology* **9**, 279-292 (2016).
8. Scallan, E. et al. Foodborne Illness Acquired in the United States—Major Pathogens. *Emerging Infectious Diseases* **17**, 7-15 (2011).
9. Heiman, K.E. et al. *Escherichia coli* O157 Outbreaks in the United States, 2003–2012. *Emerging Infectious Diseases* **21**, 1293-1301 (2015).
10. Gu, W. et al. Use of random forest to estimate population attributable fractions from a case-control study of *Salmonella enterica* serotype Enteritidis infections. *Epidemiology and Infection* **143**, 2786-2794 (2015).
11. Pedersen, M.L. et al. Rapid spread of Neisseria gonorrhoeae ciprofloxacin resistance due to a newly introduced resistant strain in Nuuk, Greenland, 2012–2015: a community-based prospective cohort study. *BMJ Open* **6**, e011998 (2016).
12. Molton, J.S. et al. The Global Spread of Healthcare-Associated Multidrug-Resistant Bacteria: A Perspective From Asia. *Clinical Infectious Diseases* **56**, 1310-1318 (2013).

13. Bialvaei, A.Z. & Samadi Kafil, H. Colistin, mechanisms and prevalence of resistance. *Current Medical Research and Opinion* **31**, 707-721 (2015).
14. Ryan, K.J., Ray, C.G. & Sherris, J.C. Sherris medical microbiology: an introduction to infectious diseases. (McGraw-Hill, 2004).
15. Farber, J.M., Ross, W.H. & Harwig, J. Health risk assessment of *Listeria monocytogenes* in Canada. *International Journal of Food Microbiology* **30**, 145-156 (1996).
16. Gracias, K.S. & McKillip, J.L. A review of conventional detection and enumeration methods for pathogenic bacteria in food. *Can J Microbiol* **50**, 883-890 (2004).
17. Ling, L.L. et al. A new antibiotic kills pathogens without detectable resistance. *Nature* **517**, 455-459 (2015).
18. Law, J.W.-F., Ab Mutalib, N.-S., Chan, K.-G. & Lee, L.-H. Rapid methods for the detection of foodborne bacterial pathogens: principles, applications, advantages and limitations. *Frontiers in Microbiology* **5**, 770 (2014).
19. Busse, H.-J., Denner, E.B.M. & Lubitz, W. Classification and identification of bacteria: current approaches to an old problem. Overview of methods used in bacterial systematics. *Journal of Biotechnology* **47**, 3-38 (1996).
20. Hilario, E. in Protocols for Nucleic Acid Analysis by Nonradioactive Probes. (eds. E. Hilario & J. Mackay) 27-38 (Humana Press, Totowa, NJ; 2007).
21. Monis, P.T. & Giglio, S. Nucleic acid amplification-based techniques for pathogen detection and identification. *Infection, Genetics and Evolution* **6**, 2-12 (2006).
22. Olsen, J.E. et al. Probes and polymerase chain reaction for detection of food-borne bacterial pathogens. *International Journal of Food Microbiology* **28**, 1-78 (1995).
23. Shirai, H. et al. Polymerase chain reaction for detection of the cholera enterotoxin operon of Vibrio cholerae. *Journal of Clinical Microbiology* **29**, 2517-2521 (1991).
24. Klančnik, A. et al. Quantification of Listeria monocytogenes cells with digital PCR and their biofilm cells with real-time PCR. *J Microbiol Methods* **118**, 37-41 (2015).
25. Montazeri, E.A. et al. Identification of methicillin-resistant *Staphylococcus aureus* (MRSA) strains isolated from burn patients by multiplex PCR. *Burns* **41**, 590-594.
26. Kumar, A., Grover, S. & Kumar Batish, V. Application of multiplex PCR assay based on genes for detection of *Escherichia coli* O157:H7 in milk. *The Journal of General and Applied Microbiology* **59**, 11-19 (2013).

27. Belgrader, P. et al. PCR detection of bacteria in seven minutes. *Science* **284**, 449-450 (1999).
28. Starbuck, M.A.B., Hill, P.J. & Stewart, G.S.A.B. Ultra sensitive detection of *Listeria monocytogenes* in milk by the polymerase chain reaction (PCR). *Lett Appl Microbiol* **15**, 248-252 (1992).
29. Daly, P., Collier, T. & Doyle, S. PCR-ELISA detection of Escherichia coli in milk. *Lett Appl Microbiol* **34**, 222-226 (2002).
30. Kobayashi, N. et al. Detection of mecA, femA, and femB genes in clinical strains of staphylococci using polymerase chain reaction. *Epidemiology and Infection* **113**, 259-266 (1994).
31. Giesendorf, B.A. et al. Rapid and sensitive detection of *Campylobacter* spp. in chicken products by using the polymerase chain reaction. *Applied and Environmental Microbiology* **58**, 3804-3808 (1992).
32. Lin, C.K. & Tsen, H.Y. Use of two 16S DNA targeted oligonucleotides as PCR primers for the specific detection of Salmonella in foods. *Journal of Applied Bacteriology* **80**, 659-666 (1996).
33. Filion, M. Quantitative Real-time PCR in Applied Microbiology. (Caister Academic Press, 2012).
34. Le Monnier, A. et al. Diagnosis of *Listeria monocytogenes* Meningoencephalitis by Real-Time PCR for the hly Gene. *Journal of Clinical Microbiology* **49**, 3917-3923 (2011).
35. Eyigor, A. & Carli, K.T. Rapid Detection of Salmonella from Poultry by Real-Time Polymerase Chain Reaction with Fluorescent Hybridization Probes. *Avian Diseases* **47**, 380-386 (2003).
36. Tyagi, A., Saravanan, V., Karunasagar, I. & Karunasagar, I. Detection of Vibrio parahaemolyticus in tropical shellfish by SYBR green real-time PCR and evaluation of three enrichment media. *International Journal of Food Microbiology* **129**, 124-130 (2009).
37. Deurenberg, R.H. et al. Rapid detection of Panton–Valentine leukocidin from clinical isolates of *Staphylococcus aureus* strains by real-time PCR. *FEMS Microbiol Lett* **240**, 225-228 (2004).

38. Nolan, T. & Bustin, S.A. PCR Technology: Current Innovations, Third Edition. (CRC Press, 2013).
39. Soumet, C. et al. Identification by a multiplex PCR-based assay of *Salmonella Typhimurium* and *Salmonella Enteritidis* strains from environmental swabs of poultry houses. *Lett Appl Microbiol* **29**, 1-6 (1999).
40. Mehrotra, M., Wang, G. & Johnson, W.M. Multiplex PCR for Detection of Genes for *Staphylococcus aureus Enterotoxins*, Exfoliative Toxins, Toxic Shock Syndrome Toxin 1, and Methicillin Resistance. *Journal of Clinical Microbiology* **38**, 1032-1035 (2000).
41. Nho, S.W. et al. Identification of high-risk *Listeria monocytogenes* serotypes in lineage I (serotype 1/2a, 1/2c, 3a and 3c) using multiplex PCR. *Journal of Applied Microbiology* **119**, 845-852 (2015).
42. Jothikumar, N. & Griffiths, M.W. Rapid Detection of *Escherichia coli O157:H7* with Multiplex Real-Time PCR Assays. *Applied and Environmental Microbiology* **68**, 3169-3171 (2002).
43. Loens, K. & ., U.A. Development and Evaluation of an in Vitro Nucleic Acid Sequence-Based Amplification (NASBA) System for Diagnosis of Respiratory Tract Infections. (Universiteit Antwerpen (Belgium), 2007).
44. D'Souza, D.H. & Jaykus, L.A. Nucleic acid sequence based amplification for the rapid and sensitive detection of *Salmonella enterica* from foods. *Journal of Applied Microbiology* **95**, 1343-1350 (2003).
45. Fykse, E.M. et al. Detection of Vibrio cholerae by Real-Time Nucleic Acid Sequence-Based Amplification. *Applied and Environmental Microbiology* **73**, 1457-1466 (2007).
46. Chen, L. et al. Real-Time Nucleic Acid Sequence-Based Amplification Assay for Rapid Detection and Quantification of agr Functionality in Clinical Staphylococcus aureus Isolates. *Journal of Clinical Microbiology* **50**, 657-661 (2012).
47. Uyttendaele, M., Schukkink, R., van Gemen, B. & Debevere, J. Detection of *Campylobacter jejuni* added to foods by using a combined selective enrichment and nucleic acid sequence-based amplification (NASBA). *Applied and Environmental Microbiology* **61**, 1341-1347 (1995).

48. Blais, B.W., Turner, G., Sooknanan, R. & Malek, L.T. A nucleic acid sequence-based amplification system for detection of *Listeria monocytogenes* hlyA sequences. *Applied and Environmental Microbiology* **63**, 310-313 (1997).
49. Ye, L. et al. Development of a real-time loop-mediated isothermal amplification assay for the sensitive and rapid detection of *Listeria monocytogenes*. *Lett Appl Microbiol* **61**, 85-90 (2015).
50. Malorny, B. et al. Standardization of diagnostic PCR for the detection of foodborne pathogens. *International Journal of Food Microbiology* **83**, 39-48 (2003).
51. Myint, M.S., Johnson, Y.J., Tablante, N.L. & Heckert, R.A. The effect of pre-enrichment protocol on the sensitivity and specificity of PCR for detection of naturally contaminated Salmonella in raw poultry compared to conventional culture. *Food Microbiology* **23**, 599-604 (2006).
52. Hoorfar, J. Rapid Detection, Characterization, and Enumeration of Foodborne Pathogens. (ASM Press, 2011).
53. Price, C.P. & Newman, D.J. Principles and Practice of Immunoassay. (Palgrave Macmillan UK, 1991).
54. Crowther, J.R. ELISA: Theory and Practice. (Humana Press, 1995).
55. Wong, R. & Tse, H. Lateral Flow Immunoassay. (Humana Press, 2008).
56. Ball, H.J. & Finlay, D. in Mycoplasma Protocols. (eds. R. Miles & R. Nicholas) 127-132 (Humana Press, Totowa, NJ; 1998).
57. van Zijderveld, F.G., van Zijderveld-van Bemmel, A.M. & Anakotta, J. Comparison of four different enzyme-linked immunosorbent assays for serological diagnosis of *Salmonella enteritidis* infections in experimentally infected chickens. *Journal of Clinical Microbiology* **30**, 2560-2566 (1992).
58. McCourt, M.T. et al. Sandwich ELISA detection of *Clostridium perfringens* cells and α-toxin from field cases of necrotic enteritis of poultry. *Vet Microbiol* **106**, 259-264 (2005).
59. Nagaraj, S., Ramlal, S., Kingston, J. & Batra, H.V. Development of IgY based sandwich ELISA for the detection of *staphylococcal enterotoxin* G (SEG), an egc toxin. *International Journal of Food Microbiology* **237**, 136-141 (2016).

60. Fu, S.-W., Zhang, Y.-L. & Zhou, D.-Y. Development of an ELISA kit using monoclonal antibody to *Clostridium difficile* toxin A. *World Journal of Gastroenterology : WJG* **10**, 2747-2749 (2004).
61. Picard, B., Alessandri, J.M. & Duval-Iflah, Y. Double-sandwich enzyme-linked immunosorbent assay for determination of *Escherichia coli* heat-labile porcine enterotoxins. *Vet Microbiol* **17**, 83-90 (1988).
62. Notermans, S. & Wernars, K. Immunological methods for detection of foodborne pathogens and their toxins. *International Journal of Food Microbiology* **12**, 91-102 (1991).
63. Shi, L. et al. A novel method to detect *Listeria monocytogenes* via superparamagnetic lateral flow immunoassay. *Analytical and Bioanalytical Chemistry* **407**, 529-535 (2015).
64. Song, C., Liu, J., Li, J. & Liu, Q. Dual FITC lateral flow immunoassay for sensitive detection of Escherichia coli O157:H7 in food samples. *Biosensors and Bioelectronics* **85**, 734-739 (2016).
65. Liu, C.-C. et al. *Salmonella* detection using 16S ribosomal DNA/RNA probe-gold nanoparticles and lateral flow immunoassay. *Food Chemistry* **141**, 2526-2532 (2013).
66. Winchester, D.J. & Winchester, D.P. Breast Cancer. (B.C. Decker, 2006).
67. Benoit, K.T. The Hallmarks of Cancer. (Dict, 2012).
68. Clinic, M. The Mayo Clinic Breast Cancer Book. (RosettaBooks, 2012).
69. Andolina, V. & Lillé, S. Mammographic Imaging: A Practical Guide. (Wolters Kluwer/Lippincott Williams & Wilkins Health, 2011).
70. Gøtzsche, P.C. Mammography Screening: Truth, Lies and Controversy. (Radcliffe Pub, 2012).
71. Ueno, E., Shiina, T., Kuboto, M. & Sawai, K. Research and Development in Breast Ultrasound. (Springer Japan, 2006).
72. Morris, E. & Liberman, L. Breast MRI: Diagnosis and Intervention. (Springer, 2005).
73. Vlaardingerbroek, M.T. & Boer, J.A. Magnetic Resonance Imaging: Theory and Practice. (Springer, 2003).
74. Sauter, E.R., Klein-Szanto, A., MacGibbon, B. & Ehya, H. nipple aspirate fluid and ductoscopy to detect breast cancer. *Diagnostic Cytopathology* **38**, 244-251 (2010).
75. Elk, R. & Morrow, M. Breast Cancer For Dummies. (Wiley, 2011).

76. Moskowitz, M. Screening for breast cancer: How effective are our tests? a critical review. *CA: A Cancer Journal for Clinicians* **33**, 26-39 (1983).
77. Gorges, T.M. et al. Circulating tumour cells escape from EpCAM-based detection due to epithelial-to-mesenchymal transition. *BMC Cancer* **12**, 178 (2012).
78. Krebs, M.G. et al. Molecular analysis of circulating tumour cells-biology and biomarkers. *Nat Rev Clin Oncol* **11**, 129-144 (2014).
79. Lianidou, E.S. & Markou, A. Circulating tumor cells in breast cancer: detection systems, molecular characterization, and future challenges. *Clin Chem* **57**, 1242-1255 (2011).
80. Nagrath, S. et al. Isolation of rare circulating tumour cells in cancer patients by microchip technology. *Nature* **450**, 1235-1239 (2007).
81. Baccelli, I. et al. Identification of a population of blood circulating tumor cells from breast cancer patients that initiates metastasis in a xenograft assay. *Nat Biotechnol* **31**, 539-544 (2013).
82. Brock, G. et al. Liquid biopsy for cancer screening, patient stratification and monitoring. *Translational Cancer Research* **4**, 280-290 (2015).
83. Vlassov, A.V., Magdaleno, S., Setterquist, R. & Conrad, R. Exosomes: Current knowledge of their composition, biological functions, and diagnostic and therapeutic potentials. *Biochimica et Biophysica Acta (BBA) - General Subjects* **1820**, 940-948 (2012).
84. An, T. et al. Exosomes serve as tumour markers for personalized diagnostics owing to their important role in cancer metastasis. *2015* (2015).
85. Sokolova, V. et al. Characterisation of exosomes derived from human cells by nanoparticle tracking analysis and scanning electron microscopy. *Colloids and Surfaces B: Biointerfaces* **87**, 146-150 (2011).
86. Smith, Z.J. et al. Single exosome study reveals subpopulations distributed among cell lines with variability related to membrane content. *2015* (2015).
87. Harris, D.A. et al. Exosomes Released from Breast Cancer Carcinomas Stimulate Cell Movement. *PLoS ONE* **10**, e0117495 (2015).
88. Zhang, H.G. Emerging Concepts of Tumor Exosome–Mediated Cell-Cell Communication. (Springer New York, 2012).

89. Sáenz-Cuesta, M., Otaegui, D. & Mittelbrunn, M. Novel clinical applications of extracellular vesicles. (2015).
90. Gruhl, F., Rapp, B. & Länge, K. in Molecular Diagnostics, Vol. 133. (eds. H. Seitz & S. Schumacher) 115-148 (Springer Berlin Heidelberg, 2013).
91. Rajmohan Joshi, R.M.J. Biosensors. (Isha Books, 2006).
92. Velusamy, V. et al. An overview of foodborne pathogen detection: In the perspective of biosensors. *Biotechnol Adv* **28**, 232-254 (2010).
93. Rasooly, A. & Herold, K.E. Biosensors for the analysis of food- and waterborne pathogens and their toxins. *J AOAC Int* **89**, 873-883 (2006).
94. Sadana, A. Biosensors: Kinetics of Binding and Dissociation Using Fractals. (Elsevier, 2003).
95. Chang, H.K. et al. Rapid, label-free, electrical whole blood bioassay based on nanobiosensor systems. *ACS Nano* **5**, 9883-9891 (2011).
96. Arlett, J.L., Myers, E.B. & Roukes, M.L. Comparative advantages of mechanical biosensors. *Nat Nano* **6**, 203-215 (2011).
97. Etayash, H., Jiang, K., Thundat, T. & Kaur, K. Impedimetric Detection of Pathogenic Gram-Positive Bacteria Using an Antimicrobial Peptide from Class IIa Bacteriocins. *Analytical Chemistry* **86**, 1693-1700 (2014).
98. Jiang, K. et al. Rapid label-free detection of E. coli using antimicrobial peptide assisted impedance spectroscopy. *Analytical Methods* (2015).
99. Etayash, H. & Thundat, T. in Encyclopedia of Nanotechnology. (ed. B. Bhushan) 1-9 (Springer Netherlands, 2015).
100. Etayash, H. et al. Real-time Detection of Breast Cancer Cells Using Peptide-functionalized Microcantilever Arrays. *Scientific Reports* **5**, 13967 (2015).
101. Orazem, M.E. & Tribollet, B. Electrochemical Impedance Spectroscopy. (Wiley, 2011).
102. Ghindilis, A.L. et al. Development of real-time assays for impedance-based detection of microbial double-stranded DNA targets: Optimization and data analysis. *Biosensors and Bioelectronics* **35**, 87-93 (2012).
103. Messing, D.S., Ghindilis, A. & Schwarzkopf, K. Impedimetric biosignal analysis and quantification in a real-time biosensor system. *Conf Proc IEEE Eng Med Biol Soc* **2010**, 2730-2734 (2010).

104. Hammond, Jules L. et al. Electrochemical biosensors and nanobiosensors. *Essays in Biochemistry* **60**, 69-80 (2016).
105. Messing, D.S., Ghindilis, A. & Schwarzkopf, K. An improved algorithm for quantifying real-time impedance biosensor signals. *Conf Proc IEEE Eng Med Biol Soc* **2011**, 2740-2744 (2011).
106. Mansfeld, F., Huet, F., Mattos, O.R. & Division, E.S.C. New Trends in Electrochemical Impedance Spectroscopy (EIS) and Electrochemical Noise Analysis (ENA): Proceedings of the International Symposium. (Electrochemical Society, Incorporated, 2001).
107. Choi, H. et al. A label-free DC impedance-based microcytometer for circulating rare cancer cell counting. *Lab Chip* **13**, 970-977 (2013).
108. Chung, Y.K. et al. An electrical biosensor for the detection of circulating tumor cells. *Biosens Bioelectron* **26**, 2520-2526 (2011).
109. Wee, K.W. et al. Novel electrical detection of label-free disease marker proteins using piezoresistive self-sensing micro-cantilevers. *Biosens Bioelectron* **20**, 1932-1938 (2005).
110. Mannoor, M.S., Zhang, S., Link, A.J. & McAlpine, M.C. Electrical detection of pathogenic bacteria via immobilized antimicrobial peptides. *Proc Natl Acad Sci U S A* **107**, 19207-19212 (2010).
111. Nwankire, C.E. et al. Label-free impedance detection of cancer cells from whole blood on an integrated centrifugal microfluidic platform. *Biosensors and Bioelectronics* **68**, 382-389 (2015).
112. Kang, G., Yoo, S.K., Kim, H.I. & Lee, J.H. Differentiation Between Normal and Cancerous Cells at the Single Cell Level Using 3-D Electrode Electrical Impedance Spectroscopy. *IEEE Sensors Journal* **12**, 1084-1089 (2012).
113. Holmes, D. et al. Leukocyte analysis and differentiation using high speed microfluidic single cell impedance cytometry. *Lab on a Chip* **9**, 2881-2889 (2009).
114. Arya, S.K. et al. Breast tumor cell detection at single cell resolution using an electrochemical impedance technique. *Lab on a Chip* **12**, 2362-2368 (2012).
115. Perez-Gonzalez, V.H. et al. in IET Nanobiotechnology, Vol. 10 263-275 (Institution of Engineering and Technology, 2016).
116. Jones, D.P. Biomedical Sensors. (Momentum Press, 2010).

117. Binnig, G., Quate, C.F. & Gerber, C. Atomic force microscope. *Phys Rev Lett* **56**, 930-933 (1986).
118. Thundat, T., Zheng, X.-Y., Chen, G. & Warmack, R. Role of relative humidity in atomic force microscopy imaging. *Surface science* **294**, L939-L943 (1993).
119. Karnati, C. et al. Organophosphorus hydrolase multilayer modified microcantilevers for organophosphorus detection. *Biosens Bioelectron* **22**, 2636-2642 (2007).
120. Mertens, J. et al. Label-free detection of DNA hybridization based on hydration-induced tension in nucleic acid films. *Nat Nanotechnol* **3**, 301-307 (2008).
121. Cha, B.H. et al. Detection of Hepatitis B Virus (HBV) DNA at femtomolar concentrations using a silica nanoparticle-enhanced microcantilever sensor. *Biosens Bioelectron* **25**, 130-135 (2009).
122. Hansen, K.M. et al. Cantilever-based optical deflection assay for discrimination of DNA single-nucleotide mismatches. *Anal Chem* **73**, 1567-1571 (2001).
123. Braun, T. et al. Quantitative time-resolved measurement of membrane protein-ligand interactions using microcantilever array sensors. *Nat Nanotechnol* **4**, 179-185 (2009).
124. Maraldo, D. & Mutharasan, R. 10-minute assay for detecting Escherichia coli O157:H7 in ground beef samples using piezoelectric-excited millimeter-size cantilever sensors. *J Food Prot* **70**, 1670-1677 (2007).
125. Waggoner, P.S. & Craighead, H.G. Micro- and nanomechanical sensors for environmental, chemical, and biological detection. *Lab Chip* **7**, 1238-1255 (2007).
126. Li, M., Tang, H.X. & Roukes, M.L. Ultra-sensitive NEMS-based cantilevers for sensing, scanned probe and very high-frequency applications. *Nat Nano* **2**, 114-120 (2007).
127. Hansen, K.M. & Thundat, T. Microcantilever biosensors. *Methods* **37**, 57-64 (2005).
128. Etayash, H. & Thundat, T. in Encyclopedia of Nanotechnology. (ed. B. Bhushan) 1-9 (Springer Netherlands, Dordrecht; 2014).
129. Nordström, M. et al. SU-8 Cantilevers for Bio/chemical Sensing; Fabrication, Characterisation and Development of Novel Read-out Methods. *Sensors* **8**, 1595-1612 (2008).
130. Chapman, P.J. et al. Differentially ligand-functionalized microcantilever arrays for metal ion identification and sensing. *Anal Chem* **79**, 7062-7068 (2007).

131. Hwang, K.S. et al. Peptide receptor-based selective dinitrotoluene detection using a microcantilever sensor. *Biosens Bioelectron* **30**, 249-254 (2011).
132. Etayash, H., Khan, M.F., Kaur, K. & Thundat, T. Microfluidic cantilever detects bacteria and measures their susceptibility to antibiotics in small confined volumes. *Nature Communications* **7**, 12947 (2016).
133. Fletcher, P.C. & Louisville, U.o. Alternative Piezoresistor Designs for Maximizing Cantilever Sensitivity. (University of Louisville, 2008).
134. Letant, S.E., Hart, B.R., Van Buuren, A.W. & Terminello, L.J. Functionalized silicon membranes for selective bio-organism capture. *Nat Mater* **2**, 391-395 (2003).
135. Zimmermann, J.L., Nicolaus, T., Neuert, G. & Blank, K. Thiol-based, site-specific and covalent immobilization of biomolecules for single-molecule experiments. *Nat. Protocols* **5**, 975-985 (2010).
136. Zougagh, M. & Rios, A. Micro-electromechanical sensors in the analytical field. *Analyst* **134**, 1274-1290 (2009).
137. Gunda, N.S.K. & Mitra, S.K. Challenges and Opportunities for Capillary Based Biofunctionalization of Microcantilever Arrays. *Journal of The Electrochemical Society* **161**, B3167-B3172 (2014).
138. Alexander, B. et al. Rapid functionalization of cantilever array sensors by inkjet printing. *Nanotechnology* **15**, 873 (2004).
139. Fuchise, K. et al. A Photolithographic Approach to Spatially Resolved Cross-Linked Nanolayers. *Langmuir* **31**, 3242-3253 (2015).
140. van Oorschot, R. et al. A microfluidic AFM cantilever based dispensing and aspiration platform. *EPJ Techniques and Instrumentation* **2**, 4 (2015).
141. Gopal, A., Hoshino, K. & Zhang, J.X. in Encyclopedia of Nanotechnology. (ed. B. Bhushan) 1397-1404 (Springer Netherlands, Dordrecht; 2012).
142. Lam, Y., Abu-Lail, N.I., Alam, M.S. & Zauscher, S. Using microcantilever deflection to detect HIV-1 envelope glycoprotein gp120. *Nanomedicine* **2**, 222-229 (2006).
143. Alvarez, M. et al. Nanomechanics of the formation of DNA self-assembled monolayers and hybridization on microcantilevers. *Langmuir* **20**, 9663-9668 (2004).
144. Wang, J. et al. Rapid Detection of Pathogenic Bacteria and Screening of Phage-Derived Peptides Using Microcantilevers. *Analytical Chemistry* **86**, 1671-1678 (2014).

145. Timurdogan, E., Alaca, B.E., Kavakli, I.H. & Urey, H. MEMS biosensor for detection of Hepatitis A and C viruses in serum. *Biosens Bioelectron* **28**, 189-194 (2011).
146. Wu, G. et al. Bioassay of prostate-specific antigen (PSA) using microcantilevers. *Nat Biotech* **19**, 856-860 (2001).
147. Campbell, G.A. & Mutharasan, R. Method of measuring Bacillus anthracis spores in the presence of copious amounts of Bacillus thuringiensis and Bacillus cereus. *Anal Chem* **79**, 1145-1152 (2007).
148. Campbell, G.A. & Mutharasan, R. Piezoelectric-excited millimeter-sized cantilever (PEMC) sensors detect Bacillus anthracis at 300 spores/mL. *Biosens Bioelectron* **21**, 1684-1692 (2006).
149. Sharma, H. & Mutharasan, R. hlyA gene-based sensitive detection of Listeria monocytogenes using a novel cantilever sensor. *Anal Chem* **85**, 3222-3228 (2013).
150. Huber, F. et al. Direct detection of a BRAF mutation in total RNA from melanoma cells using cantilever arrays. *Nat Nanotechnol* **8**, 125-129 (2013).
151. Mulchandani, A. in Enzyme and Microbial Biosensors: Techniques and Protocols. (eds. A. Mulchandani & K.R. Rogers) 3-14 (Humana Press, Totowa, NJ; 1998).
152. Heller, A. Electrical wiring of redox enzymes. *Acc Chem Res* **23**, 128-134 (1990).
153. Selan, L. et al. Reliability of a bioluminescence ATP assay for detection of bacteria. *Journal of Clinical Microbiology* **30**, 1739-1742 (1992).
154. Tzanavaras, P.D. & Zacharis, C.K. Reviews in Pharmaceutical and Biomedical Analysis. (Bentham e Books, 2010).
155. Jayasena, S.D. Aptamers: An Emerging Class of Molecules That Rival Antibodies in Diagnostics. *Clin Chem* **45**, 1628-1650 (1999).
156. Zhu, K. et al. Recent Developments in Antibody-Based Assays for the Detection of Bacterial Toxins. *Toxins* **6**, 1325-1348 (2014).
157. Banada, P.P. & Bhunia, A.K. in Principles of Bacterial Detection: Biosensors, Recognition Receptors and Microsystems. (eds. M. Zourob, S. Elwary & A. Turner) 567-602 (Springer New York, New York, NY; 2008).
158. Byrne, B., Stack, E., Gilmartin, N. & O'Kennedy, R. Antibody-Based Sensors: Principles, Problems and Potential for Detection of Pathogens and Associated Toxins. *Sensors (Basel, Switzerland)* **9**, 4407-4445 (2009).

159. Song, S. et al. Aptamer-based biosensors. *TrAC Trends in Analytical Chemistry* **27**, 108-117 (2008).
160. Cui, Y., Kim, S.N., Naik, R.R. & McAlpine, M.C. Biomimetic peptide nanosensors. *Acc Chem Res* **45**, 696-704 (2012).
161. Dennison, S.R. et al. A Novel Form of Bacterial Resistance to the Action of Eukaryotic Host Defense Peptides, the Use of a Lipid Receptor. *Biochemistry* (2013).
162. Humblot, V. et al. The antibacterial activity of Magainin I immobilized onto mixed thiols Self-Assembled Monolayers. *Biomaterials* **30**, 3503-3512 (2009).
163. Bai, L. et al. Peptide-based isolation of circulating tumor cells by magnetic nanoparticles. *Journal of Materials Chemistry B* (2014).
164. Dhayal, B. et al. Detection of Bacillus subtilis spores using peptide-functionalized cantilever arrays. *J Am Chem Soc* **128**, 3716-3721 (2006).
165. Cheng, C.I., Chang, Y.-P. & Chu, Y.-H. Biomolecular interactions and tools for their recognition: focus on the quartz crystal microbalance and its diverse surface chemistries and applications. *Chemical Society Reviews* **41**, 1947-1971 (2012).
166. Dong, Z.-M. & Zhao, G.-C. Label-free detection of pathogenic bacteria via immobilized antimicrobial peptides. *Talanta* **137**, 55-61 (2015).
167. McAlpine, M.C. et al. Peptide-nanowire hybrid materials for selective sensing of small molecules. *J Am Chem Soc* **130**, 9583-9589 (2008).
168. Kulagina, N.V., Lassman, M.E., Ligler, F.S. & Taitt, C.R. Antimicrobial peptides for detection of bacteria in biosensor assays. *Anal Chem* **77**, 6504-6508 (2005).
169. Pavan, S. & Berti, F. Short peptides as biosensor transducers. *Anal Bioanal Chem* **402**, 3055-3070 (2012).
170. Guo, X. et al. Carbohydrate-based label-free detection of Escherichia coli ORN 178 using electrochemical impedance spectroscopy. *Anal Chem* **84**, 241-246 (2012).
171. Peelman, F. et al. Characterization of functional residues in the interfacial recognition domain of lecithin cholesterol acyltransferase (LCAT). *Protein Engineering* **12**, 71-78 (1999).
172. Cai, D. et al. A molecular imprint nanosensor for ultrasensitive detection of proteins. *Nature nanotechnology* **5**, 597-601 (2010).

173. Farahi, R.H., Passian, A., Tetard, L. & Thundat, T. Critical Issues in Sensor Science To Aid Food and Water Safety. *ACS Nano* **6**, 4548-4556 (2012).
174. Donnenberg, M.S. & Narayanan, S. How to diagnose a foodborne illness. *Infect Dis Clin North Am* **27**, 535-554 (2013).
175. Gracias, K.S. & McKillip, J.L. A review of conventional detection and enumeration methods for pathogenic bacteria in food. *Can J Microbiol* **50**, 883-890 (2004).
176. Li, Y., Cu, Y.T. & Luo, D. Multiplexed detection of pathogen DNA with DNA-based fluorescence nanobarcodes. *Nat Biotechnol* **23**, 885-889 (2005).
177. Johnson, R.P. et al. Detection of Escherichia coli O157:H7 in meat by an enzyme-linked immunosorbent assay, EHEC-Tek. *Appl Environ Microbiol* **61**, 386-388 (1995).
178. Soleymani, L., Fang, Z., Sargent, E.H. & Kelley, S.O. Programming the detection limits of biosensors through controlled nanostructuring. *Nat Nanotechnol* **4**, 844-848 (2009).
179. Sorgenfrei, S. et al. Label-free single-molecule detection of DNA-hybridization kinetics with a carbon nanotube field-effect transistor. *Nat Nanotechnol* **6**, 126-132 (2011).
180. Slinker, J.D., Muren, N.B., Gorodetsky, A.A. & Barton, J.K. Multiplexed DNA-modified electrodes. *J Am Chem Soc* **132**, 2769-2774 (2010).
181. Nilsson, K.G. & Mandenius, C.F. A carbohydrate biosensor surface for the detection of uropathogenic bacteria. *Biotechnology (N Y)* **12**, 1376-1378 (1994).
182. Bergwerff, A.A. & van Knapen, F. Surface plasmon resonance biosensors for detection of pathogenic microorganisms: strategies to secure food and environmental safety. *J AOAC Int* **89**, 826-831 (2006).
183. Swaminathan, B. & Feng, P. Rapid detection of food-borne pathogenic bacteria. *Annu Rev Microbiol* **48**, 401-426 (1994).
184. Zasloff, M. Antimicrobial peptides of multicellular organisms. *Nature* **415**, 389-395 (2002).
185. Yang, L. & Bashir, R. Electrical/electrochemical impedance for rapid detection of foodborne pathogenic bacteria. *Biotechnol Adv* **26**, 135-150 (2008).
186. Mannoor, M.S. et al. Graphene-based wireless bacteria detection on tooth enamel. *Nat Commun* **3**, 763 (2012).

187. Etayash, H., Norman, L., Thundat, T. & Kaur, K. Peptide-bacteria interactions using engineered surface-immobilized peptides from class IIa bacteriocins. *Langmuir* **29**, 4048-4056 (2013).

188. Cotter, P.D., Hill, C. & Ross, R.P. Bacteriocins: developing innate immunity for food. *Nat Rev Microbiol* **3**, 777-788 (2005).

189. Hu, Y., Zuo, P. & Ye, B.C. Label-free electrochemical impedance spectroscopy biosensor for direct detection of cancer cells based on the interaction between carbohydrate and lectin. *Biosens Bioelectron* **43**, 79-83 (2013).

190. Cotter, P.D., Ross, R.P. & Hill, C. Bacteriocins - a viable alternative to antibiotics? *Nat Rev Microbiol* **11**, 95-105 (2013).

191. Drider, D. et al. The continuing story of class IIa bacteriocins. *Microbiol Mol Biol Rev* **70**, 564-582 (2006).

192. Derksen, D.J., Stymiest, J.L. & Vederas, J.C. Antimicrobial leucocin analogues with a disulfide bridge replaced by a carbocycle or by noncovalent interactions of allyl glycine residues. *J Am Chem Soc* **128**, 14252-14253 (2006).

193. Jacquet, T. et al. Antibacterial activity of class IIa bacteriocin Cbn BM1 depends on the physiological state of the target bacteria. *Res Microbiol* **163**, 323-331 (2012).

194. Kjos, M., Nes, I.F. & Diep, D.B. Class II one-peptide bacteriocins target a phylogenetically defined subgroup of mannose phosphotransferase systems on sensitive cells. *Microbiology* **155**, 2949-2961 (2009).

195. Ramnath, M. et al. Expression of mptC of Listeria monocytogenes induces sensitivity to class IIa bacteriocins in Lactococcus lactis. *Microbiology* **150**, 2663-2668 (2004).

196. Bodapati, K.C. et al. Design, synthesis and evaluation of antimicrobial activity of N-terminal modified Leucocin A analogues. *Bioorg Med Chem* **21**, 3715-3722 (2013).

197. Costa, F. et al. Covalent immobilization of antimicrobial peptides (AMPs) onto biomaterial surfaces. *Acta Biomater* **7**, 1431-1440 (2011).

198. Ghindilis, A.L. et al. Development of real-time assays for impedance-based detection of microbial double-stranded DNA targets: optimization and data analysis. *Biosens Bioelectron* **35**, 87-93 (2012).

199. Zhu, T. et al. Detection of bacterial cells by impedance spectra via fluidic electrodes in a microfluidic device. *Lab on a Chip* **10**, 1557-1560 (2010).

200. Ghosh Dastider, S. et al. Efficient and Rapid Detection of Salmonella Using Microfluidic Impedance Based Sensing. *Journal of Sensors* **2015**, 8 (2015).
201. Lillehoj, P.B. et al. Rapid, Electrical Impedance Detection of Bacterial Pathogens Using Immobilized Antimicrobial Peptides. *Journal of Laboratory Automation* **19**, 42-49 (2014).
202. Hause, L.L., Komorowski, R.A. & Gayon, F. Electrode and Electrolyte Impedance in the Detection of Bacterial Growth. *IEEE Transactions on Biomedical Engineering* **BME-28**, 403-410 (1981).
203. Sensors, safety and SPR. *Nature* **403**, 343-344 (2000).
204. Li, Y., Karlin, A., Loike, J.D. & Silverstein, S.C. A critical concentration of neutrophils is required for effective bacterial killing in suspension. *Proc Natl Acad Sci U S A* **99**, 8289-8294 (2002).
205. Barreiros dos Santos, M. et al. Highly sensitive detection of pathogen Escherichia coli O157:H7 by electrochemical impedance spectroscopy. *Biosens Bioelectron* **45**, 174-180 (2013).
206. Kjos, M. et al. Target recognition, resistance, immunity and genome mining of class II bacteriocins from Gram-positive bacteria. *Microbiology* **157**, 3256-3267 (2011).
207. Liebana, S. et al. Rapid detection of Salmonella in milk by electrochemical magneto-immunosensing. *Biosens Bioelectron* **25**, 510-513 (2009).
208. Dapra, J., Lauridsen, L.H., Nielsen, A.T. & Rozlosnik, N. Comparative study on aptamers as recognition elements for antibiotics in a label-free all-polymer biosensor. *Biosens Bioelectron* **43**, 315-320 (2013).
209. Fernandez, F. et al. A label-free and portable multichannel surface plasmon resonance immunosensor for on site analysis of antibiotics in milk samples. *Biosens Bioelectron* **26**, 1231-1238 (2010).
210. Causey, L.D. & Dwyer, D.S. Detection of low affinity interactions between peptides and heat shock proteins by chemiluminescence of enhanced avidity reactions (CLEAR). *Nat Biotechnol* **14**, 348-351 (1996).
211. Zhang, Z., Zhu, W. & Kodadek, T. Selection and application of peptide-binding peptides. *Nat Biotech* **18**, 71-74 (2000).

212. Diep, D.B. et al. Common mechanisms of target cell recognition and immunity for class II bacteriocins. *Proc Natl Acad Sci U S A* **104**, 2384-2389 (2007).

213. Fournier, P.-E. et al. Modern clinical microbiology: new challenges and solutions. *Nat Rev Micro* **11**, 574-585 (2013).

214. de Wildt, R.M.T., Mundy, C.R., Gorick, B.D. & Tomlinson, I.M. Antibody arrays for high-throughput screening of antibody-antigen interactions. *Nat Biotech* **18**, 989-994 (2000).

215. Rivoire, N. et al. Evaluation of the resazurin assay for the detection of multidrug-resistant Mycobacterium tuberculosis in Madagascar. *Int J Tuberc Lung Dis* **11**, 683-688 (2007).

216. Diacon, A.H. et al. Time to detection of the growth of Mycobacterium tuberculosis in MGIT 960 for determining the early bactericidal activity of antituberculosis agents. *Eur. J. Clin. Microbiol. Infect. Dis.* **29**, 1561-1565 (2010).

217. Boehme, C.C. et al. Rapid Molecular Detection of Tuberculosis and Rifampin Resistance. *N Engl J Med* **363**, 1005-1015 (2010).

218. Kosaka, P.M. et al. Detection of cancer biomarkers in serum using a hybrid mechanical and optoplasmonic nanosensor. *Nat Nano* **9**, 1047-1053 (2014).

219. Mader, A. et al. Discrimination of Escherichia coli Strains using Glycan Cantilever Array Sensors. *Nano Letters* **12**, 420-423 (2012).

220. Zhang, Q. et al. A self-bended piezoresistive microcantilever flow sensor for low flow rate measurement. *Sensors and Actuators A: Physical* **158**, 273-279 (2010).

221. Burg, T.P. et al. Weighing of biomolecules, single cells and single nanoparticles in fluid. *Nature* **446**, 1066-1069 (2007).

222. Faheem Khan, M. et al. Nanomechanical identification of liquid reagents in a microfluidic channel. *Lab on a Chip* **14**, 1302-1307 (2014).

223. Son, S. et al. Direct observation of mammalian cell growth and size regulation. *Nat Meth* **9**, 910-912 (2012).

224. CDC Incidence and Trends of Infection with Pathogens Transmitted Commonly Through Food — Foodborne Diseases Active Surveillance Network,10 U.S. Sites, 2006–2013. *MMWR Morb Mortal Wkly Rep* **63**, 328-332 (2014).

225. Jiang, W. et al. Elucidation of functional groups on gram-positive and gram-negative bacterial surfaces using infrared spectroscopy. *Langmuir* **20**, 11433-11442 (2004).

226. Ojeda, J.J. et al. Characterization of the cell surface and cell wall chemistry of drinking water bacteria by combining XPS, FTIR spectroscopy, modeling, and potentiometric titrations. *Langmuir* **24**, 4032-4040 (2008).
227. Rebuffo-Scheer, C.A., Schmitt, J. & Scherer, S. Differentiation of Listeria monocytogenes serovars by using artificial neural network analysis of Fourier-transformed infrared spectra. *Appl Environ Microbiol* **73**, 1036-1040 (2007).
228. Nicolaou, N., Xu, Y. & Goodacre, R. Fourier transform infrared and Raman spectroscopies for the rapid detection, enumeration, and growth interaction of the bacteria Staphylococcus aureus and Lactococcus lactis ssp. cremoris in milk. *Anal Chem* **83**, 5681-5687 (2011).
229. Mader, A. et al. Discrimination of Escherichia coli strains using glycan cantilever array sensors. *Nano Lett* **12**, 420-423 (2012).
230. Kang, D.-K. et al. Rapid detection of single bacteria in unprocessed blood using Integrated Comprehensive Droplet Digital Detection. *Nat Commun* **5** (2014).
231. Zeng, S., Baillargeat, D., Ho, H.-P. & Yong, K.-T. Nanomaterials enhanced surface plasmon resonance for biological and chemical sensing applications. *Chemical Society Reviews* **43**, 3426-3452 (2014).
232. Kjos, M., Salehian, Z., Nes, I.F. & Diep, D.B. An extracellular loop of the mannose phosphotransferase system component IIC is responsible for specific targeting by class IIa bacteriocins. *J Bacteriol* **192**, 5906-5913 (2010).
233. Etayash, H. et al. Surface-Conjugated Antimicrobial Peptide Leucocin A Displays High Binding to Pathogenic Gram-Positive Bacteria. *ACS Applied Materials & Interfaces* **6**, 1131-1138 (2014).
234. LongoG et al. Rapid detection of bacterial resistance to antibiotics using AFM cantilevers as nanomechanical sensors. *Nat Nano* **8**, 522-526 (2013).
235. Fass, L. Imaging and cancer: A review. *Molecular oncology* **2**, 115-152 (2008).
236. Gupta, G.P. & Massague, J. Cancer metastasis: building a framework. *Cell* **127**, 679-695 (2006).
237. Stott, S.L. et al. Isolation of circulating tumor cells using a microvortex-generating herringbone-chip. *Proc Natl Acad Sci U S A* **107**, 18392-18397 (2010).
238. Zemp, R.J. Nanomedicine: Detecting rare cancer cells. *Nat Nano* **4**, 798-799 (2009).

239. Yu, M. et al. RNA sequencing of pancreatic circulating tumour cells implicates WNT signalling in metastasis. *Nature* **487**, 510-513 (2012).
240. Mostert, B., Sleijfer, S., Foekens, J.A. & Gratama, J.W. Circulating tumor cells (CTCs): detection methods and their clinical relevance in breast cancer. *Cancer Treat Rev* **35**, 463-474 (2009).
241. Alix-Panabieres, C. & Pierga, J.Y. [Circulating tumor cells: liquid biopsy]. *Bull Cancer* **101**, 17-23 (2014).
242. Alix-Panabieres, C. & Pantel, K. Technologies for detection of circulating tumor cells: facts and vision. *Lab Chip* **14**, 57-62 (2014).
243. Schoenfeld, A. et al. The detection of micrometastases in the peripheral blood and bone marrow of patients with breast cancer using immunohistochemistry and reverse transcriptase polymerase chain reaction for keratin 19. *Eur J Cancer* **33**, 854-861 (1997).
244. He, W. et al. In vivo quantitation of rare circulating tumor cells by multiphoton intravital flow cytometry. *Proc Natl Acad Sci U S A* **104**, 11760-11765 (2007).
245. Castells, A. et al. Detection of colonic cells in peripheral blood of colorectal cancer patients by means of reverse transcriptase and polymerase chain reaction. *Br J Cancer* **78**, 1368-1372 (1998).
246. Lee, S.K. et al. Nanowire substrate-based laser scanning cytometry for quantitation of circulating tumor cells. *Nano Lett* **12**, 2697-2704 (2012).
247. Yoon, H.J. et al. Sensitive capture of circulating tumour cells by functionalized graphene oxide nanosheets. *Nat Nanotechnol* **8**, 735-741 (2013).
248. Gaitas, A., Malhotra, R. & Pienta, K. A method to measure cellular adhesion utilizing a polymer micro-cantilever. *Appl Phys Lett* **103**, 123702 (2013).
249. Shekhawat, G.S. & Dravid, V.P. Nanomechanical sensors: Bent on detecting cancer. *Nat Nanotechnol* **8**, 77-78 (2013).
250. Wu, G. et al. Bioassay of prostate-specific antigen (PSA) using microcantilevers. *Nat Biotechnol* **19**, 856-860 (2001).
251. Soudy, R. et al. Proteolytically stable cancer targeting peptides with high affinity for breast cancer cells. *J Med Chem* **54**, 7523-7534 (2011).
252. Ahmed, S. et al. Peptide arrays for screening cancer specific peptides. *Anal Chem* **82**, 7533-7541 (2010).

253. Kenny, L.M. et al. Phase I trial of the positron-emitting Arg-Gly-Asp (RGD) peptide radioligand 18F-AH111585 in breast cancer patients. *J Nucl Med* **49**, 879-886 (2008).
254. Desgrosellier, J.S. & Cheresh, D.A. Integrins in cancer: biological implications and therapeutic opportunities. *Nat Rev Cancer* **10**, 9-22 (2010).
255. Pasqualini, R., Koivunen, E. & Ruoslahti, E. Alpha v integrins as receptors for tumor targeting by circulating ligands. *Nat Biotechnol* **15**, 542-546 (1997).
256. Dareing, D.W., Tian, F. & Thundat, T. Effective mass and flow patterns of fluids surrounding microcantilevers. *Ultramicroscopy* **106**, 789-794 (2006).
257. Wang, J. et al. Rapid detection of pathogenic bacteria and screening of phage-derived peptides using microcantilevers. *Anal Chem* **86**, 1671-1678 (2014).
258. Bai, L. et al. Peptide-based isolation of circulating tumor cells by magnetic nanoparticles. *Journal of Materials Chemistry B* **2**, 4080-4088 (2014).
259. Etayash, H., Jiang, K., Thundat, T. & Kaur, K. Impedimetric Detection of Pathogenic Gram-Positive Bacteria Using an Antimicrobial Peptide from Class IIa Bacteriocins. *Anal Chem* **86**, 1693-1700 (2014).
260. DeMello, A.J. Control and detection of chemical reactions in microfluidic systems. *Nature* **442**, 394-402 (2006).
261. Kolonin, M.G. et al. Ligand-directed surface profiling of human cancer cells with combinatorial peptide libraries. *Cancer Res* **66**, 34-40 (2006).
262. Rangel, R. et al. Combinatorial targeting and discovery of ligand-receptors in organelles of mammalian cells. *Nat Commun* **3**, 788 (2012).
263. Chou, J. et al. Effects of sample delivery on analyte capture in porous bead sensors. *Lab Chip* **12**, 5249-5256 (2012).
264. Jacob, K., Sollier, C. & Jabado, N. Circulating tumor cells: detection, molecular profiling and future prospects. *Expert Rev Proteomics* **4**, 741-756 (2007).
265. Balic, M. et al. Comparison of two methods for enumerating circulating tumor cells in carcinoma patients. *Cytometry B Clin Cytom* **68**, 25-30 (2005).
266. Thery, C., Ostrowski, M. & Segura, E. Membrane vesicles as conveyors of immune responses. *Nat Rev Immunol* **9**, 581-593 (2009).
267. Fidler, I.J. The pathogenesis of cancer metastasis: the 'seed and soil' hypothesis revisited. *Nat Rev Cancer* **3**, 453-458 (2003).

268. Melo, S.A. et al. Glypican-1 identifies cancer exosomes and detects early pancreatic cancer. *Nature* **523**, 177-182 (2015).

269. Dey-Hazra, E. et al. Detection of circulating microparticles by flow cytometry: influence of centrifugation, filtration of buffer, and freezing. *Vascular Health and Risk Management* **6**, 1125-1133 (2010).

270. Tauro, B.J. et al. Comparison of ultracentrifugation, density gradient separation, and immunoaffinity capture methods for isolating human colon cancer cell line LIM1863-derived exosomes. *Methods* **56**, 293-304 (2012).

271. Im, H. et al. Label-free detection and molecular profiling of exosomes with a nano-plasmonic sensor. *Nat Biotech* **32**, 490-495 (2014).

272. Tatischeff, I. et al. Fast characterisation of cell-derived extracellular vesicles by nanoparticles tracking analysis, cryo-electron microscopy, and Raman tweezers microspectroscopy. *Journal of Extracellular Vesicles* **1**, 10.3402/jev.v3401i3400.19179 (2012).

273. Issadore, D. et al. Miniature magnetic resonance system for point-of-care diagnostics. *Lab on a chip* **11**, 2282-2287 (2011).

274. Ko, J., Carpenter, E. & Issadore, D. Detection and isolation of circulating exosomes and microvesicles for cancer monitoring and diagnostics using micro-/nano-based devices. *Analyst* **141**, 450-460 (2016).

275. Palmieri, V. et al., Vol. 16 16:2583 (Nanoparticle Research 2014).

276. Gengrinovitch, S. et al. Glypican-1 Is a VEGF165 Binding Proteoglycan That Acts as an Extracellular Chaperone for VEGF165. *Journal of Biological Chemistry* **274**, 10816-10822 (1999).

277. Mrvar-Brečko, A. et al. Isolated microvesicles from peripheral blood and body fluids as observed by scanning electron microscope. *Blood Cells, Molecules, and Diseases* **44**, 307-312 (2010).

278. Van Der Pol, E. et al. Optical and non-optical methods for detection and characterization of microparticles and exosomes. *Journal of Thrombosis and Haemostasis* **8**, 2596-2607 (2010).

279. Etayash, H., McGee, A.R., Kaur, K. & Thundat, T. Nanomechanical sandwich assay for multiple cancer biomarkers in breast cancer cell-derived exosomes. *Nanoscale* **8**, 15137-15141 (2016).
280. Tirinato, L. et al. SERS analysis on exosomes using super-hydrophobic surfaces. *Microelectronic Engineering* **97**, 337-340 (2012).
281. Bodapati, K.C. et al. Design, synthesis and evaluation of antimicrobial activity of N-terminal modified Leucocin A analogues. *Bioorganic & Medicinal Chemistry* **21**, 3715-3722 (2013).
282. Messing, D.S., Ghindilis, A. & Schwarzkopf, K. in Engineering in Medicine and Biology Society, EMBC, 2011 Annual International Conference of the IEEE 2740-2744 (2011).
283. Hoshino, A. et al. Tumour exosome integrins determine organotropic metastasis. *Nature* **527**, 329-335 (2015).
284. Grasso, L. et al. Molecular screening of cancer-derived exosomes by surface plasmon resonance spectroscopy. *Analytical and Bioanalytical Chemistry* **407**, 5425-5432 (2015).
285. Scallan, E. et al. Foodborne illness acquired in the United States--major pathogens. *Emerg Infect Dis* **17**, 7-15 (2011).
286. Gould, L.H. et al. Surveillance for foodborne disease outbreaks - United States, 1998-2008. *MMWR Surveill Summ* **62**, 1-34 (2013).
287. Etayash, H., Norman, L., Thundat, T. & Kaur, K. Peptide-Bacteria Interactions using Engineered Surface-Immobilized Peptides from Class IIa Bacteriocins. *Langmuir* **29**, 4048-4056 (2013).
288. Hashem Etayash, S.A., Ramana Dangeti and Kamaljit Kaur Peptide Bacteriocins - Structure Activity Relationships *Current Topics in Medicinal Chemistry* **16**, 220 - 241 (2015).
289. Kong, J. & Yu, S. Fourier transform infrared spectroscopic analysis of protein secondary structures. *Acta Biochim Biophys Sin* **39**, 549-559 (2007).

Appendix

Chapter 2

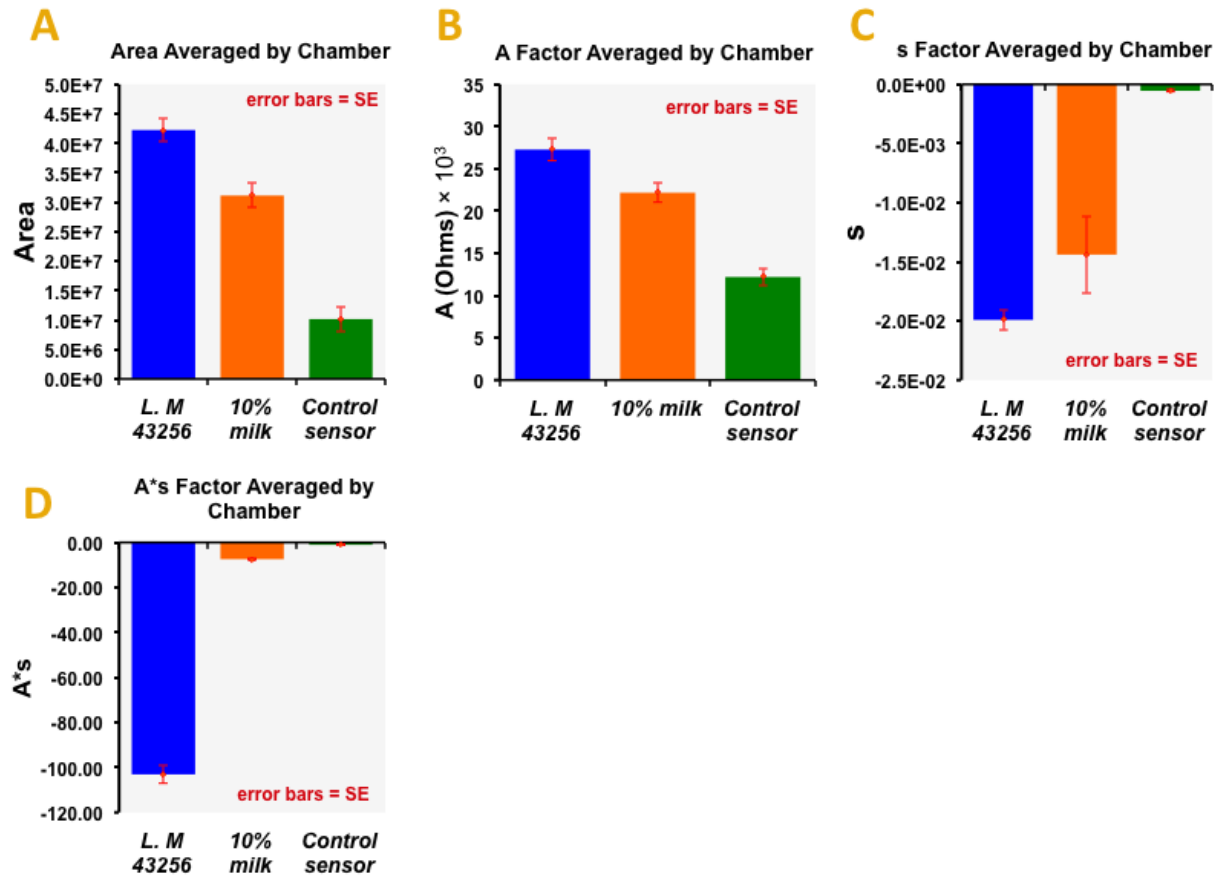

Appendix Figure 1. Binding kinetic parameters of normalized impedance signals to peptide sensor responses to 10% milk contaminated with *L. monocytogenes* (*L. M*) at 10^3 cfu mL^{-1}; **(A)** area under the binding curve, **(B)** Amplitude A **(C)** s value and **(D)** A × s. Bars represent an average of five replications.

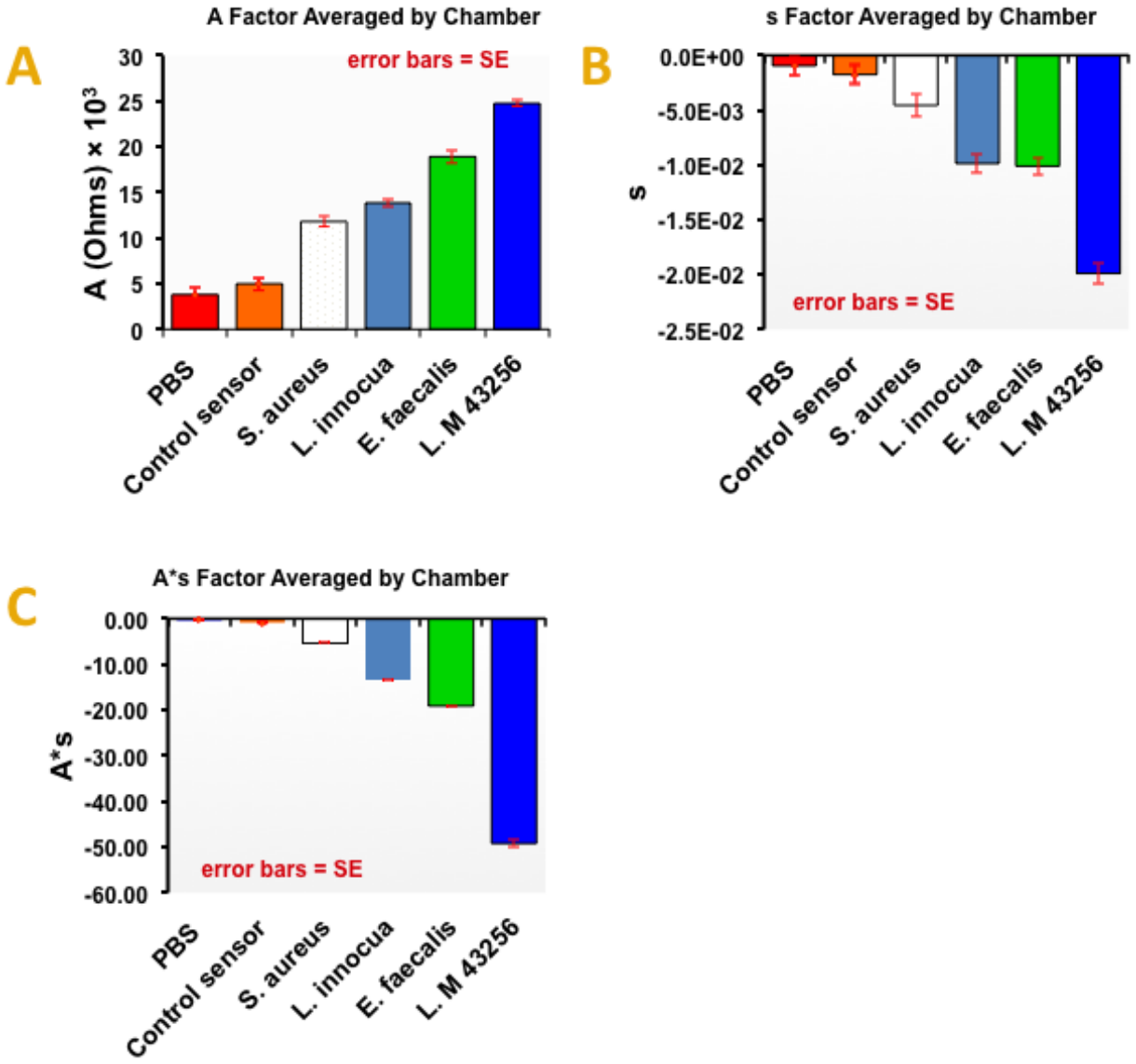

Appendix Figure 2. Binding curve parameters of normalized impedance signal responses to peptide sensor interactions to bacterial species. **(A)** Amplitude A **(B)** time constant (s value) and **(C)** A × s value, the initial binding rate. The studies were performed with contaminated buffer samples with different bacterial species at concentrations of 10^3 cful mL^{-1}. Bars represent an average of five replications.

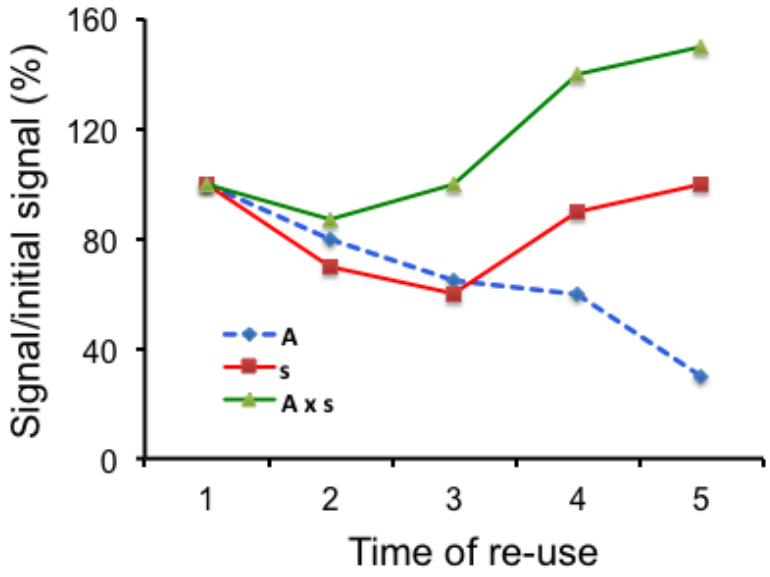

Appendix Figure 3. Changes of the binding curve parameters as a result of the peptide sensor array regeneration (x-axis). The amplitude A (blue), time constant (red) and A × s (green). The array performance after regeneration was evaluated against *Listeria monocytogenes* at a concentration of 10^3 cfu mL^{-1} in 1X PBS solution at fixed frequency. The values were calculated as percentage of the initial measurements obtained during the first time use.

Chapter 3:

Materials and Methods:

1. Ligands and bacteria:

In our bacterial detection study, the target strain of bacteria was *Listeria monocytogenes* (*L. monocytogenes*) – a facultative, food-borne pathogen with a mortality rate exceeds 20%.[224] Two *L. monocytogenes* targeting-molecules were employed, anti-*L. monocytogenes* monoclonal antibody (mAb) and *Listeria*-selective antimicrobial peptide (AMP). The mAb were purchased from MyBioSource, Inc. San Diego, California USA. The antimicrobial peptide (Leucocin A of class IIa bacteriocin), having a sequence of 37 amino acids (KYYGNGVHCTKSGCSVNWGE--AFSAGVHRLANGGNGFW), was chemically synthesized using Fmoc-solid phase peptide synthesis (SPPS) as described in previous reports[233, 287]. We have chosen Leucocin A of class IIa bacteriocins because of its selectivity, potent activity against *L. monocytogenes*, ample stability and its applicable use in biosensing technologies as conveyed heretofore[97, 287]. A negative peptide (seq. CTKSGCSVNWGEAF), with no biological activity against bacteria[288] was used as a control for comparisons. Stocks of bacterial cells, *L. monocytogenes* ATCC 43256 (grown in TSBYE, 37 °C), *Listeria innocua ATCC* 33090 (grown in TSBYE, 37 °C), *Staphylococcus aureus ATCC* 13565 (grown in APT broth, 37 °C), and gram-negative *E.coli DH5α* (grown in LB media), were obtained from CanBiocin Edmonton Inc., subcultured, maintained and handled in a level II biosafety cabinet.

2. **Bimaterials microchannel cantilever (BMC):**

U-shaped microfluidic channel was made-up on top of a silicon nitride microcantilever having a dimension of 32 μm width, 600 μm lengths and a height of 3 μm (**Fig 1 in the main contents)**. The cantilever was made bimetallic by coating the bottom side with a gold film (300 nm thickness). The inside part however, was kept as a thin layer of silicon nitride. The two openings at the bottom of the lever, inlet and outlet, are attached to teflon tubes and adjusted to direct fluid flow (samples) in and out the microfluidic channel. The BMC chip settles in a holder made of polyether ether ketone (PEEK), connected to large tubes for fluid delivery. A polydimethylsiloxane (PDMS) seal is used to achieve a sealed contact between the PEEK holder and the BMC chip. An external-cavity quantum cascade lasers (QCLs) were concomitant the cantilever setup and used as a source of infrared (IR) light. When the BMC irradiated with a

series of different IR wavelengths, the deflection is measured by reflecting a visible laser (635 nm) to a positive sensitive detector (PSD) attached to the system.

3. **BMC surface functionalization:**

The BMC channel consists of silicon nitride (Si_3N_4) was initially rinsed with piranha solution [30% H2O2/H2SO4, 1:3 (v/v)], chloroform, MQ-water and subjected to ambient atmosphere to ensure complete oxidation of the Si_3N_4 and formation of silicon dioxide assembles [*Note, piranha is extremely reactive, caution is strongly recommended*]. The formed silanol groups (Si - OH) were chemically attached to an ethanolamine linker ($NH_2C_2H_4OH$, Sigma Aldrich), which was further conjugated to the bacteria-targeting ligands (AMP or/ mAb). In details, ethanolamine hydrochloride (300 mg) was dissolved in DMSO (1 mL) under gentle heating at ~70 C in a crystallization dish. It was allowed then to cool down and degassed in a desiccator at aspirator vacuum for 30 min. A solution of ~100 μL was subsequent passed through the BMC several times during the day and the chip was sealed by Teflon and incubated overnight in the solution to ensure a complete coupling. Next, the chip was rinsed with ethanol and dried under stream of nitrogen gas. Either AMP /or mAb solution (0.8 mg mL^{-1}), activated by NHS/EDC for 10 min, was injected to the BMC chip five times, ~50 μL once every 2 hr to ensure a widespread assembling. The solution was also kept overnight in the microchannel to certify the functionalization (**Fig S1)**. Prior experiments, the BMC were washed with MQ-water, ethanol and dried under stream of nitrogen gas.

4. Surface characterization and ligands density measurements:

In the initial experiments the resonance frequency and the infrared-induced nanomechanical deflection of the BMC functionalized with self-assembled monolayers (SAMs) of ethanolamine (1^{st} SAM), and AMP or/ anti-listeria monoclonal antibody (mAb) as 2^{nd}SAM were collected individually. Using a Quantum Cascade Laser (QCL) (MIRCat, Day Light Solutions), the BMC was irradiated with tunable IR light at different wavenumber spans, QCL1 (from 1615 cm^{-1} – 1365 cm^{-1}), QCL2 (1365 cm^{-1} – 1170 cm^{-1}) and QCL3 (1700 cm^{-1} – 999 cm^{-1}) to achieve a longer range of IR signatures. The average IR nanomechanical spectrum (average of the amplitude) represents the averaged measurements of five independent experiments performed

under same conditions. The average amplitudes were plotted against wavenumbers cm^{-1} to present the nanomechanical deflection and the IR fingerprint spectra of the delivered samples.

We examined the surface functionalization process by observing the changes in the nanomechanical IR readings, resonance frequency and nanodeflection of the cantilever compared to the background spectrum of silicon nitride. The 1st SAM (ethanolamine layer) was detected by appearance of a distinctive absorption peak at ~1600 cm^{-1}, suggesting a primary amine absorption peak (**Fig S2a**). The peak however, nearly vanished subsequent loading of the 2nd SAM (AMP or/mAb adlayer), signifying the success of the peptide conjugation to the ethanolamine layer and indicating a constant adlayer formation (**Fig S2a**). The adlayer of the AMP and/or mAb was also defined by the appearance of a strong absorption peak at 1533 cm^{-1}, which corresponds well to the amide II absorption band[197, 289]. Furthermore, the differential analysis of amplitudes of nanomechanical deflections (**Fig S2b**) and the resonance frequency shifts (**Fic S2c**) showed the differences in the mass densities of the two adsorbed layers (1st and 2nd SAMs), and indicated the attainment of the sensor surface activation.

To ensure a high surface density of the immobilized ligands on the surface of the BMC chip, we performed preliminary tests, where diluted samples of antimicrobial peptide (Leucocin A) and mAb (0.2, 0.4, 0.6, 0.8, and 1 mg ml^{-1}) were introduced into the BMC sensor and subjected to nanomechanical readings. The nanomechanical cantilever bending was computed and results were presented as differential deflection against concentration of the peptide in the samples (**Fig S3**). Results suggested that a concentration of 0.8 mg mL^{-1} is an optimum to achieve maximum surface density of both AMP and mAb. Based on the results, we used the highest concentration of 0.8 mg mL^{-1} for immobilization of the ligands in the BMC microchannel.

5. **BMC measurements; bacterial detection/sensitivity and selectivity**:

BMC fabrication, instrumentation for data acquisition and software for data analysis are described in our previous report[222]. Here, by passing the fluid through the channel, the device is not only detecting the change in the total mass density of the cantilever, but it also identifies the molecular fingerprint of the present molecules in the sample by providing the nanomechanical IR

spectra of the entire delivery. Initially, the measurements was performed to characterize the surface of the channel and to endorse the surface functionalization processes, as illustrated above.

In the bacterial detection experiments, artificially contaminated samples with *L. monocytogenes* at 10^3 cfu mL^{-1} (100 cells /100 µl were conceded through the BMC sensors, incubated and subjected to the nanomechanical readings. Three different readings, IR signatures, magnitude of nanomechanical cantilever deflections and resonance frequency shifts were measured. To estimate the device sensitivity and limit of detection, diluted samples with bacterial cells suspended in water at a range of 10^3 – 10^6 cfu ml^{-1}were subjected to the sensors readings. Various strains of bacteria were also exposed to the BMC sensors in order to determine the sensors selectivity. Each experiment was repeated at least five times under same conditions and at different time sets. Signals of the readings were plotted with respect to the wavenumber of IR light that generates nanomechanical IR spectra of the analytes inside the BMC. The IR spectral features are often overlapped. Thus, some data preprocessing were performed to analyze the data, such as binning, smoothing, and second derivative transformation analysis. Binning reduces the number of data points in a spectrum, smoothing eliminates noise by averaging neighboring data points. Second-derivative transformation separates overlapping absorption bands and removes baseline offsets.

6. <u>Confocal microscopy:</u>

A Stock solution of the CyQUANT dye (a green color probe) was made by following the manufacture protocol. Briefly, CyQUANT probe reagent (0.8 μL) was dissolved in HBSS buffer (200 μL) and stored in dark condition at 4 °C. Bacterial cells (*L. monocytogenes, or L. innocua, or S. aureus, or E. coli DH5α*) were pulled from the culture by centrifugation and re-suspended in fresh 1× PBS solution. The supernatant was eliminated and the bacterial cells at a concentration of 10^6 cfu ml^{-1} were incubated with CyQUANT solution (100 μL) for ~30 min at 37 °C. The cells were pelleted by centrifugation again and resuspended in fresh 1 × PBS buffer. Samples of stained bacterial cells were then introduced into the AMP-coated BMC sensor and the mAb-coated BMC, independently for ~30 min. A gentle wash of the BMC sensors with 1 × PBS was performed prior any microscopic examination. The captured bacterial cells were

examined using a Quorum WaveFX spinning disk confocal microscopy (Quorum Technologies Inc., Guelph, Canada) through a magnification20×/1.4. All captured images were recorded using a Quorum digital camera and were analyzed using a velocity three-dimensional image analysis software.

7. Sensor re-usability:

Effective regeneration is a key for successful sensor assays. Therefore, a valuable investment would be establishing a suitable re-generation condition that allows a number of recycling with maintaining a sufficient activity and efficient performance. The BMC chip of both, AMP-coated and mAb-coated sensors, was simply re-generated via two steps. First, the sensors were vigorously washed with a regeneration solution of 10 mM glycine-HCl at pH (3.0, 2.5, 2.0 or 1.5), independently. The microfluidic channel was then rinsed with 70% ethanol in order to remove all adsorbed materials and making the functionalized BMC sensor accessible again for further detection assays. Performance of the re-generated BMC chips was evaluated against *L.* monocytogenes at 100 cells per 100 μL. The nanomechanical deflection was measured at the indicated bacteria infrared signature of both regenerated sensors (AMP-coated or mAb-coated BMC). The average calculated values were obtained as percentage of responses with respect to the initial deflection values obtained at the first time use. The condition of suitable regeneration was determined by using different pH values as indicated. **Fig S6** shows the sensors performance after BMC regeneration. It turns out that regeneration of the AMP-coated BMC at all conditions tested restore the immobilized receptors response to the analyte to a constant level, which is 80% or more with best regeneration achieved at pH 2.5 and 3.0. Accordingly, the regeneration can be performed confidently at pH 3.0 or 2.5. In contrast to the AMP sensor, the repeated usage of the mAb-coated BMC sensor after its regenerations at harsh environment (pH 2.0 and 1.5) had resulted in dramatic loss of its binding activity to more than 50%, which indicate that the immobilized mAb may undergo unfolding and denaturation (**Fig S6**). However, the sensor was sufficiently stable at milder conditions (pH 2.5 and 3.0) where a restored response reaches ~80%. The results suggest that mAb-coated BMC can be regenerated at pH 2.5 – 3.0 (or possibly higher), but it loses significant activity at lower pH. Steps for BMC sensor regeneration may need further optimizations using further reagents since milder conditions showed to preserve the sensor performance.

8. **Bacteria drug resistance**

All chemicals, culture media, reagents and antibiotics (ampicillin and kanamycin), with analytical grade, were obtained from Sigma-Aldrich. The ampicillin is a β-lactam containing antibiotics, penicillin alike, that act by inhibition of bacterial cell-wall synthesis through its interference with the peptidoglycan biosynthesis. The kanamycin; on the other hand, is an aminoglycoside subtype that kills bacteria by causing a membrane-damage and inhibiting DNA and RNA synthesis. *E. coli DH5α* is a well-known strain with its sensitivity to ampicillin and its resistance to kanamycin. The AMP (Leucocin A) was also applied in this study in order to verify applicability of the sensor to detect various drug-resistances and to explore response of the bacteria to antibiotics and antimicrobial peptides. Leucocin A is very unique class IIa bacteriocin peptide, with very strong activity against *L. monocytogenes.* The peptide acts by targeting specific membrane allocated receptor found on the surface membrane of bacterial cells that is known as mannose phosphotransferase[288]. Interestingly, some bacterial cells express this receptor and others do not; some cells have higher expression level of this receptor than others and some cells develop resistance gene to modify this targeted receptor. In order to identify bacterial resistance to this AMP, we have used two different strains of bacteria, *E. coli DH5α* and *L. monocytogenes*. While *L. monocytogenes* is very sensitive to Leucocin A, DH5α-strain is unsusceptible to it [288].

9. Bacteria preparations

As described previously, frozen stocks of bacteria, stored at -80°C in glycerol-supplemented media, were initially streaked in agar growth media and few bacterial colonies were collected afterward and incubated overnight at 37°C in 1 ml of broth media (LB for *E. coli* DH5 and TSBYE for *L. monocytogenes* 43256). After incubation, the bacterial culture was centrifuged; bacteria were precipitated and re-suspended in a phosphate buffered saline – pH 7.4.

10. BMC sensor preparation, calibration and detection of bacterial-drug resistance

Our home-made silicon nitride microchannel cantilevers coated from bottom with a thin film of gold layer (300 nm) and having dimensions of 32 μm width, 600 μm lengths and a microchannel height of 3 μm were embedded on it. Initially, the BMC was treated with (3-aminopropyl)

triethoxysilane (APTES) – a linker molecule that promotes adherence of bacterial cells to the cantilever surface. The linker provides loose attachment of the cells to the cantilever surface without affecting its metabolic and viable activities _ENREF_78[234]. Specifically, the BMC was subjected to a 0.2% solution of APTES in MQ water for approximately 3-5 min and then rinsed with ultrapure water. The BMC sensor was introduced into the sensor chamber for analysis and calibration. The calibration was performed by injecting buffer solution free from bacteria, and taking its nanomechanical reading as a baseline for measuring the subsequent experiments. Bacteria cells either *E. coli*, in case of (ampicillin and kanamycin or *Listeria monocytogenes*, in case of the AMP Leucocin A, were diluted at 10^{-5} and introduced into the BMC. The cells were left to incubate for ~10 min at room temperature and were then rinsed gently with PBS to remove any floating bacterial cells. Standard LB media or LB media containing antibiotics were injecting individually to the BMC sensor and data of the resonance frequency, cantilever deflection and IR signatures were measured simultaneously after each step. The measurements were performed at 5 min from the injection and after 30 min from the injection. The measurement was performed also after the antibiotics were removed and re-introduced LB media again. In addition, in order to enhance the metabolism of the bacteria, we introduced 5% glucose solution to bacteria after exposure to antibiotics and measured the sensor response 10 min later. The experiments are intended to elaborate the viability of the cells and its susceptibility to the treatments. Due to overlapping, the IR spectral preprocessing such as binning, smoothing, and second derivative transformation analysis were performed to analyze the data. Binning reduces the number of data points in a spectrum, smoothing eliminates noise by averaging neighboring data points. Second-derivative transformation separates overlapping absorption bands and removes baseline offsets. In addition, in order to differentiate intact from dead bacteria. IR Multivariate analysis, analogous to principal component analysis (PSA), was performed to differentiation life from dead bacteria. The analysis involved applying a stepwise variable selection to decrease the multidimensionality of the data into its most significant scores as described previously.

11. Bacteria viability assay (Microscopy)

The viability of bacterial cells attached to the inner walls of the cantilever was evaluated using a live/dead Bacterial Viability Kit (Life Technologies Inc., Burlington, ON, Canada). Live/dead

bacterial viability stains includes CyQUANT green and propidium iodide (PI). The two dyes were prepared separately by dilution in MQ-water (1:10) and then mixed together in equivalent ratio (1:1 vol/vol). The mixed live/dead solution (~ 10 µL) was introduced into BMC contains bacteria had exposed either to ampicillin or kanamycin. The BMC left for 10 min in darkness at room temperature prior to analysis. The captured bacteria were examined using a Quorum WaveFX spinning disk confocal microscopy (Quorum Technologies Inc., Guelph, Canada) through a magnification20×/1.4. All captured images were recorded using a Quorum digital camera and were analyzed using a velocity three-dimensional image analysis software.

12. <u>Statistical analysis:</u>

All nanomechanical measurements were averaged and each experiment was performed at least five times. Data are presented as mean ± SD throughout the manuscript. The statistical difference was tested either using the unpaired t-test or the one way ANOVA test. In all statistical analysis the significance level (P value) was sat at as 0.05.

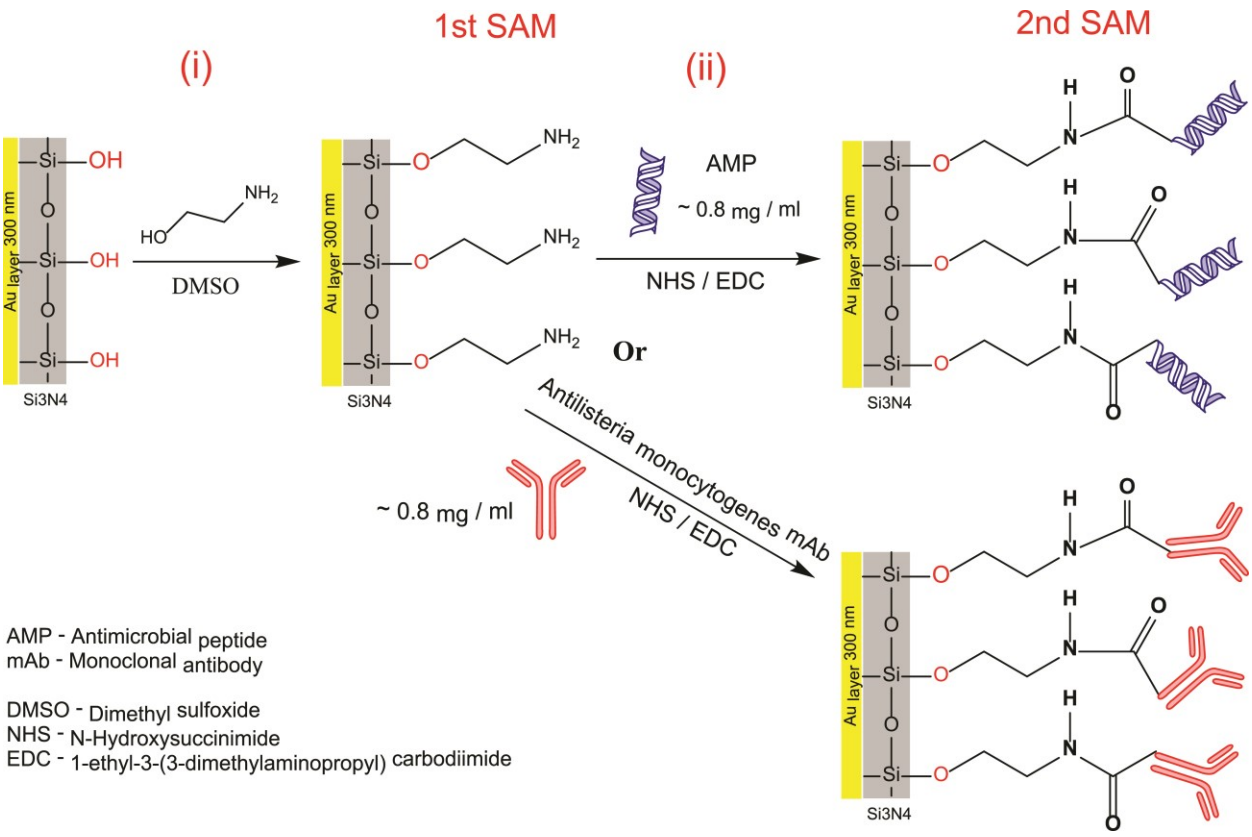

Appendix Figure 4. BMC ligands attachment. Chemistry of the BMC surface functionalization illustrates the two steps of the AMP/ or mAb of immobilization strategy. Ethanolamine interacts with the oxidized silicon nitride surface (**i**), forming free amine groups (1st SAM) accessible for conjugation with pre-activated carboxylates of the AMP or mAb (**ii**) to custom an AMP or mAb adlayer (2nd SAM) as indicated. DMSO: Dimethylsulfoxide; NHS: N-hydroxysuccinimide; EDC: 1-Ethyl-3-(3-dimethylaminopropyl) carbodiimide.

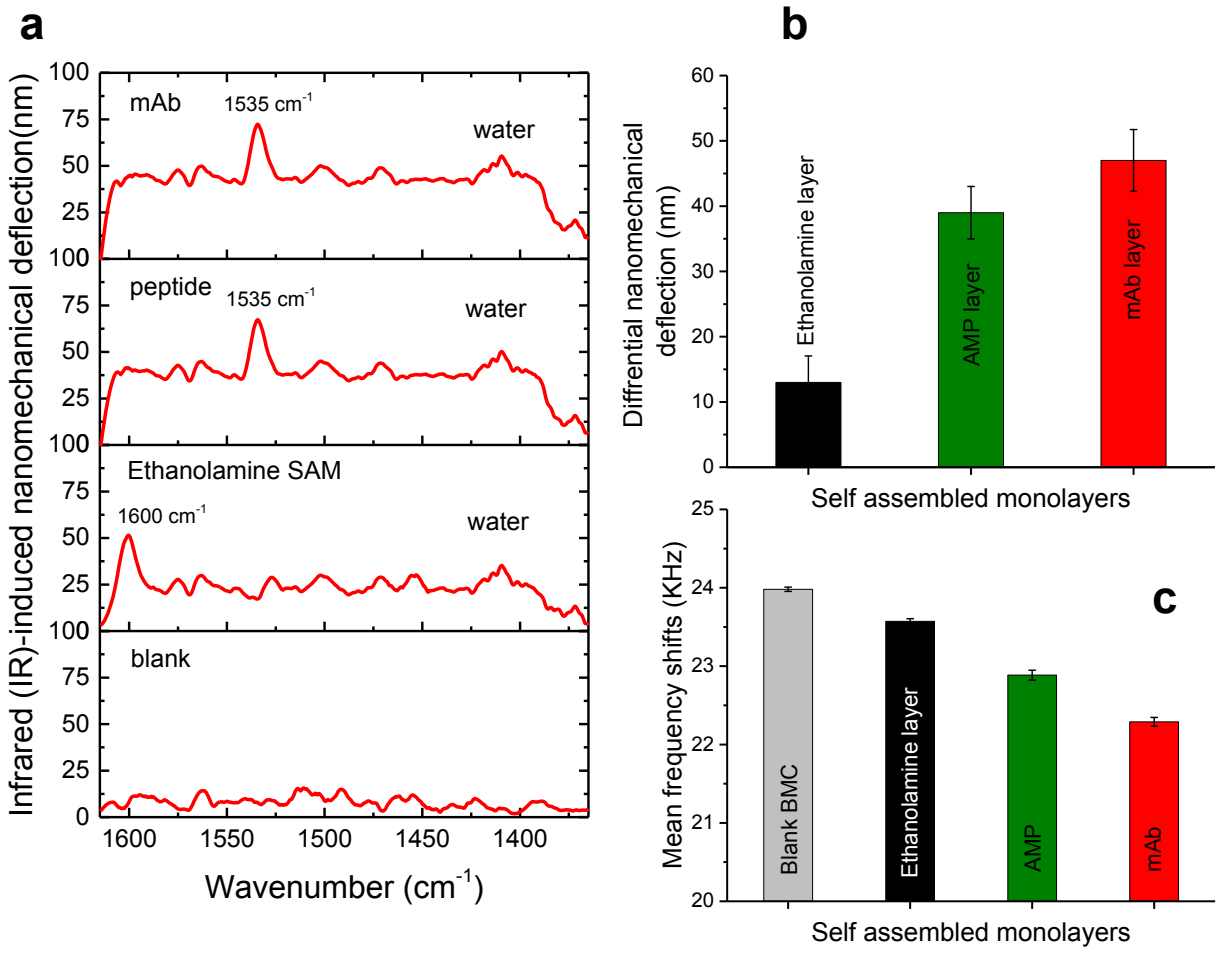

Appendix Figure 5. Infrared signature, cantilever nanomechanical deflections and frequency shifts exhibit BMC surface functionalization. (**a**), integrated IR signals present SAM layers on the cantilever surface. Appearance of a 1ry amine band around 1600 cm^{-1} (ethanolamine panel) is an indicative signal of the ethanolamine layer-adherence. Its extinction and appearance of amide II band (1553 cm^{-1}) is a definite signal of a second SAM formation (mAb /or peptide adlayer). IR spectra were smoothed 30% and are representative of five replicates. (**b)** Differential nanomechanical deflections of the cantilever show the response of the BMC to the adhered adlayers. Averaged values are presented with error bars indicating standard deviations (n=5). (**c**) BMC resonance frequency shifts as a result of surface functionalization. Frequency drops down as higher density molecules attach to the inside shallow of the microchannel, 1st SAM (ethanolamine), AMP adlayer, mAb adlayer. Changes in the resonance frequency are measured with respect to the surface functionalization.

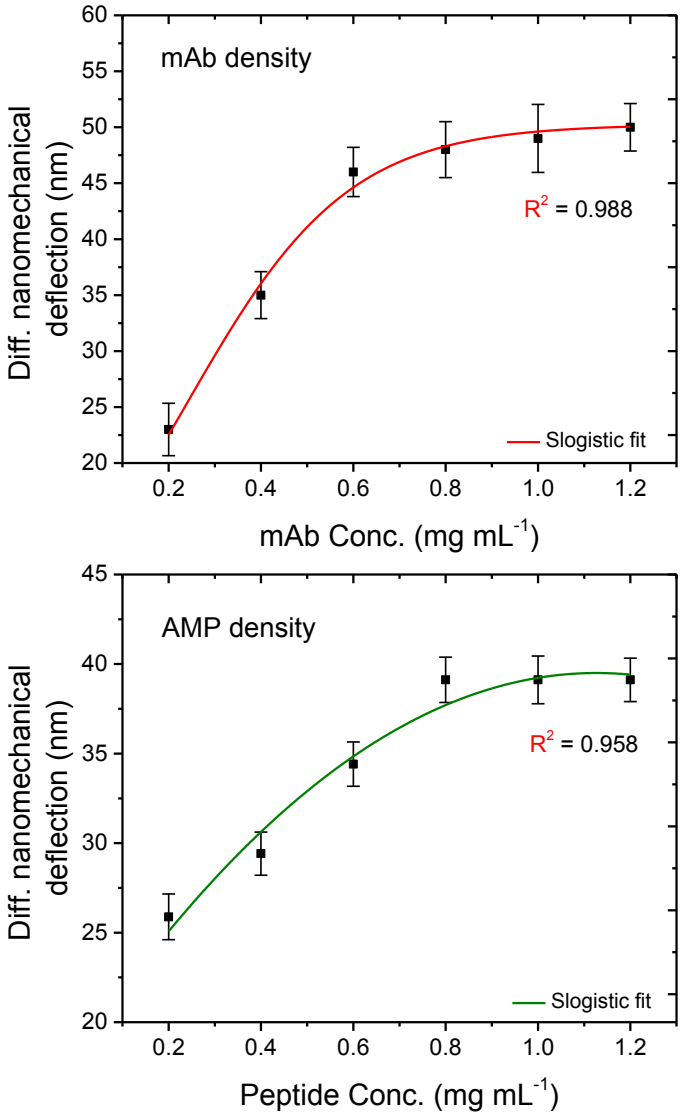

Appendix Figure 6. adsorption density of the AMP and mAb on the BMC surface. The differential nanomechanical deflection induced is plotted against various ligand (AMP or mAb) concentrations in the sample (0.2 mg ml^{-1}, 0.4 mg ml^{-1}, 0.6 mg ml^{-1}, 0.8 mg ml^{-1}, 1 mg ml^{-1}, 1.2 mg ml^{-1}). The solid line represents the Slogistic calibration fit and error bars represent standard deviations (n = 5). The study suggested density saturation at 0.8 mg ml^{-1}, which was used subsequently for surface functionalization.

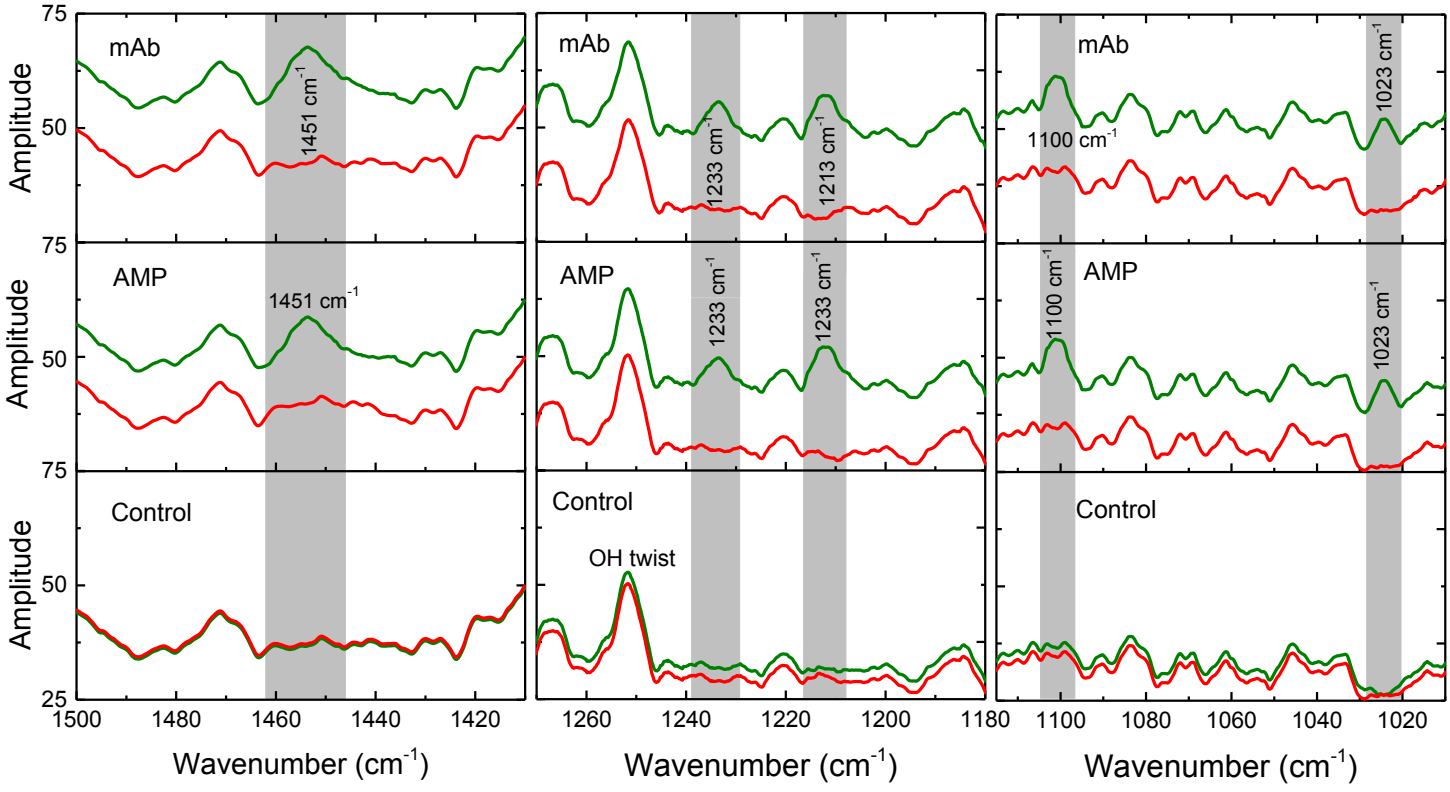

Appendix Figure 7. IR-induced nanomechanical spectra show the fingerprint of L. monocytogenes at different wavelengths. As indicated, the spectra display linear nanomechanical signals associated with specific IR signatures of each adhesion layer added to the BMC. Adhesion or/ binding of bacteria (L. monocytogenes) to the immobilized ligands (mAb and AMP) show definite bacteria infrared absorption bands at different wavenumbers. In all spectra, red lines represent samples with no bacteria while the green lines represent the response to samples containing bacteria (100 cell /µL). While the mAb and AMP represent BMC coated with a monoclonal antibody and an antimicrobial peptide (Leucocin A), respectively, the control denotes a BMC coated with a negative peptide, which has no affinity to bacteria. The observed bacteria IR absorption bands, as specified above, 1451 cm^{-1}, 1233 cm^{-1}, 1213 cm^{-1}, 1100 cm^{-1} and 1023 cm^{-1} in the spectra correspond well to bacteria IR fingerprints illustrated previously by FTIR. Note that the presented spectra are smoothed (30%) short cut data of a wide range infrared spectrum.

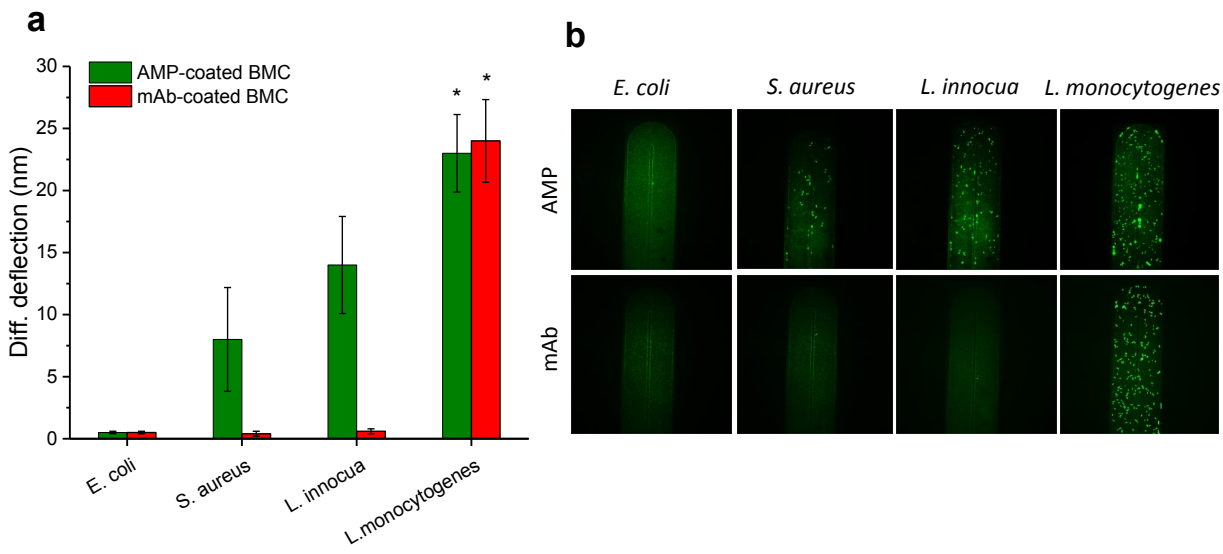

Appendix Figure 8. nanomechanical deflection in response to various strains of bacteria. Charts show the differential cantilever deflection in response to various strains of bacteria. The results indicate statistical significant response to *L. monocytogenes* compared to other strains with a P values > 0.05 (n = 5). b, confocal microscopy images show attached bacteria onto the AMP and mAb functionalized BMC sensors.

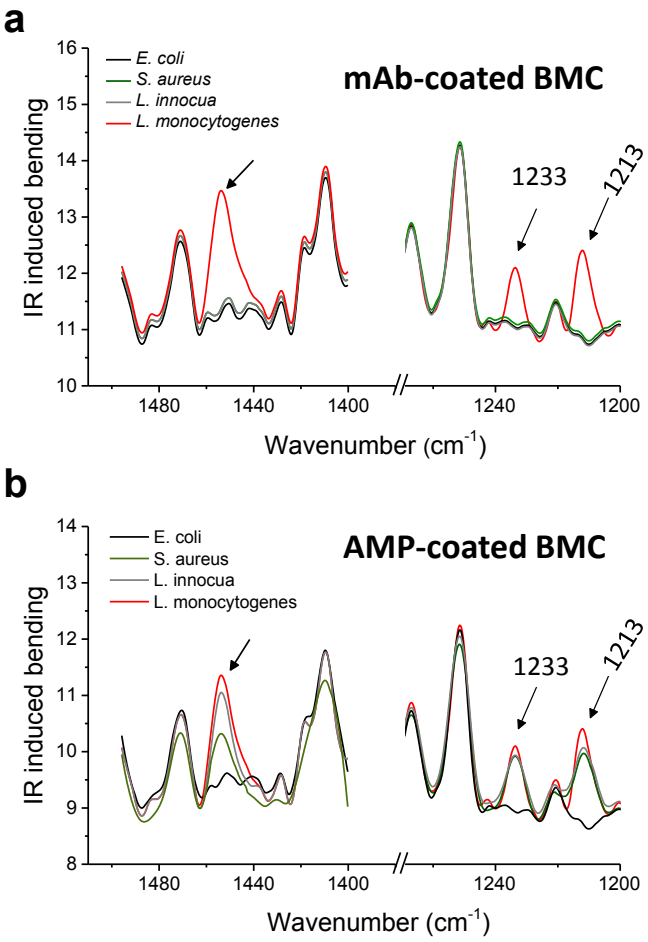

Appendix Figure 9. The nanomechanical infrared spectra of captured bacteria inside the BMC sensors. Representative IR deviation analyzed spectra in the mid-IR region for bacteria strains as indicated, detected by exposure to a mAb-coated BMC sensor (a) or an AMP-coated BMC sensor. The IR absorption bands of the bacteria at ~ 1213 cm^{-1}, 1233 cm^{-1} and 1451 cm^{-1}, without extensive algorithmic preprocess (binning, smoothing and second deviation transformation) show the difference between strains of bacteria.

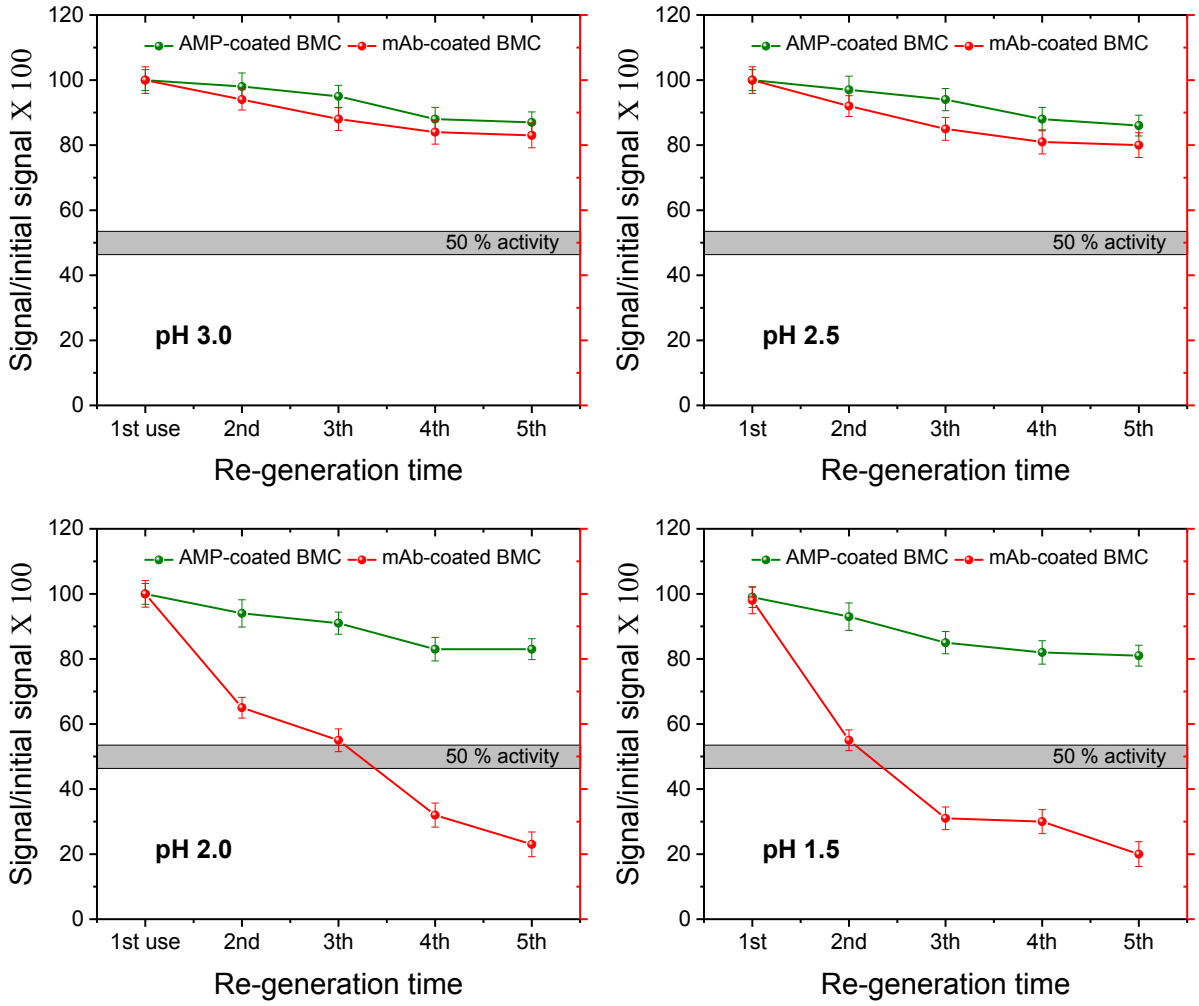

Appendix Figure 10. BMC sensors re-usability. As indicated, performance of the BMC sensors, either the AMP-coated (green) or mAb-coated BMC (red) are shown after exposure to a repeated cycle of regeneration at various pH. Restored responses to analytes were presented as a percentage with respect to the sensors responses at their first time use. Each response is an average calculation of five replicates and error bars correspond to standard deviations.

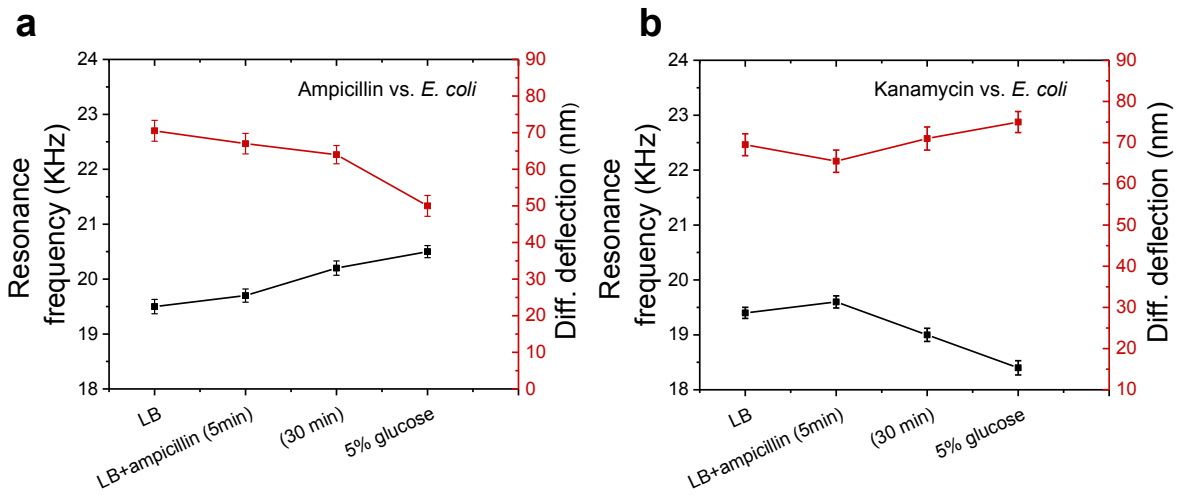

Appendix Figure 11. Experiment shows the cantilever deflection and resonance frequency shift in response to bacteria metabolism. *E. coli* DH5α exposed to ampicillin (a) and kanamycin (b); the cantilever (deflection, frequency) measurements were performed as indicated, starting from bacteria in LB, adding antibiotics (10 μg ml^{-1}), 30 min after exposure to the antibiotics and 10 min after adding a 5% glucose solution. The results represent an average of 5 replicates performed at the same condition with error bars indicating standard deviation.

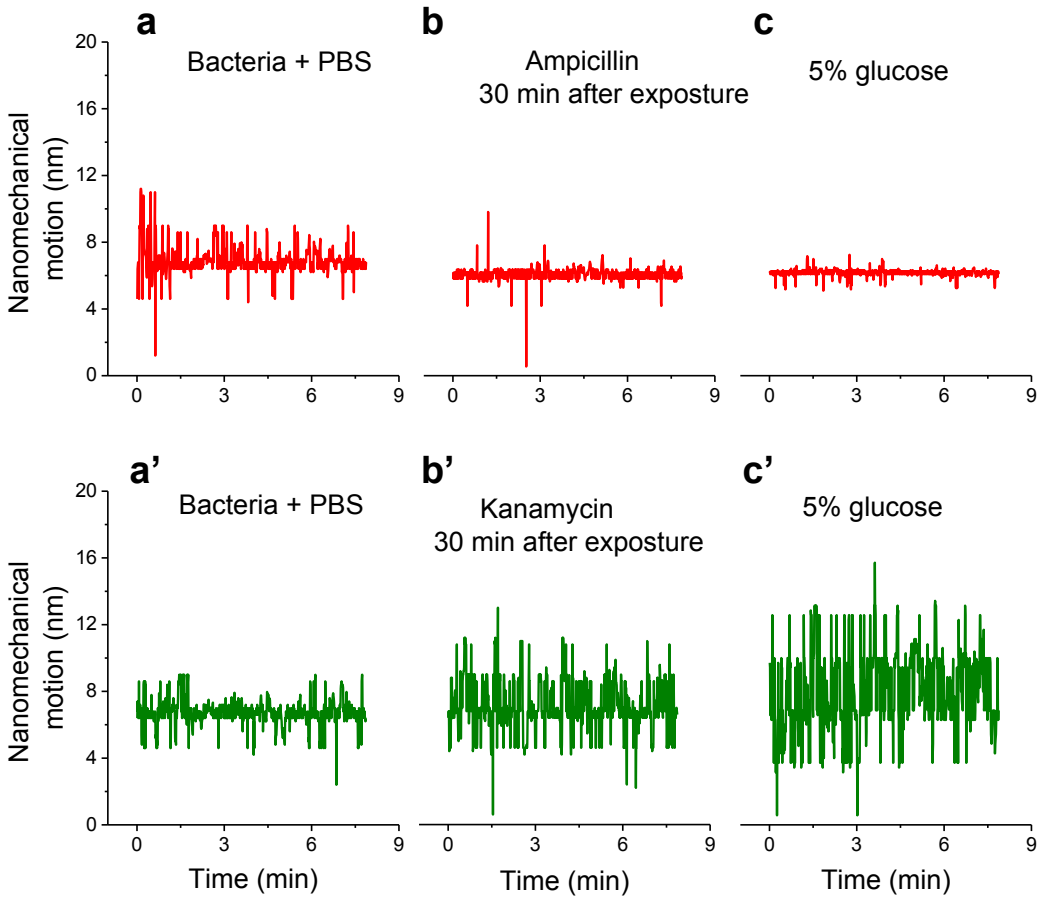

Appendix Figure 12. Enhancement of nanomechanical BMC oscillation by bacteria (*E. coli*) metabolism. Nanomechanical fluctuation of bacteria exposed to ampicillin (upper panel) or to kanamycin (lower panel). **a** and **a'** are a result of bacteria in PBS, **b** and **b'** show a result of exposure to antibiotics, ampicillin or kenamycin, respectively (measurement after 30 min of exposure). **c** and **c'** shows the nanomechanical motion after exposure to 5% glucose solution by 10 min. The results suggested that *E. coli* is killed by ampicillin but it resisted kanamycin. Removal of antibiotic to introduce 5% glucose to the bacteria enhanced the metabolism of the bacteria exposed to kanamycin to increase the nanomechanical fluctuation., while introducing ampicillin did not change the cantilever fluctuation, indicating that bacteria is killed.

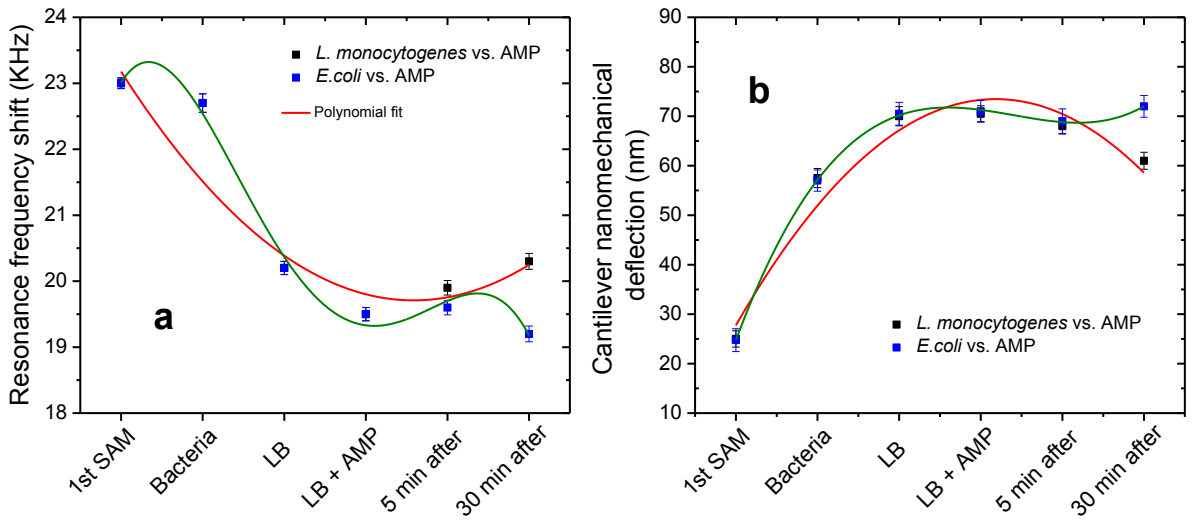

Appendix Figure 13. Susceptibility of bacteria to the antimicrobial peptide Leucocin A. While the figure (**a**) shows resonance frequency shift as a result of bacteria (*L. monocytogenes and E. coli*) exposure to Leucocin A, figure (**b**) displays differential nanomechanical deflection as a result of exposure to Leucocin A at a concentration of 0.1 μg ml^{-1}. When Leucocin A was introduced into *L. monocytogenes* we see clear upward shift of the resonance frequency (**a red line**); however, when it was introduced into *E. coli* (**a green line**) a clear drop in the resonance frequency is observed after 30 min from the treatment. This suggests viability of the cells and its resistance to the antibacterial activity of Leucocin A. The experiment also describes the relation between the amplitude of BMC nanomechanical deflection and bacteria metabolic activity as indicated. During Leucocin A injection, we observe a slight drop in the nanomechanical deflection after 5 min of Leucocin A introduction. However, measurements at 30 min of exposure showed a decrease in the amplitude of deflection of *L. monocytogenes* sensor (**b red line**) and an increase in the amplitude of deflection for *E. coli* sensor (**b green line**). It is expected that Leucocin A has killed most of *L. monocytogenes* cells and deactivate its metabolic processes as what happen with ampicillin. The AMP however, has no effect on the *E. coli* cells; after few min from first shock the cells had recovered its metabolism. This causes an enhancement in the nanomechanical amplitude of deflection and decrease in the resonance frequency. Data is presented as a mean ± SD.

Chapter 4

Appendix Table 1. Short ligand peptide probes used in the study

Peptide	Targeting receptor	$[M+H]^{+1}$ Obs.	Calc.	Rt (min)	Yield %
18-4 (WxEAAYQrFLC)	Unknown	1398.2	1397.5	26	61%
Ref-1 (XEPAYQRFTC)	none	1225.2	1225.2	25	62%
cRGDfC	Integrin $\alpha v\beta 3$	579.5	578.7	22	66%
Ref-2 (cRADfC)	none	592.6	592.7	25	60%

RP-HPLC retention time (Rt) of synthetic peptides was measured using Vydac C18 analytical column with a gradient of (mobile phase 1 for peptides 1 and 2) 15 – 50% ACN/water (0.1% TFA) in 50 min with a flow rate of 1 mL min^{-1} or (mobile phase 2 for peptides 3 and 4) 15 – 55% ACN/water (0.1% TFA) in 50 min with a flow rate of 1 mL/min. Lower case letters denote D-amino acids. X is Nle (norleucine), and Ref indicates reference peptides for the targeting peptides.

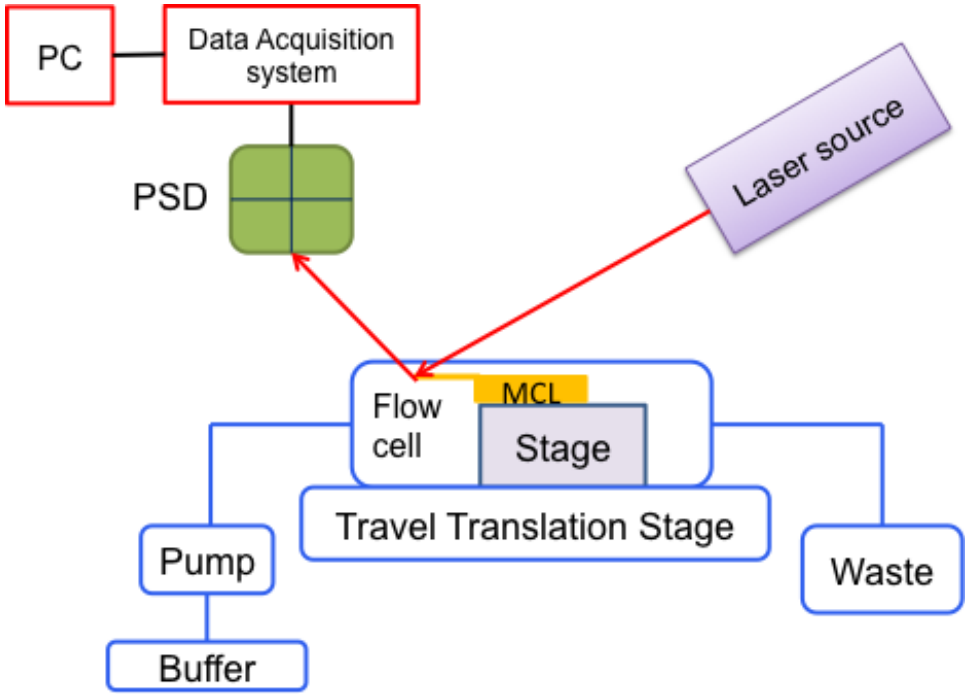

Appendix Fugure 14. Schematic diagram of an in-house built microcantilever detection system. The parts for the sensor were purchased from Thorlabs. Inc (Newton, New Jersey, USA), while the levers were obtained from Concentris GmbH – Switzerland. The system consists mainly of the flow cell, where the cantilever is mounted to two ports, inlet and outlet, to receive and eject the delivered samples. Red diode laser beam reflect off the free end of the cantilever where the peptide is immobilized which then is focused on a positive sensitive detector (PSD) to detect changes.

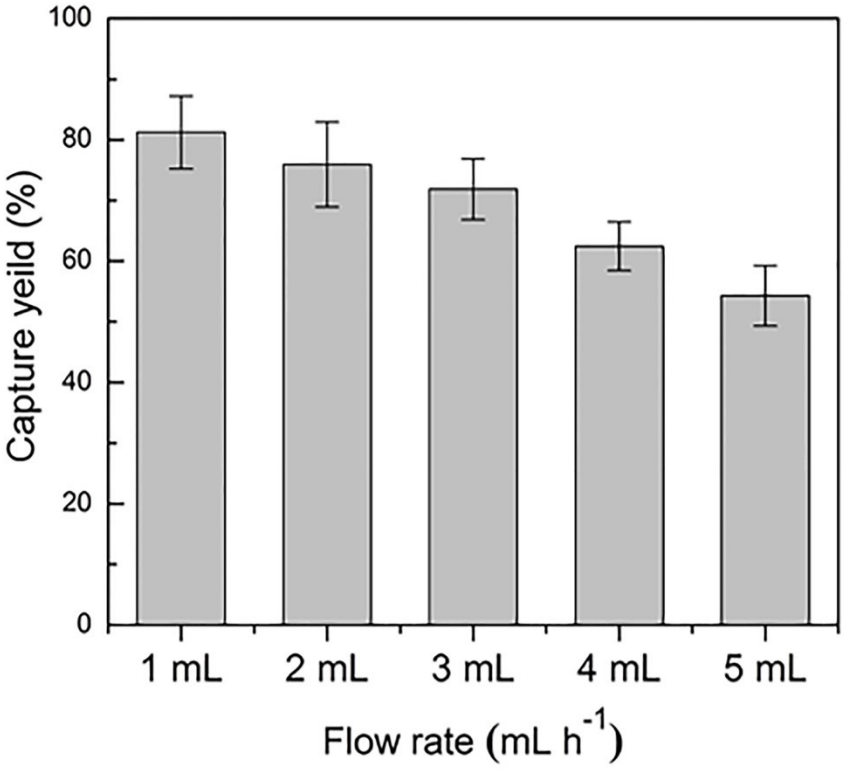

Appendix Figure 15. Capture yield as a function of flow rate (mL h-1) from buffer solution spiked with MCF7 cells (100 cells mL^{-1}). The responses were taken for a cantilever array sensor functionalized with peptide **18-4**. Each percentage is an average calculation of three replicates and error bars indicate corresponding standard deviations.

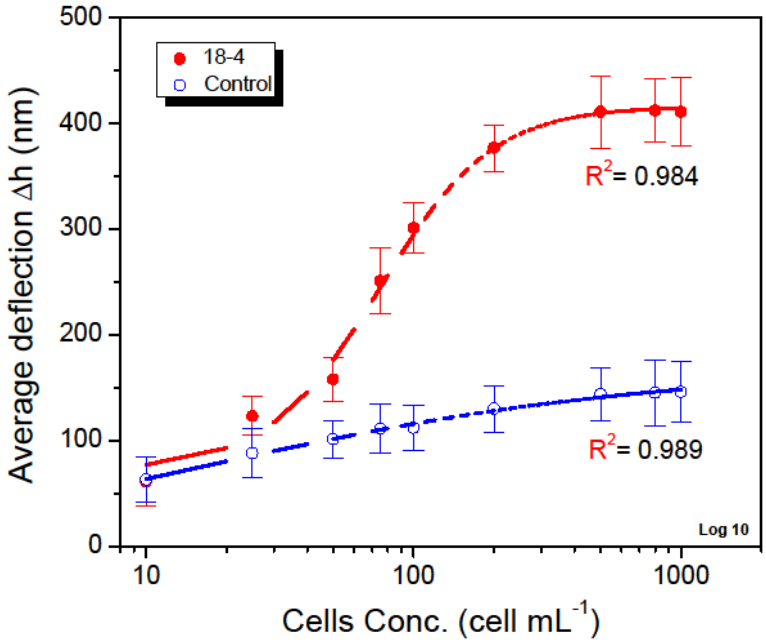

Appendix Figure 16. Concentration dependent pattern of the peptide-based cantilever sensor. The differential deflection of peptide **18-4** functionalized cantilever array (red) and control peptide cantilever (blue) was read after injection of serial concentration of MCF7 cancer cells spiked in phosphate buffered saline as indicated. The dashed lines show the sigmoid fit of the nanomechanical response as a function of MCF7 concentrations. Cantilever differential deflection represents an average calculation of eight replicates and error bars indicate standard deviations.

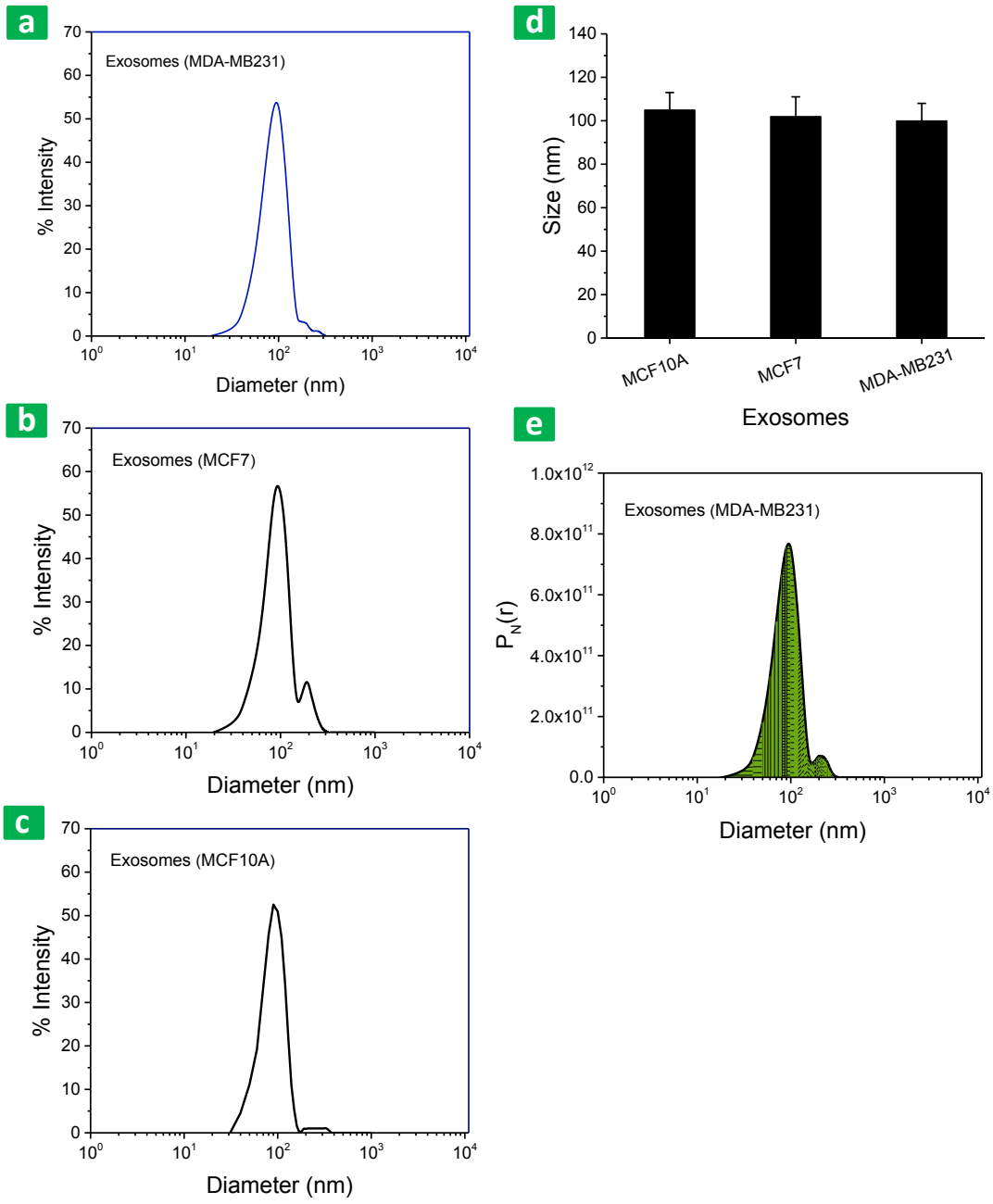

Appendix Figure 17. Dynamic Light Scattering (DLS) determines the absolute exosomes size distribution for the tested cell lines as indicated in spectra **a, b** and **c**. An averaged size determined by DLS is presented in figure **d**. The difference from SEM (~89 ±5 nm) compared to

Dynamic Light Scattering (around ~102 ±8 nm) is due to the fact that the DLS monitors the hydrodynamic diameter of the exosomes in solution. In addition, larger particles contribute more strongly to the light scattering than the smaller particles which cause more shifts in the distribution values. Values of an average calculation of three replicated is presented with ± s.d. **e.** Concentration of exosomes (vesicles per mL) as it recovered from the vesicles' distribution, $P_N(r)$ represents the number of vesicles per mL.

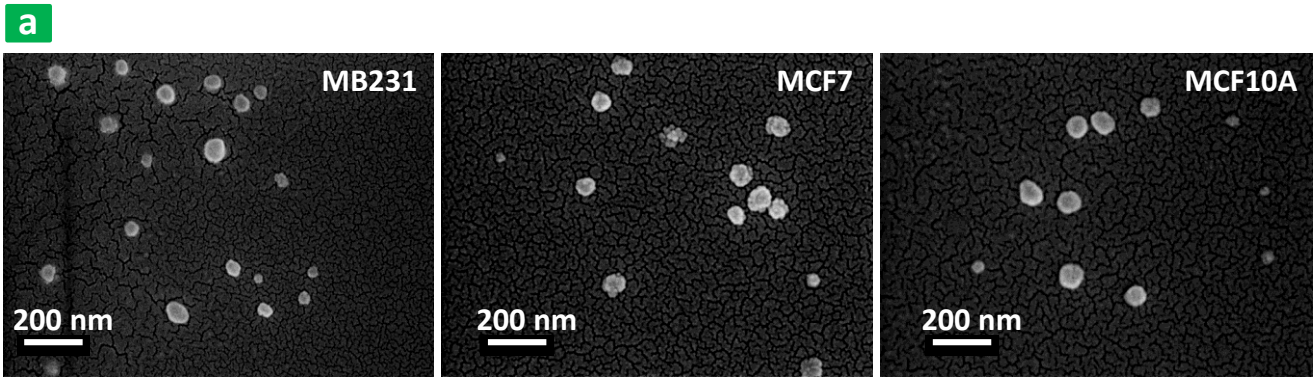

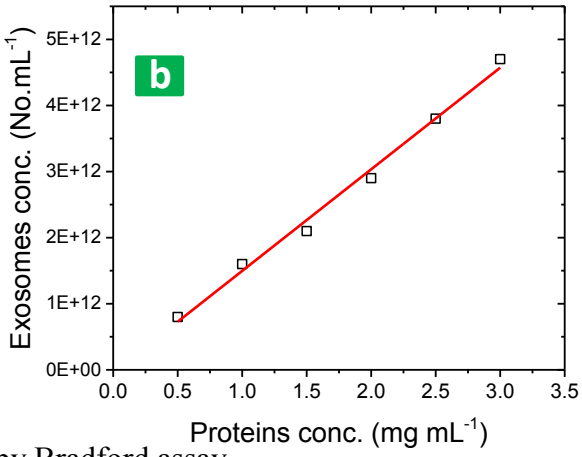

Appendix Figure 18. Scanning Electron Microscopy (SEM) images of exosomes produced breast cell lines as indicated, MB231, MCF7 (cancerous cells) and MCF10A (noncancerous cells). The result shows comparable exosomal distribution with an average size value of ~89 ±5 nm in all experiments. Figure **b** represents a linear correlation between quantification of exosomal proteins measured by Bradford assay (mg per mL) and concentration of the exosomes (number per mL) measured by Dynamic Light Scattering. The plot indicates a linear relationship between the vesicles number and protein concentration. An average of three replicate measurements is presented.

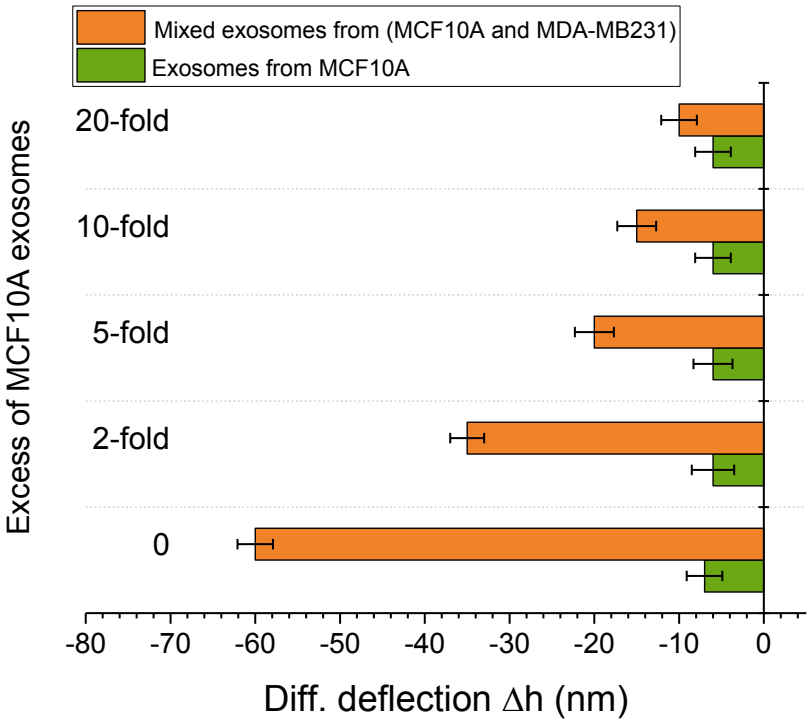

Appendix Figure 19. Differential nanomechanical deflection (Δh) measured after injection of different ratios of exosomes from cancer cells (MDAA-MB231) and noncancerous exosomes from MCF10A cell line. The results indicate significant deflection in presence of cancer cell-derived exosomes in comparison to the reference (exosomes only from MCF10A). The results indicate that the antiGPC1-functionalized cantilever can still detect cancer cell-derived exosomes in the presence of a 20-fold excess of non-cancerous exosomes. Mean values are presented with error bars indicating s.d.

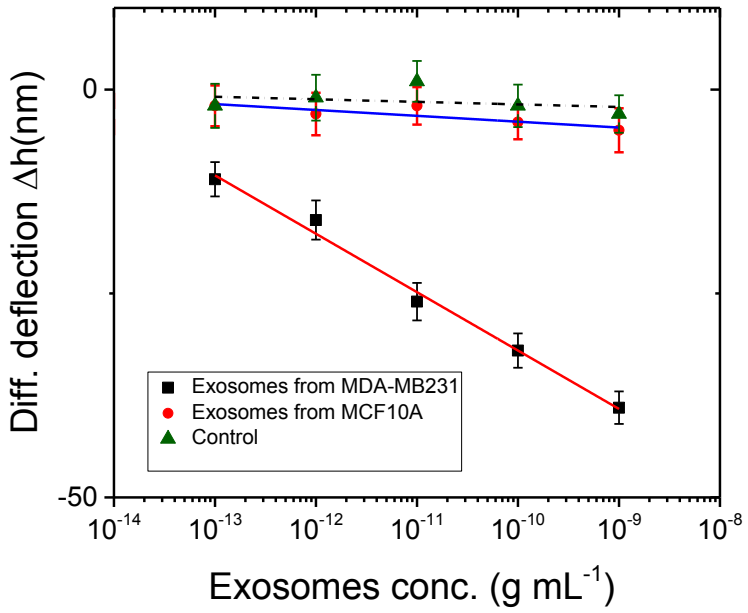

Appendix Figure 20. Exosomes concentration as a function of fixed antiGPC1-coated NPs. Enhanced nanomechanical bending (nm) is scaled proportionally with the exosomes concentration in the samples. The plot shows a limit of detection of 10^{-13} g mL^{-1} at which the cantilever signal is statistically significant from those observed with normal cells-derived exosomes and the reference control. The control signal is a microcantilever-coated with only cysteamine, exposed to exosomes at the same concentrations as indicated, then exposed to antiGPC1-coated NPs at fixed concentration (2×10^{-12} g mL^{-1}). Values represent an average calculation of three replicates and error bars indicate s.d.

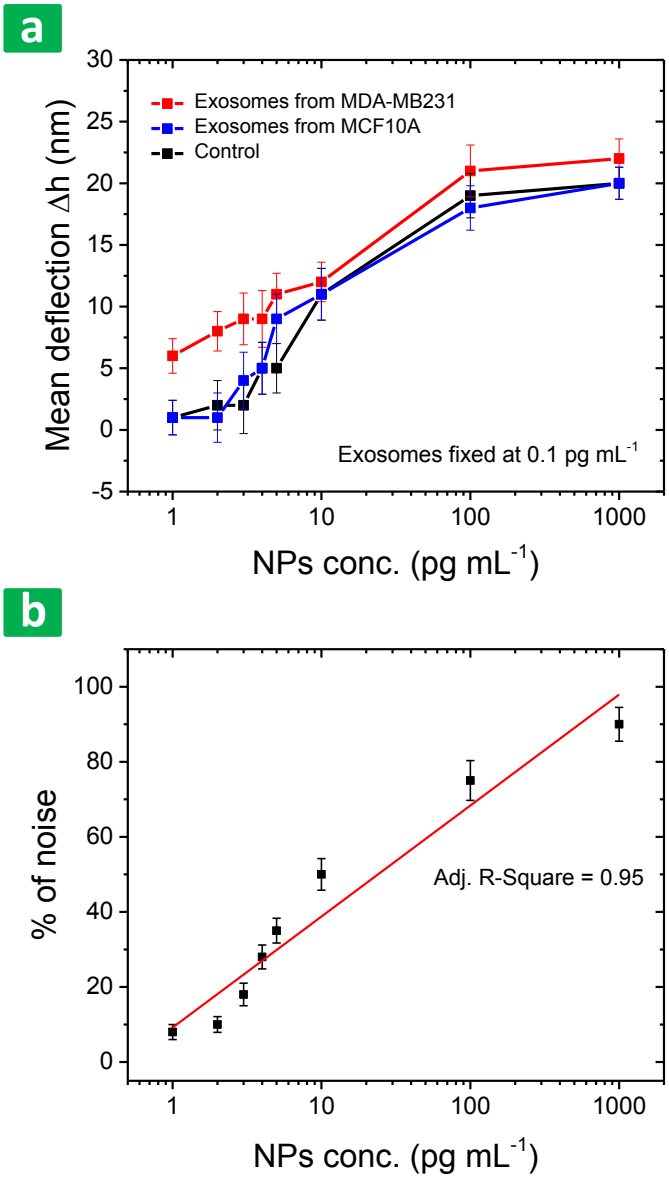

Appendix Figure 21. Microcantilever sandwich assay, nanomechanical deflection (nm) as a function of concentration of antiGPC1-coated nanoparticles (NPs). **a.** Deflection of the cantilever due to exposure to different concentrations of NPs at fixed concentration of exosomes (1×10^{-13} or o.1 pg mL^{-1}). Results represent mean ± s.d. of three replicates. **b.** The noise ratio of the cantilever increases as a function of the number of NPs at the tested exosomes level (0.1 pg mL^{-1}). In other words, the generated signals of the cantilever become less significant by increasing the number of functionalized NPs, indicating a saturation point at 2×10^{-12} g mL^{-1} or/ 2 pg mL^{-1} NPs concentration (maximum significance and minimum noise). The results suggest

that the maximum number of antiGPC1-coated NPs on the surface is ~400 for exosomes concentration 200, based on the calculated mass and number of NPs provided by the manufacturer. This agrees well with our geometrical calculation that estimates number of NPs on the surface to ~500. This leads us to suggest also that the enhanced cantilever surface stress may be due to NPs binding to more than one exosome at a time. The noise represents the percentage of the subtracted values of cantilevers' deflection (MBA-MD231) from the reference control values.